Universidade de Aveiro Departamento de Química
2017

João Tiago Viana de Matos

Matéria Orgânica em Aerossóis Atmosféricos Urbanos: Caracterização Molecular utilizando Técnicas Analíticas de Alta Resolução

Organic Matter in Atmospheric Aerosols: Molecular Characterization Using High-Resolution Analytical Techniques

Universidade de Aveiro Departamento de Química
2017

João Tiago Viana de Matos

Matéria Orgânica em Aerossóis Atmosféricos Urbanos: Caracterização Molecular utilizando Técnicas Analíticas de Alta Resolução

Organic Matter in Atmospheric Aerosols: Molecular Characterization Using High-Resolution Analytical Techniques

Tese apresentada à Universidade de Aveiro para cumprimento dos requisitos necessários à obtenção do grau de Doutor em Química realizada sob a orientação científica do Doutor Armando da Costa Duarte, Professor Catedrático do Departamento de Química da Universidade de Aveiro, e da Doutora Regina Maria Brandão de Oliveira Duarte, Equiparada a Investigadora Principal do Centro de Estudos do Ambiente e do Mar (CESAM) da Universidade de Aveiro.

Apoio financeiro da FCT e do FSE no âmbito do III Quadro Comunitário de Potencial Apoio e do Programa Operacional Humano (POPH) do QREN (SFRH/BD/84247/2012) e dos projetos de investigação *ORGANOSOL* (PTDC/CTE-ATM/118551/2010) and *CN-linkAIR* (PTDC/AAG-MAA/2584/2012).

Para a minha afilhada Salomé.

o júri

Presidente

Maria Herminia Deulonder Correia Amado Laurel
Professora Catedrática da Universidade de Aveiro

Armando da Costa Duarte
Professor Catedrático da Universidade de Aveiro

Maria Arminda Costa Alves
Professora Catedrática da Faculdade de Engenharia da Universidade do Porto

Carlos Manuel de Melo Pereira
Professor Auxiliar com Agregação da Faculdade de Ciências da Universidade do Porto

Mário Emanuel Campos de Sousa Diniz
Professor Auxiliar da Faculdade de Ciências e Tecnologia da Universidade Nova de Lisboa

Artur Manuel Soares Silva
Professor Catedrático da Universidade de Aveiro

agradecimentos

A realização desta dissertação não seria possível sem a ajuda e colaboração de diversas pessoas, a quem endereço os meus mais sinceros agradecimentos.

Aos meus orientadores, Professor Doutor Armando Duarte e Doutora Regina Duarte, pela confiança, disponibilidade e compreensão demonstrada ao longo de todo o doutoramento.

Ao Professor Doutor Artur Silva pela disponibilidade para a aquisição dos espetros de NMR uni- e bidimensionais e pela a sua contribuição e ajuda na interpretação destes mesmos espetros.

Às minhas colegas de laboratório, nomeadamente a Sandra Freire, Catarina Loureiro, Andreia Paula e Sónia Lopes, que muito contribuíram para os resultados alcançados neste trabalho.

Aos meus pais e irmã por todo o apoio e suporte que me deram ao longo de todos estes anos.

À minha namorada, que me acompanhou nos bons e (principalmente) nos maus momentos, e pelo seu amor e apoio incondicional.

À Fundação para a Ciência e Tecnologia, pelo suporte financeiro através da bolsa de Doutoramento (Ref. SFRH/BD/84247/2012).

A todas as outras pessoas que direta ou indiretamente contribuíram para a realização deste trabalho.

A todos muito obrigado!

palavras-chave

Aerossóis orgânicos urbanos; Matéria orgânica solúvel em água; Matéria orgânica solúvel em meio alcalino; Cromatografia líquida bidimensional abrangente; Matriz de emissão-excitação; Análise de fatores paralelos - mínimos quadrados alternados; Espectroscopia de ressonância magnética nuclear uni- e bidimensional.

resumo

Esta dissertação focou-se na caracterização química de amostras de aerossóis atmosféricos finos recolhidas numa região urbana situada na costa da Europa Ocidental, durante oitenta semanas, e representativas das diferentes estações do ano. Os dados adquiridos proporcionam um maior conhecimento sobre a composição molecular da fração orgânica dos aerossóis, bem como uma visão global sobre a contribuição de diferentes fontes e sazonalidade dos componentes carbonáceos e inorgânicos nos aerossóis. A cromatografia líquida bidimensional abrangente foi utilizada para investigar a heterogeneidade química e mapear a hidrofobicidade *vs.* distribuição de peso molecular das frações de ácidos mais hidrofóbicos da matéria orgânica solúvel em água (*WSOM*, na sigla em inglês) de aerossóis atmosféricos, revelando que a *WSOM*, amostrada nas estações quentes, é enriquecida em estruturas alifáticas, enquanto que a *WSOM* recolhidas nas estações frias contém estruturas com ligações π conjugadas juntamente com estruturas alifáticas. Foi também realizado uma comparação das características estruturais da matéria orgânica presente em extratos aquosos e extratos alcalinos, sequencialmente extraídos de aerossóis finos. Para isso, foi utilizado um método quimiométrico multidirecional para decompor conjuntos de espectros de fluorescência em modo matriz excitação-emissão de *WSOM* e de matéria orgânica solúvel em meio alcalino (*ASOM*, na sigla em inglês), numa tentativa de identificar as estruturas fluorescentes atmosfericamente mais relevantes, bem como a sua variabilidade anual. A metodologia utilizada demonstrou diferenças sazonais num dos componentes fluorescentes identificados nas amostras de *WSOM*, contrastantes com os resultados obtidos para as amostras *ASOM*, nas quais os componentes identificados foram constantes ao longo do ano. A espectroscopia de ressonância magnética nuclear (RMN) de protão foi igualmente utilizada para investigar e comparar as características estruturais das frações de *WSOM* e *ASOM*, mostrando que estas frações contêm grupos funcionais de protão semelhantes, mas com uma diferente distribuição relativa ao longo do ano. As amostras recolhidas nas estações frias apresentam um carácter menos alifáticos e oxidado e com uma maior contribuição de estruturas aromáticas que as amostras recolhidas nas estações quentes. Adicionalmente, a aplicação das técnicas bidimensionais (2D) de RMN forneceram uma excecional resolução e uma incomparável representação da assinatura molecular das amostras, o que permitiu obter um perfil detalhado da composição estrutural destas frações, assim como decifrar as suas principais fontes de emissão ao longo do ano. As frações *ASOM* são menos hidrofílicas e estruturalmente diversas das frações de *WSOM*, sendo estas últimas constituídas maioritariamente por estruturas alifáticas ramificadas ricas em hétero-átomos, de origem primária (antropogénica e natural) e secundária. Estruturas do tipo da lignina, sacarídeos, dissacarídeos, e anidrosacarídeos foram identificados nas amostras de *WSOM,* refletindo a influência queima de biomassa. Os dados espectrais obtidos para cada ligação H-C identificada foram também utilizados para construir um modelo estrutural semi-quantitativo da fração *WSOM*, o qual poderá ser utilizado em futuros estudos acerca do efeito da composição química e estrutural dos aerossóis orgânicos no respetivo comportamento e impacto na química da atmosfera.

keywords

Urban organic aerosols; Water-soluble organic matter; Alkaline-soluble organic matter; Comprehensive two-dimensional liquid chromatography; Emission – excitation matrix; Parallel factor analysis - alternating least squares; One- and two-dimensional nuclear magnetic resonance spectroscopy.

abstract

This dissertation focus on the chemical characterization of fine atmospheric aerosol samples collected at an urban site in the Western European Coast, during eighty weeks, representative of different seasons. The acquired data set provide a comprehensive and new insight on the molecular composition of the organic fraction of the aerosol components, as well as, provide a seasonal source apportionment overview of both carbonaceous and inorganic aerosol components. Comprehensive two-dimensional liquid chromatography was introduced to investigate the chemical heterogeneity and map the hydrophobicity *vs.* molecular weight distribution of the most hydrophobic acid fractions in water-soluble organic matter (WSOM) from atmospheric aerosols, revealing that the WSOM samples collected in warm seasons are enriched in aliphatic structures, while those from colder seasons exhibit a higher degree of structures with conjugation of π-bonds alongside aliphatic structures. A comparison of the features of the organic matter present in water and alkaline extracts, sequentially extracted, from fine aerosol samples during different seasons, are also carried out. For that, a multiway chemometric method was used to decompose sets of excitation-emission matrices fluorescence spectra of WSOM and alkaline-soluble organic matter (ASOM), in an attempt to identifying the most atmospherically-relevant fluorescent structures, as well as their variability over seasons. The method shows differences between the colder and warmer seasons in the fluorescence map of one WSOM fluorescent component, which contrast with the results obtained for the ASOM, where the fluorescence signatures were found to be constant along the seasons. Proton nuclear magnetic resonance (^{1}H NMR) spectroscopy was used for investigating and comparing the structural features of WSOM and ASOM, showing that these fractions hold similar ^{1}H functional groups; however, they differ in terms of their relative distribution throughout the different seasons. Samples collected during the cold seasons have a less aliphatic and oxidized character and higher contributions from aromatic groups than those from warmer conditions. Furthermore, a synergistic combination of 2D NMR techniques provided an exceptional resolution and depicted unsurpassed resolved molecular signatures, which allowed portraying the annual background of the structural composition of these fractions, as well as deciphering their major source types over seasons. The ASOM fractions are less hydrophilic and structurally diverse than their WSOM counterparts. This latter component is mostly composed of heteroatom-rich branched aliphatics, having both primary (natural and anthropogenic) and secondary origin. Lignin, disaccharides, and anhydrosaccharides signatures were also identified in the WSOM samples, reflecting the biomass burning influence. The derived dataset on the H–C molecules backbone were also used to build a semi-quantitative structural model of WSOM, which can be used as a proxy to further distil key features on the atmospheric behaviour of organic aerosols.

Table of contents

List of figures and tables

Figures

Tables

List of abbreviations

1D	One-dimensional
2D	Two-dimensional
3D	Three-dimensional
AAS	Atomic absorption spectrometer
ALS	Alternating least squares
AMS	On-line aerosol mass spectrometry
Aut.	Autumn
ASOC	Alkaline-soluble organic carbon
ASOM	Alkaline-soluble organic matter
BBOA	Biomass burning organic aerosol
CMB	Chemical mass balance
COSY	Correlation spectroscopy
CP-MAS	Cross-polarization with magic-angle spinning
DAD	Diode array detector
DOC	Dissolved organic carbon
EC	Elemental carbon
EEM	Excitation-emission matrix
ESI	Electrospray ionization
FID	Flame ionization detector
FT-ICR	Fourier transform ion cyclotron resonance
GC–MS	Gas chromatography coupled to mass spectrometry
GC×GC	Comprehensive two-dimensional gas chromatography
HILIC	Hydrophilic interaction liquid chromatography
HMBC	Heteronuclear multiple bond correlation
HR-MS	High-resolution mass spectrometry
HSQC	Heteronuclear single-quantum correlation
LC–MS	Liquid chromatography coupled to mass spectrometry
LC×LC	Comprehensive two-dimensional liquid chromatography
LOD	Limit of detection
MALDI	Matrix-assisted laser desorption/ionization
MCR-ALS	Multivariate curve resolution-alternating least squares
MS	Mass spectrometry

MOA	Marine organic aerosol
M_p	Molecular weight at peak maximum
M_w	Molecular weight
NMR	Nuclear magnetic resonance
NOM	Natural organic matter
NPOC	Non-purgeable organic carbon
OA	Organic aerosol
OBGC	Orthogonal background correction
OC	Organic carbon
PALC	P*er* aqueous liquid chromatography
PARAFAC	Parallel factor analysis
PC	Pyrolytic carbon
PCA	Principal component analysis
$PM_{2.5}$	Particulate matter with aerodynamic diameter ≤ 2.5 µm
$PM_{2.5-10}$	Particulate matter with aerodynamic diameter between 2.5 and 10 µm
PMF	Positive matrix factorization
RP	Reversed-phase
SEC	Size-exclusion chromatography
SIA	Secondary inorganic aerosol
SPIDER	Saturation pulse induced dipolar exchange with recoupling
SOA	Secondary organic aerosol
Spr.	Spring
Sum.	Summer
SVOCs	Semi-volatile organic compounds
TOC	Total organic carbon
TOCSY	Total correlation spectroscopy
TOF-MS	Time-of-flight mass spectrometry
Win.	Winter
WINSOC	Water-insoluble organic carbon
WSOC	Water-soluble organic carbon
WSOM	Water-soluble organic matter

Chapter 1

Aims and structure of dissertation

This chapter presents a general introduction to the research topic providing an overview on the importance of the study of atmospheric aerosols. This chapter also presents a description and aims of the PhD research project, as well as, the dissertation structure.

1.1. Overview and significance of atmospheric aerosols

An aerosol is a system consisting of a gas with either solid or liquid particles in suspension; typically, the particle diameters are in the range between ~ 1 nm and ~ 100 μm. Since it is virtually impossible to supply a gas without particles, each gas could be considered as a part of the aerosol system [1,2]. Consequently, an atmospheric aerosol is made of solid and/or liquid particles suspended in air. Some examples of these particles are smoke, fog, smog, and clouds [3]. However, in atmospheric science, clouds are usually considered as separate phenomena, since in this field the term aerosol is normally used to describe the suspended particles that contain a large proportion of condensed matter other than water [2].

Atmospheric particulate matter can have a wide variety of different physicochemical characteristics strongly linked to the nature of its source. In this context, aerosols can be classified according to their emission source, i.e., in natural and anthropogenic aerosols. In addition, atmospheric particulate matter can also be discriminated according to their formation mechanism, i.e., in primary particles and secondary particles. The primary particles are liquid or solid particles directly emitted by natural (e.g., volcanic eruptions, and wind-driven re-suspension of dust, salt and pollens), or anthropogenic sources (e.g., biomass burning, incomplete combustion of fossil fuels, and vehicle emissions). Figure 1.1 shows the distribution, on a global scale, of some of these primary atmospheric particles according to the principal emission sources scenarios. In red and orange it is represented dust raised from Earth surface, the blue colour represents the sea salt particles, the green represents smoke rising from fires, and the white represents sulphates of volcanic eruptions and emissions from burning fossil fuels. Secondary particles, on the other hand, are liquid droplets or solid particles formed in the atmosphere by gas-to-particle conversion using different physicochemical processes (i.e., new particle formation by nucleation and condensation of gaseous precursors) [2]. The concentration and composition of the aerosols in the atmosphere is thereby extremely variable, since the residence time in atmosphere of these particles as well as their spatial and temporal distribution are connected to highly complex systems (e.g., meteorological conditions).

In urban areas, activities associated with large population densities have become the most important sources of atmospheric particles and aerosol precursor gases, which exert a

major impact not only in a regional but also in a global scale [4]. The biomass burning and fossil-fuel combustion, which produce, among other, large amounts of black carbonaceous particles, and the road dust, construction, and industrial activities which produce larger mechanically generated aerosols, are among the major sources of primary aerosols in urban environments. On the other hand, the combustion-related release of precursor gases, such as oxides of nitrogen and sulphur, are very common in urban areas, generating significant amounts of secondary nitrate (NO_3^-) and sulfate (SO_4^{2-}) aerosols [4]. The production of these primary and secondary atmospheric aerosols, especially those from biomass burning and fossil-fuel combustion, have massively increased since preindustrial time, and, nowadays, its impact in the air quality, visual perception, and human health, are one of the most important public concerns in urban centres, particularly in heavily polluted cities [2,4]

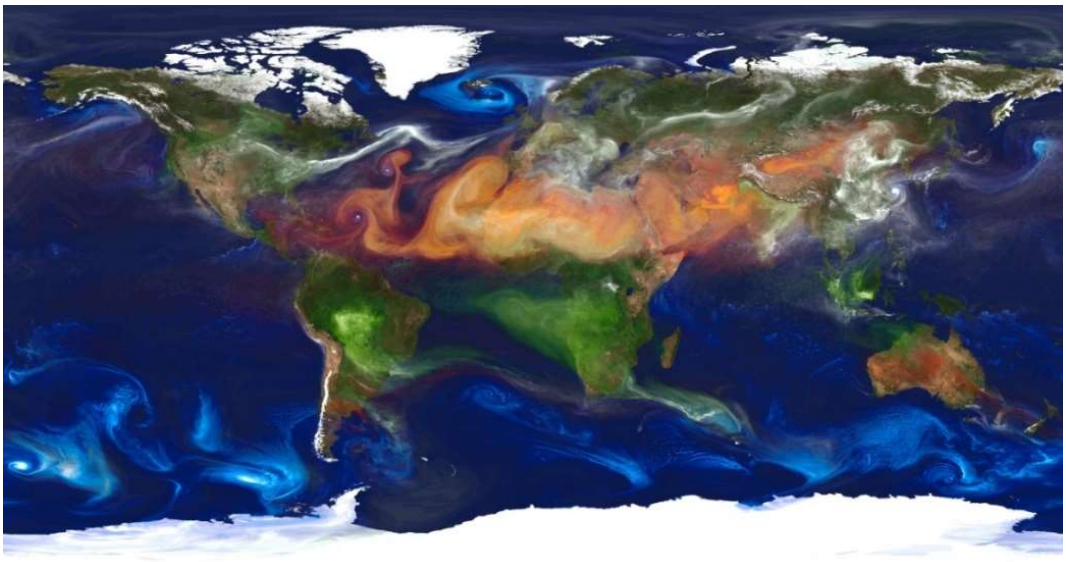

Figure 1.1 Distribution of aerosols on a global scale: results produced by the Discover supercomputer of NASA Center for Climate Simulation at Goddard Space Flight Center, Greenbelt, Md. (Image credit: William Putman, NASA/Goddard).

Nowadays, the study and characterization of aerosols, as well as their effects on climate and public health, are some of the most predominant topics in atmospheric and environmental analytical chemistry. This can be easily verified by the increasing number of research papers and citations addressing the topic of atmospheric aerosols in the latest years. As shown in Figure 1.2, the number of papers that discuss this topic almost tripled in the last decade, and the number of citations increased from a few dozens to more than ten thousand, which highlights the importance of this topic in the field of environmental sciences.

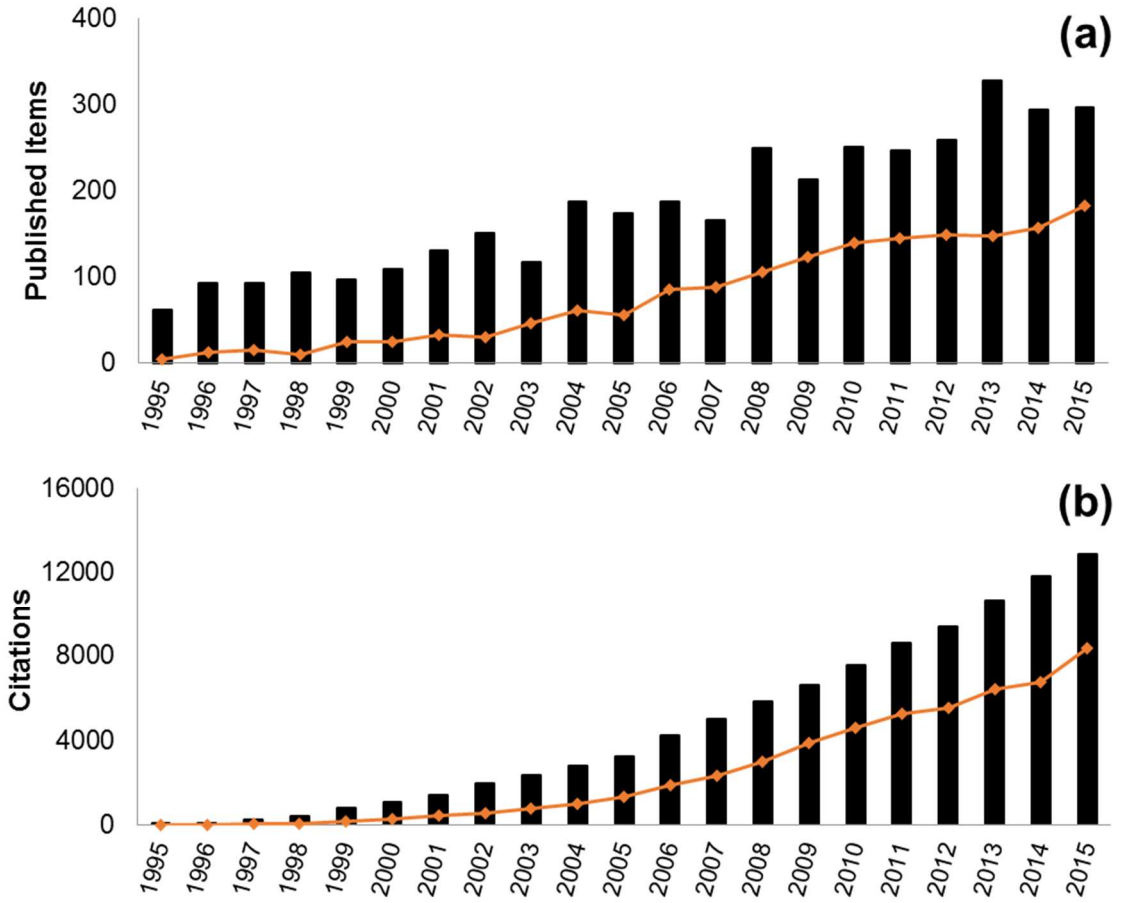

Figure 1.2 (a) Number of publications in each year and (b) citations in each year with the keywords "Atmospheric Aerosols" (columns) and "Organic Aerosols" (line) between the years 1995 and 2016. The search has been made in all databases of the science search engine ISI web of knowledge (http://apps.isiknowledge.com) on the 29th of Aug. 2016.

In the same fashion, the interest on the fraction of natural organic matter (NOM) in atmospheric aerosols, often referred to as organic aerosol (OA), has become a topic of paramount importance for the atmospheric research community. This component can be the predominant fraction of fine particulate matter ($PM_{2.5}$, particles with aerodynamic diameter ≤ 2.5 μm), accounting for more than 40% of the total fine aerosol mass in urban and continental areas [5,6], and has a profound effect on the radiative climate forcing [5,7], atmospheric chemistry [8,9], and human health [10,11]. The chemical composition and physical properties of OA and their dynamic change in the atmosphere have been the subject of extensive research over the past two decades [12,13], as emphasized in Figure 1.2. It is now well established that OA comprise a multitude of molecular structures, physical properties, and sources (primary and secondary formation) [8,12]. However, coping with OA complexity still is a major impairment in advancing our understanding about its

molecular composition, as well as its physical properties, sources, transformation, and climatic impact [12,13]. Investigating the chemical properties of OA components is especially relevant at urban areas, where their ambient concentrations and hazardous properties are linked to adverse health effects [14]. Understanding OA significance is, therefore, a focus of major scientific and also a relevant policy concern.

1.2. Description and aims of the PhD research project

The main goal of this PhD research project was to provide new insights on the spatiotemporal variability of the structural and functional groups composition of OA in fine aerosols collected in an urban area (Aveiro) at the north western coastal region of Portugal. For this purpose, fine aerosol samples collected on a weekly basis, during different seasons (i.e., winter (Win.), spring (Spr.), summer (Sum.), and autumn (Aut.)) on pre-fired quartz filters, using a high-volume sampler, will be the basis for the investigation. The characterization and measurement of the OA will lay mainly in the fraction of water-soluble organic matter (WSOM), extracted and isolated from the urban aerosol samples following already existing protocols [15,16].

In addition to the WSOM, and in order to further improve the current knowledge on the whole OA component, this PhD project will also make an attempt to characterize the water-insoluble organic fraction, namely the fraction dissolved in alkaline medium, for further comparison to its water-soluble organic counterpart and to assess the contribution of different groups of organic structures to the aerosol organic material. This urban aerosol fraction, comprising the alkaline-soluble organic matter (ASOM) is often neglected in most field studies and, therefore, is usually left under-characterized. However, ASOM constitute a highly variable fraction of the total fine aerosol mass and hence may significantly affect the atmospheric behaviour of the air particles.

The work of this dissertation produced eight scientific papers, namely: 1) “Tracing of aerosol sources in an urban environment using carbonaceous, major ions, Sr isotope, and mineralogical compositional data” published in *Environmental Science and Pollution*

Research [17]; 2) "Natural organic matter in urban aerosols: comparison between water and alkaline soluble components using excitation – emission matrix fluorescence spectroscopy and multiway data analysis", published in *Atmospheric Environment* [18]; 3) "A simple approach to reduce dimensionality from comprehensive two-dimensional liquid chromatography coupled with a multichannel detector", published in *Analytica Chimica Acta* [19]; 4) "Profiling water soluble organic matter from urban aerosols using comprehensive two-dimensional liquid chromatography", published in *Aerosol Science and Technology* [20]; 5) "Two chemically distinct light-absorbing pools of urban organic aerosols: A comprehensive multidimensional analysis of trends" published in *Chemosphere* [21]; 6) "Challenges in the identification and characterization of free amino acids and proteinaceous compounds in atmospheric aerosols: A critical review", published in *Trends in Analytical Chemistry* [22]; 7) "^{1}H NMR studies of water- and alkaline-soluble organic matter from fine urban atmospheric aerosols", published in *Atmospheric Environment* [23]; and, 8) "Persistence of urban organic aerosols composition: decoding their structural complexity" that is under review.

1.3. Dissertation structure

This dissertation is organized into 10 chapters, starting with a general description and a contextualization of the scientific relevance and specific objectives of the research work (Chapter 1). Chapter 2 presents a state of the art in the study of the OA fraction and Chapter 3 describes the conditions and time schedule of the sampling campaigns for the $PM_{2.5}$ samples, and the extraction and isolation of the water-soluble and alkaline-soluble organic fractions. Chapter 4 presents a comprehensive characterization on the carbonaceous and major water-soluble inorganic ions composition of $PM_{2.5}$. The acquired data resulted in a seasonal source apportionment overview of both carbonaceous and inorganic aerosol components. In Chapter 5, a new data treatment procedure for deal with the multidimensional data from comprehensive two-dimensional liquid chromatography (LC×LC) coupled to a diode array detector (DAD) is introduced [19]. As described in Chapter 6, this new procedure, has been used for unravelling and resolving the heterogeneity of WSOM, and to provide a deeper insight into how size-distinguished aerosol WSOM fractions differ in hydrophobicity during

different seasonal events. In Chapter 7 there is a comparison of the fluorescence features of the NOM present in water and alkaline extracts from the urban fine aerosol samples collected during different seasons. In this study a multiway chemometric method (Parallel Factor Analysis - Alternating Least Squares (PARAFAC-ALS)) was used for decomposing sets of excitation-emission matrices (EEM) fluorescence spectra of WSOM and ASOM, in an attempt to identify the most atmospherically-relevant fluorescent features, as well as their variability over seasons and potential sources. In Chapter 8, solution-state proton nuclear magnetic resonance (^{1}H NMR) spectroscopy was applied to characterize the structural features of WSOM and ASOM in order to assess the functional characteristics of fine aerosol WSOM and ASOM, and also to identify the major sources of these fractions at an urban location. Chapter 9 describes the synergistic combination of 2D NMR techniques, namely gradient-selected ^{1}H–^{1}H homonuclear Correlation Spectroscopy (*g*COSY), gradient-selected ^{1}H–^{13}C Heteronuclear single-quantum correlation (*g*HSQC), and gradient-selected ^{1}H–^{13}C Heteronuclear Multiple Bond Correlation (*g*HMBC), for decoding the structural features of WSOM and ASOM from fine atmospheric aerosols collected in Winter and Summer seasons. Finally, Chapter 10 presents the main conclusions of this thesis and puts forward some suggestions for future research.

Chapter 2

Study of the OA fraction

This chapter presents an introduction to the study of OA and discusses the main difficulties in their analytical characterization. This chapter also presents a state of the art of the high-resolution analytical techniques currently used in the study of this organic fraction from atmospheric aerosols.

2.1. Composition of atmospheric particles

The diversity of sources, transformations, and removal processes, as well as the spatial and temporal variability of atmospheric aerosols end up translating into a large heterogeneity of the chemical composition of atmospheric particles. In general, the particulate matter in the lower atmosphere (troposphere) comprises a complex mixture of highly water soluble inorganic salts (e.g., SO_4^{2-}, NO_3^-, ammonium (NH_4^+) salts and sea salt), siliceous crustal minerals (e.g., soil dust, and combustion ash), carbonaceous materials (organic compounds ranging from very soluble to insoluble and elemental carbon (EC)), and water [24–26].

As reviewed by Duarte [27], the components that make up the atmospheric particles are not equally distributed among all size ranges, and there is a strong dependence between the size of atmospheric particles and the presence of specific chemical structures in their composition. Therefore, the large particles, namely the $PM_{2.5-10}$ fraction (particulate matter with aerodynamic diameter between 2.5 and 10 μm) is primarily made up of chemical species characteristic of the Earth's crust, such as carbonate, silicon, aluminium, iron, calcium, and manganese and particles of marine origin, such as magnesium, sodium, and chlorine. These coarse particles may still contain a small fraction of carbonaceous material (1.2 to 31% of the total particle mass, depending on the study) [4,27]. However, the high concentration of carbonaceous compounds is usually associated with fine particles (20 to 50% of the total particle mass). Fine particles, namely the $PM_{2.5}$, are normally formed by gas-to-particle conversion and emitted to the atmosphere from combustion processes and, consequently, the major components of these particles are: a) inorganic species, such as SO_4^{2-}, NO_3^-, and NH_4^+; b) carbonaceous compounds; and c) some other trace elements (i.e., cadmium, lead, vanadium, barium, nickel, selenium, and chromium) from combustion processes [4,27].

From the perspective of the atmospheric aerosols characterization, while considerable progress has been made in understanding the physical and chemical properties of their inorganic component, the knowledge about their carbonaceous fraction, namely its structural and molecular composition, remains limited due to its formidable chemical complexity [24,28].

2.1.1. Carbonaceous fraction of atmospheric aerosols

The carbonaceous particles make up a large amount of the total atmospheric particulate matter and it is known that these particles play a part in the Earth's radiative balance and in climate change, although its true role is still far from being known [29]. The carbonaceous particles can be mainly allocated in three groups: carbonate minerals, EC, and organic carbon (OC) [30]. The carbonate minerals (e.g., calcite and dolomite) are derived from primary sources such as soil dust, and they are usually studied in conjunction with the other highly water soluble inorganic salts since they are usually negligible at submicron particles size range [29,30]. The EC also called black carbon or graphitic carbon, a strong absorber of visible and near-infrared light, is a primary aerosol generated as a by-product of incomplete combustion of fossil fuels sources, making up (typically) 5 to 20% of the total fine particulate mass. These particles are entirely non-volatile and are composed entirely of carbon that exists only in the particle phase [24,28,29]. Finally, the OC is the carbon related to organic compounds that can be derived from both primary and secondary sources. These organic compounds can make up more than 50% of the total fine particulate mass and, consequently, may represent, in several cases, the main fraction in atmospheric fine particles [26,29]. However, the determination of the OC fraction by the identification of each organic compound present in the atmospheric aerosols is extremely difficult, even for the most advanced analytical techniques, due to the countless different organic compounds with a wide range of chemical and thermodynamic properties [24,30,31].

2.2. Composition of the OA fraction

As reviewed by Kanakidou *et al.* [5], the fraction of the organic components of atmospheric aerosols, often referred to as OA, can be the predominant fraction of suspended matter mass, accounting for ~ 20 – 50% of the total fine particulate mass at continental mid-latitudes and reach 90% in tropical forested areas. Its distribution can have global (e.g., climate change) and local (e.g., toxicity hazards for human health) impacts [31]. The OA have already been widely recognized and identified as an active element in the process of cloud condensation and also as a source of ice formation nuclei. Several studies have

shown that OA are an important part of the total number of cloud condensation nuclei and their activation capability can be even comparable to SO_4^{2-} particles, which are considered as the most effective cloud condensation nuclei [31]. However, the true ability for most organic compounds to be cloud condensation nuclei has not yet been explored and their hygroscopic growth mechanism is still very uncertain and poorly understood [31]. Furthermore, despite the fact that the vast majority of organic components in the atmospheric aerosol remains yet to be identified, it is known that this fraction contains highly toxic compounds such as oxy- and nitro-polycyclic aromatic hydrocarbons and polychlorinated dibenzodioxins [32]. Consequently, and taking into account that these organic compounds are present in the fine fraction of atmospheric aerosols, which are sufficiently small to penetrate the membranes of the respiratory tract and be transported by the blood throughout the body, represents a serious hazard to human health.

The OA fraction covers a huge variety of molecular structures with different physicochemical properties and sources. However, the lack of knowledge regarding the inherent complexity of their chemical nature is nowadays one of the major impairments, not only to an improved understanding of atmospheric organic matter chemistry and composition, but also to predict how these compounds affect the climate system, atmospheric processes, and human health. Despite the enormous challenge that arises from unravelling the complexity of the OA into their individual components and structures, this quest, when accomplished, will provide unparalleled rewards towards a better understanding of their role in various atmospheric processes [33].

2.2.1. Water-soluble OA fraction

Due to the myriad of organic components that make part of the OA, the chemical composition and properties of the bulk organic matter remains poorly understood. A usual way towards unravelling the inherent complexity of this organic fraction is to group the different organic compounds by their general physicochemical properties. Many of the analytical techniques applied in earlier studies for the identification and characterization of organic molecules in atmospheric particles required the samples to be in liquid state; thus, the most exploited property had been solubility in different solvents [34].

Some of the earliest studies were based on the solubility of many of the components in nonpolar organic solvents (e.g., benzene, ether, hexane, and cyclohexane). This choice of organic solvents for the extraction of organic compounds from atmospheric particles was due mostly to its compatibility with gas chromatography coupled to mass spectrometry (GC–MS) [34,35], and by using those solvents, several individual non-polar organic compounds were identified by gas chromatography based systems. However, when following this methodology, the total mass of organics identified only accounts for less than 15% of the total mass of the OC fraction [35]. Furthermore, later studies also showed that several organic compounds in atmospheric particles absorb water, and from these, several contributed as cloud condensation nuclei. Hence, a need for a better characterization of this presumably water-soluble fraction was then aroused [34]. When water was used to extract organic compounds from the atmospheric particles, it was found that it improved extraction efficiency substantially and removed considerably more organic components from these particles than any organic solvent [35]. In fact, the realization that several organic compounds have strong polarity, surface activity, solubility and affinity for water, and that a highly variable fraction (10 – 80%) of the OA fraction are water-soluble, has promoted the development of new methodologies to explain the abundance, composition, origin, and atmospheric relevance of this OA component [13,31].

The growing interest on the WSOM has been fuelled by the realization that this organic fraction can potentially alter some aerosol properties (e.g., hygroscopic properties, surface tension behaviour, effective density) and thereby have an important role in several atmospheric processes [13]. As reviewed by Duarte and Duarte [13], the WSOM can affect the way on how particles act as cloud condensation nuclei; by absorbing solar radiation and atmospheric heating, this fraction contributes to the direct effect of aerosols on climate system; and WSOM can be important as a temporal source of OC to surface waters and, consequently, it could play an important role in the global carbon cycle. Furthermore, another important aspect in the study of WSOM is their source and formation mechanisms. Currently, these issues are still poorly known, although the major sources of these compounds appear to be biomass burning and secondary formation. Nevertheless, the atmospheric WSOM and their precursor gases can also be modified in the atmosphere by oxidative processes and, thereby, becoming less volatile, more hygroscopic and, consequently, more water soluble [33].

Several procedures and methodologies have been developed to study the chemical composition of this water-soluble organic fraction [15,16,36,37]. These studies are usually carried out using a combination of total OC (TOC) analysis, isolation and fractionation procedures, and characterization of molecular fragments and intermolecular bonds by different analytical techniques (see section 2.3.2). These studies have demonstrated that this fraction consists of a highly diverse suite of oxygenated compounds, including dicarboxylic acids, keto-carboxylic acids, aliphatic aldehydes and alcohols, saccharides, anhydrosaccharides, aromatic acids, phenols, but also amines, amino acids, organic NO_3^-, and organic SO_4^2 [15,16,23,30,38]. These studies also show that despite WSOM from different aerosol sources exhibit the same main carbon functional groups, their relative abundances are quite different [33].

Despite the enormous efforts to unravel the predominant structures in WSOM from OA, little is still known about their chemical composition, functional groups and sub-structural components. Consequently, the majority of the physicochemical properties of the water-soluble components, as well as their sources, formation mechanisms and fate in atmosphere, are also poorly understood [33]. Furthermore, due to its dynamic nature, it is likely that fractions collected from different environments or seasons and with different formation processes will exhibit different classes of compounds. Consequently, the establishment of general models for the structure of the water-soluble fraction of OA still is far from being a reality, and a lot of work and study is needed to understand their actual impact on a regional and global scale.

2.2.2. Alkaline-soluble OA fraction

Besides the water-soluble organic component, the OA also contain water-insoluble organic matter, which is often neglected in most field studies and, therefore, left under-characterized. The chemical composition, sources, and behavior of this aerosol organic fraction that is not extractable with ultrapure water is emerging as an important research topic when assessing the environmental and health impacts of OA as a whole. This organic fraction can comprise up to 90% of aerosol OC [39–41], and it has been indicated to represent local fresh emissions, containing most of the primary fossil material emitted through human activity [40–42]. The available studies rely on the use of high-resolution

mass spectrometry (HR-MS) analysis with electrospray ionization (ESI) and, therefore, they have used organic solvents (e.g., methanol, acetonitrile, or pyridine) for extracting the water-insoluble organic species from laboratory generated secondary OA, (SOA) [43,44], and ambient rural aerosol samples [41]. In the field aerosol samples, pyridine extracted a less polar and more aliphatic fraction of the OA compared to water or acetonitrile, which extracted chemically similar organic matter components [41]. These preliminary studies suggest that the organic solvent-extractable OA fractions could have molecular characteristics distinct from their water-soluble counterparts. Nevertheless, it must be emphasized that the water- and organic solvent-extracted OC fractions were not sequentially obtained, which means that solvents exhibiting different polarities than water (e.g., methanol and acetonitrile) could still extract similar organic matter components. Anyhow, the questions of the chemical composition and origin of this non-ultrapure water-extractable OA are also far from being resolved.

Based on its own definition, the aerosol organic fraction which is not readily soluble in ultrapure water is expected to have a more hydrophobic character than its water-soluble counterpart. As such, one could presume that this organic fraction can be dissolved in a medium other than an organic solvent. The use of an alkaline medium (e.g., 0.1 M sodium hydroxide, NaOH) following a first ultra-pure water extraction step, could be a good alternative to investigate the less polar and more aliphatic OA fraction. Adopting this procedure, Feczko *et al.* [45] reported that the yearly average concentration of ASOM can account to up 14% of the aerosol OC in six different background European sites. Despite these results, the ASOM fraction still is a poorly understood fraction, which makes its structural characterization a new challenge for the atmospheric research community.

2.3. Advanced analytical techniques for characterization of OA

2.3.1. On-line vs off-line techniques

Nowadays, there is a wide range of methodologies that can be used to mitigate the complexity and, therefore, to characterize the structural and chemical composition of

atmospheric particles, namely its organic fraction. Ideally, the analysis of OA should provide, in a continuous way, a complete chemical analysis of the sample, and thus ensuring a continuous size and time resolution [46]. However, currently, there is no technique capable of providing this sort of information. Thus, analytical techniques can be broadly divided into two major groups, on-line and off-line. The on-line methodologies mainly ensure temporal resolution, while the off-line methodologies mainly ensure the chemical resolution.

On-line or *in situ* methodologies, allow an on-site analysis of the OA providing real-time or near-real-time information. When using these methodologies, the analysis is performed almost at the same time that the particles are sampled and with very fast acquisition rates; the measurements provide high temporal resolution of the samples without sampling artefacts [3,13]. In the past years, on-line aerosol mass spectrometry (AMS) analysis has become one of the techniques of choice for real-time field measurements of atmospheric aerosol, especially due to its high-sensitivity, universality, and robustness [3]. Several reviews have recently presented the benefits of these instrumental set-ups for OA assessment [3,47–50]. Furthermore, on-line particle-into-liquid samplers combined with TOC detectors and/or ion chromatography can be used to provide essential physicochemical information about fast changes in composition and concentration of the water-soluble fraction of atmospheric aerosols [51]. However, these on-line techniques provide limited information on specific compounds and less details on individual species when compared with the off-line assemblies [13,26,47] and, consequently, their use is still far from replacing the off-line techniques in the structural characterization of OA.

Off-line methodologies are usually based on highly complex spectroscopic systems that can be associated with some separation method, and they are used to provide detailed information on the chemical characteristics and functional groups assessment of the organic component of atmospheric particles collected by filter-based techniques [3,26]. Despite the high spectral resolution that these techniques can provide, and the truly insight into the several chemical features of the OA, these techniques have some drawbacks, namely the fact that these analytical techniques usually require large amounts of sample (particles collected from several days to weeks) resulting in low temporal resolution, which may also lead to some problems of sample representativeness [3]. Furthermore, the use of long sampling times increases the risk of the incidence of sampling artefacts during atmospheric aerosol

collection, which are translated by volatilization/condensation processes that may occur on the filter, or particles surface, for semi-volatile organics, as well as oxidation of filter deposited organics by strong oxidants, such as ozone.

2.3.2. Spectroscopic methods for studying OA

2.3.2.1. Sample preparation

For off-line studies of the organic fraction of atmospheric aerosols, it is necessary to use an extraction method capable of separating these organic components from the whole atmospheric particulate matter, thus making them more amenable to a structural inquiry by spectroscopic methods. Consequently, based on the chosen extraction procedure, the analytical technique employed will only characterize a subset of the organic compounds sampled on a filter. As mentioned in section 2.2.1, water can extract a high percentage of organic compounds and is currently the most used approach for the analysis of OA. However, one important concern before pursuing a spectroscopic study is to ensure that the WSOM is free from inorganic species (e.g., paramagnetic trace elements) that may interfere with the application of advanced analytical techniques (e.g., NMR). The application of a previous isolation procedure is thus a crucial step, and it must allow the recovery of an unbiased and uncontaminated fraction of WSOM from the original atmospheric sample.

Even for analytical methods that require the sample in the solid-state (e.g., solid-state NMR), the water-soluble fraction is the fraction normally considered for the analysis of the organic fraction, instead of the original particulate matter. While there may be advantages in analysing the organic fraction in the original sample without any pre-treatment, in practice due to the presence of many sources of interference (e.g., inorganic component), the low amount of the OA component (usually below 35% of the total mass), and the difficulty in extracting the sample in the solid state from the sampling filters, makes it very difficult (or nearly impossible) to withdraw structural information on the organic fraction from the original particulate matter [13,33]. Thus, for the analytical methodologies which require the sample in the solid state, the water-soluble fraction must be transformed to a solid by freezing or drying processes prior to analysis.

2.3.2.2. Application of NMR spectroscopy

NMR spectroscopy belongs to the set of off-line analytical techniques that provides a thorough knowledge resolution on the functional groups, and a detailed description and structural identification of the main substructures present in the OA. This technique has gradually become one of the most predominant tools in the study of OA, namely their water-soluble fraction [13,33]. However, the deep insightful on the sample complexity provided by this technique comes at a cost in terms of temporal resolution, since NMR techniques require large amounts of sample and, therefore, the sample to be analysed comes from several sampling hours or even days. Nowadays, the most widely used NMR based method in the analysis of aerosol WSOM is the one-dimensional (1D) solution-state ^{1}H NMR [37,52–57]. As reviewed by Duarte and Duarte [13], the potential of 1D solution-state ^{1}H NMR has already been exploited for the identification of functional groups, molecular modelling, and determination of source, seasonal and temporal characteristic profiles of the water-soluble fraction of the OA. However, a 1D solution-state ^{1}H NMR spectrum of the aerosol WSOM is often characterized by the presence of a strong overlapping of analytical signals. On this occurrence, it is only possible to identify some generic structural features thus making it not advisable to attempt the identification of specific molecular structures by 1D solution-state ^{1}H NMR techniques alone [33]. Furthermore, these techniques, exhibit a very low sensitivity for detecting functional groups that do not carry protons (e.g., substituted aromatic compounds), or containing groups with rapidly exchangeable protons (e.g., carboxyl and hydroxyl groups) [13].

One of the first examples of the application of 1D solution-state ^{1}H NMR to the study of OA, namely their water-soluble fraction, was conducted by Decesari *et al.* [52] to identify chemical features and evaluate the seasonal variation of fine aerosol WSOM. In this study, representative samples of a cycle of four annual seasons were analysed and the obtained spectra consisted mainly of very broad poorly resolved peaks, derived from the overlap of several individual minor contributions. Nevertheless, on the basis of the high density of sharp peaks superimposed to the unresolved signals located in well-defined spectral windows, the authors were able to assign four categories of functional groups carrying carbon-hydrogen bonds, namely: aliphatic protons in extended alkyl chains, located in the region between δ ^{1}H 0.5 and 1.9 ppm of the spectrum; protons bound to aliphatic carbon atoms adjacent to

unsaturated groups, such as alkenes, carbonyl, imino and aromatic groups, located in the region between δ ^{1}H 1.9 and 3.2 ppm of the spectrum; protons bound to oxygenated aliphatic carbons atoms, such as aliphatic alcohols, ethers, and esters, located in the region between δ ^{1}H 3.3 and 4.1 ppm of the spectrum; and aromatic protons located in the region between δ ^{1}H 6.5 and 8.3 ppm of the spectrum. By integrating the four spectral regions in each sample, Decesari *et al.* [52] pointed out that, despite the four samples have approximately the same functional groups, the relative proton abundance of these functional groups, changes from sample to sample, and consequently from season to season. As recently reviewed by Duarte and Duarte [33], the overall set of data provided by the quantitative integration of each spectral region from different studies that have used ^{1}H NMR analysis for the characterization of aerosol WSOM, have shown that in these samples the majority of the protons is confined in aliphatic structures, followed by oxygenated aliphatic compounds and unsaturated aliphatic groups, and only a small portion in aromatic structures. Another NMR based technique successfully applied in the last fifteen years, for investigating the distribution of carbon functional groups in water-soluble fraction of the OA, is the 1D solid-state cross-polarization with magic-angle spinning (CP-MAS) ^{13}C NMR spectroscopy [15,36,58–60]. This technique allows a semi-quantitative measure of the relative contribution of the different carbon functional groups to the OC present in the sample and, consequently, it can be used for investigating the composition and the structural variability of the water-soluble organic fraction with modifications in sampling parameters (e.g., aerosol sources, sampling sites, and meteorological conditions) [33]. Furthermore, although intuitively the analysis in solution-state of the WSOM could make more sense, in practice 1D solid-state CP-MAS ^{13}C NMR presents some advantages for the analysis of this fraction especially when compared to 1D solution-state ^{1}H NMR spectroscopy or even to 1D solution-state ^{13}C NMR spectroscopy. Some of these advantages have been recently reviewed by Duarte and Duarte [13,33] and include: the solid-state technique is a non-destructive method, allowing the sample to be used for further complementary structural analysis and a better comparison of results; this technique is not affected by the solvent which can cause changes in the chemical shifts of the sample, hide some sample chemical resonances by the solvent signals, or even loss of some peaks namely those of the carboxylic acids, due to the presence of rapidly exchangeable protons; and finally, the solution-state NMR spectra may present lower resolution and sensitivity due to the low solubility of some

organic components in the selected solvent. A major limitation of the 1D solid-state CP-MAS ^{13}C NMR techniques is the difficulty in obtaining high-quality NMR spectra due to the relative low carbon content of the OA samples. This fact requires the need for combining several samples collected under similar ambient conditions in order to obtain sufficient sample mass for analysis (~ 20 – 100 mg of sample, depending on the size of the NMR probe) [13,33]. It must be emphasized, however, that under this circumstances the acquisition of a high-quality ^{13}C NMR spectrum is made at the expense of pursuing studies on near real-time variations of the chemical composition of OA. Nevertheless, this technique can be used for assessing the seasonal variability of OA, as performed by Duarte *et al.* [15] in atmospheric aerosols collected at a rural-coastal location with high agricultural activity. In this study, the typical CP-MAS ^{13}C NMR spectra are very broad with overlapping peaks, mainly located in four regions corresponding to four major carbon functional groups, namely: unsubstituted saturated aliphatic carbons located in the δ ^{13}C 0 – 50 ppm spectral region; aliphatic carbons singly bonded to one oxygen or nitrogen atom, located in the δ ^{13}C 60 – 95 ppm spectral region; aromatic and unsaturated carbons located in the δ ^{13}C 110 – 160 ppm region; and carboxyl, ester and amide carbons located in the δ ^{13}C 160 – 190 ppm region. The remaining ^{13}C resonances (corresponding to 4 – 15% of the total NMR peak area, depending on the season) can be explained by minor peaks from other functional groups such as: carbons of methyl groups of methyl ethers, located in the region between δ ^{13}C 50 – 60 ppm of the spectrum; aliphatic carbons bonded to two oxygen atoms, such as anomeric carbons of polysaccharides, located in the region between δ ^{13}C 95 – 110 ppm of the spectrum; aromatic carbons bonded to one oxygen atom, located in the region between δ ^{13}C 140 – 160 ppm of the spectrum; and carbonyl carbons of aldehydes and ketones, located in the region between δ ^{13}C 190 – 230 ppm of the spectrum. Although the spectra from the different seasons present the same main carbon functional groups, their relative abundances are quite different. These differences can be easily observed in Figure 2.1, which compares the relative abundance of the main carbon functional groups obtained by Duarte *et al.* [15] for WSOM from atmospheric aerosols collected in a rural-coastal location in the winter (Figure 2.1a) and in the summer (Figure 2.1b). These two graphs clearly show the differences in composition of OA in two seasons, with the summer sample being more enriched in aliphatic structures (61.6% of total NMR peak area) than the winter sample (40.5% of total NMR peak area), whereas the latter has a higher percentage of aromatic structures (15.3%

of total NMR peak area) likely derived from wood burning processes during the colder period [15]. Sannigrahi *et al.* [36] also conducted a CP-MAS ^{13}C NMR study of the WSOM from atmospheric aerosols collected in a urban location (Atlanta, USA) in summer. The results of this study indicate the presence of the same carbon functional groups as those present in the rural-coastal location, and their relative abundances (shown in Figure 2.1c) are also very close to those obtained in the same season in the rural-coastal location. Overall, the results obtained by Duarte *et al.* [15] and Sannigrahi *et al.* [36] provide clear evidence that the WSOM from atmospheric aerosols is mostly aliphatic (41 – 62% of total NMR peak area), followed by oxygenated aliphatics (18 – 22%) and carboxylic acid (8.3 – 9.5%) functional groups.

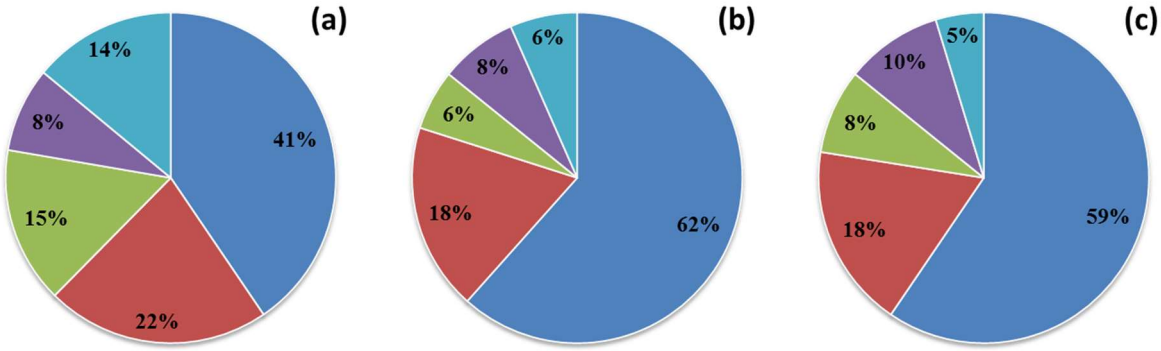

Figure 2.1. Percentage distribution of the main carbon functional groups (■ aliphatics, ■ oxygenated aliphatics, ■ aromatics; ■ carbocyclic acids; and ■ other ^{13}C resonances) for WSOM from atmospheric aerosols collected in rural-coastal location with high agricultural activity in the (a) winter and (b) summer, and (c) for WSOM from atmospheric aerosols collected in a urban location in summer, based on the data collected by Duarte *et al.* [15] and Sannigrahi *et al.* [36].

Despite the advantages of solid-state NMR over the solution-state NMR, no other nuclei, except the ^{13}C, was yet used for the analysis of the WSOM from atmospheric aerosols. This fact appears to play opposite with the requisite of studying other species present in the OA, such as nitrogen-containing organic species. In this later case, although it is possible to use ^{15}N as a nucleus, the CP-MAS ^{15}N NMR spectroscopy show a sensitivity 50 times lower than that of the CP-MAS ^{13}C NMR spectroscopy [33]. One strategy that could be forwarded to overcome this problem may be based on the recent developments made in the advanced spectral editing techniques for solid-state NMR, namely the ^{13}C–{^{14}N} Saturation pulse induced dipolar exchange with recoupling (SPIDER) spectral editing approach. These techniques provide deeper insights into the molecular connectivity and

functional groups, including those containing nitrogen, which are usually hidden in solid-state CP-MAS ^{13}C NMR data [33]. However, the absence of "know-how" in the use of these solid-state NMR spectral editing techniques (e.g., selecting the correct pulse sequence, handling and interpretation of the data), remain one of the major limitations to its application to the study of the OA [33].

A set of NMR-based methodologies that are emerging for the analysis of OA, are the two-dimensional (2D) solution-state NMR techniques [16,61–63]. These techniques have proven to be very useful to solve the spectral information overlaid in 1D NMR spectra, by separating the data into a second frequency dimension. The combinations of the data from some of these 2D solution-state NMR techniques, namely $^{1}H–^{1}H$ homonuclear (COSY and Total Correlation Spectroscopy (TOCSY)) and $^{1}H–^{13}C$ heteronuclear (HSQC and HMBC) connectivity, improve the spectral resolution and provide a deeper insight into the C–H backbone of the organic compounds from the atmospheric aerosols [33]. Despite the fact that the use of solution-state 2D NMR techniques to OA analysis is still very limited, the existing studies [16,61] have demonstrated the potential of these high-resolution NMR techniques for a comprehensive description of the substructures present in OA, as well as to identifying molecular fingerprints of the different aerosol sources and formation mechanisms. However, one of the most important drawbacks of these techniques is the required time for signal acquisition, which can reach several days, thus limiting its application, at least on a routine basis. Nevertheless, as already shown by Duarte and Duarte [13,33], the keys to develop an accurately knowledge about the OA lies on the development of analytical procedures taking advantage of the synergistic application of all of the aforementioned techniques (i.e., 1D solid-state NMR, 1D solution-state NMR, and 2D solution-state NMR), as well as its association with other advanced analytical techniques, namely the HR-MS. Furthermore, due to the inherent complexity of the OA fraction, the application of a chromatographic separation procedure prior to NMR analysis can directly provide major advances in the knowledge gained from the sample. Although chromatographic systems hyphenated with NMR (i.e., 1D solution-state ^{1}H NMR) are already applied for the characterization of extremely complex environmental samples, namely NOM from aquatic environments [64,65], to the best of my knowledge, these have not been used for reducing the heterogeneity of the OA. Furthermore, taking into account the results of the recently developed method for resolving the chemical heterogeneity of

NOM, based on a LC×LC system [66], the development of protocols based on those two analytical techniques may provide valuable clues for unfolding the complexity of OA.

2.3.2.3. Application of mass spectrometry

Over the last decade, there has been a rapidly development of mass spectrometry (MS) techniques and an increase in their application to atmospheric aerosols studies, especially for the molecular identification of its organic components [46]. As already mentioned (section 2.3.1), many of these developments were applied in on-line analyses of ambient aerosols. However, in this chapter, the focus will be placed in the off-line MS techniques, which allow a detailed characterization of OA, whilst providing little temporal resolution. Off-line MS methodologies, especially when associated with chromatographic separation procedures, allow a high selectivity and molecular discrimination of the compounds constituents of OA [46]. This hyphenated technique has been widely used in target analysis aiming at a quantitative identification of specific organic compounds and chemical markers for aerosols source apportionment [46], and the most widely used methodology for the chemical characterization of OA compounds is GC–MS [46]. This powerful, sensitive and selective hyphenated assemblage allows the separation, identification, and quantification of specific organic species within atmospheric aerosols. Several studies using GC–MS for molecular identification and quantification of target compounds from OA have recently been reviewed [13,22,46,48], and the main classes of compounds included aliphatic acids, aromatic compounds, amino acids, multifunctional oxygenated compounds, polyols, sugars, nitrogenated compounds, and polycyclic aromatic hydrocarbons. However, this methodology usually requires time-consuming derivatization procedures, especially for the analysis of highly polar and less volatile compounds [13]. Liquid chromatography coupled to mass spectrometry (LC–MS) has become in recent years a real alternative to GC–MS for the analysis of individual compounds in OA. Although it is less quantitative, this technique is especially suited for the analysis of high-molecular-mass, thermally unstable and/or very polar molecules without derivatization [48,67]. The most recent examples of application of LC–MS to molecular identification and quantification of target compounds from OA have also been recently reviewed [13,22,46,48]. The main classes of compounds studied using this technique include aliphatic, alicyclic and aromatic carboxylic acids, organosulfates, carbohydrate-like substances, and amino acids and other

organo-nitrogen compounds. However, the complexity of the OA can be an impediment for the use of these type of 1D methodologies (i.e., GC–MS and LC–MS) since the chromatograms obtained often exhibit several overlapping peaks and the majority of the compounds are either very poorly resolved or not resolved at all [67]. One possible way to deal with this problem is to increase the chromatographic resolution by including a second chromatographic dimension, as in comprehensive multidimensional chromatographic systems. In this context, comprehensive 2D gas chromatography (GC×GC) coupled with time-of-flight mass spectrometer (TOF-MS) has been successfully applied to the study of ambient OA, resulting in the separation of more than 10,000 organic components (i.e., oxidized monoterpenes, acyclic alkanes, alkenes, ketones, aldehydes, alcohols, acids, and aromatics) from a urban and coniferous forest locations [68–70]. In the same way as in GC separations, the lack of chromatographic resolution of the LC–MS systems can be overcome using LC×LC. Despite its application being confined to only one study, the LC×LC system has already been coupled to ESI-TOF-MS to identifying and quantifying carboxylic acids in rural and urban aerosol samples [71]. These multidimensional separation techniques provide a characteristic separation pattern of a specific class of compounds together with their MS information, which can be quite useful for associating sample fingerprinting with the different parameters causing aerosols variability, such as the aerosol sources and the actual meteorological conditions [13].

In addition to the hyphenated techniques, there are other MS-based techniques that have also been used for acquiring detailed structural information on OA. An example of this application is the development of a methodology using matrix-assisted laser desorption/ionization (MALDI) TOF-MS for the analysis of biological aerosols, such as *E. coli* bacteria particles [72]. Nowadays, probably the most emerging systems based on MS for the analysis of OA are HR-MS, namely the Fourier Transform Ion Cyclotron Resonance (FT-ICR) MS, with soft ionization techniques (e.g., ESI, MALDI). In such analytical systems, the soft ionization provide intact molecular ions and the HR-MS can provide up to 25 billion theoretical plates of separation, which allows a rapid and definitive molecular mass determination of intact polar macromolecules that are difficult to analyse by the traditional hyphenated techniques [73]. As pointed by Wei *et al.* [73], these systems can achieve a separation efficiency performance more than 3 orders-of-magnitude larger that the state of the art advanced gas or liquid separation-based techniques. As recently reviewed

[13,46], the applications of these HR-MS techniques have increased, mainly aiming at the identification of the molecular elemental composition of thousands of individual organic components for further investigations on the influence of the aerosol sources on the composition of OA. It should also be mentioned that a detailed interpretation of the huge amount of MS data generated by these high resolution techniques requires data processing methods capable of handling all of this information. Furthermore, the compound molecular formula only allows an attempt to propose possible chemical structures, with the assistance of a spectral database or a reference. Thus, when such information is not available, it becomes highly recommendable to associate the information obtained from the HR-MS systems with that acquired by another "structural analysis" technique, namely the NMR spectroscopy [13,67].

2.3.2.4. Data processing and treatment

Regardless of the sophistication and high-resolution analytical techniques used, the quality of the results is always dependent on the capacity to extract useful information from the produced data. However, the processing and treatment of the data acquired by many of the techniques presented in this chapter is not a trivial task. Some of these techniques can provide information regarding hundreds or even thousands of different compounds, which may cause a severe overlap of the different analytical signals obtained from a complex sample. In addition, the data produced by these techniques, especially when combined with chromatographic techniques, may easily exceed more than three or four analytical dimensions. Nowadays, one of the biggest limitations to a larger application of these advanced instrumental techniques is the lack of knowledge and analytical expertise for interpreting the huge and complex data sets produced [13]. The lack of knowledge to deal with these data, associated with the chemical complexity of OA, has limited the study of this fraction to the identification of some target components, the identification of some functional chemical groups, and the determination of source and temporal characteristic patterns. In this sense, almost all applications of chemometric tools in the study of ambient aerosols has been focused on the extraction, from the acquired data, of different patterns that may be associated with source profiles and source contributions; the so-called source apportionment methodologies. As recently reviewed by Alier *et al.* [74], there are several source apportionment methodologies already in use, namely the chemical mass balance (CMB) and

some multivariate factor analysis methodologies, such as principal component analysis (PCA), positive matrix factorization (PMF), and multivariate curve resolution-alternating least squares (MCR-ALS). The CMB model uses compounds associated with specific sources as references (e.g., levoglucosan as a tracer of biomass burning) in order to attempt to identify the contribution of that particular source. Consequently, this methodology is mainly limited to the study of well-known emission source profiles [74,75]. On the other hand, multivariate factor analysis methodologies allow identifying profiles, based on numerical factors, from experimental data. These factors, although not corresponding to a particular spectrum of a pure chemical compound, may be related to emission sources and/or functional chemical groups. As pointed out by Alier *et al.* [74], the MCR-ALS and PMF provide similar results, whereas the PCA methodology produces profiles with the weakest physical meaning. As an example of the application of these methods to the study of OA is the recent work presented by Paglione *et al.* [57], in which MCR-ALS was applied to ^{1}H NMR data from WSOM from atmospheric aerosols. According to this work, a total of 5 factors were able to be identified: two factors were associated with chemical tracers (e.g., methane-sulphonic acids and low-molecular weight (M_w) amines); other two factors were associated with "aged" components (one of which was also associated with aged biomass burning particles); and the fifth factor was associated with primary wood burning particles and showed a chemical composition dominated by anhydrosugars, other polyols and phenolic compounds [57]. This study also showed a concordance of these factors with the results provided by PMF analysis of the AMS data [57]. The combination of this powerful mathematical algorithms with the aerosol data provided by the diverse high-resolution off-line and on-line analytical techniques has an enormous potential for the identification of the main chemical structures present in OA, as well as their quantification and source apportionment. Yet, its implementation still is in its embryonic stage.

Chapter 3

Sampling campaigns and experimental procedures

This chapter provides information regarding the aerosol sampling campaigns, including methods and equipment used, as well as location, duration, and acquired meteorological data. Information regarding the methods of extraction is also provided, namely for the extraction of the water and alkaline soluble organic matter.

3.1. Aerosol sampling

Under the research programme of two urban aerosol projects (*ORGANOSOL* and *CN-linkAIR*), high-volume aerosol samples were collected at the city of Aveiro (40º37′44′′N, 08º39′22′′W), Portugal, on a weekly basis (7 days in continuum) in order to collect enough material for subsequent structural characterization. The aerosol samples were collected on pre-fired (at 500 °C) quartz fibre filters (20.3 × 25.4 cm; Whatman QM-A) with an airflow rate of 1.13 m^3 min^{-1}. The high-volume sampler (model TE-6070V, Tisch Environmental, Inc.), shown in Figure 3.1a, and schematized in Figure 3.1b, was provided with a pre-separator for excluding particles larger than 2.5 µm. This cut-off size was accomplished using a PM_{10} inlet (model TE-6001, Tisch Environmental, Inc., Figure 3.1c) and a $PM_{2.5}$ single-stage impactor (model TE-231, Tisch Environmental, Inc., Figure 3.1d). The total mass of $PM_{2.5}$ samples was determined by weighing the filter under ambient temperature and controlled moisture (relative humidity of ≈ 50%) conditions before and after sampling. The filters were then wrapped up in aluminium foil and stored frozen until further analysis.

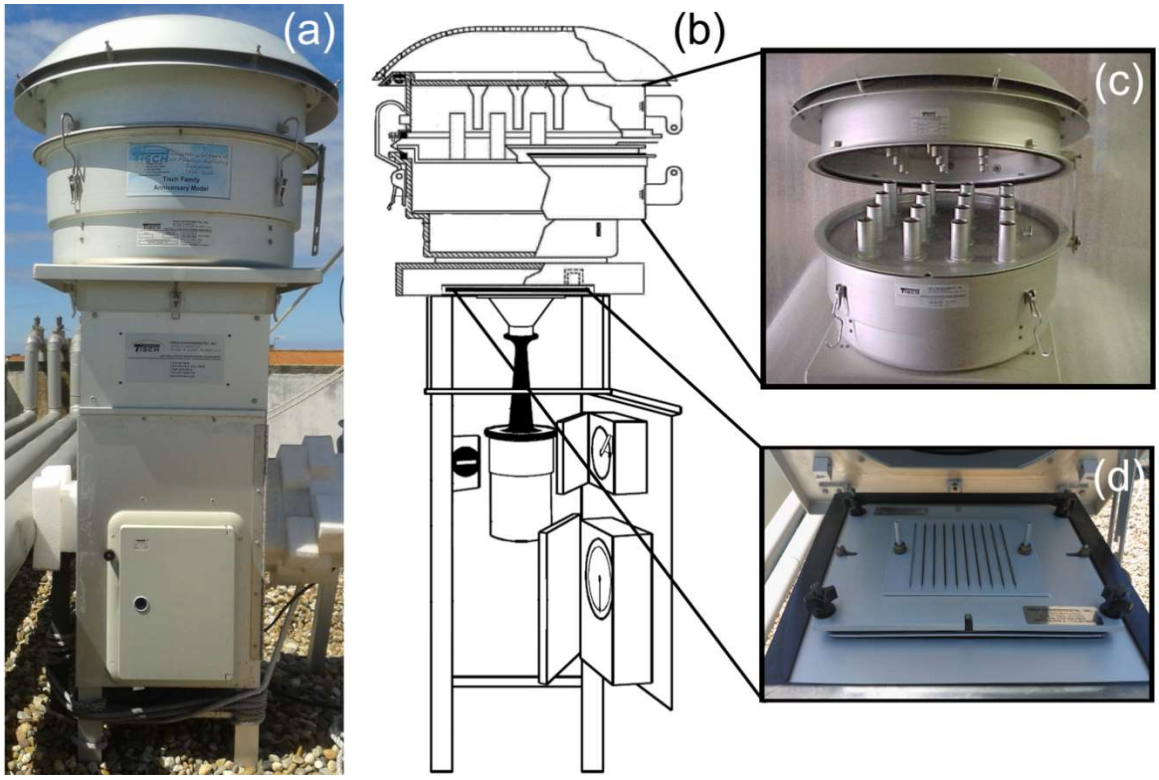

Figure 3.1 (a) Photo and (b) schematic of the high-volume sampler with the enlarged photo of the (c) selective PM_{10} inlet, and (d) $PM_{2.5}$ single-stage impactor.

3.2. Description of the sampling campaigns

The aerosol samples were collected during intensive field campaign, which began in November of 2009 and ended in July 2014. This sampling period was divided in 3 sampling campaigns: a) 37 samples are collected from November 2009 to March 2011 in Sampling campaign I; b) 23 samples are collected from January 2013 to December 2013 in sampling campaign II; and c) 20 samples are collected from January 2014 to July 2014 in sampling campaign III. In annexed Table A. 1 is provided all the detailed information regarding the sampling dates for each sampling campaign.

Throughout this intensive sampling period, no attempts were made to control any adsorption/desorption phenomena on the filter. Consequently, some volatilisation/ condensation processes may have occurred on the filter, or particles surface, for semi-volatile organics. Also, oxidation of filter deposited organics by strong oxidants (e.g., ozone) may have occurred during aerosol collection. Therefore, in a similar fashion to what has been considered in previous works (e.g., Duarte *et al.* [15]), the measured concentrations for oxygenated organic species, water-soluble OC (WSOC) in particular, should be considered an upper limit of the true atmospheric levels. Nevertheless, preliminary aerosol sampling campaigns, carried out by Freire [76], using the tandem filter method (i.e., sets of two (front and back) quartz fibre filters directly on top of each other), were carried out in order to study the occurrence of volatilization and/or adsorption phenomena during aerosol collection and, simultaneously, deduce on the relative importance of secondary formation processes to the fluorescent features of urban aerosol WSOM. In this work, a total of 12 filter pairs were collected (also on a weekly basis) during a warmer period, encompassing the periods of the Sum. 2008, Spr. 2009, and Sum. 2009.

3.3. Extraction of WSOM and ASOM from aerosol samples

Each collected filter was firstly extracted with 150 mL of ultra-pure water (18 MΩ cm) by mechanical stirring during 5 min plus ultrasonic bath during 15 min. The final slurry obtained after stirring was filtered through a hydrophilic polyvinylidene fluoride (PVDF)

membrane filter (Durapore®, Millipore, Cork, Ireland) of 0.22 μm pore size. For the ASOM extraction, each slurry residue obtained from the previous WSOM extraction was soaked in 100 mL of NaOH 0.1 M (Fisher Scientific, Loughborough, UK) under an inert atmosphere (N_2). Then, each residue mixture was placed in an ultrasonic bath for 10 min, acidified with HCl 12 M (Riedel-de Haën, Seelze, Germany) to pH 3.0, and filtered through a PVDF membrane filter of 0.22 μm pore size.

3.4. Grouping the aerosol samples

To ensure enough mass for the subsequent structural analysis, the extracts need to be batched together according to similar ambient conditions, namely, air temperature (Figure 3.2), relative humidity (Figure 3.3), precipitation (Figure 3.4), wind direction and velocity (Figure 3.5), and the origin of the air masses (Table 3.1), in groups of three to five samples representative of the different seasonal periods (i.e., Aut. 2009, Spr. 2010, Sum. 2010, Aut. 2010, Win. 2010, Spr. 2011, Win. 2013, Spr. 2013, Sum. 2013, Aut. 2013, Win. 2014, Spr. 2014, and Sum. 2014). However, since there was variation in atmospheric conditions, in some of these seasons, namely in Spr. 2010, Aut. 2010, Aut. 2013, and Spr. 2014, these seasons were further divided into, Spr. A 2010, Spr. B 2010, and Spr. C 2010; Aut. A 2010, and Aut. B 2010; Aut. A 2013 and Aut. B 2013; and Spr. A 2014, Spr. B 2014, and Spr. C 2014, respectively. The Spr. 2010 season was divided mainly due to the variations on the air temperature, with median values of 12.6, 15.4, and 19.0 ºC (Figure 3.2) for Spr. A 2010, Spr. B 2010, and Spr. C 2010, respectively. Additionally, Spr. B 2010 samples were collected during the volcanic eruptions that occurred in Iceland during that sampling period [76]. In the case of Aut. 2010, the split has been made due to the median value of air temperature, which was much higher in Aut. A 2010 (17 ºC) than in Aut. B 2010 (12.5 ºC, Figure 3.2), and the highest value of total precipitation recorded during the sampling days of Aut. B 2010, compared with the days of Aut. A 2010 (Figure 3.4). In the case of Aut. 2013, the split has been carried out due to the differences in the median value of air temperature between Aut. A 2013 (18.4 ºC) and Aut. B 2013 (10.2 ºC, Figure 3.2), the highest value of total precipitation registered in Aut. A 2013, whilst no precipitation has been recorded in Aut. B

2013 (Figure 3.4), and in Aut. A 2013, the air masses over the urban site mainly originated from the maritime surroundings, whereas in Aut. B 2013, the air masses mainly originated from the continent surroundings by the northeasterly winds, as shown in Figure 3.5 and Table 3.1. In the case of Spr. 2014 season, the split was justified by the differences in the median value of air temperature during Spr. A (13.1 ºC) compared to those recorded during Spr. B and Spr. C (15.5 and 16.5 ºC, respectively) (Figure 3.2), and the differences in the total precipitation accumulated in Spr. A (30 mm) compared to those registered during Spr. B (44 mm) and Spr. C (79 mm) (Figure 3.4).

The Sum. 2010 and Sum 2013 seasons, were also divided into Sum. A 2010, Sum. B 2010 and Sum. A 2013, Sum. B 2013, respectively. In these cases, the samples were divided due to the high number of forest fires which took place during the second period (B) of these summer sampling seasons. Table 3.1 shows which samples were batched together for the representativeness of each season from each sampling campaign.

Table 3.1 Summarized information regarding the samples batched together for each sampling campaign.

Sampling campaign	Season	Samples	Sampling Date	Origin of Air Masses[(a)]
I	Aut. 2009	s01 to s04	23 Nov. 2010 – 21 Dec. 2009	Maritime
	Spr. A 2010	s05 to s07	08 Mar. 2010 – 13 Apr. 2010	Maritime/Continental
	Spr. B 2010	s08 to s11	20 Apr. 2010 – 18 May 2010	Maritime/Continental
	Spr. C 2010	s12 to s14	18 May 2010 – 22 Jun. 2010	Maritime/Continental
	Sum. A 2010	s15 to s18	22 Jun. 2010 – 26 Jul. 2010	Maritime/Continental
	Sum. B 2010	s19 to s21	26 Jul. 2010 – 16 Aug. 2010	Maritime/Continental
	Aut. A 2010	s22 to s24	20 Sep. 2010 – 11 Oct. 2010	Maritime
	Aut. B 2010	s25 to s29	02 Nov. 2010 – 07 Dec. 2010	Maritime/Continental
	Win. 2010	s30 to s33	27 Dec. 2010 – 01 Feb. 2011	Continental
	Spr. 2011	s34 to s37	01 Mar. 2011 – 29 Mar. 2011	Maritime/Continental
II	Win. 2013	s01 to s04	30 Jan. 2013 – 27 Feb. 2013	Maritime/Continental
	Spr. 2013	s05 to s08	05 Apr. 2013 – 03 May 2013	Maritime/Continental
	Sum. A 2013	s09 to s12	01 Jul. 2013 – 02 Aug. 2013	Maritime/Continental
	Sum. B 2013	s13 to s15	02 Sep. 2013 – 23 Sep. 2013	Continental
	Aut. A 2013	s16 to s19	30 Sep. 2013 – 28 Oct. 2013	Maritime
	Aut. B 2013	s20 to s23	11 Nov. 2013 – 09 Dec. 2013	Continental
III	Win. 2014	s01 to s04	08 Jan. 2014 – 05 Feb. 2014	Maritime
	Spr. A 2014	s05 to s08	19 Feb. 2014 – 19 Mar. 2014	Maritime/Continental
	Spr. B 2014	s09 to s12	03 Apr. 2014 – 01 May 2014	Maritime/Continental
	Spr. C 2014	s13 to s16	19 May 2014 – 16 Jun. 2014	Maritime/Continental
	Sum. 2014	S17 to s20	30 Jun. 2014 – 28 Jul. 2014	Maritime/Continental

[(a)] Origin of air masses during each season, based on air mass back trajectories assessed by means of the the HYbrid Single Particle Lagrangian Integrated Trajectory (HYSPLIT) model (24 h interval, 7 days), using the Global Data Assimilation System (GDAS) meteorological database, and accessed via National Oceanic and Atmospheric Administration (NOAA) Air Resources Laboratory READY website [77,78].

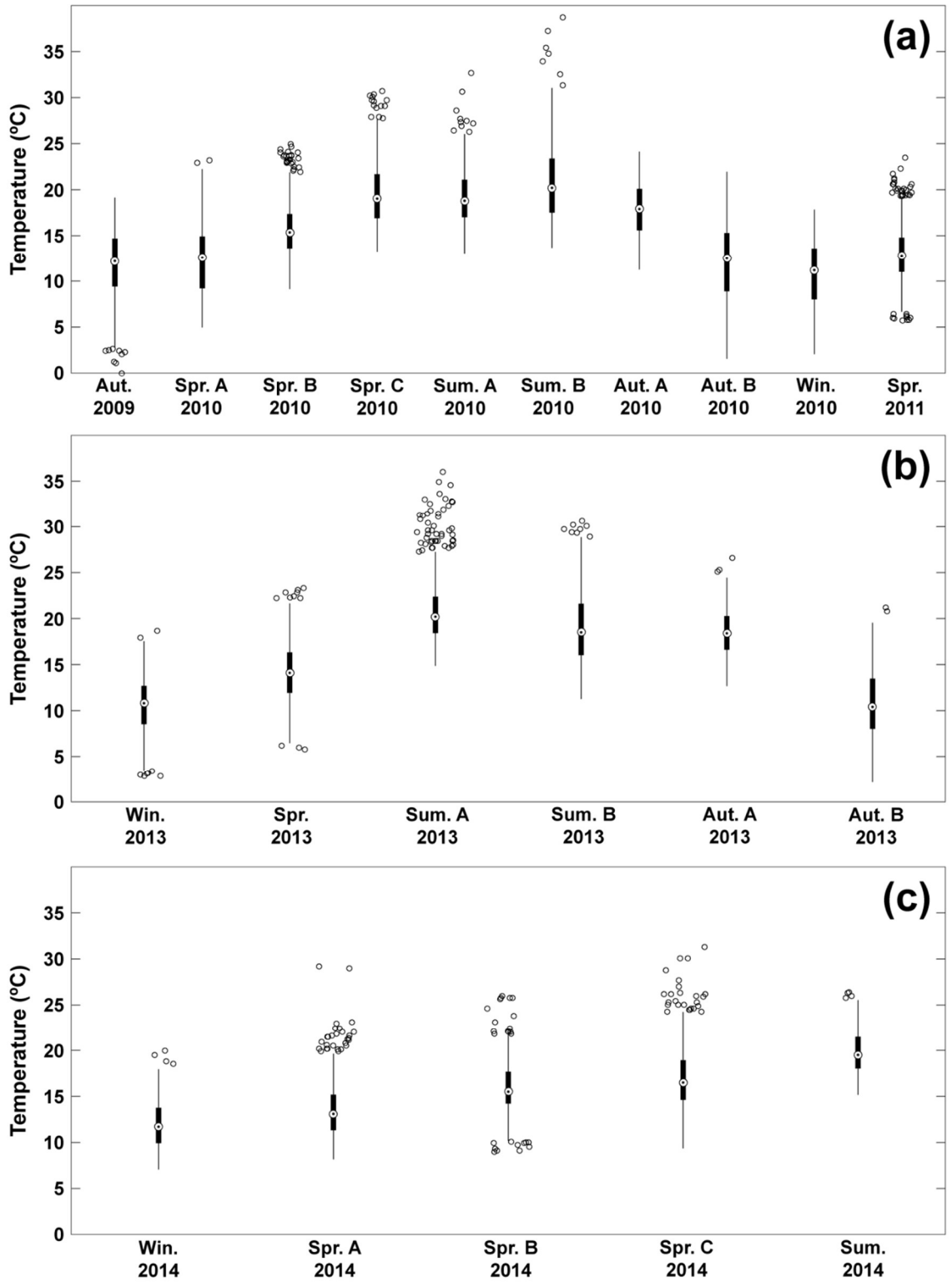

Figure 3.2 Variability of the air temperature recorded on an hourly basis for each season described in Table 3.1, during (a) Sampling campaign I, (b) Sampling campaign II, and (c) Sampling campaign III (meteorological data provided by the Portuguese Sea and Atmosphere Institute and by the Department of Physics of the University of Aveiro).

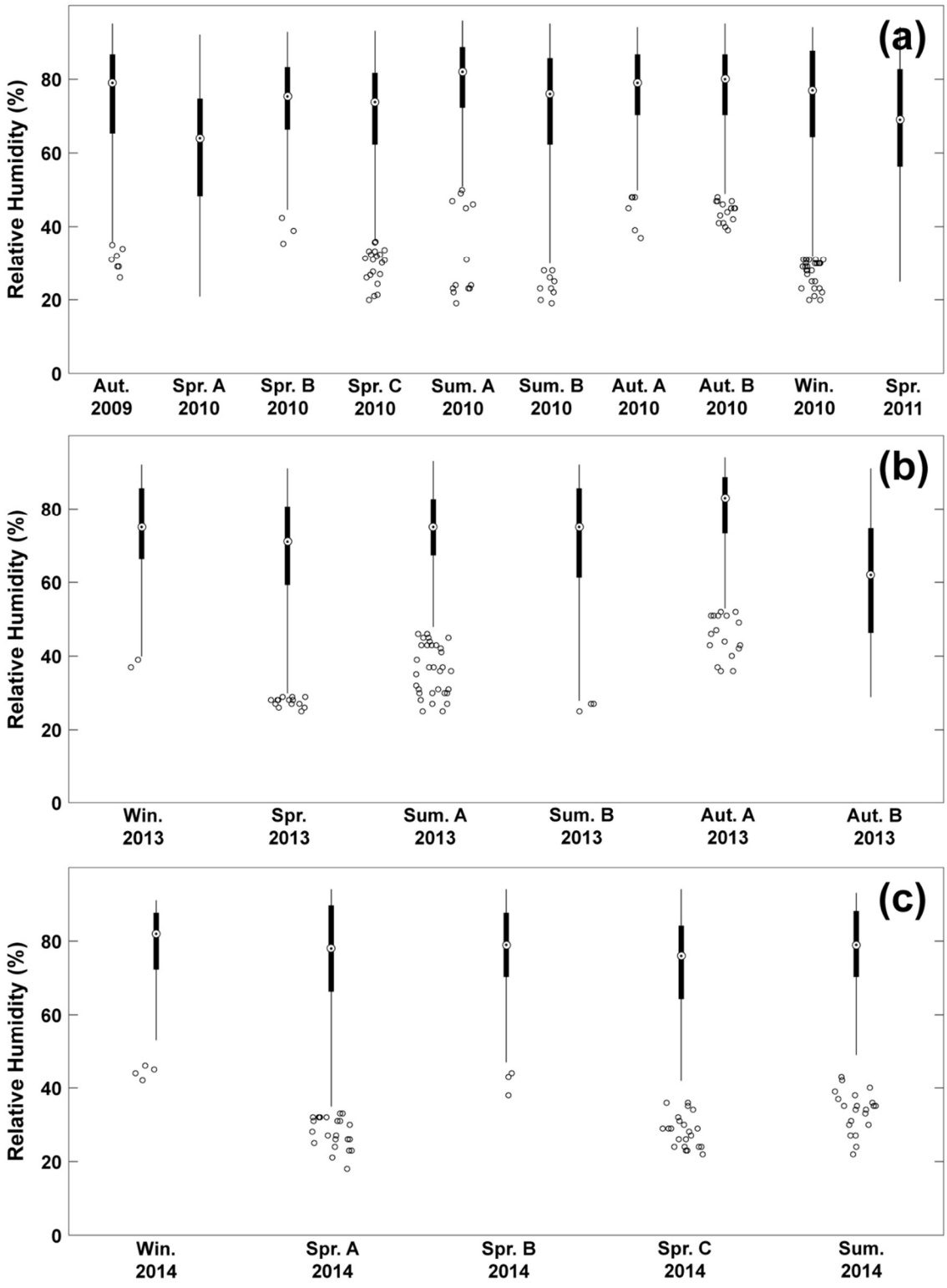

Figure 3.3 Relative humidity recorded on an hourly basis for each season described in Table 3.1, during (a) Sampling campaign I, (b) Sampling campaign II, and (c) Sampling campaign III (meteorological data provided by the Portuguese Sea and Atmosphere Institute and by the Department of Physics of the University of Aveiro).

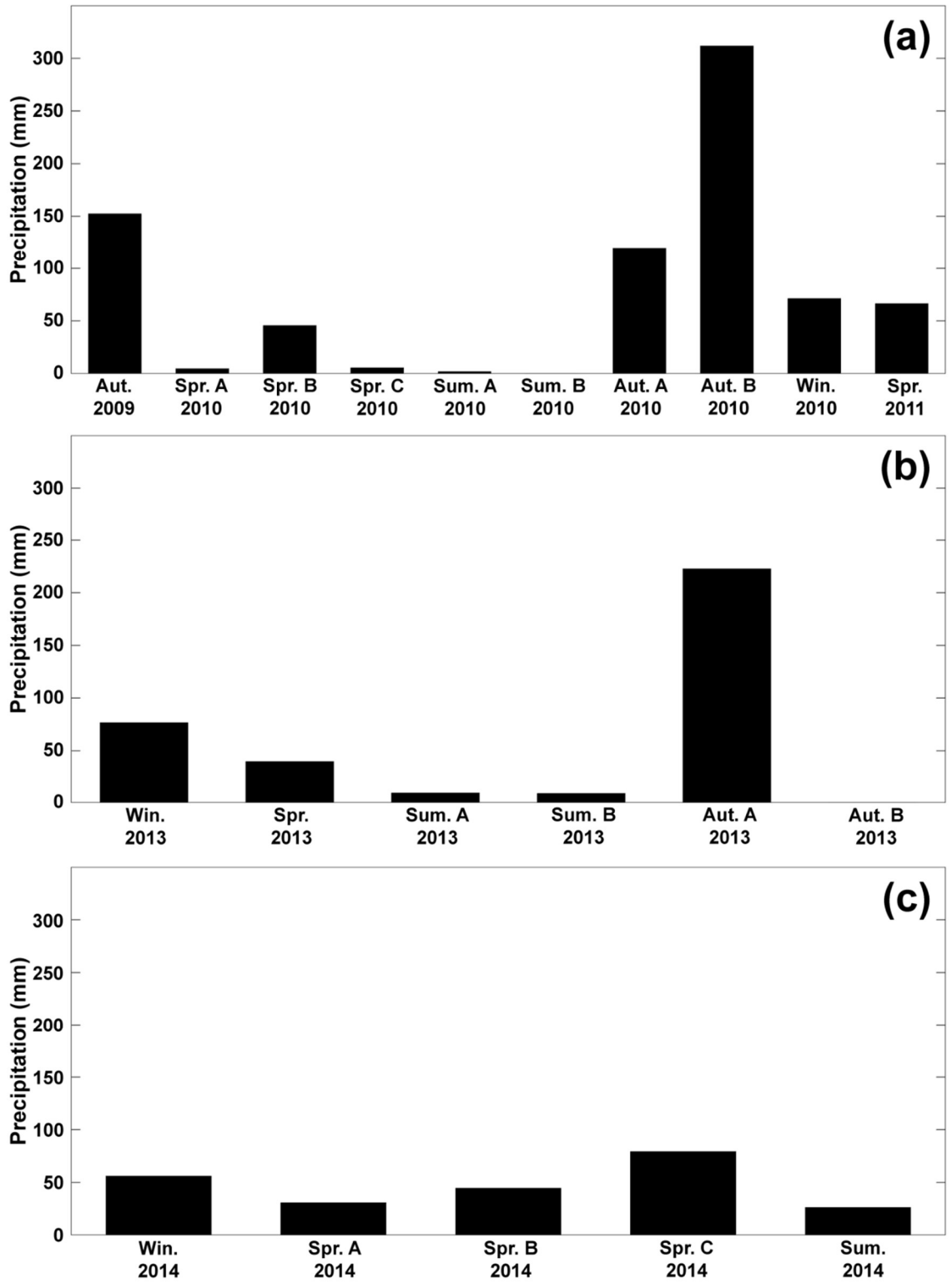

Figure 3.4 Total of precipitation recorded on an hourly basis for each season described in Table 3.1, during (a) Sampling campaign I, (b) Sampling campaign II, and (c) Sampling campaign III (meteorological data provided by the Portuguese Sea and Atmosphere Institute and by the Department of Physics of the University of Aveiro).

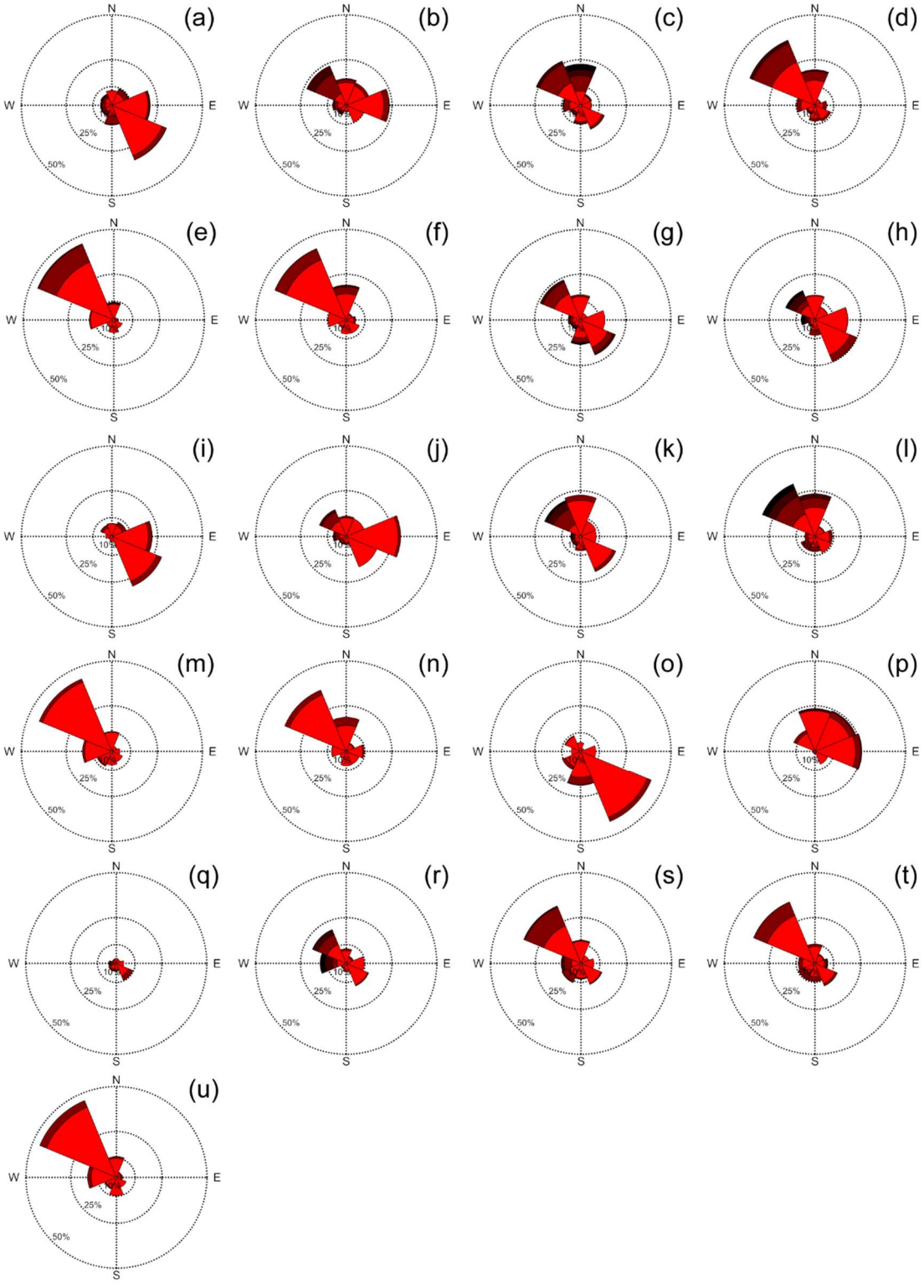

Figure 3.5 Wind rose plot showing the wind speed (■ 0 – 4, ■ 4 – 6, ■ 6 – 8, and ■ 6 – 8 m/s) and direction for (a) Aut. 2009, (b) Spr. A 2010, (c) Spr. B 2010, (d) Spr. C 2010, (e) Sum. A 2010, (f) Sum. B 2010, (g) Aut. A 2010, (h) Aut. B 2010, (i) Win. 2010, and (j) Spr. 2011 samples from sampling campaign I, (k) Win. 2013, (l) Spr. 2013, (m) Sum. A 2013, (n) Sum. B 2013, (o) Aut. A 2013, and (p) Aut. B 2013 samples from sampling campaign II, and (q) Win. 2014, (r) Spr. A 2014, (s) Spr. B 2014, (t) Spr. C 2014, and (u) Sum. 2014 samples from sampling campaign III.

3.5. Isolation and fractionation of WSOM from aerosol samples

Each pooled WSOM sample was isolated/fractionated by adsorption onto a Supelite™DAX-8 resin, following a well-established analytical protocol [15,16]. Briefly, the aqueous extracts were acidified to pH 2.2 with 6 M HCl (Riedel-de Haën, Seelze, Germany) and then pumped onto a glass column (35 mL) containing the Supelite™DAX-8 resin at a flow rate of 0.8 mL min^{-1}. After this concentration stage, the organic matter adsorbed onto the resin was washed with one column volume of ultrapure water at the same flow rate to remove the inorganic species. Then, the organic matter retained in the resin was back eluted with a solution of methanol/ultrapure water in the proportion of 3:2. All eluates were evaporated almost to dryness (final volume < 1 mL) in a rotary evaporator, at 30 ºC, and then re-dissolved in ultrapure water. The highly conjugated compounds of the WSOM samples that are recovered from the Supelite™DAX-8 resin are referred to as "WSOM hydrophobic acids", whereas the most hydrophilic and of low molecular size compounds not retained by the resin are referred to as "WSOM hydrophilic acids".

3.6. Determination of the carbon content in aerosol samples

3.6.1. Determination of OC and EC content in the aerosol samples

The determination of OC and EC contents in the aerosol samples was performed at the Portuguese Agency of Environment, using a Lab OC-EC Aerosol Analyzer (Sunset Laboratory Inc.) following a thermo-optical method as described by Birch and Cary [79]. As with other procedures (thermal and thermo-optical) applied into the analysis of OC and EC in aerosol samples, the contents of OC and EC are operationally defined. Briefly, in a O_2-free He atmosphere, a small portion (1.5 cm^2) of the quartz fibre filter is heated in four increasing temperature steps (60 sec at 315 ºC, 60 sec at 475 ºC, 60 sec at 615 ºC, and 90 sec at 870 ºC) to remove all OC from the filter. During this first stage of analysis, a fraction of OC is pyrolytically converted to EC, called pyrolytic carbon (PC). This pyrolytic conversion is continuously monitored by measuring the transmission of a laser beam through the filter. As the organic compounds are vaporized, they are immediately oxidized to CO_2 in an oven under an O_2 rich flux of He. The CO_2 containing flow of He is then reduced to CH_4, which

is then detected and measured by a flame ionization detector (FID). At the end of the fourth step of the temperature program, the oven is cooled to 550 ºC (50 sec). After this step, the flow of He is switched to a 2% O_2/He mixture in the sample oven and the temperature is stepped up to 940 °C. During this second stage of analysis, both the original EC and the PC are oxidized to CO_2 due to the presence of O_2 in the carrier gas. As previously, the CO_2 is then reduced to CH_4 and detected by the FID. The darkness of the filter is continuously monitored throughout all stages of the analysis. Finally, after all carbon has been oxidized from the sample, a known volume and concentration of CH_4 is injected into the sample oven in order to calibrate each measurement to a known quantity of carbon. This also provides a means of checking the operation of the instrument. Based on the FID response and laser transmission data, the quantities of OC and EC are calculated for each sample.

3.6.2. Determination of dissolved OC content in the WSOM and ASOM

The dissolved OC (DOC) content of each aqueous and alkaline extract of the aerosol samples was measured by means of a Shimadzu (Kyoto, Japan) TOC-5000A analyser, using the non-purgeable OC (NPOC) method. Briefly, the procedure starts by acidifying 10 mL of each standard/sample with 6 μL of 6 M HCl (pH < 3.0) immediately before sparging with ultra-high purity air for 2 min. Then, each standard/sample was injected (25 μL) into the TC furnace of the analyser, where it was catalytically oxidized to CO_2 according to the principles of the NPOC method. For NPOC quantification, standards were prepared from reagent grade potassium hydrogen phthalate in ultrapure water in the range of 0 to 1 mgC L^{-1}. For each sample, five determinations of NPOC were considered and only the mean values of areas with standard deviation less than 200 (peak area count) and/or a variation coefficient less than 2% were considered as acceptable.

Chapter 4

Tracing of aerosol sources using chemical characterization

This chapter aims at performing a comprehensive assessment of carbonaceous species (OC, WSOC, and EC) and major water-soluble inorganic ions (SO_4^{2-}, NO_3^-, NH_4^+, chloride (Cl^-) potassium (K^+), and sodium (Na^+)) in $PM_{2.5}$ samples collected throughout the seasons, in order to infer the potential local and regional sources.

4.1. Introduction

Atmospheric aerosols are implicated as key drivers of regional and global climate variability, exerting also a strong impact on various biogeochemical processes and on human health (e.g., [2,14,80–82]. One of the most important attributes of aerosols for both climate and health impacts is the aerosol composition. Fine aerosol particles, $PM_{2.5,}$ have a heterogeneous chemical composition, which includes OC, EC, inorganic ions, crustal material, and trace metals [14]. The enrichment of fine particles in water-soluble components (both organic and inorganic) and their mixing state plays an important role in several atmospheric processes. For example, WSOC can change the hygroscopic nature of aerosol surfaces, leading to alterations in the cloud condensation nuclei activity of the particles [5,83], whereas its inorganic counterpart can determine not only the aerosol acidity, thus influencing acidic cloud and rain formation [84], but also impact the rate of several reactions occurring on the aerosol droplet [85]. Therefore, knowledge on the chemical properties of the aerosol particles is vital to explore its dynamics as well as its sources and formation mechanisms. Furthermore, targeting and controlling their chemical composition is also essential for climatic and epidemiological studies, whose results are critical to support and evaluate informed policies on atmospheric pollution reduction at regional and global levels [86–89].

Within the framework of various European aerosol research activities, different studies on the chemical characteristics of particulate matter have been reported for urban, suburban, rural and mountain areas in western, southern, and central Europe (e.g., [90–94]). Although some of these studies are based on large-scale monitoring surveys [95], they are also usually based on short sampling campaigns, and still report a large variability in $PM_{2.5}$ chemical characteristics (mainly, carbonaceous, SO_4^{2-}, NO_3^-, sea salt, and dust constituents). Pio *et al.* [93] reports a comprehensive study on the $PM_{2.5}$ compositions at rural and background sites in Europe, by focusing on the major fractions of $PM_{2.5}$ (inorganic ions, EC and OC, and its sub-fractions, WSOC and water-insoluble OC (WINSOC)) over a time span of 2 years. However, it has to be mentioned that one of the rural background sites studied by Pio *et al.* [93] is located approximately 6 km southeast from the urban area focused in this study. Since the rural background site is characterized by small-scale forests and agricultural fields (horticulture and maize growing), the emissions from these sources are not expected

to substantially contribute to the atmospheric load at the urban area, where the anthropogenic contribution derived from urban emissions is expected to be higher than in the rural background site. The authors [93] concluded that similar amounts of organic and inorganic matter are found in the nonurban European atmosphere (except in Azores, classified as marine background site). The authors also reported that most (50 – 80%) of OC is water-soluble, allowing them to suggest that, in addition to SO_4^{2-}, OC must be considered when discussing the role of clouds on European climate. Despite the existing data, there is still a large gap in relevant field information regarding the major inorganic and organic (including WSOC and WINSOC) $PM_{2.5}$ constituents over long time periods at different sites throughout European regions.

In this chapter the seasonal variation of well-known water-soluble inorganic ions, EC, WSOC, and WINSOC fractions and their relative contribution to ambient urban $PM_{2.5}$ load are investigated. The acquired data taken together with the structural information on the WSOM described in previous studies [18,23,60], provides a good characterization of the urban $PM_{2.5}$, thus allowing to infer about the potential local and regional sources.

4.2. Materials and methods

4.2.1. WSOM samples

This study was conducted using the WSOM extracts from a total of 43 high-volume $PM_{2.5}$ samples, representative of eleven seasons from Sampling campaign II and III: Win. 2013, Spr. 2013, Sum. A 2013, Sum. B 2013, Aut. A 2013, Aut. B 2013, Win. 2014, Spr. A 2014, Spr. A 2014, Spr. B 2014, Spr. C 2014, and Sum. A 2014. All the information regarding these samples, as well as the procedures for extraction are described in Chapter 3.

4.2.2. Inorganic ion analysis

The determination of the water-soluble SO_4^{2-}, NO_3^-, and Cl^- ions content in the aqueous extracts of the high-volume $PM_{2.5}$ samples was carried out on a Dionex 2000i/SP

Ion Chromatograph with a conductivity detector. The anions were separated on a AS4A SC column (25 cm × 4 mm I.D) with an AG4A-SC guard column 4 mm I.D, and were detected by suppressed conductivity detector, using an Anion Micro-Membrane AMMS-I with regenerate of 25 mN sulfuric acid (H_2SO_4). The injection volume was 10 µL, and the flow rate was 2.0 mL min^{-1}. The chromatograms were recorded on a Chromjet integrator from Dionex. The minimum detection limits were 0.55 mg L^{-1} for SO_4^{2-}, 0.89 mg L^{-1} for NO_3^-, and 0.83 mg L^{-1} for Cl^-. The water-soluble NH_4^+ ion content in each sample was determined by a colorimetric indophenol method, as proposed by Solorzano [96]. The minimum detection limit for NH_4^+ was 0.07 mg L^{-1}. The water-soluble Na^+ and K^+ ions concentrations were determined by flame atomic absorption spectrometer (AAS). The flame AAS measurements were carried out using a GBC model Avanta Sigma equipped with hollow cathode lamps as the radiation source. An acetylene – air flame was used, and the gas flow rates and the burner height were adjusted to obtain the maximum absorbance signal for each element. The minimum detection limits were 0.14 mg L^{-1} for Na^+ and 0.13 mg L^{-1} for K^+.

4.3. Results and discussion

4.3.1. Chemical characterization of urban $PM_{2.5}$ samples

Seasonal distribution of average $PM_{2.5}$, OC, EC, and WSOC concentrations for the 17 months sampling period is depicted in Figure 4.1. A graph showing the variation of the $PM_{2.5}$ mass concentrations and carbonaceous fractions for each collected sample is provided in Annexes (Figure A. 1). The $PM_{2.5}$ mass concentration levels are in the 6.44 – 49.2 µg m^{-3} and 2.03 – 35.5 µg m^{-3} ranges, with median values of 20.5 µg m^{-3} (average: 19.4 ± 10.0 µg m^{-3}) and 12.8 µg m^{-3} (average: 14.5 ± 8.93 µg.m^{-3}) for the Sampling campaign II and Sampling campaign III (see Chapter 3), respectively. During both sampling periods, the median values of $PM_{2.5}$ concentrations were below the European annual $PM_{2.5}$ threshold of 25 µg m^{-3} regulated by 2008/50/EC. In addition, the median and average values of $PM_{2.5}$ concentrations during both sampling periods seem to comply with the obligation for reducing national exposure by the year 2015 (exposure concentration obligation of 20 µg m^{-3}, fixed by 2008/50/EC, and based upon measurements in urban background

locations). Nevertheless, the $PM_{2.5}$ limit of 20 μg m^{-3} was exceeded during 12 weeks in the Sampling campaign II and 4 weeks in the Sampling campaign III (i.e., 4 weeks in Win. 2013, 2 weeks in Sum. A 2013, 2 weeks in Sum. B 2013, 1 week in Aut. A 2013, 3 weeks in Aut. B 2013, 1 week in Win. 2014, 2 weeks in Spr. A 2014, and 1 week in Spr. B). The $PM_{2.5}$ concentrations found in this study are of the same order of magnitude for the annual average values reported for other northwestern (e.g., Glasgow, Manchester, and Uccle), southern (e.g., Las Palmas and Huelva), and central (e.g., Debrecen, Basel, and Zurich) European urban background sites, being also closer to values reported for rural background places (e.g., Chaumont, Hohenpeisenb, Streithofen, and Hortobágy) in central Europe [90]. For a rural site near the city of Aveiro, Pio *et al.* [93] reported an annual mean $PM_{2.5}$ mass of 23 μg m^{-3} (sampling took place between July 2002 and July 2004), which is somewhat higher than the median concentrations found in the city of Aveiro.

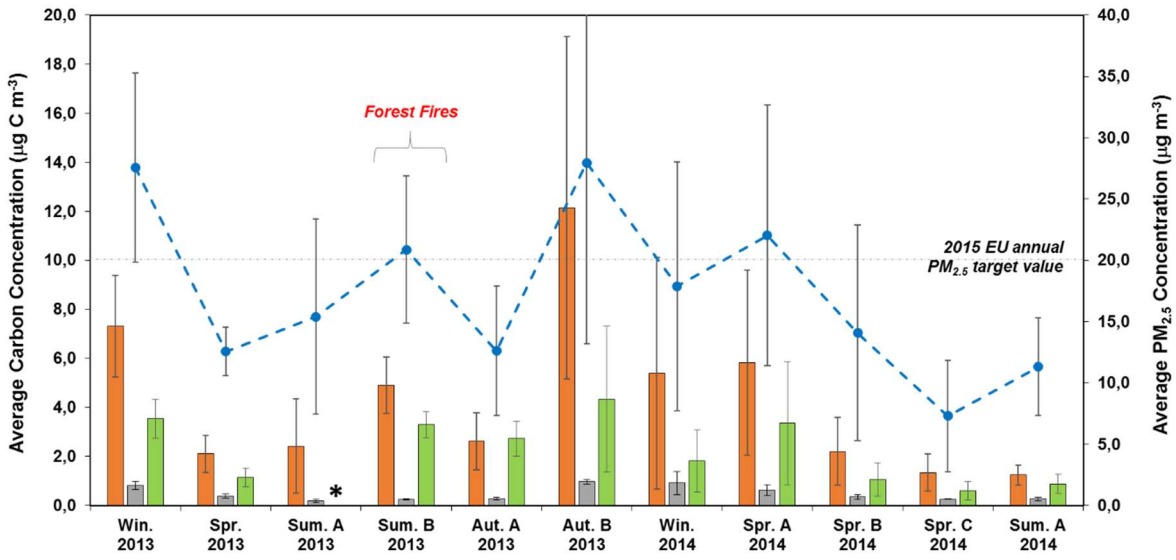

Figure 4.1 Average atmospheric concentrations of ■ OC (μg C m^{-3}), ■ EC (μg C m^{-3}), ■ WSOC (μg C m^{-3}), and -●- urban $PM_{2.5}$ (μg m^{-3}) in different seasonal periods. Error bars represent the standard deviation of the mean concentrations for the different seasonal periods. (*) denotes data unavailable for the content of WSOC fraction in $PM_{2.5}$ samples collected in Sum. A 2013 period. The $PM_{2.5}$ limit of 20 μg m^{-3} fixed by 2008/50/EC for the year 2015 is represented by a dashed dot grey line. The samples collected under forest fire events are also highlighted.

Overall, higher average $PM_{2.5}$ concentrations were observed in colder periods compared to dryer warm conditions. An exception is, however, observed for Sum. B 2013, which exhibits average $PM_{2.5}$, OC, and WSOC concentrations close to those found in the colder seasons, which could be attributed to the primary emissions from the forest fires events during this sampling period [23,60]. Apart from this exception, the ambient

concentrations of OC, EC, and WSOC follow a similar seasonal trend, with higher values during the colder seasons and lower during the warmer seasons. In this regard, a strong negative correlation was observed between each of these carbonaceous fractions and the median weekly temperature (p-value < 0.009, Table A. 2 in Annexes). This seasonal trend has been quite well documented for other European sites [15,35,93,97], although an opposite trend has been observed in Bologna [94], mountain sites in Central Europe [93], and in North America [98,99]. In this study, the increase in the concentrations of the various carbonaceous fractions during the colder seasons, namely in Win. 2013, Aut. B 2013, and Win. 2014, may be related to an increase of domestic heating and a less warm weather (see Figure 3.2) which favors the particulate phase of semi-volatile organics [15,35]. The lower spring and summer values are probably resulting from photochemical oxidation processes, which prevail during these warm conditions. On the other hand, the notable lower average ambient concentrations of OC, EC, and WSOC in Aut. A 2013 could be related to a change in source profiles and an exceptional warm weather (favoring the gas phase of semi-volatile organics) during this sampling period.

The OC is the predominant $PM_{2.5}$ carbonaceous component accounting for 73 – 96% of the total carbon within the 17 months sampling period (OC concentrations: 0.85 – 22.2 μg C m^{-3} and 0.79 – 12.5 μg C m^{-3} in the Sampling campaign II and Sampling campaign III, respectively). As seen in Figure 4.1, an important fraction of OC is water soluble. The WSOC concentrations are in the range of 0.81 – 8.73 μg C m^{-3} and 0.33 – 6.16 μg C m^{-3} in the Sampling campaign II and Sampling campaign III periods, respectively. The WSOC/OC ratios exhibit a clear seasonal dependence, with the lowest average values (≈ 36%) being observed for Aut. B 2013 and Win. 2014 seasons. These results suggest some solubility of primary organic compounds and/or aging of these compounds, even in colder seasons, likely accompanied by compositional changes, especially in the WSOM fraction [23,60]. The acquired data also reveals an increase of the average WSOC/OC ratios in both Aut. A 2013 (≈ 82%) and Spr. A 2014 (≈ 55%) sampling periods. These features could be related to the onset of exceptionally warm weather conditions (air temperature typically above 15 ºC during day-time in both sampling periods, whereas the lowest air temperatures were recorded during the night) and its consequences: increased mixing height, shift in the partitioning of semi-volatile organic compounds (SVOCs) between gas and particle phase, some solubility of primary OC and/or atmospheric aging of OC, and nonexistence/ending of

biomass burning events and/or domestic heating in the nearby houses [35,97]. It should also be mentioned that up to 70% of the OC was found to be WINSOC, which means that an important fraction of the OA is still eluding the current available analytical window.

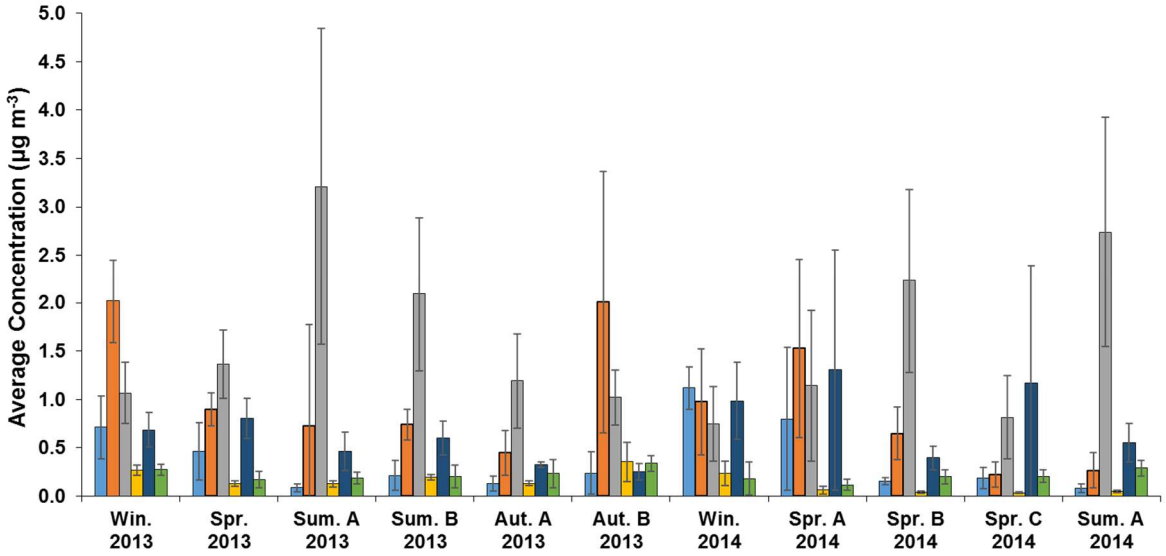

Figure 4.2 Average atmospheric concentrations (µg m^{-3}) of water-soluble ions Cl^-, NO_3^-, SO_4^{2-}, K^+, Na^+, and NH^{4+} in urban $PM_{2.5}$ in different seasonal periods. Error bars represent the standard deviation of the mean concentrations for the different seasonal periods.

Figure 4.2 depicts the seasonal distribution of the average concentrations of the major water-soluble ions in the $PM_{2.5}$ samples during the 17 months sampling period. A graphic representation of the variation of the analysed water-soluble ions for each collected sample is provided in Annexes (Figure A. 2). As expected, the major contributor to the levels of inorganic ions in warmer conditions is SO_4^{2-}. This trend is generally associated with enhanced photochemistry, low levels of precipitation, decrease in the renewal of air masses at regional scale or the increment of the summer mixing layer depth favouring the regional mixing of polluted air masses [100]. A distinction has been also made between the non-sea-salt and sea-salt fractions of SO_4^{2-}, with the former being calculated by subtracting the sea-salt SO_4^{2-} fraction taken as 0.25 times the sea-salt fraction of Na^+ [93]. The obtained results are plotted in Figure 4.3 and they clearly show that most of the SO_4^{2-} (62 – 95%) present in the urban $PM_{2.5}$ samples is likely to be non-sea-salt SO_4^{2-} aerosols (the complete dataset is provided in Figure A. 3, in Annexes). A positive correlation was also observed between the levels of SO_4^{2-} and the median weekly temperature (p-value < 0.0003, Table A. 2 in Annexes). Although this SO_4^{2-} component could be related to anthropogenic SO_2 emissions, the atmospheric oxidation of marine dimethyl-sulphide emissions from phytoplankton has

also to be considered as a potential source of non-sea-salt SO_4^{2-} aerosols at this coastal urban site [93,101].

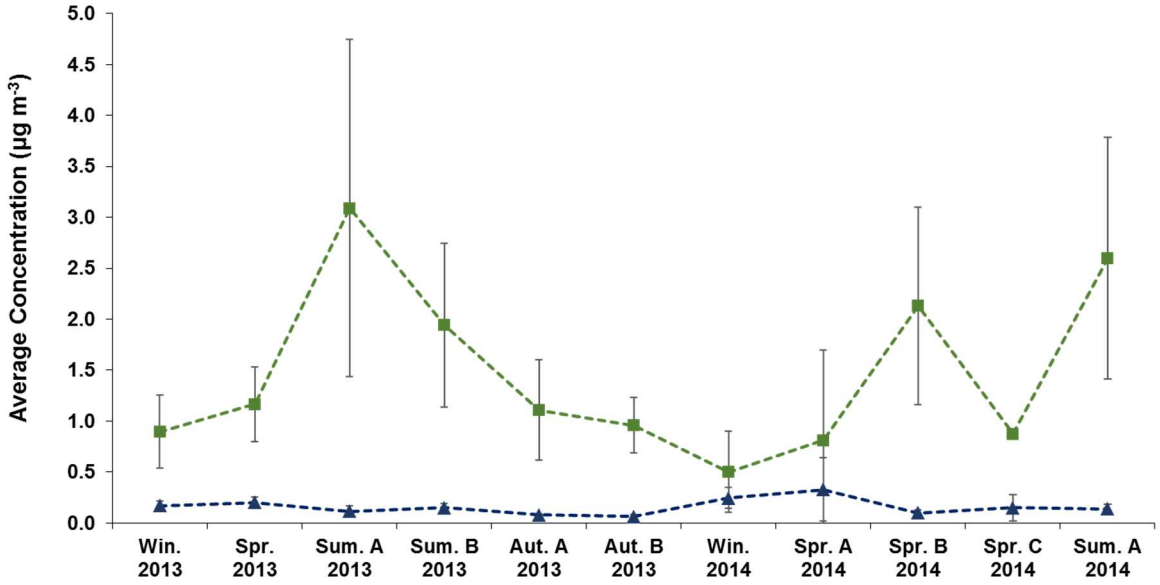

Figure 4.3 Average atmospheric concentrations (µg m^{-3}) of -■- non-sea-salt SO_4^{2-} and -▲- sea-salt SO_4^{2-} in urban $PM_{2.5}$ in different seasonal periods. Error bars represent the standard deviation of the mean concentrations for the different seasonal periods.

Average atmospheric NH_4^+ concentrations present a less pronounced seasonal trend. However, significant seasonality was observed for the average concentrations of NO_3^- and K^+ (p-value < 0.0002, Table A. 2 in Annexes), with the highest values being observed in less warm conditions, particularly in Win. 2013 and Aut. B 2013 seasons. In the case of NO_3^-, this outcome is likely to be associated with the low temperature conditions promoting the gas-to-particle conversion of semi-volatile NH_4NO_3 particles (a positive correlation was observed between the levels of NO_3^- and NH_4^+ (p-value < 0.009, Table A. 2 in Annexes). A similar pattern has been reported by Pio *et al.* [93], Terzi *et al.* [102], Mantas *et al.* [100], and Tositti *et al.* [94], for rural and urban European sites. For K^+, a well-known biomass burning tracer [93], this seasonal trend is in line with the previous findings that these urban $PM_{2.5}$ samples in colder periods are clearly impacted by biomass combustion sources [60]. It should also be mentioned that, the average concentrations of K^+ in $PM_{2.5}$ samples collected in Sum. B 2013 (0.17 – 0.23 µg m^{-3}) are of the same order of magnitude of those found in less warm seasons, indicating potential transport from biomass combustion sources occurring during this summer period. Also noteworthy is the high average concentrations of both Cl^- and Na^+ ions observed in Win. 2014 and Spr. A 2014 seasons, which seems to be in

agreement with a transport of marine aerosols from the Atlantic Ocean during these periods (Table 3.1). Considering that at continental sites, Na^+ can be used as an unambiguous tracer of the sea-salt aerosol, the mass fraction of sea-salt was calculated by combining the Na^+ concentration, Cl^- concentration, and the sea-salt contributions of magnesium, calcium, K^+ and SO_4^{2-}, as suggested by Pio *et al.* [93]. As shown in Figure 4.4, the contribution of sea-salt to urban $PM_{2.5}$ mass is higher in these two seasons (and also in Spr. 2013) than in the remaining seasonal periods, accounting for 12 – 14% of the aerosol mass. In general, the water-soluble ionic concentrations at the city of Aveiro are comparable to those previously found by Pio *et al.* [93] at a rural site, in the outskirts of the city of Aveiro. An exception is verified for NH_4^+, for which the authors reported an average atmospheric concentration six times higher than those found in this study. It is well-known that the atmospheric concentrations of NH_4^+ are strongly influenced by anthropogenic activities [103,104]. In the particular case of the rural site, one cannot disregard the influence of nitrogen-based synthetic fertilizers applied in the agriculture sector as an important emission source of NH_4^+ into the atmosphere [103,104]. The water-soluble ionic concentrations in Aveiro are typically at the lower level of the annual and/or seasonal average values ranges reported for other central and southern European urban background sites [94,100,102].

It appears from Figure 4.4 (and Figure A. 4 in Annexes) that organic matter (estimated as 1.6 × OC, based on elemental analysis performed on the WSOC fractions [60]) dominates the urban $PM_{2.5}$ mass in colder periods (40 – 68%, on a seasonal basis), specifically in Win. 2013 and Win. 2014, Aut. B 2013, and Spr. A 2014. In contrast, its contribution is weakened in warmer periods (18 – 33%). Again, an exception is observed for Sum. B 2013, where the organic matter accounts for 36 – 40% of $PM_{2.5}$ mass, which has been previously suggested to be associated with emissions from biomass burning in forest fires events. The median of the total carbonaceous fraction (organic matter plus EC) contributes to ≈ 36% of the urban $PM_{2.5}$ mass during the 17 months sampling period. This observation is in good agreement with the average values previously reported for European urban [95,100,102] and rural [93] sites. As shown in Figure 4.4, secondary inorganic aerosols (calculated as the sum of non-sea salt SO_4^{2-}, NO_3^-, and NH_4^+) were also major components of $PM_{2.5}$ mass (9 – 28%, on a seasonal basis), with a markedly higher contribution in Sum. A 2013 (≈ 26%) and Sum. 2014 (≈ 28%). On a seasonal basis, the mass of analyzed inorganic ions plus the carbonaceous matter (EC plus organic matter) explains

42 – 82% of the urban $PM_{2.5}$ aerosol mass. The unidentified fraction of the $PM_{2.5}$ mass, accounting here for 18 – 58%, is usually attributed to water bounded to hygroscopic inorganic and organic material, but it can also result from the presence of unidentified species (water-insoluble crustal materials) or from an underestimation of the organic matter content [93,102].

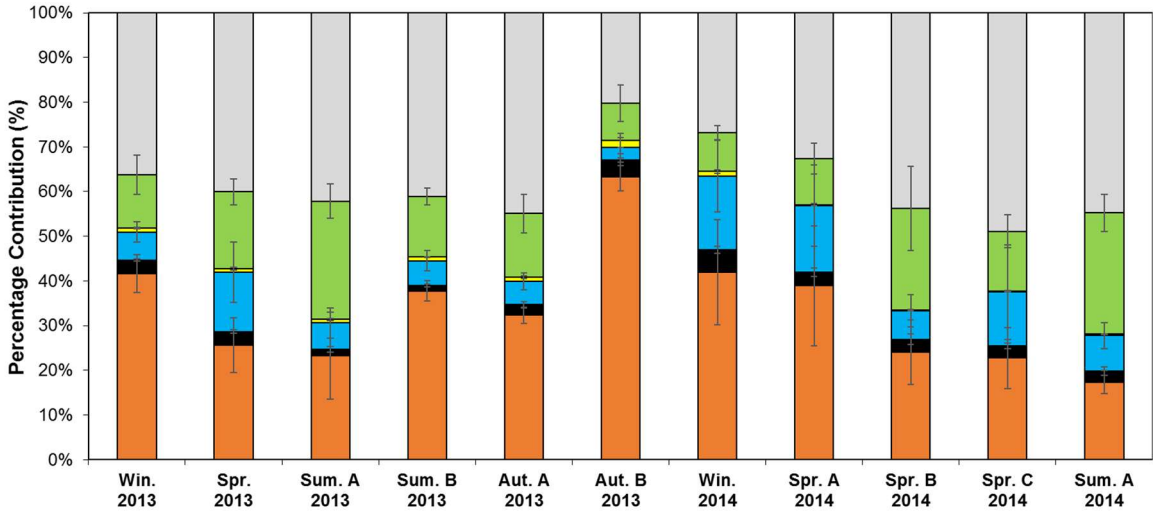

Figure 4.4 Percentage contribution (average values) of organic matter, EC, sea salt, non-sea-salt K+, and secondary inorganic aerosol (SIA) to the urban $PM_{2.5}$ mass in different seasonal periods. "Unknown" represents the difference between total mass, measured by gravimetry, and total analysed mass. Error bars represent the standard deviation of the mean percentages for the different seasonal periods.

4.3.2. Major sources of $PM_{2.5}$ samples at the Western European Coast

A tentative source identification can be pursued for the urban $PM_{2.5}$ at the Western European Coast by combining the carbonaceous and inorganic data set obtained here with the structural characterization of the aerosol WSOM described by Duarte *et al.* [60]. It can be concluded that primary natural sea-salt aerosols and mineral dust are continually present throughout the sampling period, as well as the EC component (although the contribution of the latter increases during winter). In this regard, the EC measured at the studied urban location has a likely primary origin, with a possible major contribution of emissions from the incomplete combustion of fossil fuels, namely from road transport [105,106]. Nevertheless, other EC sources such as biomass burning, in winter, and plumes of wild fires, in summer [106,107], are also likely to contribute to the EC present in the urban $PM_{2.5}$ samples during these periods. The sources of OA (including its water-soluble fraction) are

mainly non-fossil-fuel and markedly different between colder and warmer seasons. In colder seasons, the $PM_{2.5}$ WSOM fractions have less aliphatic and oxidized character and higher contributions from aromatic groups (namely, lignin-derived structures) than those of warmer conditions [23,60]. These structural data alongside a higher content in water-soluble K^+, suggests that biomass burning primary emissions are the main source of carbonaceous aerosol in colder periods, although the presence of aged and processed organic and inorganic aerosols cannot be ruled out (supported by data obtained in this study for the WSOC/OC ratios and SIA fractions, alongside the structural features of $PM_{2.5}$ WSOM described by Duarte *et al.* [60]). In warmer seasons, secondary *in situ* organic and inorganic (mainly SO_4^{2-}) aerosol formation from anthropogenic and/or biogenic precursors is likely to be predominant. Nonetheless, primary emissions from intense forest fires events can also become an important source of carbonaceous $PM_{2.5}$ in urban environments.

4.4. Conclusions

The extensive dataset acquired for urban $PM_{2.5}$ at the Western European Coast shows that organic matter dominates the identifiable urban $PM_{2.5}$ mass, followed by secondary inorganic aerosols (non-sea salt SO_4^{2-}, NO_3^-, and NH_4^+). Additionally, it has been demonstrated that an important fraction of OC is water-soluble (17 months range of 30 – 93%), whose content and structural characteristics are markedly different between colder and warmer seasons [60]. These findings suggest that besides discussing the role of the complex "aerosol WSOC-inorganic" system in cloud and rain formation, one should also discuss the potential impact for the biogeochemical cycling of this OA material. On the basis of the chemical (organic and inorganic) and mineralogical composition data, it is clear that both primary (sea-salt, mineral dust, fossil fuel, wood burning) and secondary (e.g., atmospheric aging, photooxidation and/or gas-to-particle conversion) sources contribute to the chemical composition of the urban $PM_{2.5}$ at the Western European Coast. Primary natural sea-salt aerosols and mineral dust, and fossil-related EC are continually present throughout the sampling period. During warmer conditions, the OA is found to be mainly secondary, whereas during colder periods, biomass burning primary emissions are the main source of carbonaceous aerosols.

This study in combination with the compositional studies of Duarte *et al.* [60] demonstrate that a thorough and long-term chemical characterization provides meaningful and interpretable information on urban $PM_{2.5}$ origin (primary and secondary). This study has also enabled a clear perception of the influence of weather conditions and the impact of different emission sources on the $PM_{2.5}$ levels and composition (organic and inorganic). The proposed approach can be easily adapted to other regional settings to better assessing the sources and chemical components of atmospheric $PM_{2.5}$, and it can be an added value in planning effective abatement strategies for improving air quality.

Chapter 5

Extracting information from a LC×LC system with a multichannel detector

This chapter presents a new and simple approach to deal with the large amount of data generated by LC×LC coupled to a multichannel detector, such as DAD, in order to extract useful information for the identification of patterns from complex samples.

5.1. Introduction

Both the increasing need for dealing with complex mixtures from different science fields (i.e., genomic, proteomic and metabolomics) and the low potential of 1D separation techniques to differentiate such complex mixtures, have led to the urgency for developing new separation methods, mostly based on comprehensive 2D chromatographic techniques [108,109]). The impressive resolving power and the high peak capacities of these techniques make them perfectly adequate to deal with complex samples encompassing hundreds or even thousands of chromatographic peaks in a wide range of concentrations. However, the data handling processes within the framework of these techniques, of which LC×LC is an example, still is one of the major drawbacks that have impaired their wider application [108,110]. This weakness becomes even more evident when these techniques are coupled to a multichannel detector, such as DAD or MS. The huge three-way matrix produced by these systems, which can achieve a four-way data array when analysing replicates, makes it very difficult to extract the relevant information from the chromatograms. Despite the powerful algorithms recently introduced to deal with such huge data structures [111,112], a full characterization of each individual peak in a complex sample still is a very time consuming task, and, in some cases, almost impossible to accomplish. An alternative to address this problem is to develop non-targeted cross-sample analysis [113] in order to obtain a chromatographic profile of each sample. This method aims at obtaining a global profile of each sample instead of the individual characterization of each chromatographic peak. By gathering as much information as possible from each sample, the conclusions withdrawn from the non-targeted cross-sample analysis are based either in the similarities or in variations of the chromatographic profile when compared to those of other samples or available standards.

The association of multichannel detectors to multi-dimensional separation techniques, such as LC×LC–DAD, can be of great help for accomplishing the chemical pattern recognition of complex organic samples. There is, however, an application problem to deal with 3D data matrix. Usually, the comparison of chromatographic profiles and the identification of patterns rely on the visual inspection of the analyst and in image based tools. However, the 3D matrices obtained from systems such as LC×LC–DAD cannot be plotted without reducing the dimensionality of data to two-dimensions (e.g., building an individual

2D chromatogram for each DAD wavelength, plotting the sum of the responses for all spectral channels, and using the original 2D matrix before the data folding). Therefore, Chapter 5 presents the development a methodology to obtain a non-target profile of samples analysed by means of a LC×LC–DAD system, using an algorithm to identify the coordinates of the maximum of each peak, not only in the chromatographic dimensions, but also in the spectra obtained from the DAD. The 3D coordinates produced by these maxima are then used to build a 3D map representative of the sample.

5.2. Method development

5.2.1. Correction of the background

The variations in the background signal of the chromatogram have to be removed at a first stage. Filgueira *et al.* [114] have recently introduced an orthogonal background correction (OBGC) approach, which theoretically could also be applied for removing the 2D background for each wavelength from the LC×LC–DAD data. In their approach, the authors used a 1D baseline correction method based on a median filter with a moving window applied orthogonally to the second dimension. The filter window size needs to be at least twice the width of the widest peak in the chromatogram. For the present study, some improvements to this approach are required because the chromatographic data show regions with some overlapped peaks along the first dimension. Consequently, the window size used in the algorithm needs to be twice the width of the overlapped region, in order to ensure that the median is not deviated by the intensity of the analytical signal. However, the use of such window size will cause a loss of sensitivity of the algorithm, which becomes unable to identify an actual deviation from the background. Therefore, an improvement to the performance of the algorithm has been incorporated in a MATLAB subroutine with the following steps: a) the OBGC approach (with a median filter) is applied to the data in order to identify an initial estimate of the background; b) all values above a threshold multiplied by the initial estimate obtained by the OBGC approach are removed from the original data; and c) the same OBGC approach is applied again but with a narrower window. These steps are repeated in a loop until the background is properly quantified.

The proof of concept was made by adding a background deviation, shown in Figure 5.1a, to a simulated chromatogram shown in Figure 5.1b. For that, simulated chromatograms were produced in *MATLAB* environment, with the following Gaussian model for testing the procedures for removing the background and noise:

$$Z(x,y) = z_0 \times \exp -1/2 \times \left[\left(\left(x - {}^1t_R \right) / {}^1\sigma \right)^2 + \left(\left(y - {}^2t_R \right) / {}^2\sigma \right)^2 \right] \quad (1)$$

where Z(x,y) is the height at time *x* and y in the first dimension and the second dimension, respectively, z_0 is the maximal peak height, ${}^1t_R$ and ${}^2t_R$ are the retention times of the peak in the first dimension and the second dimension, respectively (i.e., peak coordinates), and ${}^1\sigma$ and ${}^2\sigma$ are the standard deviations of the Gaussian peak on the first dimension and the second dimension, respectively. In addition, to simulate the deviations in background, the following polynomial function was used:

$$B(x,y) = \left(a \times x \right) - \left(b \times x^2 \right) + \left(c \times y^2 \right) \quad (2)$$

where *B(x,y)* is the height at time *x* and y in the first dimension and the second dimension, respectively, and *a*, *b*, *c* are constants. The added noise was generated and uniformly distributed using the *rand()* function from *MATLAB* of pseudorandom numbers within the range of 0 and 0.02. The background deviation identified by means of the methodology proposed by Filgueira *et al.* [114] is shown in Figure 5.1c, while in Figure 5.1d it is shown the chromatogram obtained after the removal of the deviation by the Filgueira *et al.* [114] approach. Figure 5.1e shows the deviation of the background identified by the improved methodology proposed in this study, and Figure 5.1f shows the chromatogram obtained after the removal of this deviation. For estimating the volume of a 2D chromatogram, and consequently identify the loss of intensity generated by the background removal process, all values of the 2D matrix are summed up and the result multiplied by the spacing of the grid in both dimensions. Following this procedure, the volume value of the original simulated chromatogram (Figure 5.1b) was estimated as being 1.50. The chromatogram with the background deviation removed as proposed by Filgueira *et al.* [114] (Figure 5.1d) has a volume value of 1.11, while the chromatogram with the background deviation removed by the improved methodology (Figure 5.1f) has a volume value of 1.38, which is much closer to the original value of 1.50 than the estimate of 1.11.

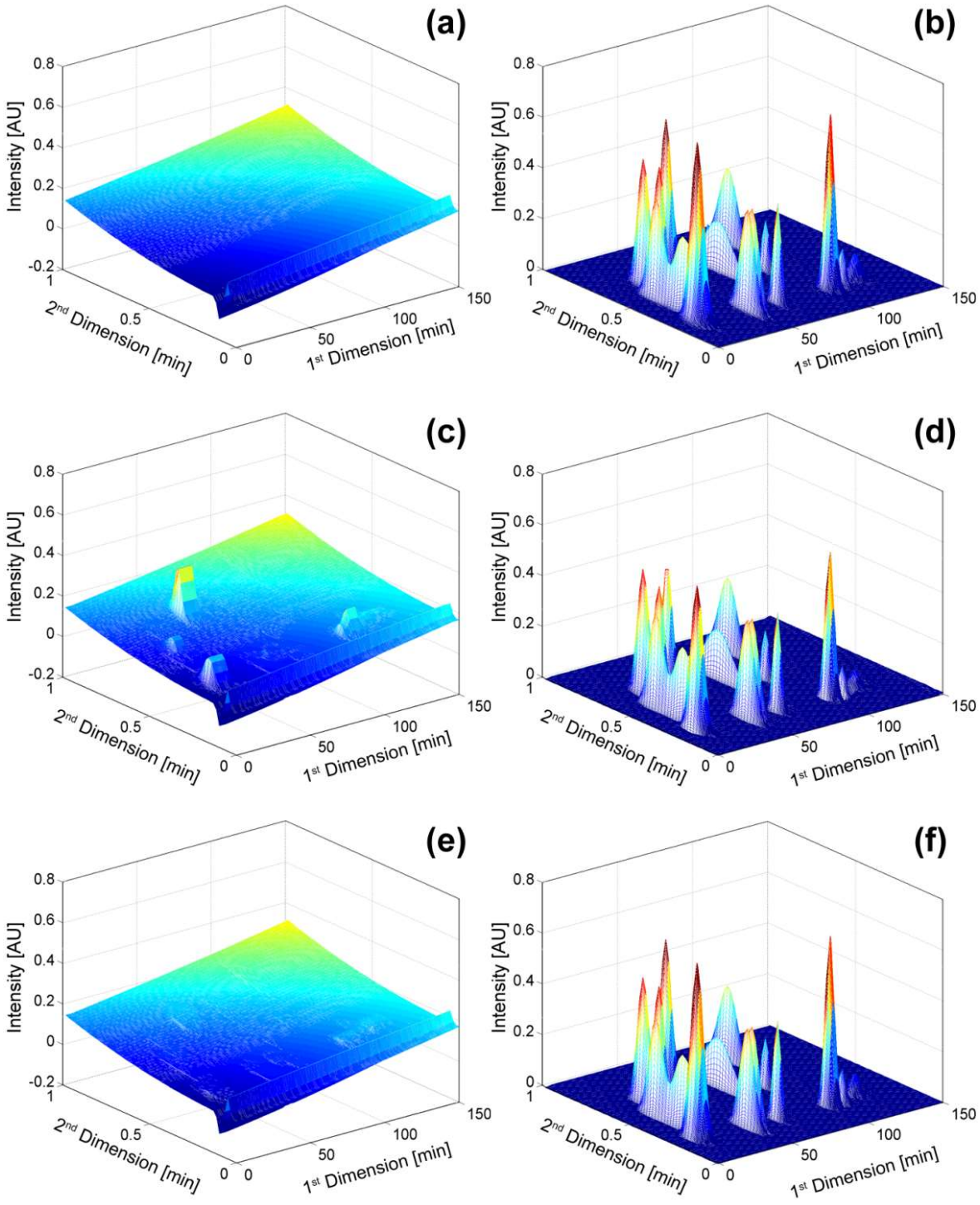

Figure 5.1 (a) Background deviation added to (b) simulated chromatogram; (c) background deviation estimated by Filgueira *et al.* [114] and (d) chromatogram obtained by subtraction (a+b-c); (e) background deviation estimated by the methodology presented in this chapter and (f) chromatogram obtained by subtraction (a+b-e).

5.2.2. Identification of the 3D chromatographic maxima

In chromatography, the location of each chromatographic peak is usually defined by the retention time where the signal reaches its maximum intensity. Mathematically, the location of these maxima of intensity can be translated into the concept of regional maximum, i.e., a value from a data array in which all the neighbouring values are smaller than this value [115]. The number of neighbouring values however depends on the dimensionality of the collected data. For example, a 1D data vector only has two neighbours for each maximum, but this value increases to 8 neighbours in a 2D matrix, and reaches 26 neighbours in a 3D data cube. In this context, since the data from a LC×LC–DAD system have a 3D structure, a regional maximum search algorithm will test, for each data point, whether all the surrounding 26 neighbour values are lower in order to identify each maximum. The operation mode of this algorithm is schematically shown in Figure 5.2, in which $\mathbf{M_{(i,j,k)}}$ represents the value under test of the 3D matrix, at row **i**, column **j**, and plane **k**, and the remaining values are the surrounding 26 neighbours of the value $\mathbf{M_{(i,j,k)}}$. Once all the regional maxima are detected, then this algorithm will produce a new matrix containing the intensity of each regional maximum, as well as their 3D coordinates corresponding to the retention time in the first dimension, the retention time in the second dimension, and the wavelength in which this maximum occurred.

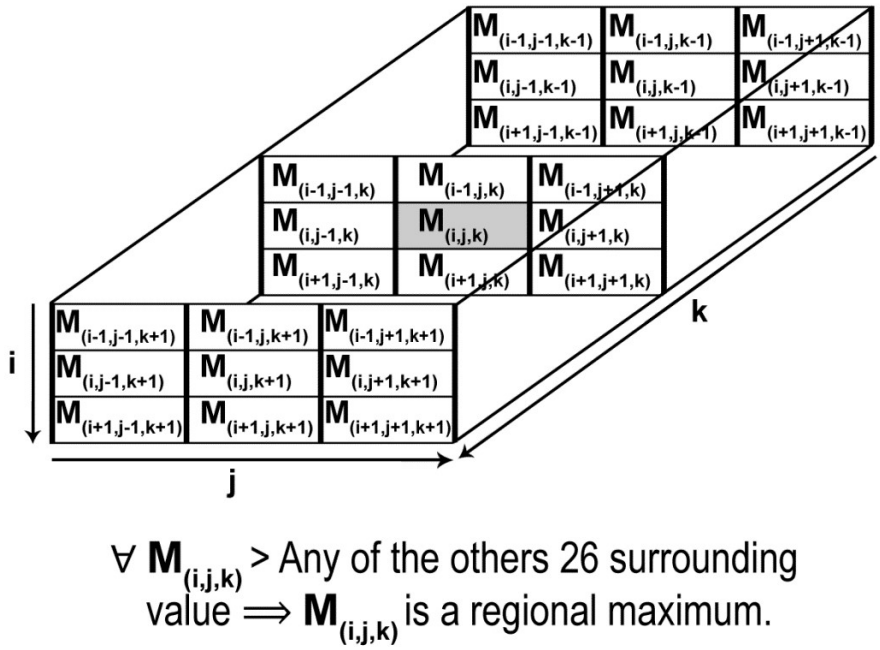

Figure 5.2 Method of operation of the 3D regional maxima search algorithm.

After identifying the entire 3D regional maxima, it is necessary to identify which of these 3D maxima are actually derived from the chromatographic components. In practice, any variability in the data acquisition and noise from the detector may cause the identification and assignment of a regional maximum caused by such variability. Thus, it is necessary to define a threshold, above which the existence of a detectable component will be considered as significant. However, the signal/noise ratio is not constant throughout the entire span of DAD wavelengths and, consequently, to ensure the proper functioning of the methodology, it is necessary to assign for each wavelength, a threshold value. These thresholds can be calculated on the basis of the IUPAC definition of limit of detection (LOD) [116]:

$$LOD = \overline{X_\lambda} + k + S_\lambda \tag{3}$$

where $\overline{X_\lambda}$ is the mean of the background and noise signal, k is a value manually chosen for the acceptation level, and S_λ is the standard deviation of the background and noise signal. After all the spurious data points caused by low levels of random background noise are identified, they are then subsequently removed from the regional maxima matrix. On way to estimate the background noise signal, it was used a simulation of the background noise obtained from the chromatographic data by applying an algorithm similar to that used to remove background variations, but with a narrower window to be more sensitive to the noise signal.

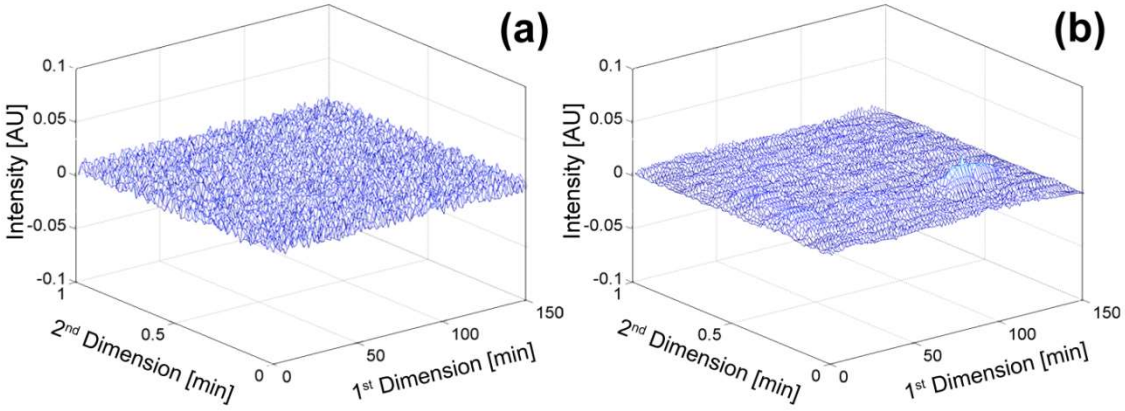

Figure 5.3 (a) Simulated noise added to chromatogram of Figure 5.1b, and (b) noise estimated by the methodology under study.

The simulated chromatogram shown in Figure 5.1 was used to test this approach by adding to it the random noise shown in Figure 5.3a. The application of the suggested algorithm for removal of background variations was applied to the resulting chromatogram, and the "blank" extracted is very similar to the original noise, as shown in Figure 5.3b. The values of LOD calculated by Eq. (3) are also very similar: 0.0091 and 0.0092 for the initial added noise (Figure 5.3a) and the noise calculated by the above mentioned algorithm (Figure 5.3b), respectively.

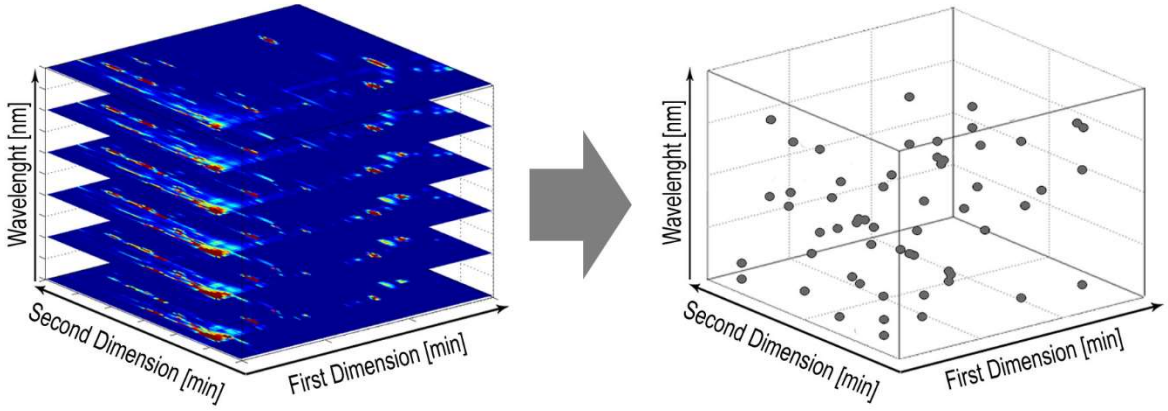

Figure 5.4 Schematic representation of the 3D coordinates of the sample components

Figure 5.4 presents a schematic representation of the possible results of the 3D regional maxima obtained for a given LC×LC–DAD chromatogram after the application of the proposed methodology. This method can be quickly and easily applied to a large matrix of data and it will enable the differentiation of patterns and the comparison of profiles between samples from different academic or industrial trials, and even between different samples. For the particular case of this work, the applicability of the developed methodology was assessed by performing a non-target LC×LC–DAD analysis of WSOM hydrophobic acids from urban atmospheric aerosol samples, presented in Chapter 6.

This method can also be used for intra-sample comparison, being easily adapted for screening and monitoring contaminants or adulterations in a sample, because any intra-sample change will change the number of peaks, and/or the location of maxima. It is also important to highlight that for each of the regional maximum identified, there is an associated intensity value, which can be used to make a qualitative assessment of the variation in the concentrations of the peaks identified in each sample. This methodology can also be used in optimization problems. As recently highlighted, the optimization of chromatographic

systems with multi-dimensional detectors, such DAD, remains an issue because the spectral information is often overlooked [117]. In this context, it is possible to incorporate the results of this methodology in chromatographic response functions to be used in optimization processes. The optimization model based on chromatographic response functions [117], when no other parameter such as resolution and time of analysis is added, will promote the best result as the one with the highest number of components, which is particularly suitable for non-target analysis.

5.3. Conclusions

In this chapter, a new method has been developed to reduce dimensionality from a three-way data extracted from a comprehensive 2D chromatographic system coupled to a multichannel detector in order to allow a graphical representation of the chromatographic and spectral profile. The huge potential resulting from the association of multichannel detectors to multi-dimensional separation techniques can be explored by using this simple approach, which allows obtaining a chemical pattern representation of each sample. As a result of improvements included in the background removal process, it was possible to extract from more than a million data points of the original raw data matrix, about a hundred data points capable of producing a fingerprint of the samples under study. This method can be quickly and easily applied to a large matrix of data, thus allowing the differentiation of patterns and the comparison of profiles between samples from different academic or industrial trials. It can also be used in chromatographic optimization functions of non-target analysis of complex samples, which is currently being pursued in our laboratory.

Chapter 6
Characterization and seasonal profiling of WSOM using LC×LC–DAD

This chapter presents the use of LC×LC–DAD technique for unravelling the chemical heterogeneity and mapping the hydrophobicity vs. M_w distribution of the substructures in fine urban aerosol WSOM collected during different seasons, as well as identifying different patterns associated with these substructures throughout the seasons.

6.1. Introduction

As already reviewed in section 2.3, numerous off-line methodologies have been developed to study the chemical composition of aerosol WSOM, usually combining TOC analysis, isolation procedures, and characterization by different analytical techniques. Despite these valuable efforts, it is clear that the substantial heterogeneity of WSOM limits the quality of structural data obtained by high-resolution instrumental techniques, thus making their interpretation extremely difficult. In this sense, the synergistic application of any chromatographic separation protocol, based on hydrophobicity, polarity, M_w, or the combination of two independent separation mechanisms, prior to an off-line structural inquiry of the fractionated materials can be of particular value for unfolding the molecular complexity of aerosol WSOM.

For the purpose of resolving the chemical heterogeneity of WSOM from atmospheric aerosols, LC×LC coupled to a DAD was employed for the first time to map the hydrophobicity vs. M_w distribution of fine urban aerosol WSOM hydrophobic acids collected during different seasons. The specific objectives of this chapter include: 1) highlighting the potential of LC×LC for separating the complex aerosol WSOM; 2) determining how its size-distributed fractions differ in hydrophobicity; 3) assessing the M_w properties of the studied WSOM samples; and 4) discerning on a seasonal profile of variation of the M_w properties of urban aerosol WSOM hydrophobic acids. This new chromatographic approach was originally developed to improve the resolution and reduce the heterogeneity of Suwannee River Fulvic Acids standard material and Pony Lake Fulvic Acids reference material [66]. This pivotal study employed a mixed-mode hydrophilic interaction chromatography (HILIC) column in the first dimension and a size-exclusion chromatography (SEC) column in the second dimension. The packing of the mixed-mode HILIC column features an alkyl long chain with hydrophilic diol functional groups at the end, thus allowing this packing material to be used in either HILIC mode (with organic-rich mobile phase) or reversed-phase (RP) mode (with water-rich mobile phase). Within the framework of LC×LC of organic matter, the mixed-mode HILIC column was operated under aqueous RP conditions, which led the authors to employ the term *per* aqueous liquid chromatography (PALC) in order to distinguish the features of this chromatographic mode from traditional HILIC and RP [66]. In a similar fashion, the same designation will be used

in the present study. Nevertheless, an important enhancement has been introduced here in regard to the previous seminal research work: the present study takes advantage of the full UV – Vis spectrum provided by the DAD, while the former uses a DAD operating only at a single wavelength. Using the full UV – Vis spectrum preceded of a comprehensive chromatographic system becomes especially useful for non-target analysis and identification of patterns based on the information extracted from complex organic mixtures. As a result, the sample-to-sample comparison is improved, and sample characterization is facilitated especially when LC×LC is combined with the informing power of a multichannel detector. Nevertheless, extracting useful information from a large amount of multi-dimensional data still is one of the major drawbacks for a wider application of LC×LC–DAD procedures [110]. Therefore, in this chapter, a mathematical procedure described in Chapter 5 and published by Matos *et al.* [19] has been also used to deal with the large amount of data generated by the PALC×SEC–DAD system and draw a 3D fingerprinting for each WSOM sample, which alongside the other samples, can be used to identify different patterns associated with the specific properties of each sample under study.

6.2. Materials and methods

6.2.1. WSOM hydrophobic acids

This study was conducted using the WSOM hydrophobic acids fractions from five representative WSOM samples of different seasons: Aut. 2009, Sum. B 2010, Aut. B 2010, Win. 2010, and Spr. 2011. All the information regarding these samples, as well as the procedures for extraction and isolation are already described in Chapter 3.

6.2.2. Instrumentation and chromatographic conditions

The schematics of the instrumentation setup and the complete description of the LC×LC system used in this experimental procedure can be found in Duarte *et al.* [66]. The first dimension, using an Acclaim Mixed-Mode HILIC-1 column (Dionex; diameter 4.6 mm; length 150 mm; comprised of 5 μm high-purity, porous, spherical silica particles with

120 Å diameter pores bonded with alkyldiol functional groups), was operated in isocratic mode, in PALC conditions, using a mobile phase composition consisting of 20 mM of ammonium acetate (pH adjusted to 6.0 with 1.1 mM of acetic acid) and 10% (v/v) of acetonitrile. The flow rate in the first dimension was 0.020 mL min^{-1} and the temperature of the analytical column was maintained at 30 ºC. The second dimension using a PSS Suprema 30 Å analytical column (Polymer Standards Service GmbH; diameter 8 mm; length 150 mm; particle size 10 μm; separation range 100 – 30,000 Da; stationary phase polyhydroxymethacrylate copolymer) was also operated in isocratic mode with a mobile phase composition consisting of 20 mM of ammonium hydrogen carbonate (pH 8.0) and 11% (v/v) of acetonitrile. The flow rate was 2.5 mL min^{-1} and the temperature of the analytical column was also maintained at 30 ºC. The outlet of the second dimension column was connected to a diode array detector (JASCO, model MD-2010) operating at 2 nm intervals in a range between 234 and 300 nm. The first and second dimensions were interfaced with an eight-port high pressure two-position interfacing valve (VICI®AG International, Schenkon, Switzerland) equipped with two identical 50 μL sampling loops. The modulation time was set at 150 s, and the valve was controlled by a PSS WinGPC Unity software (Polymer Standards Service GmbH, Mainz, Germany) by receiving a start-up signal from a PSS Universal Data Center (model UDC 810). Before the PALC×SEC–DAD analyses, the WSOM hydrophobic acids solutions were diluted in 10% of the mobile phase (v/v) of the first dimension. The M_w distribution, obtained by the SEC column in the second chromatographic dimension was calibrated using sodium polystyrene sulfonate standards (M_w at peak maximum (M_p): 186, 891, 2240, 3420, and 8390 Da, obtained from Sigma Aldrich) and HPLC grade acetone 5% (v/v), which also served as permeation volume probe. These standards were prepared by dissolving an appropriate amount of each compound in the mobile phase of the second dimension. The PALC and SEC separation mechanisms were further evaluated using the following organic compounds of known atmospheric relevance: D(+)-Glucose, D(+)-Trehalose dihydrate, Levoglucusan, Citric acid, Adipic acid, Catechol, Glycine, and L-Isoleucine. The molecular formula and M_w of these eight organic compounds are available in Table 6.1. Since some of these compounds do not have strong chromophoric groups, their detection was performed using an evaporative light-scattering detector (SEDEX, model 80-LT-ELSD) operating at 60 °C and 3.5 bar.

Table 6.1 Molecular formula and M_w of the eight organic compounds used for evaluation of the PALC and SEC separation mechanisms.

Name	Molecular formula	M_w (Da)
1. Citric acid	$C_6H_8O_7$	192
2. Adipic acid	$C_6H_{10}O_4$	146
3. D(+)-Glucose	$C_6H_{12}O_6$	180
4. D(+)-Trehalose dihydrate	$C_{12}H_{22}O_{11}.2H_2O$	378
5. Glycine	$C_2H_5NO_2$	75.1
6. Levoglucosan	$C_6H_{10}O_5$	162
7. L-Isoleucine	$C_6H_{13}NO_2$	131
8. Catechol	$C_6H_6O_2$	110

6.2.3. Data acquisition and data treatment

Data acquisition was carried out using ChromNav Chromatography Data System software version 1.17.01 (JASCO Corporation, Tokyo, Japan), exported as ASCII and then processed using laboratory made algorithms coded in MATLAB environment (The Mathworks Inc., Natick, MA, USA). In this study, the new method described in Chapter 5, and recently published by Matos *et al.* [19], was applied to remove the variations in the background signal of the chromatograms, as well as, to identify the 3D regional maxima of each chromatographic peak generated in the LC×LC–DAD system, i.e., retention times at the peak maximum in the first and second dimensions, and the wavelength of the maximum UV absorption, allowing to obtain a graphical representation of the chromatographic and spectral profiles. In this procedure, a value of 5 was taken as the acceptation level threshold (k) of the Eq. (3) (Chapter 5).

6.3. Results and discussion

6.3.1. Assessing the separation mechanisms in both dimensions

The interpretation of the size distribution of WSOM hydrophobic acids obtained by means of SEC is not straightforward. The SEC separation is usually not strictly based on the molecular size of the analytes with respect to the average pore size of the stationary phase. In this separation mode, apart from the size exclusion separation mechanism, the occurrence of non-size exclusion effects (e.g., hydrophobic interactions, ion-exchange and ion-

exclusion effects) due to the interaction with the column stationary phase cannot be neglected for several compounds. Moreover, it is of common knowledge that the calibration of the molecular size distribution in a SEC column should be carried out with standards of the same molecular type as the samples under study (e.g., similar M_w and charge distribution). However, since the chemical composition and properties of the bulk aerosol WSOM is still poorly understood [118], this option becomes impossible to fulfil. Furthermore, some conceptual models of aerosol WSOM suggest that small and heterogeneous compounds may be self-assembled into supramolecular conformations stabilized mainly by weak forces, such as van der Waals, π–π, or CH–π [119]. Consequently, WSOM could have different properties, particularly with regard to M_w and charge distribution, compared to the individual molecular forms usually identified in these samples. The occurrence of non-size exclusion effects and the lack of adequate standards to calibrate the SEC column are, therefore, the most significant drawbacks in the characterization of the size-exclusion distribution of WSOM as a whole.

The development of the chromatographic conditions applied in this study followed the method suggested by Duarte *et al.* [66] for PALC×SEC analysis of Fulvic Acids reference materials. The authors used sodium polystyrene sulfonate standards to calibrate a SEC column identical to the one applied in the present study. According to Chin *et al.* [120], these standards show good agreement with the M_w of aquatic Fulvic Acids reference, as determined by techniques based on colligative properties (i.e., vapour pressure osmometry and small-angle X-ray scattering). The same calibration procedure based on sodium polystyrene sulfonate standards was followed in this work, taking into account that aerosol WSOC hydrophobic acids and aquatic Fulvic Acids hold similar carbon functional groups [15]. Nevertheless, it should also be highlighted that due to the very wide molecular and structural heterogeneity of aerosol WSOM samples, one cannot ensure that the calibration of M_w is accurate for all the individual compounds present in the sample. To test this hypothesis, the chromatographic behaviour of eight organic compounds with atmospheric relevance (i.e., D(+)-Glucose, D(+)-Trehalose dihydrate, Levoglucosan, Citric acid, adipic Acid, Catechol, Glycine, and L-Isoleucine) was studied under similar experimental conditions in the PALC×SEC system. These results are presented in Figure 6.1. In terms of the separation by the SEC mechanism, the M_p values obtained for each organic compound were: 176 Da for Citric acid, 169 Da for Adipic acid Da, 70.4 Da for D(+)-Glucose, 80.5 Da

for the D(+)-Trehalose dihydrate, 76.2 Da for Glycine, 50.7 Da for Levoglucosan, 57.3 Da for L-Isoleucine, and 144 Da for Catechol. These results, when compared with the M_w values reported in Table 6.1, show that carbohydrates (i.e., D(+)-Glucose, D(+)-Trehalose dihydrate, Levoglucosan) and L-Isoleucine are eluting later than expected. In these cases, the compounds can be adsorbed onto the SEC packing material due to hydrophobic interaction and/or ion exchange mechanisms, yielding an estimate of the M_w lower than the actual M_w value of the compounds. Furthermore, one cannot disregard the fact that none of these four compounds with an underestimated M_w value exhibit intense chromophoric groups and, therefore, they are likely to be absent from the PALC×SEC–DAD chromatograms. This fact suggests the possibility that the M_w value of some of the WSOM hydrophobic acids components can also be underestimated. Moreover, organic compounds with larger M_w could also show some unexpected interactions with the SEC stationary phase. Nevertheless, these interactions are more likely to occur with small M_w compounds since they can access more easily the pores of the stationary phase (i.e., larger surface contact area) and, consequently, can experience adsorption and/or some electrostatic interactions onto the SEC packing material [121].

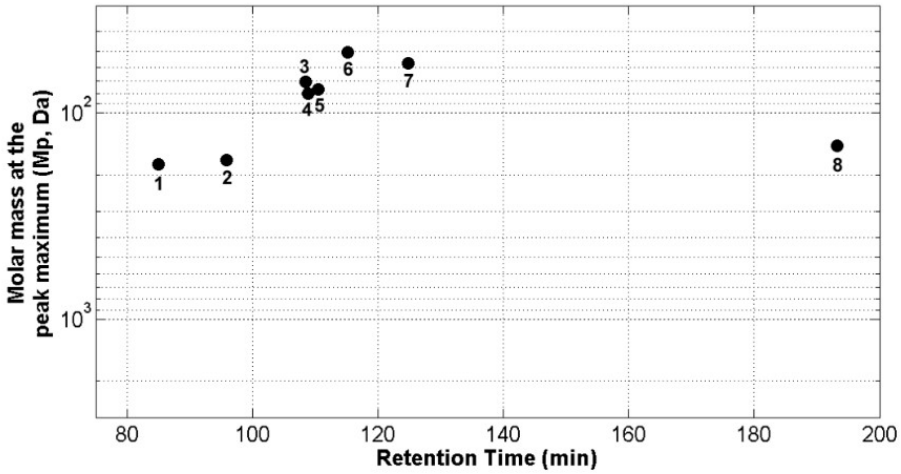

Figure 6.1 2D representation of the peak regional maxima location in the PALC×SEC–ELSD chromatogram of (1) Citric acid, (2) Adipic acid, (3) D(+)-Glucose, (4) D(+)-Trehalose dihydrate, (5) Glycine, (6) Levoglucosan, (7) L-Isoleucine, and (8) Catechol.

The separation of the eight atmospherically relevant compounds in the first chromatographic dimension also allows assessing the hydrophobic separation by means of the PALC mechanism (Figure 6.1). As expected, the compounds are eluting according to their hydrophobic character in the following order: Citric acid (85.0 min) < Adipic acid (95.8

min) < D(+)-Glucose (109 min) < D(+)-Trehalose dihydrate (109 min) < Glycine (111 min) < Levoglucosan (115 min) < L-Isoleucine (125 min) < Catechol (193 min). This chromatographic trend can be used as an indicator for mapping the hydrophobicity of more complex organic mixtures, such as the WSOM hydrophobic acids.

6.3.2. PALC×SEC–DAD analysis of WSOM hydrophobic acids

In this work, the acquisition of the full UV – Vis spectrum provided by the DAD have arisen some problems in the representation and interpretation of the raw data, since the 3D data matrices obtained from any LC×LC–DAD system cannot be represented without reducing the dimensionality of data, e.g., by plotting the sum of the responses for all spectral channels, or using the original 2D matrix before data folding [19]. Using the first option, Figure 6.2 shows the chromatographic profile built on the basis of the total sum of intensities of the PALC×SEC–DAD data obtained for each aerosol WSOM hydrophobic acid sample studied. As it can be seen in Figure 6.2, the PALC×SEC method allowed the separation of the WSOM hydrophobic acids samples into several fractions, with most of the UV absorption contour plots displaying different elution patterns. Apparently, these fractions exhibit different molar mass distributions and chemical characteristics in terms of hydrophobicity throughout the year. No less important, it is also noteworthy that samples from different years but collected during the same season, i.e., Aut. 2009 and Aut. B 2010 (Figure 6.2a and Figure 6.2c, respectively), have a very similar chromatographic profile. Due to the small number of studied samples, definite conclusions on the seasonality of the chemical characteristics of WSOM samples cannot be totally ascertained by means of the PALC×SEC–DAD method. Notwithstanding this fact, the findings obtained in this study suggest that the WSOM hydrophobic acids exhibit fairly similar profiles in terms of M_w distribution and hydrophobicity for the same season, but in different years.

The strategy of combining two independent separation mechanisms in a single chromatographic run and the degree of separation attained for the five complex WSOM hydrophobic acids samples, underlines the remarkable potential of LC×LC technique for resolving the chemical heterogeneity of these complex unknown organic mixtures, which

would be impossible to achieve using only 1D separation techniques. In order to further understand and explore the PALC×SEC–DAD data obtained for each WSOM hydrophobic acids sample, the 3D regional maxima of each chromatographic peak (retention times at the peak maximum in the first and second dimensions and the wavelength of the maximum UV absorption) were identified according to the procedure developed in Chapter 5 and published by Matos and co-workers [19]. This dataset was then used to build a map of "hydrophobicity vs. M_w distribution" for each WSOM hydrophobic acids sample.

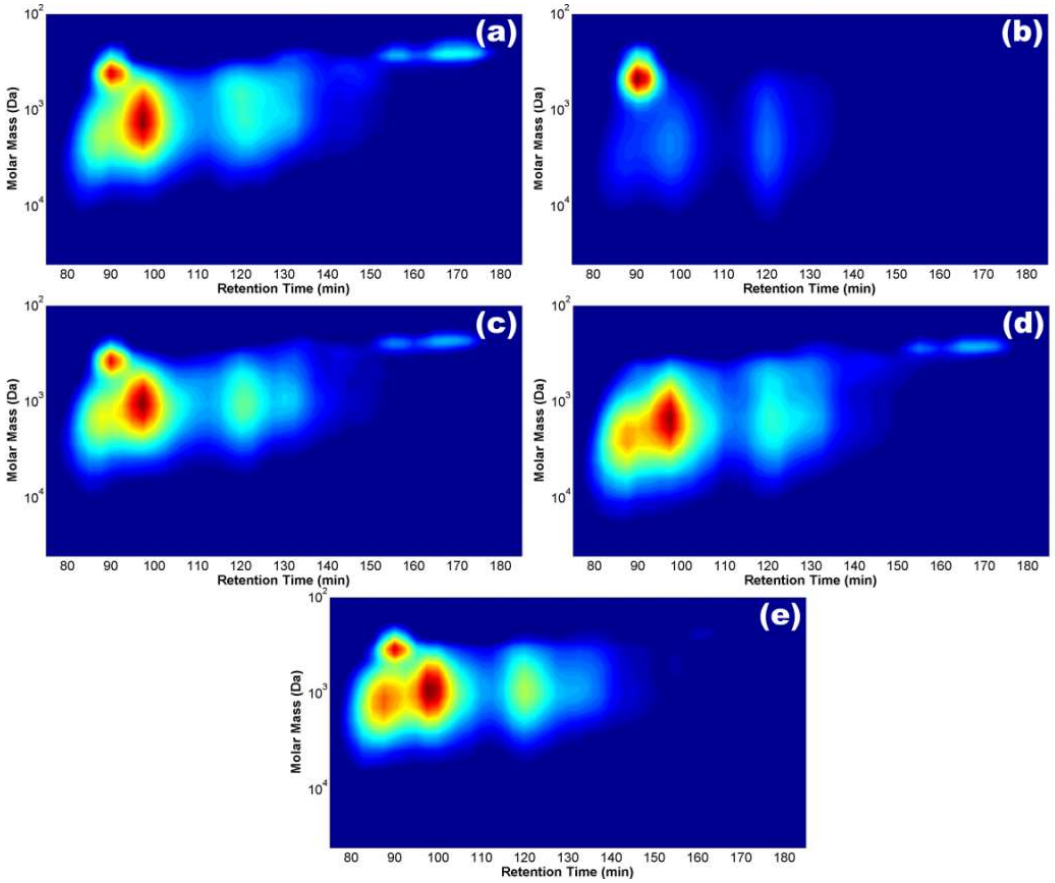

Figure 6.2 Total sum of intensities for the PALC×SEC–DAD chromatogram of the WSOM hydrophobic acids from (a) Aut. 2009, (b) Sum. B 2010, (c) Aut. B 2010, (d) Win. 2010, and (e) Spr. 2011 urban aerosol samples.

Figure 6.3 shows the coordinates of the peak regional maxima of the PALC×SEC–DAD chromatogram of the urban aerosol WSOM hydrophobic acids collected during the different seasons (Sum. B 2010, Aut. B 2010, Win. 2010, and Spr. 2011) over one year. In terms of M_w distribution, the WSOM hydrophobic acids from Sum. B 2010 (Figure 6.3a) exhibits six chromatographic peaks with different characteristics in terms of hydrophobicity and molar mass, of which four have high M_p values (using the M_p value of 1000 Da as the

threshold) in the range of 1901 – 2689 Da, and two of these have the highest hydrophobicity. The two peaks with the lowest M_p values are also located in the lower range of hydrophobic character. For the WSOM hydrophobic acids from the Spr. 2011 sample (Figure 6.3d), considered to be collected during a warmer period, six chromatographic peaks are also portrayed, most of them at retention times in the first dimension similar to those of the Sum. B 2010 sample and, consequently, with similar hydrophobicity, but with lower values of M_p (< 1081 Da). The presence of chromatographic peaks with apparently high M_p values (> 1000 Da) in the aerosol WSOM hydrophobic acids collected during warmer periods, Sum. B 2010 sample in particular, may be explained by the long residence time in the atmosphere of low M_w organic compounds that undergo oligomerization and/or polymerization reactions mediated by solar radiation, thereby resulting in molecular structures with higher M_w [122]. On the other hand, the decrease in air temperature in the colder seasons appears to have an effect on the hydrophobicity and M_w distribution of the aerosol WSOM hydrophobic acids. Indeed, the Aut. B 2010 and Win. 2010 samples (represented in Figure 6.3b and Figure 6.3c, respectively), have a profile close to each other, but quite different from those of the Sum. B 2010 and Spr. 2011 samples. The WSOM hydrophobic acids from both Aut. B 2010 and Win. 2010 samples contain almost double of the chromatographic peaks compared to those of the warm season samples, with a wide range of M_p values and hydrophobicity (M_p values ranging between 232 – 1406 Da and 267 – 2689 Da for the Aut. B 2010 and Win. 2010 samples, respectively). Interestingly, the chromatographic profile of the WSOM hydrophobic acids from both Aut. B 2010 and Win. 2010 samples exhibit a cluster of chromatographic peaks with retention times higher than 130 minutes and, therefore, with high hydrophobicity, but with very low M_p values (between 267 and 389 Da). Besides reflecting the different structural and chemical properties of the organic structures in the WSOM hydrophobic acids across the different M_w fractions, these results may also suggest that the most hydrophobic structures have lower M_w values. According to the work of Duarte and Duarte [123], the occurrence of organic compounds with such a low M_p range in these atmospheric aerosol samples may be indicative of the presence of freshly emitted SVOCs with low M_w values. Nonetheless, the presence of fractions exhibiting somewhat higher M_p values in these same samples (ranging from 589 to 860 Da) could be associated with the emission to the atmosphere of organic particles from other sources than those of SVOCs (e.g., wood burning).

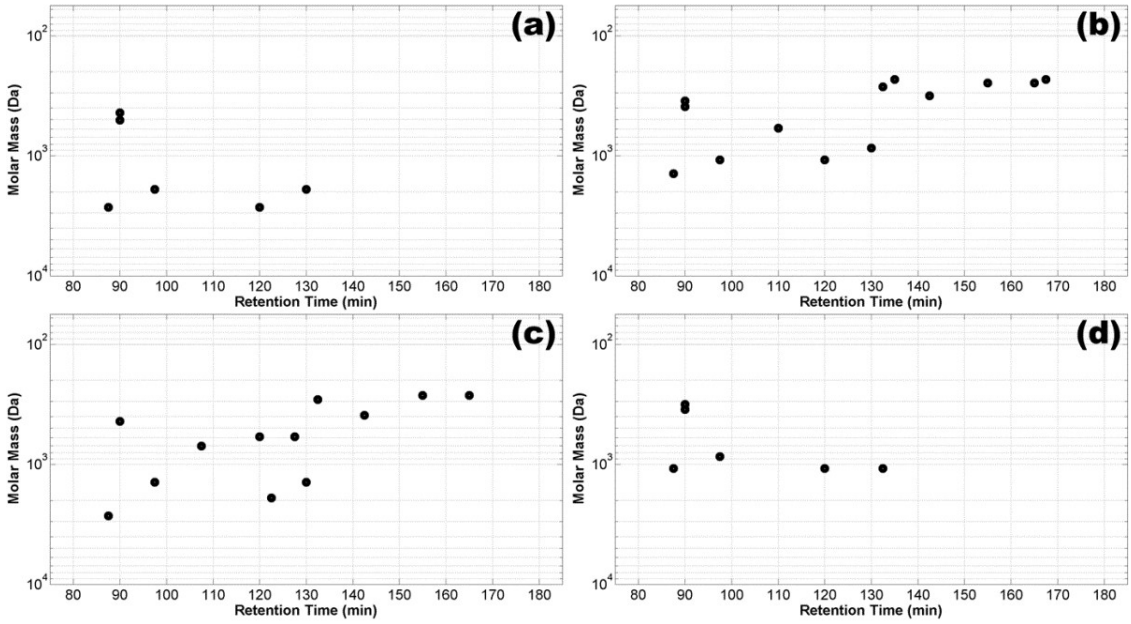

Figure 6.3 Representation of the peak regional maxima location of the PALC×SEC–DAD chromatogram of the WSOM hydrophobic acids from (a) Sum. B 2010, (b) Aut. B 2010, (c) Win. 2010, and (d) Spr. 2011 urban aerosol samples.

Despite the obvious differences between the chromatographic profiles of the samples, the application of the total sum of intensities originates a loss of spectral information and, consequently, reduces the amount of information available for the characterization of such complex samples. In order to avoid this loss, the mathematical approach used in this work for the identification of chromatographic peaks also provides information on the wavelengths that each chromatographic peak shows the maximum of absorbance [19]. With this information, a 3D map was created using the complete 3D regional maxima of each chromatographic peak generated by the PALC×SEC–DAD system. Figure 6.4 shows the obtained profiles for each of the aerosol WSOM hydrophobic acids collected in the different seasons (Sum. B 2010, Aut. B 2010, Win. 2010, and Spr. 2011). As depicted in Figure 6.4, the vast majority of the organic compounds of the warmer season samples, i.e., Sum. B 2010 and Spr. 2011 (represented in Figure 6.4a, and Figure 6.4d, respectively), have UV absorbance below 254 nm. The only exceptions to this profile are three maxima (one for the Sum. B 2010 sample and the other two for the Spr. 2011 sample), with low hydrophobicity and molar mass, which have UV absorbance near 290 nm. On the other hand, the organic compounds from the colder season samples, i.e., Aut. B 2010 and Win. 2010 (represented in Figure 6.4b and Figure 6.4c, respectively), have absorbance uniformly distributed over the entire acquired UV spectrum. Figure 6.4 also seems to show

a relationship between the decrease in the values of M_p and a shift towards higher wavelengths throughout all seasons. Since UV absorptivity at lower wavelengths (near 220 nm) is usually associated with the presence of more aliphatic structures (because of their low content in C=C bond systems), and that at higher wavelengths (> 254 nm) is usually related with the presence of more unsaturated bond systems, such as those of aromatic structures, can be suggested that fractions with lower M_p values may be enriched in organic structures with a higher degree of conjugation of π-bond systems.

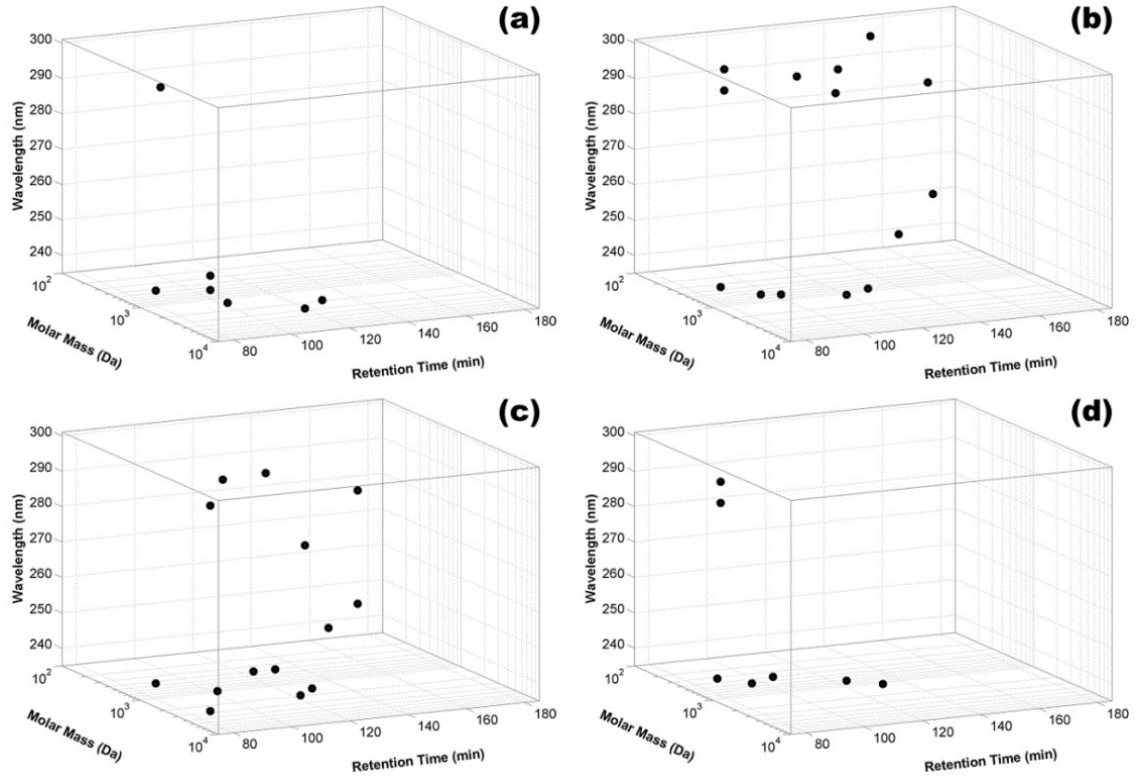

Figure 6.4 3D representation of the peak regional maxima location of the PALC×SEC–DAD chromatogram of the WSOM hydrophobic acids from (a) Sum. B 2010, (b) Aut. B 2010, (c) Win. 2010, and (d) Spr. 2011 urban aerosol samples.

Taking into account these results, it can be argued that the WSOM hydrophobic acids from warmer seasons, namely the Sum. B 2010 and Spr. 2011 samples, are enriched in aliphatic structures, while those from colder seasons, i.e., Aut. B 2010 and Win. 2010, exhibit a higher degree of structures with conjugation of π-bonds (e.g., aromatics) alongside aliphatic structures. These results appear to be in agreement with those obtained by Duarte *et al.* [15] and Sannigrahi *et al.* [36], who applied solid-state ^{13}C NMR spectroscopy for investigating the distribution of carbon functional groups in WSOM hydrophobic acids from

atmospheric aerosols collected, respectively, in a rural-coastal location in winter and summer seasons, and in an urban location in summer. The results from these studies indicate that the summer sample are more enriched in aliphatic and oxygenated aliphatic structures (approx. 60 and 18% of total NMR peak area, respectively) [15,36] than the winter sample (approx. 40 and 18% of total NMR peak area, respectively), whereas the latter has a higher percentage of aromatic structures (15% of total NMR peak area) likely derived from wood burning processes for house heating [15].

6.4. Conclusions

The results obtained in this study highlight the potential of 2D chromatographic techniques, namely the LC×LC–DAD, for unravelling the complexity of the substructures present in WSOM from fine atmospheric aerosols. In this study, LC×LC–DAD provided a unique insight into the molecular distributions within the complex hydrophobic acid fractions of WSOM samples, which allowed us to differentiate patterns and comparing profiles of the aerosol WSOM samples in order to understand how their chemical characteristics vary in relation to the perturbation of the atmospheric system under study. Furthermore, this study also demonstrates that the combination of PALC and SEC separation mechanisms in a single run provide a new perspective on the structural heterogeneity of WSOM, allowing to visualize differences between chromatographic fractions in terms of M_w distribution and hydrophobicity. This fact constitutes an enormous advantage in comparison to the traditional 1D chromatographic approach. Moreover, even if one tries to replicate these results using only 1D techniques, this would need at least several chromatographic analysis and tedious procedures for collecting different chromatographic fractions. Nevertheless, there is still room for upgrading the developed PALC×SEC procedure, namely further improving the chromatographic resolution and decreasing the total time of analysis. Besides extending the range of the organic matter separation, the data obtained by LC×LC–DAD is amenable to a proposed mathematical procedure that allows a graphical representation of the chromatographic and spectral profiles, and produces patterns associated with each sample, thus providing valuable clues for unfolding the complexity of the NOM present in OA.

Chapter 7

Study of WSOM and ASOM using EEM fluorescence spectroscopy

This chapter compares the fluorescence features of the organic matter present in water and alkaline extracts using a multiway chemometric method (PARAFAC-ALS) for decomposing sets of EEM fluorescence spectra of WSOM and ASOM from fine urban aerosols.

7.1. Introduction

As extensively reviewed in Chapter 2, the majority of the physicochemical properties of the WSOM and ASOM fractions of atmospheric aerosol, as well as their sources, formation mechanisms, and fate in the atmosphere are still poorly understood. The obvious lack of knowledge on these fractions leads us to develop new strategies for assessing its chemical features and identify their structural differences. For this purpose, this work also applies three-dimensional (3D) excitation – emission matrix (EEM) fluorescence spectroscopy to study the main fluorophores present in both WSOM and ASOM fractions, sequentially extracted from $PM_{2.5}$ collected at the selected urban location during different seasons. As recently reviewed by Andrade-Eiroa *et al.* [124], this technique has been extensively used for providing important information on the chemical nature, structural groups, conformation, and heterogeneity of chromophoric NOM from different environmental matrices, including also WSOM from aerosols [125,126]. The application of this technique has also increased in the last decade due to the association of multiway chemometric methods, namely PARAFAC-ALS [127].

In this chapter, I have also take advantage of this powerful chemometric tool for decomposing sets of EEM spectra of WSOM and ASOM in order to identify the location and intensity of independent fluorescent components from the PARAFAC-ALS models and, consequently, to characterize the dominant individual fluorescent moieties in both WSOM and ASOM from urban aerosols. From the comparison of the spectral features obtained for each OA fraction, an attempt to identify the most atmospherically-relevant fluorescent structures will be pursued, as well as their variability over seasons.

7.2. Materials and methods

7.2.1. WSOM and ASOM samples

This study was conducted using a total of 60 aerosol WSOM and ASOM extracts from the sampling campaigns I, II, and III, and 12 aerosol WSOM tandem filter samples

from the Freire [76] campaign. All the information regarding these samples is described in Chapter 3.

7.2.2. EEM Fluorescence spectroscopy and data processing

The fluorescence spectra of each WSOM and ASOM sample were recorded on a spectrophotometer JASCO (Tokyo, Japan), model FP-6500, using a 1 cm path-length quartz cuvette. Excitation and emission wavelength ranges were set from 220 to 400 nm and 230 to 500 nm, respectively, and their scanning intervals were set at 10 nm and 5 nm, respectively. The excitation and emission slit widths were fixed at 10 nm and the scan speed was set at 100 nm/min. For each day of analysis, a spectrum of a sample of ultra-pure water was acquired under the same experimental conditions and used as blank. In order to improve the quality of the recorded spectra and to reduce some unwanted effects (e.g., light scattered off the sample, and inner filter effects) which cause deviation from the spectrum trilinearity, an EEM correction method was used, based on the procedure proposed by Murphy *et al.* [127,128]. The instrument-specific spectral deviation matrix was obtained from the outer product of the vectors of excitation and emission correction factors, which were acquired according to the manufacturer instructions using Rhodamine B as the quantum counter for excitation spectrum and a quartz diffuser for emission spectra. The inner filter effects were taken into account using a correction matrix developed from the absorbance spectra (210 – 500 nm, with a spacing of 1 nm), recorded on a Shimadzu spectrophotometer (Kyoto, Japan), model UV 2101PC, using a 1 cm path-length quartz cuvette. After that, each spectrum was normalized according to the area under the water Raman peak of the blank at 350 nm (converting the data intensity to Raman Units, R.U.), and the blank was subtracted. Finally, the Rayleigh scatter and the Raman peaks remaining after blank-subtraction were removed, and the missing values were interpolated.

7.2.3. PARAFAC modelling

PARAFAC-ALS analysis was carried out in MATLAB (Mathworks Inc., Natick, MA) environment using the N-way Toolbox [129]. The models were developed using the EEM data normalized to their total intensity, but this normalization was reversed after the validation of the model following the procedure of Murphy *et al.* [127]. All models produced

were constrained to non-negative values and unimodality in the emission dimension. In order to identify the number of components which best suited each model, several tests using two to eight components were performed. The convergence criterion was set at $1E^{-10}$. All models were validated using the recently published drEEM Toolbox [127], which assists in the identification of outliers, and also performs the Core consistency diagnostic [130] and the split-half analysis. The percentage residual error of models and the visual inspection of the identified components were also taken into account for the validation of the PARAFAC model.

7.3. Results and discussion

7.3.1. Identification of the PARAFAC components

Figure 7.1 shows four selected EEM fluorescence spectra (after data pre-treatment), representative of the typical fluorescence profiles of WSOM and ASOM fractions extracted from atmospheric aerosol samples collected in summer and winter. In spite of the obvious difference in terms of fluorescence intensity between the EEM spectra of the aerosol organic fractions collected in summer and winter seasons, the global fluorescence profile is almost the same for all samples. Therefore, in this work, it was initially assumed that the fluorophore existing in each WSOM and ASOM sample was stable enough to produce a PARAFAC model containing 3 components. Sixty samples of each fraction were used to identify the mathematical components, which might explain the annual variance of each type of fluorescent compounds. A split-half analysis validation method, with the samples being sorted into four subsets according to each sampling season, was used in order to verify this hypothesis. Nevertheless, in this study, it was not possible to validate the PARAFAC model for the whole WSOM samples using the split-half analysis since there are significant differences between the components computed from the summer and winter samples. As a consequence, instead of an annual model, two models were created for the WSOM samples: the first was representative of the warmer seasons, whilst the second was representative of the colder seasons. Each of these models has been validated using the split-half analysis of two subsets, with representative samples of the autumn and winter periods for the colder

seasons, and of spring and summer periods for the warmer seasons. For the colder season model, the explained variance of the model and the core consistency value was 99.66% and 78.40%, respectively, while for the warmer season model these values were 99.79% and 79.97%, respectively. In the case of the ASOM samples, it was possible to validate the PARAFAC model using the four subsets with representative samples of each season, thus ensuring that there are no significant differences in the PARAFAC components throughout the year. In this model, the explained variance of the model and the core consistency value was 99.78% and 83.17%, respectively.

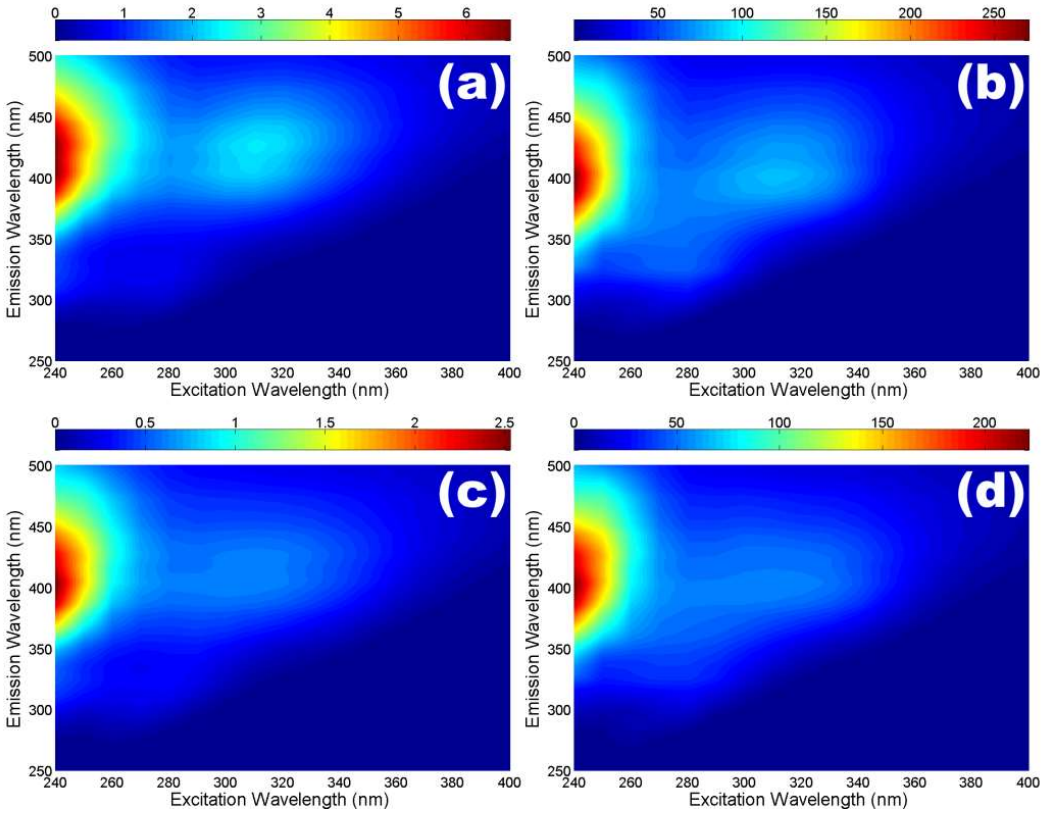

Figure 7.1 EEM spectra (fluorescence intensity in R.U.) from WSOM fractions extracted from aerosol samples collected in (a) Summer and (b) Winter, and from ASOM fractions extracted from aerosol samples collected in (c) Summer and (d) Winter.

These differences in terms of seasonal variability between the PARAFAC models of the WSOM and ASOM samples may be intrinsically linked to the different ranges of OC concentration in the aerosols samples. Table 7.1 summarizes the maximum, minimum and median values of the ambient concentrations of OC, EC, WSOC and alkaline-soluble OC (ASOC) of the urban aerosol samples collected during the colder and warmer seasons in the sampling campaigns I, II, and III, as well as the WSOC/OC and ASOC/OC ratios for these

same seasons. The analytical procedures adopted for the determination of OC and EC content in the aerosol samples, as well as the DOC content of each aqueous and alkaline extract are described in section 3.6 (Chapter 3). The concentrations of OC, WSOC, and ASOC follow a similar seasonal trend, with higher values for the aerosol samples collected in the colder season than for those collected in the warm season. On the other hand, the concentrations of EC do not exhibit a clear seasonal pattern, which is likely to be the end result of the major influence of local anthropogenic primary sources. Furthermore, some remarkable observations were also found for the WSOC/OC and ASOC/OC ratios of the aerosol samples. First of all, unlike what happens with the WSOC and ASOC concentrations, the WSOC/OC and ASOC/OC ratios are higher for the aerosol samples collected in warmer seasons than for those collected in colder season. This fact corroborates the importance of oxidation processes, likely accompanied by compositional changes especially in the WSOM fraction, during the warmer seasons. On the other hand, the differences between the maximum and minimum ASOC/OC values in both seasons are much lower than those for the WSOC/OC values. This occurrence may explain the differences in terms of seasonal variability between the PARAFAC models of the WSOM and ASOM samples, suggesting that the ASOM fraction is likely to be enriched in fluorescent compounds from *in situ* primary sources which are constant throughout the year.

Table 7.1 Maximum (Max), minimum (Min), and median (Med) values for ambient concentrations of $PM_{2.5}$, OC, EC, WSOC, and ASOC (± standard deviation in brackets), and the WSOC/OC and ASOC/OC ratios for the atmospheric aerosols collected in the warmer and colder seasons at the urban location.

		$PM_{2.5}$ (μg m^{-3})	OC (μgC m^{-3})	EC (μgC m^{-3})	WSOC (μgC m^{-3})	ASOC (μgC m^{-3})	WSOC/ OC (%)	ASOC/ OC (%)
Cold season	Min	10.8	1.95 (± 0.04)	0.02 (± 0.01)	0.84 (± 0.06)	0.28 (± 0.01)	21.8	6.70
	Max	37.0	12.9 (± 0.05)	1.44 (± 0.03)	4.95 (± 0.13)	1.82 (± 0.06)	59.8	28.7
	Med	20.1	6.62 (± 0.10)	0.38 (± 0.02)	2.18 (± 0.06)	0.88 (± 0.05)	37.3	14.0
Warm season	Min	9.72	0.57 (± 0.02)	0.11 (± 0.01)	0.37 (± 0.03)	0.05 (± 0.00)	30.0	6.80
	Max	27.0	6.53 (± 0.02)	1.11 (± 0.03)	2.89 (± 0.09)	0.70 (± 0.04)	81.0	36.6
	Med	15.0	2.36 (± 0.07)	0.56 (± 0.06)	1.18 (± 0.09)	0.41 (± 0.02)	49.7	12.6

A PARAFAC model has also been put forward using data obtained for the WSOM samples extracted from the back quartz fibre filters of the tandem filters sampling method from the work of Freire [76]. As described in section 3.2, these samples are only representative of warm seasons. Consequently, this model was validated by the split-half

analysis of two subsets with representative samples from spring and summer periods. In spite of the limited number of samples (12 samples), the explained variance of the model and the core consistency value was 99.42% and 75.65%, respectively.

7.3.2. Spectral features of WSOM and ASOM components

Figure 7.2 shows the three components (C1 to C3) identified by the PARAFAC model for the WSOM samples collected in the warm (Figure 7.2a, Figure 7.2c, and Figure 7.2e) and cold seasons (Figure 7.2b, Figure 7.2d, and Figure 7.2f). Despite the differences between the models (outlined in section 7.3.1), it is possible to find some similarities when comparing the components for each model, i.e., components C1 with the highest contribution for the WSOM PARAFAC models of the warm (Figure 7.2a) and cold seasons (Figure 7.2b); components C2 with an intermediate contribution for the WSOM PARAFAC models of the warm (Figure 7.2c) and cold seasons (Figure 7.2d); and, components C3 with the lowest contribution for the WSOM PARAFAC models of the warm (Figure 7.2e) and cold seasons (Figure 7.2f).

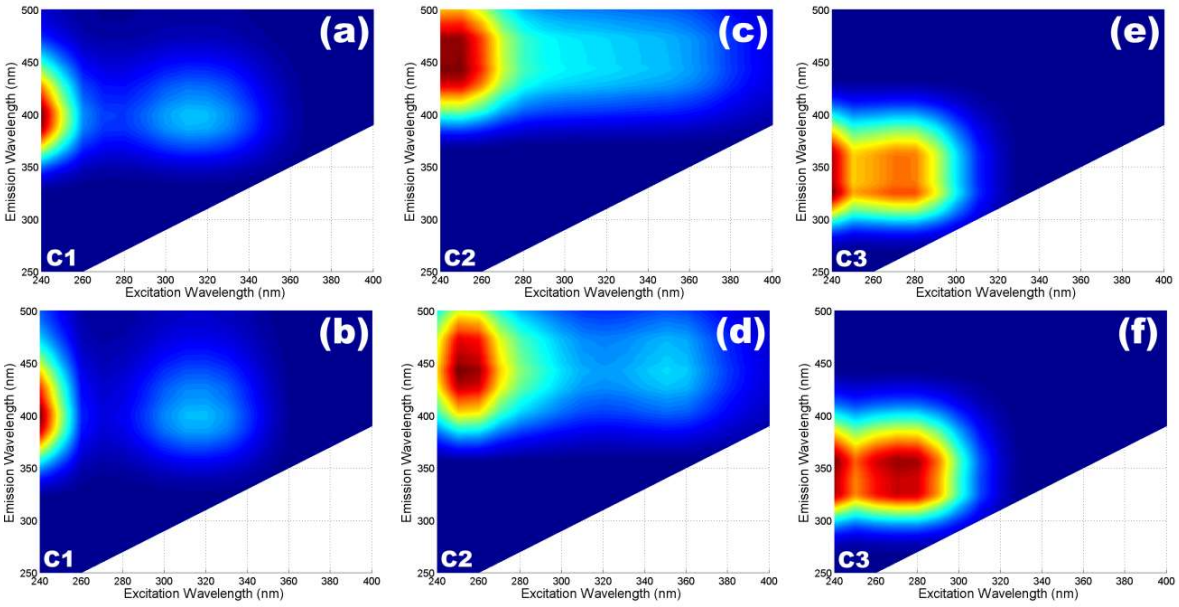

Figure 7.2. Three components (C1 to C3) identified by means of the PARAFAC models for the WSOM samples from the warm (a, c, and e) and cold seasons (b, d, and f).

Based on the location of the excitation and emission maxima of each component (data shown in Table 7.2), it is possible to verify that PARAFAC component C1 is common

to the WSOM samples from both warm (Figure 7.2a) and cold season models (Figure 7.2b). The deviation between the excitation (10 nm) and emission (2 nm) values is considered to be negligible since it is the same as the spacing fot the detector data acquisition. This similarity between seasons for component C1 suggests that the group of fluorophores contributing to this higher florescence intensity is predominantly the same throughout the whole year. On the other hand, the spectral features of PARAFAC component C2 of aerosol WSOM (Figure 7.2c and Figure 7.2d) appears to be different among the two seasons. Although the location of the emission maximum is about the same (at 442 / 444 nm), there is a clear shift in the location of the excitation maximum at lower wavelengths (< 240 nm and 250 nm for the aerosol WSOM from warmer and colder seasons, respectively). This shift to lower wavelengths of the most intense excitation maximum in C2 could be associated with a decrease in the degree of the π-electron system in the WSOM samples from warm season, most likely due to a reduction in the number of aromatic rings, and decomposition and break up of large condensed aromatic moieties into smaller fragments [131]. Furthermore, C2 of aerosol WSOM from cold season has one additional distinct excitation/emission maximum at 350 / 442 nm (Table 7.2), whereas the aerosol WSOM from warm season only shows one excitation/emission maximum. The existence of a second peak at high excitation/emission wavelengths in C2, suggests the existence of a large number of condensed aromatic moieties, conjugated bonds, and nonlinear ring systems. Finally, it is possible to verify that the spectral profile of component C3 is quite similar for both WSOM PARAFAC models (Figure 7.2 e and Figure 7.2f). However, these components in the emission fluorescence spectra are separated in an unexpected bimodal distribution. As shown in Table 7.2, there is a deviation in the location of the absolute maximum of the two bimodal distributions, appearing at 326 nm for the aerosol WSOM from warm season and at 354 nm for the aerosol WSOM from cold season. This may be due to some changes in the proportions of the organic fluorophores associated with these components. However, it is very unlikely that there is a change in the structure of the fluorophores and consequently in the functional groups associated with C3, since there is no obvious shift in the overall profile of this PARAFAC component.

Table 7.2 Spectral characteristics of the three PARAFAC components identified in the EEM datasets of the aerosol WSOM samples from warm and cold seasons, and for the aerosol ASOM samples.

	Component 1 (C1)		Component 2 (C2)		Component 3 (C3)	
	Excitation (nm)	Emission (nm)	Excitation (nm)	Emission (nm)	Excitation (nm)	Emission (nm)
WSOC Warm season	<240 (310)	398	<240	444	<240 (270)	326
WSOC Cold season	<240 (320)	400	250 (350)	442	<240 (270)	354
ASOC	<240 (320)	402	250 (360)	444	<240 (280)	350

Despite the increase in knowledge obtained for the type of components produced by the PARAFAC model for the WSOM samples, only further qualitative considerations can be made about the potential sources responsible for the fluorescent structures associated with such components. To this aim, a comparison was made between the spectral loadings of the PARAFAC components, corresponding to the excitation and emission spectra loadings, of the urban aerosol WSOM from warm season (Figure 7.2a, Figure 7.2c, and Figure 7.2e) and those of the PARAFAC components produced from the EEM datasets of the water extracts of the back filters from the sampling campaigns using the tandem filter method. The similarity of the excitation and emission loadings from the PARAFAC models was evaluated according to their visual representation as shown in Figure 7.3, and quantified by the Tucker's Congruence Coefficient (TCC) as coded in drEEM Toolbox [127]. From the TCC quantification, as pointed out by Lorenzo-seva and Berge [132], results between 0.95 and 1 imply that the two factors or components can be considered equal, and values in the range of 0.85 – 0.94 imply that the two factors are still fairly similar. The excitation and emission loadings (Figure 7.3c) of the C3 component in the aerosol WSOM samples can be considered equal to the corresponding C3 of the water extracts from the back tandem filters, since the TCC is 0.98 and 0.97 for the excitation and emission comparison, respectively. This suggests that not only the organic compounds likely responsible for the adsorptive phenomena are more water-soluble (possibly containing more polar functional groups or being more oxidized than the WIOM [133]) but also secondary formation processes are likely to be the most important contributors to the fluorescent features of urban aerosol WSOM during warmer periods. Similar conclusions can be drawn from the comparison of the C1 components (Figure 7.3a), since they both show the maximum excitation in the same location (i.e., <240 and 330), although the TCC value for the excitation is 0.94. Furthermore, the emission loadings from both C1 components can be considered equal, since they have a TCC value of 0.99.

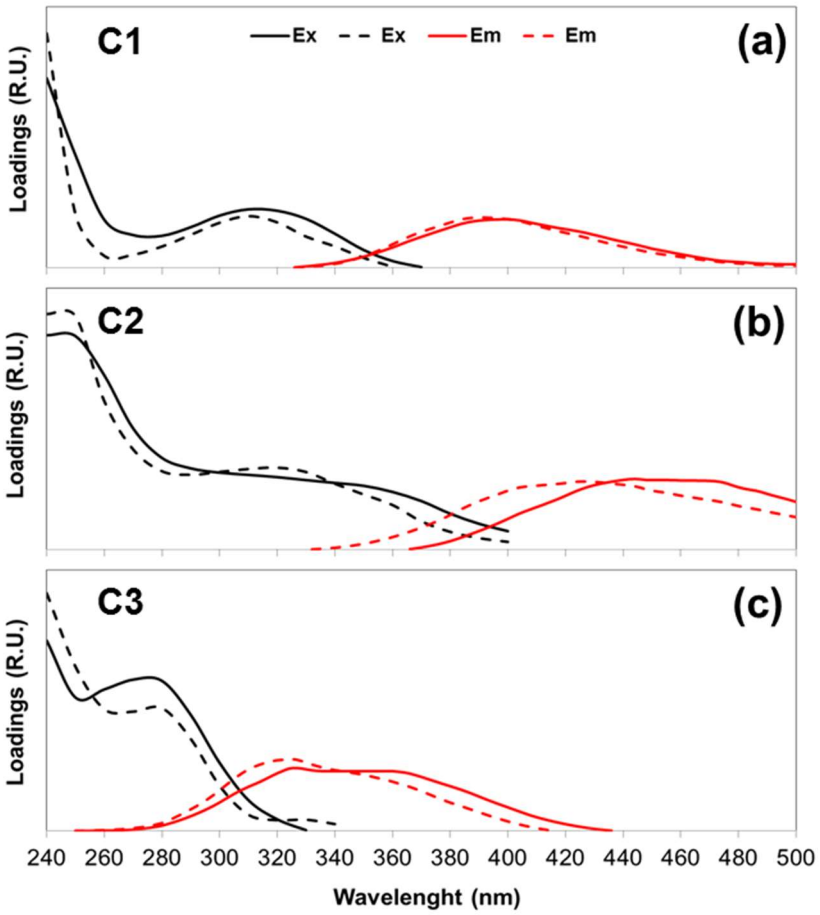

Figure 7.3. Three components (C1 to C3) excitation (Ex) emission (Em) loadings identified by the PARAFAC model for the WSOM samples collected during the warm season in the intensive field campaign (solid line) and for the water extracts of the back filters from the sampling campaigns using the tandem filter method (dashed line).

On the other hand, the fluorescent PARAFAC component C2 of the water extracts from the back tandem filter (Figure 7.3b) shows a deviation for the region of shorter wavelengths in the emission spectra, comparatively to the PARAFAC component C2 of the urban aerosol WSOM also collected during a warmer period. These differences are again highlighted by the lowest value of TCC (i.e., C2 emission value of 0.93). In addition, despite the TCC value for the comparison of both C2 excitations is very high (i.e., 0.99), the excitation loading from the back filters extracts has a second emission peak at 320 nm, while the WSOM samples from the warm season shows a shoulder extended to higher wavelengths (Figure 7.3b). The shift towards high wavelengths for C2 of the urban aerosol WSOM samples suggests that the fluorescent structures contributing to this component could derive from chemical aging processes of OA constituents. As reviewed by Pöschl [2], oxidative modification and degradation of biopolymers may convert these into water-soluble organic

structures. Moreover, condensation reactions and radical-initiated oligo- or polymerization can decrease the volatility of OA constituents and promote the formation of secondary and more water-soluble OA. Therefore, the likely presence of conjugated unsaturated bond systems in the urban aerosol WSOM samples may explain the shift towards high wavelengths of component C2 [134], and this can be used to assess the influence of chemical aging processes into the bulk composition of urban aerosol WSOM.

Figure 7.4 shows the three components loadings identified by the PARAFAC model for the ASOM samples, and ordered according to their contribution to the model. By comparing the results of this PARAFAC model for ASOM with those obtained for both WSOM fractions from warm and cold seasons (Figure 7.2), it is possible to verify that they share similar florescence profiles. Furthermore, the location of the excitation/emission maxima of each of the components (shown in Table 7.2), is almost similar in peak position to the PARAFAC components of the cold season WSOM samples. This fact may be explained by the concentration of the ASOM in the warm samples, which is lower than those collected in colder seasons and, consequently, the relative weight of the cold season samples to the annual ASOM PARAFAC model is higher than those of the warm season.

By using a one-step alkaline extraction procedure for their aerosol samples, Havers *et al.* [135] suggested that the ASOM fraction would have some structures comparable to humic and fulvic acids from soils and aquatic systems. However, in this study, even though a sequential NaOH extraction has been used, no evidence was found to support that this ASOM fraction has structures comparable to humic and fulvic-like substances. Furthermore, the obtained results indicate that no significant fluorescent differences were found to support that WSOM and ASOM have very different chromophoric compounds. Nevertheless, one cannot disregard the possibility of the ASOM fractions to exhibit the same fluorophores functional groups as those of the WSOM fractions, but arranged in different chemical structures.

The general fluorescent profiles of components C1 to C3 identified by the three models (WSOM from warm seasons, WSOM from cold seasons, and ASOM) studied in this work are already well documented for different NOM samples from different environmental matrices [124,136–141], including also atmospheric aerosols [126]. The fluorescence profile of the first and second PARAFAC components, with the highest contribution in each model,

are traditionally associated with humic-like materials of terrestrial and aquatic origin [126,136–141]. However, it is necessary to be cautious when associating the spectral features of components C1 and C2 with those of humic-like substances occurring in water and soils, since these are unlikely to resemble the NOM occurring in atmospheric aerosols. In fact, there are already some studies that point towards this direction. For example, Duarte *et al.* [15] compared the structural features of aquatic fulvic and humic acids to those of the WSOM from atmospheric aerosols and concluded that the former are not good models for describing aerosol WSOM. Consequently, associating PARAFAC components C1 and C2 to the fluorescence profiles of humic-like materials from terrestrial and aquatic environments leads to a scenario where a huge fraction of aerosol NOM is being characterized incorrectly.

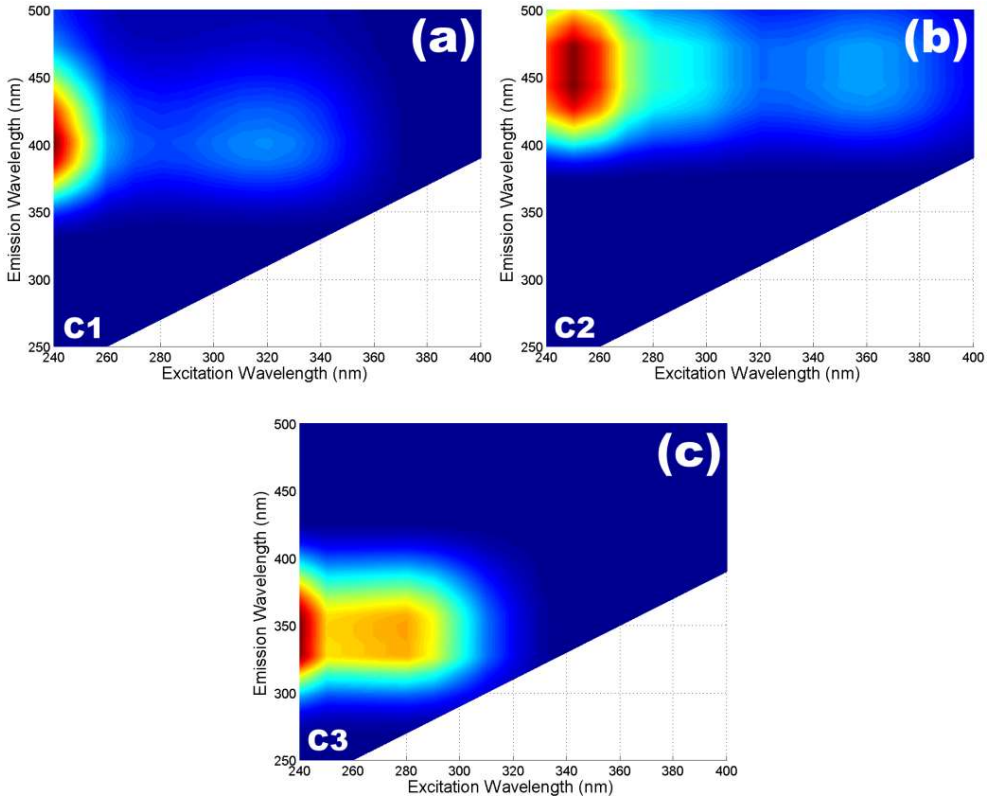

Figure 7.4. Three components (C1 to C3) identified by means of the PARAFAC models for the urban ASOM samples.

The spectral features of PARAFAC component C3, the one with the lower contribution in each model (WSOM from warm seasons, WSOM from cold seasons, and ASOM) are usually associated with proteinaceous-like material [126,136,138,140,141]. Recent studies that attempted to quantify proteins in atmospheric aerosols concluded that the

concentrations of total protein are usually quite low [22]. Nevertheless, since these C3 components are in a fluorescence region of low wavelength and high energy, the presence of protein-like substances remains plausible. Another possible explanation for the occurrence of component C3 has been proposed by Mladenov *et al.* [126], who have also reported the presence of a fluorescence peak in a similar position to that of C3 and associated this maximum with the fluorescence peak of naphthalene, a compound released from diesel combustion, which is very likely to occur in urban areas due to car traffic.

7.3.3. WSOM and ASOM seasonal variation

On the basis of the quantitative information describing the distribution of the three PARAFAC components in each sample, an attempt was carried out to assess the seasonal variations of the fluorophores in both WSOM and ASOM from atmospheric aerosols. Figure 7.5a depicts the values of fluorescence intensity at the maximum (F_{max}) for the components of the WSOM PARAFAC models from the cold (dark colours) and warm seasons (bright colours). It is necessary to bear in mind that, despite the similarities of the fluorescent profiles of the WSOM PARAFAC components from cold and warm seasons (shown in section 7.3.1), these components are originated from two different models, which may limit the conclusions drawn in this comparison. Figure 7.5b shows the F_{max} values for the three PARAFAC components identified for the ASOM fractions across the different seasons. For both WSOM and ASOM samples, the F_{max} values of the three PARAFAC components exhibit a similar profile of F_{max} intensities. Furthermore, the F_{max} intensity of the three components from ASOC PARAFAC model represents nearly 20 to 40% of the total intensity of the organic fractions under study.

On the whole, the components from WSOM and ASOM fractions have higher F_{max} values in the cold seasons than in the warm seasons, which may be explained by the decrease in atmospheric temperatures causing a shift of the SVOCs from the gas phase into the particulate phase, therefore increasing the concentration of OA in periods of low air temperature conditions. Nevertheless, one cannot disregard the occurrence of other factors affecting the partitioning phenomena of the SVOCs throughout the seasons (e.g., the nature of the aerosol and the low impact of atmospheric reactions during cold seasons) which could also affect the values of F_{max} [142]. Another possible explanation is the increase in

atmospheric particles concentration originated from combustion of fossil fuels for domestic heating [15,35]. However, there are two seasons which show an exception to the F_{max} seasonal profile: Sum. B from 2010 and Sum. B from 2013. Contrary to what would be expected, in these two warm seasons, the F_{max} intensities had a substantial increase in intensity, whose occurrence cannot be explained by the decrease in atmospheric temperature. One possible reason for this remarkable increase in intensity may be the occurrence of forest fires near the sampling site. As shown in Figure 7.5c, during the sampling periods of Sum. B from 2010 and Sum. B from 2013, there was a wide occurrence of large forest fires events in the surrounding regions of the sampling area. The release into the atmosphere of a high amount of chromophoric organic particles derived from the combustion of forest wood can thus be a fairly plausible justification for the unexpected increase in the F_{max} intensities in these two summer periods.

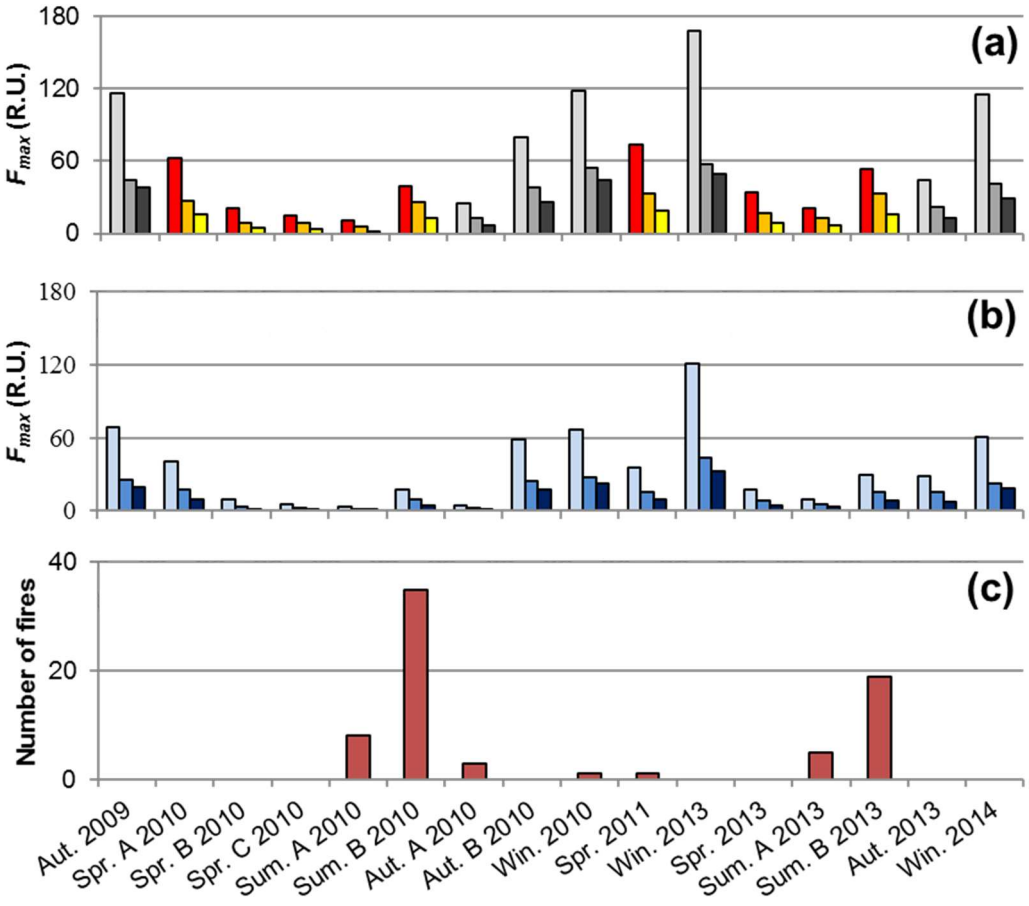

Figure 7.5. F_{max} of the three components PARAFAC-ALS models for (a) WSOM samples (■ C1, ■ C2, and ■ C3 from cold seasons; and ■ C1, ■ C2, and ■ C3 from warm seasons) and (b) ASOM samples (■ C1, ■ C2, and ■ C3), throughout the seasons. (c) Number of large forest fires that occurred in Portugal in the surrounding regions of the sampling site.

Although the F_{max} values from all PARAFAC components, for both WSOM and ASOM fractions, have the same seasonal profile, the F_{max} fluctuation of each component is neither equal nor proportional along the various seasons. Figure 7.6 shows the ratios between $F_{max}1$, $F_{max}2$, and $F_{max}3$ (F_{max} from the components with the highest, the second highest and the lowest contribution, respectively) and their fifth order polynomial trend lines, for the WSOM models (Figure 7.6a, Figure 7.6c, and Figure 7.6e) and for the ASOM models (Figure 7.6b, Figure 7.6d, and Figure 7.6f). The results for 2011 spring season were removed from these figures, since this is the only sample from the warm seasons of this year and their presence would incorrectly change the profile of the trend line. However, the values obtained for this season were equal to those obtained for the remaining spring seasons.

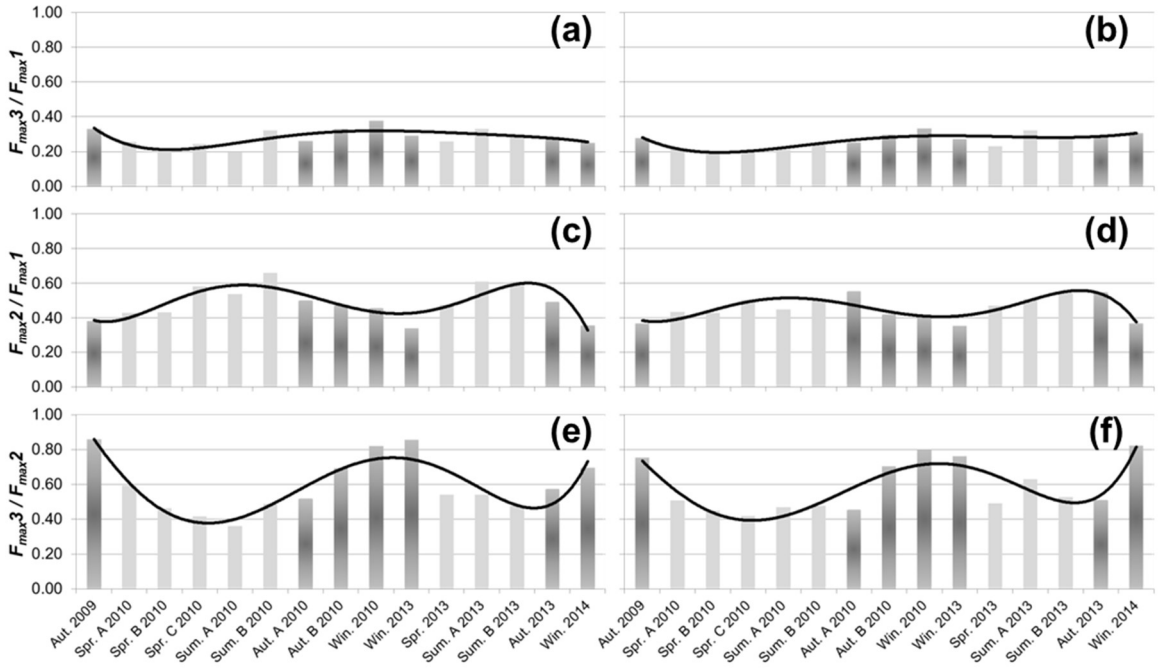

Figure 7.6. Ratio and respective fifth order polynomial trend line for (a) $F_{max}3/F_{max}1$ from WSOM PARAFAC components, (b) $F_{max}3/F_{max}1$ from ASOM PARAFAC components, (c) $F_{max}2/F_{max}1$ from WSOM PARAFAC components, (d) $F_{max}2/F_{max}1$ from ASOM PARAFAC components, (e) $F_{max}3/F_{max}2$ from WSOM PARAFAC components, and (f) $F_{max}3/F_{max}2$ from ASOM PARAFAC components.

The way in which $F_{max}1$ and $F_{max}3$ from the WSOM PARAFAC change over the seasons is quite similar, since the $F_{max}3/F_{max}1$ ratio (Figure 7.6a) and its trend line are constant throughout the seasons, being the $F_{max}3$ value approximately one-third of the value of $F_{max}1$. These results suggest that these two components may share similar origins and are affected by the same type of meteorological variables (e.g., air temperature). On the other

hand, the $F_{max}2/F_{max}1$ ratio from the WSOM PARAFAC results (Figure 7.6c) shows a seasonal trend with low values in the cold seasons, and high values in the warm seasons. This ratio implies that these two components have different origins and/or are affected differently by the weather conditions throughout the seasons. Moreover, a seasonal trend, but now with low values in warm seasons and high values in cold seasons, also appears for the $F_{max}3/F_{max}2$ ratio from the WSOM PARAFAC results (Figure 7.6e). This seasonal profile is opposite to that obtained for the $F_{max}2/F_{max}1$ ratio in Figure 7.6c, being easily explained by the fact that $F_{max}2$ in Figure 7.6e is now in the denominator of the ratio. Still, the trend obtained for this ratio is in line with the other two ratios ($F_{max}2/F_{max}1$ *and* $F_{max}3/F_{max}2$), suggesting that the components with the highest and lowest contribution to the WSOM PARAFAC model had similar origins and fate in the atmosphere, but these characteristics are not shared by the second component. The proportion of $F_{max}2$ values compared to $F_{max}1$ change from about 0.3 in the cold seasons to about 0.6 in warm seasons. In their turn, $F_{max}3$ values compared to $F_{max}2$ change from approximately 0.8 in the cold seasons to approximately 0.4 in the warm seasons. The increase in the $F_{max}2$ value in the warm seasons in relation to $F_{max}1$ and $F_{max}3$ may be explained by the increase of oxidation phenomena and other chemical aging processes during the warm season, which appears to be in accordance with the results obtained in section 7.3.2 regarding the possible sources/origin of the compounds associated with each PARAFAC component.

7.4. Conclusions

In this chapter, a non-target approach was applied for unravelling the bulk chemical composition of WSOM and ASOM sequentially extracted from urban atmospheric aerosols, in an attempt to link their fluorescent characteristics to their seasonal variability. Regarding the characteristics of the WSOM fraction, some profile changes were identified by PARAFAC modelling of EEM datasets of aerosol WSOM samples collected in the warm and cold seasons. These changes were associated with the decrease of degree of unsaturated π-bond systems in the samples from warmer seasons comparatively to those of the cold seasons. It has been also concluded that oxidation phenomena and other chemical aging processes (e.g., condensation reactions and radical-initiated oligo- or polymerization) may

have an important contribution for the fluorescence features of urban aerosol WSOM samples collected during warm seasons. On the other hand, PARAFAC modelling of the EEM datasets of aerosol ASOM seem to indicate that the fluorescent features of this fraction are more constant throughout the year, therefore, suggesting that the ASOM may be enriched in fluorescent compounds with an *in situ* origin. Additionally, no evidence has been found that ASOM fraction is structurally different from WSOM fraction. Nevertheless, this study cannot be considered conclusive about this topic since, despite proven advantages, the EEM fluorescence spectroscopy is blind to compounds that do not show any fluorescence, e.g., more aliphatic and saturated compounds.

The fluorescence intensity of the components from the PARAFAC models appear to be strongly influenced by the season of the year, showing high values in the cold seasons and low values in the warm seasons. The only exceptions were found for samples collected in the warm seasons of Sum. B from 2010 and Sum. B from 2013. The samples collected in these two seasons showed an anomalous increase of the fluorescence intensity, which appear to be related to the occurrence of forest fires, being in line with the fact that burning of forest wood is a large source of emissions of organic matter into the atmosphere.

Chapter 8

^{1}H NMR studies of WSOM and ASOM

In this chapter, solution-state ^{1}H NMR spectroscopy was applied to characterize the structural features of WSOM and ASOM hydrophobic acids, in order to compare the main functional characteristics and assess the sources of these two OA fractions at an urban location.

8.1. Introduction

As extensively reviewed in section 2.3.2, solution-state ^{1}H NMR spectroscopy, has become one of the most predominant techniques in the study of OA, namely their water-soluble fraction, since it has proved to be a very useful tool for both unraveling the functional and structural group composition of OA, and aerosol source identification.

In this chapter, the solution-state ^{1}H NMR spectroscopy was employed to investigate the structural characteristics of the WSOM and ASOM hydrophobic acids, extracted from fine atmospheric aerosols collected over different seasons. The acquired ^{1}H NMR data of both aerosol WSOM and ASOM hydrophobic acids was further interpreted as fingerprints for source contribution analysis, following the method of Decesari *et al.* [15]. With this study it is expected to obtain a deeper insight into the yet unsolved structural composition of aerosol ASOM, and to understand possible composition variations in both WSOM and ASOM fractions due changes in their sources and seasonal conditions at an urban location.

8.2. Materials and methods

8.2.1. WSOM and ASOM hydrophobic acids

This study was conducted using the WSOM hydrophobic acids and ASOM hydrophobic acids fractions from six samples representative of different seasons: Aut. 2009, Sum. A 2010, Sum. B 2010, Aut. B 2010, Win. 2010, and Spr. 2011. All the information regarding these samples, as well as the procedures for extraction and isolation are already described in Chapter 3.

Average ambient concentrations of $PM_{2.5}$, OC, WSOC, ASOC, and isolated WSOM and ASOM hydrophobic fractions from urban atmospheric aerosols, are summarized in Table 8.1.

Table 8.1 Average ambient concentrations of $PM_{2.5}$ OC, EC, WSOC, ASOC, and isolated WSOM and ASOM hydrophobic fractions from urban atmospheric aerosols during the six seasonal periods of the Sampling campaign I (± standard deviation in brackets).

Season	$PM_{2.5}$ (μg m^{-3})	OC (μg C m^{-3})	WSOC (μg C m^{-3})	ASOC (μg C m^{-3})	WSOC hydrophobic (μg C m^{-3})	ASOC hydrophobic (μg C m^{-3})
Aut. 2009	22.2 (± 3.8)	7.71 (± 0.39)	2.68 (± 0.23)	1.06 (± 0.13)	1.36 (± 0.13)	0.21 (± 0.06)
Sum. A 2010	14.6 (± 7.9)	1.07 (± 0.06)	0.66 (± 0.20)	0.16 (± 0.01)	0.28 (± 0.01)	0.06 (± 0.01)
Sum. B 2010	22.9 (± 3.6)	4.84 (± 0.09)	1.82 (± 0.13)	0.43 (± 0.05)	0.90 (± 0.11)	0.21 (± 0.04)
Aut. B 2010	22.3 (± 7.5)	6.80 (± 0.10)	1.86 (± 0.07)	0.98 (± 0.10)	0.96 (± 0.03)	0.23 (± 0.07)
Win. 2011	24.1 (± 9.3)	8.22 (± 0.12)	3.12 (± 0.20)	1.04 (± 0.10)	1.57 (± 0.02)	0.20 (± 0.03)
Spr. 2011	19.2 (± 2.5)	4.99 (± 0.10)	2.22 (± 0.18)	0.50 (± 0.09)	0.99 (± 0.03)	0.13 (± 0.04)

8.2.2. Solution-state ^{1}H NMR spectroscopy

All ^{1}H NMR spectra were acquired on a Bruker Avance-500 spectrometer operating at 500.13 MHz, equipped with a liquid nitrogen cooling CryoProbe. All spectra were run at 22 °C, under the following conditions: i) pulse with of 3.83 μsec; b) acquisition time of 2.97 sec; c) 64 k data points; d) spectral with of 11029 Hz; e) recycle delay of 1 sec; and f) 1024 scans. The dried WSOM and ASOM hydrophobic acids samples (approximately 8 mg) were dissolved in deuterated methanol (MeOH–d_4, 1 mL) and transferred to 5 mm NMR tubes. Due to the insufficient amount of ASOM fraction extracted from the Sum. A 2010 sample, it was impossible to acquire its ^{1}H NMR spectrum and only the WSOM fraction was analyzed. The identification of functional groups in the ^{1}H NMR spectra was based on their chemical shift relative to the central solvent (MeOH–d_4) peak set at δ ^{1}H 3.31 ppm.

8.3. Results and discussion

8.3.1. Solution-state ^{1}H NMR spectroscopy of WSOM and ASOM

Figure 8.1 presents the solution-state ^{1}H NMR spectra of WSOM and ASOM hydrophobic acids extracted from fine aerosol samples collected in Aut. 2009, Sum. B 2010,

Aut. 2010, Win. 2010, and Spr. 2011. Overall, all ^{1}H NMR spectra comprises a complex overlapping profile with broad bands superimposed by a relatively small number of sharp peaks. Although the characterization of specific individual organic species becomes difficult, four main categories of functional groups carrying C–H bonds can be identified: (i) δ ^{1}H 0.5 – 1.9 ppm for protons bound to carbon atoms of straight and branched aliphatic chains (C–H), which includes protons from methyl (R–CH_3), methylene (R–CH_2), and methyne (R–CH) groups; (ii) δ ^{1}H 1.9 – 3.2 ppm for protons bound to carbon atoms in α-position to unsaturated groups in allylic (H–C_α–C=), carbonyl or imino (H–C_α–C=O or H–C_α–C=N) groups, and protons in secondary and tertiary amines (H–C=NR_2 and NR_3); (iii) δ ^{1}H 3.3 – 4.1 ppm for protons bound to oxygenated saturated aliphatic carbon atoms (H–C–O) in alcohols, polyols, ethers, esters, and organic nitrate (R–CH_2–O–NO_2); and (iv) δ ^{1}H 6.5 – 8.3 ppm for protons bound to aromatic carbon atoms (Ar–H), although alkenes protons in conjugated systems can also resonate within this chemical-shift range.

For a further exploration of the ^{1}H NMR data, a quantitative integration of each spectral region was performed in order to assess the abundance of each functionality in the WSOM and ASOM hydrophobic acids, as shown in Figure 8.2. The data from Sum. A 2010 WSOM hydrophobic acids is also shown in Figure 8.2. Integrated regions for WSOM and ASOM hydrophobic acids showed a similar ^{1}H NMR profile as those reported in previous studies of WSOM form aerosols collected in industrial locations [143] and during biomass burning campaigns [144]. For both WSOM and ASOM hydrophobic acids, the saturated aliphatic protons are the most important component, followed by unsaturated and oxygenated aliphatic protons, and a lower contribution from aromatic protons. The aliphatic structures exhibit a seasonal trend, with a distinct maximum of 57.5% in Sum. A 2010 and a minimum of 44.3% in Win. 2010 season for WSOM hydrophobic acids, and a maximum of 67.1% in Sum. B (the spectra of Sum. A 2010 ASOM hydrophobic acids was not acquired) and a minimum of 47.6% in Win. 2010 season for ASOM hydrophobic acids. It is noteworthy that within each season, the ASOM hydrophobic acids exhibits a consistently higher amount of aliphatic protons than the WSOM hydrophobic acids. For most samples, two groups of peaks can be distinguished in the saturated aliphatic region at 0.8 – 0.9 ppm and 1.0 – 1.4 ppm, corresponding to methyl (CH_3) and methylenic (CH_2) protons, respectively. The CH_2/CH_3 ratio in both WSOM and ASOM hydrophobic acids are in the order of magnitude of 4 and 5, respectively, suggesting that the aliphatic structures in both

fractions have different chain lengths, being slightly higher for the ASOM hydrophobic acids.

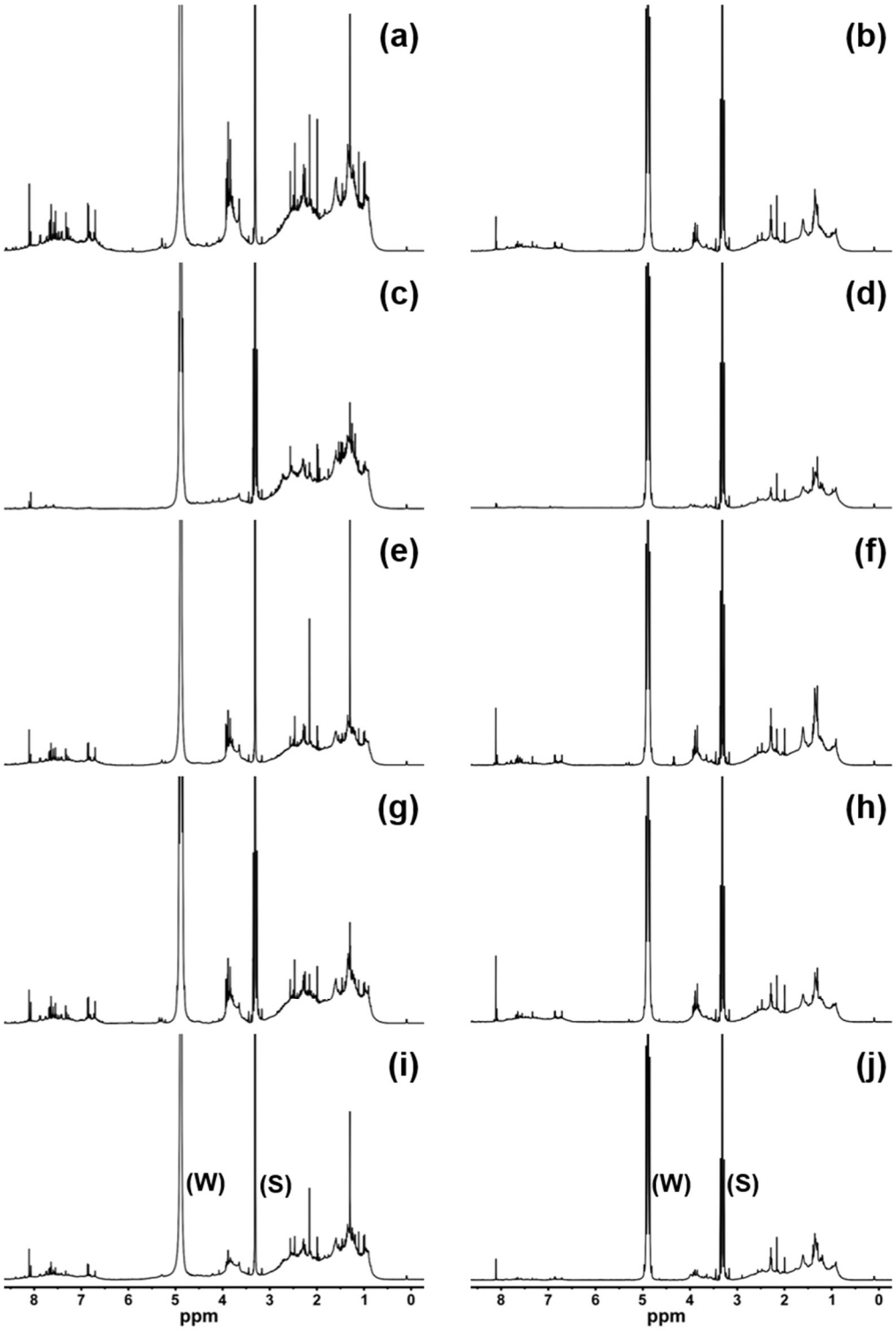

Figure 8.1 500 MHz solution-state ^{1}H NMR spectra of WSOM hydrophobic acids from (a) Aut. 2009, (c) Sum. B 2010, (e) Aut. B 2010, (g) Win. 2010, and (i) Spr. 2011 seasons, and the ASOM hydrophobic acids from (b) Aut. 2009, (d) Sum. B 2010, (f) Aut. B 2010, (h) Win. 2010, and (j) Spr. 2011 seasons. Resonance signals: Water (W) and Solvent (S) – MeOH–*d4*.

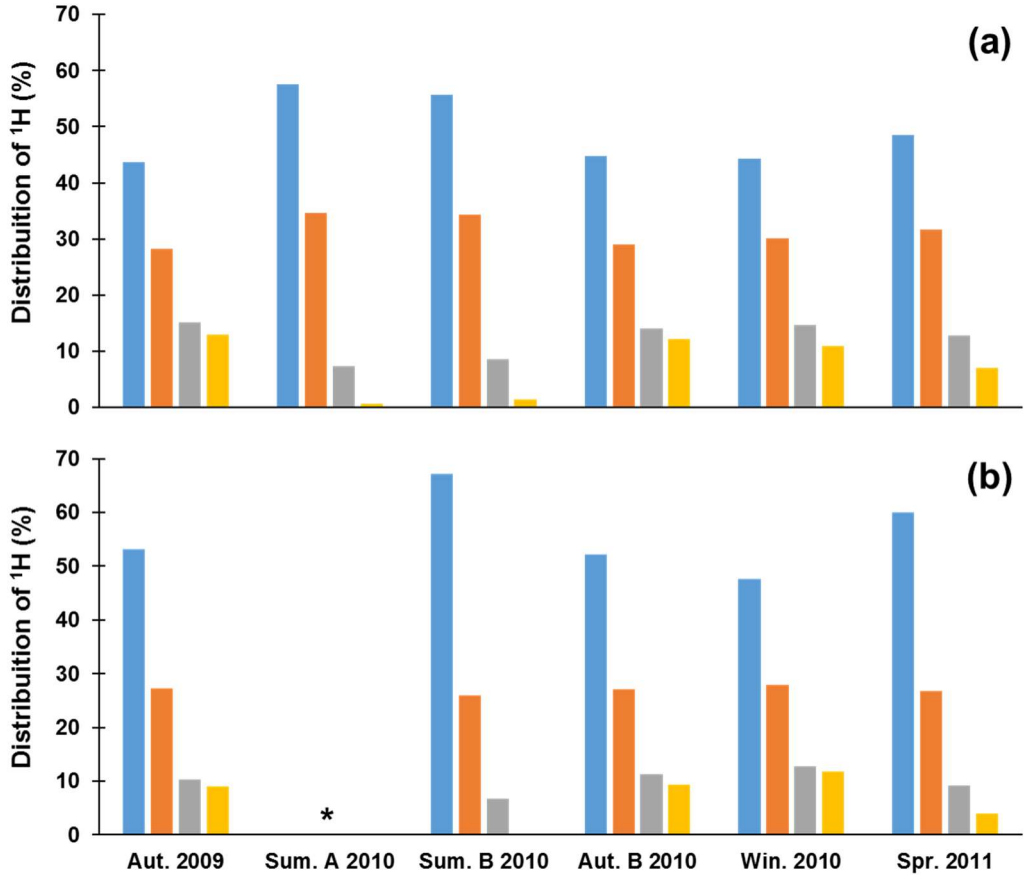

Figure 8.2 Percentage distribution of ^{1}H functional groups (i.e., H–C, H–C–C=, H–C–O, and Ar–H), from (a) WSOM and (b) ASOM hydrophobic acids from fine urban aerosol samples collected during different seasons. (*) denotes data unavailable for ASOM hydrophobic acids from Sum. A 2010 season.

Additional differences between the WSOM and ASOM hydrophobic acids are found in the spectral region associated with protons bound to unsaturated structures (H–C–C=). The WSOM hydrophobic acids show higher relative peak areas in this region than the ASOM hydrophobic acids (on average, 31.3 and 26.9%, respectively). Moreover, the relative abundance of this area in the WSOM hydrophobic acids is higher for the warmer season samples than for colder season samples, whereas no seasonal trend was observed for the ASOM fractions. This feature suggests that the WSOM hydrophobic acids is more selective for unsaturated compounds, which might be capable of contributing to sunlight absorption.

For both WSOM and ASOM hydrophobic acids, protons bound to oxygenated groups also exhibit a seasonal trend, increasing from warmer to colder seasons. The relative abundance of this area is lower in Sum. B 2010 (8.7 and 6.8%, for WSOM and ASOM hydrophobic acids, respectively), and higher in Win. 2010 (14.7 and 12.7%, for WSOM and

ASOM hydrophobic acids, respectively). These results suggest that the two solvents employed in this study may extract similar chemically portions of oxygenated components from the whole OA. The relative abundance of the spectral region assigned to aromatic protons also exhibit a seasonal trend, with higher percentages being found for both WSOM and ASOM hydrophobic acids collected in colder seasons, which could be attributed to wood-burning processes for house heating [57,60,145]. This phenomenon is also reflected in the increase of the relative abundance of protons bound to oxygenated groups for these samples, which usually suggests the presence of lignin-like compounds released from biomass burning processes [146]. Regarding the differences between the WSOM hydrophobic acids collected in Sum. A 2010 and Sum. B 2010, although both WSOM hydrophobic acids exhibit a similar NMR profile, the sample collected during Sum. A 2010 has somewhat lower percentages of oxygenated and aromatic protons than WSOM hydrophobic acids collected during Sum. B 2010 season. These differences could be due to the prevalence of forest fire events during the later season. Moreover, regarding the difference within the WSOM and ASOM hydrophobic acids collected in Aut. 2009 and Aut. 2010 seasons, the quantitative integration of ^{1}H NMR spectral regions, demonstrate that both WSOM and ASOM hydrophobic acids have similar chemical characteristics regardless of the year. This result poses now the question whether this feature also occurs for other seasons, which implies further long-term studies.

8.3.2. Source apportionment of WSOM and ASOM samples

In order to determine whether the ^{1}H functional group distribution could indicate the sources of both aerosol WSOM and ASOM hydrophobic acids, the source apportionment technique developed by Decesari *et al.* [37] was applied to all samples. By plotting the ratios of calculated carbonyl and carboxylic aliphatic groups (H–C–C=O)-to-total aliphatics (H–C–C=O/∑Aliphatics) and oxygenated aliphatic groups (H–C–O)-to-total aliphatics (H–C–O/∑Aliphatics), Decesari *et al.* [37] created source boundaries for marine OA (MOA), SOA, and aged biomass burning OA (BBOA). The contribution of H–C–C=O groups is indirectly estimated by subtraction of benzylic groups (assumed to be 16.7% of the measured H–Ar signal) from the measured H–C–C= signal. The total aliphatic carbon

includes the unfunctionalized alkyls (H–C), the unsaturated aliphatic groups (H–C–C=), and the oxygenated functional groups (H–C–O).

Figure 8.3 depicts the locations of the urban WSOM and ASOM hydrophobic acids collected in this study, in relation to the three aforementioned WSOC sources proposed by Decesari *et al.* [37]. Overall, the H–C–C=O/∑Aliphatics ratio range from 0.18 to 0.32 for the WSOM hydrophobic acids and 0.18 to 0.24 for the ASOM hydrophobic acids, whereas the H–C–O/∑Aliphatics ratio range from 0.13 to 0.28 for the WSOM hydrophobic acids, and from 0.12 to 0.23 for the ASOM hydrophobic acids. These results demonstrate that both WSOM and ASOM hydrophobic acids fell outside of the three specific fingerprint sources previously established, especially in the contribution of the H–C–C=O groups, thus suggesting that these urban OA fractions are less oxidized than those of the predefined fingerprints.

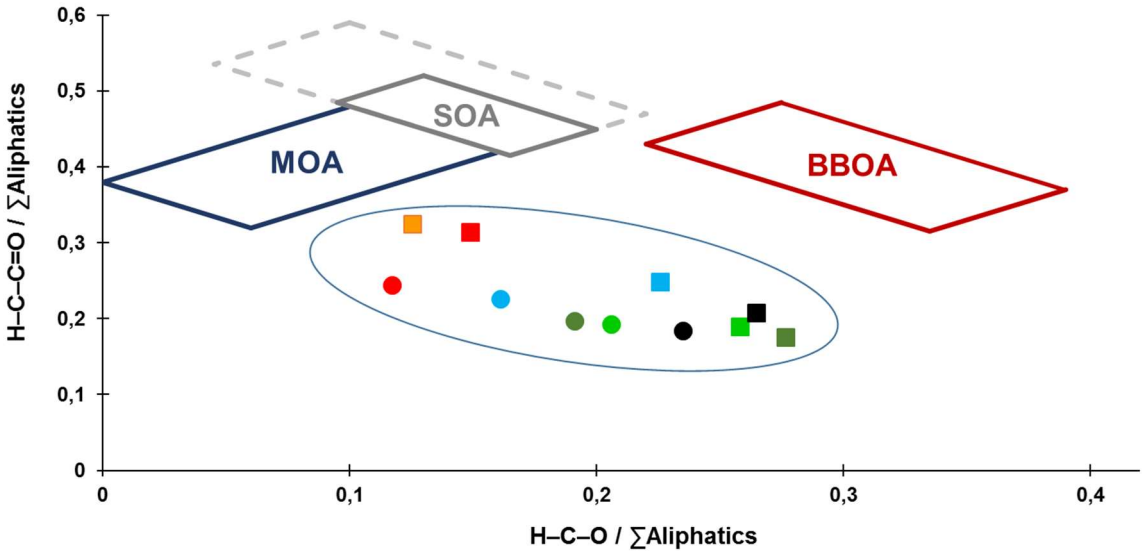

Figure 8.3 Functional group distributions for WSOM ■ Aut. 2009, ■ Sum. A 2010, ■ Sum. B 2010, ■ Aut B 2010, ■ Win. 2010, and ■ Spr. 2011 hydrophobic acids, and ASOM ● Aut. 2009, ● Sum. B 2010, ● Aut. B 2010, ● Win. 2010, ● Spr. 2011 hydrophobic acids from the fine urban aerosol samples based on the analysis of Decesari *et al.* [37]. Boxes represent boundaries for MOA, SOA, and BBOA.

It must be emphasized that the source attribution scheme of Decesari *et al.* [37] is focused on the total WSOM, whereas the present study targets only the hydrophobic acid fraction of the whole aerosol WSOM extract. In order to exclude the hypothesis that the isolation protocol is exerting a bias in WSOM composition between this study and that of Decesari *et al.* [37], a seven-day $PM_{2.5}$ sample was collected in the early autumn of 2014

(October). Its aqueous extract was freeze-dried and the obtained residue was dissolved in MeOH–*d4* for further NMR analysis of the total WSOM. The ^{1}H NMR spectra of this WSOM extract is available in Annexes (Figure A. 5). The calculated H–C–C=O/∑Aliphatics and H–C–O/∑Aliphatics ratios were 0.27 and 0.23, respectively, which are in the range of those obtained for the WSOM hydrophobic fractions. These results suggest that the employed WSOM isolation protocol (section 3.5) is unlikely to affect the comparison between this study and that of Decesari *et al.* [37], and the WSOM hydrophobic fractions can be considered as good proxies of the total aerosol WSOM.

The H–C–C=O/∑Aliphatics ratio also decreases from warmer to colder seasons, in about 45% for the WSOM hydrophobic acids and 24% for the ASOM hydrophobic acids. The H–C–C=O/∑Aliphatics ratios are also typically higher for WSOM than for ASOM fractions, underscoring the less oxidized character of the latter. This trend is more pronounced during the warmer season than during the colder periods. A higher oxidation level is usually associated to SOA formation [147]. However, the fact that data points for WSOM hydrophobic acids are falling outside the SOA boundaries during summer seems to be inconsistent with SOA being the main component of OA during warmer periods. This fact suggests that in the context of the studied urban area, the SOA might not correspond to the traditional definition generally accepted in aerosol science. This has been also referred by Gelencsér *et al.* [107] for six sites across south-central Europe, including a rural location near the city of Aveiro. In this site, fossil fuel SOA was found to account for up to 20% of the total aerosol carbon, thus suggesting that the contribution of SOA from fossil fuel combustion becomes higher in near-source areas. Primary sources should also influence the ASOM hydrophobic acids in a greater extent, and the lower percentage of variation of the H–C–C=O groups between samples may be a sign that primary emissions are likely to be constant throughout the year. Noteworthy, both WSOM and ASOM hydrophobic acids of the colder seasons exhibit similar H–C–C=O/∑Aliphatics ratios, suggesting that the primary sources may prevail over the secondary sources and they influence in an equal manner both fractions during these seasons. The H–C–C=O/∑Aliphatics ratios of both WSOM and ASOM hydrophobic acids collected in Aut. 2009 and Aut. B 2010 are also very similar, thus suggesting that the emissions sources of OA in the studied urban area should also be constant over the years, during at least the colder periods.

The fractional contribution of H–C–O did not vary outside of the values for the pre-established source regions (Figure 8.3). The H–C–O/∑Aliphatics ratios increase from warmer to colder seasons for both WSOM and ASOM hydrophobic acids. Although falling outside the pre-established boundaries of biomass burning, the higher H–C–O/∑Aliphatics ratios for the Aut. B 2010 and Win. 2010 samples could have a contribution from wood-burning emissions from house heating in these periods [146]. The effect of biomass burning emissions might also explain the differences between the WSOM hydrophobic acids collected in Sum. A 2010 and Sum. B 2010, with the latter exhibiting a higher H–C–O/∑Aliphatics ratio than the former due to the higher number of forest fires.

The results here obtained demonstrate that the boundaries of the signature boxes described by Decesari *et al.* [37], especially for SOA and biomass burning, might be different at the city of Aveiro. The lower fractional contribution of H–C–C=O groups for the urban OA and, therefore, the lower level of oxidation in comparison to the previous established source fingerprints, is in agreement with the ^{1}H NMR source apportion results of Cleveland *et al.* [56] for an industrial urban center. All these findings suggest not only the existence of distinct ^{1}H NMR signatures for different sources of OA, but also the need to improve the available source attribution data by extending this approach to other urban OA.

8.4. Conclusions

The ^{1}H NMR analysis showed that urban aerosol WSOM and ASOM hydrophobic acids hold similar proton functional groups; however, they differ in terms of their relative distribution throughout the sampling campaign I. In both fractions, the saturated and unfunctionalized aliphatics are the most abundant group, followed by the unsaturated and oxygenated aliphatic structures, and a less contribution from aromatic groups. The ^{1}H NMR data further demonstrated that winter and autumn samples are distinct from those of warmer conditions, in that they have a less aliphatic and oxidized character and higher contributions from aromatic structures.

The NMR data were also compared to the ^{1}H NMR source apportionment scheme of Decesari *et al.* [37] for MOA, SOA, and aged BBOA. This exercise failed to classify specific

source influences, and the majority of the urban WSOM and ASOM hydrophobic acids did not fall into any of the pre-determined categories. The studied samples displayed a significantly smaller contribution of H–C–C=O groups due to the lower level of oxidation, which seems to be consistent with the likely local anthropogenic origin of fine OA. It has been suggested that the boundaries of the signature boxes, especially for SOA and biomass burning, might be different at urban locations, thus requesting an improvement of the established ^{1}H NMR source apportionment model for including urban OA.

Chapter 9

Decoding the structural features of WSOM and ASOM using 2D NMR

This chapter describes the synergistic combination of 2D NMR techniques, namely $^{1}H-^{1}H$ COSY, $^{1}H-^{13}C$ HSQC, and $^{1}H-^{13}C$ HMBC, for decoding the structural and molecular information of WSOM and ASOM hydrophobic acids, sequentially extracted from fine atmospheric aerosols collected in an urban setting during Winter and Summer seasons.

9.1. Introduction

In order to further advanced understanding of the molecular nature of WSOM and ASOM hydrophobic acids, in this chapter is introduced a combination of 2D NMR techniques, namely gradient-selected $^{1}H-^{1}H$ *g*COSY, $^{1}H-^{13}C$ *g*HSQC, and $^{1}H-^{13}C$ *g*HMBC, allowing to identify the main substructures present in these two fractions, which have been sequentially extracted from fine urban aerosols collected over different seasons. Such multifaceted approach was used for providing additional and deeper understanding of the structural dynamics of both aerosol WSOM and ASOM hydrophobic acids, as well as deciphering their major sources over seasons. The spectral data and derived structural features were also used to build a semi-quantitative model of the most atmospherically-relevant structures in urban aerosol WSOM hydrophobic acids.

9.2. Materials and methods

9.2.1. WSOM and ASOM hydrophobic acids

This study was conducted using the WSOM hydrophobic acids extracted and isolated from Sum. A 2010, Sum. B 2010, and Win. 2010 samples and ASOM hydrophobic acids extracted and isolated from Sum. B 2010, and Win. 2010 samples. All the information regarding these samples, as well as the procedures for extraction and isolation have been already described in Chapter 3.

9.2.2. Solution-state 2D NMR spectroscopy

All 2D NMR spectra were acquired using a Bruker Avance-500 spectrometer operating at 500.13 and 125.77 MHz for ^{1}H and ^{13}C, respectively, and equipped with a liquid nitrogen cooling CryoProbe Prodigy^{TM}. Approximately 8 mg of each dried WSOM and ASOM hydrophobic acids sample was dissolved in deuterated methanol (MeOH–*d4*, ~ 1 mL) and transferred to 5 mm NMR tubes. As already mentioned in section 8.2.2, due to

the insufficient amount of ASOM fraction isolated from the Sum. A 2010 sample, it was impossible to acquire its 2D NMR spectra and only the corresponding WSOM fraction was characterized. The 2D NMR spectra were run at 295.1 K, under the following conditions: i) 2D *g*COSY spectra were recorded with 360 transients over 368 increments (zero-filled to 1 K) and 2 K data points with spectral widths of 5550 Hz. The recycle delay was 1 sec. The data were processed in the absolute value mode; ii) the phase sensitive ^{1}H-detected (^{1}H, ^{13}C) *g*HSQC spectrum was recorded with 376 transients over 392 increments (zero-filled to 1 K) and 2 K data points with spectral widths of 5550 Hz in F_2 and 22725 Hz in F_1. The recycle delay was 1.5 sec. A cosine multiplication was applied in both dimensions. The delays were adjusted according to a coupling constant $^{1}J_{CH}$ of 145 Hz; iii) the *g*HMBC spectrum was recorded with 436 transients over 448 increments (zero-filled to 1 K) and 2 K data points with spectral widths of 5550 Hz in F_2 and 29410 Hz in F_1. The recycle delay was 1.5 sec. A sine multiplication was applied in both dimensions. The low-pass J-filter of the experiment was adjusted for an average coupling constant $^{1}J_{CH}$ of 145 Hz and the long-range delay utilized to excite the heteronuclear multiple quantum coherence was optimized for 10 Hz.

The identification of functional groups in the NMR spectra was based on their chemical shift relative to the central solvent (MeOH–*d4*) peak set at δ ^{1}H 3.31 ppm and δ ^{13}C 49.0 ppm. The interpretation of the spectral regions and structural assignments were based on the NMR chemical shift data described in the literature for standard organic compounds and for NOM from different matrices [16,148,149], as well as on data generated by NMR simulators software's and databases (e.g., Perkin Elmer ChemBioDraw® Ultra 14.0, sdbs.db.aist.go.jp [150], NMR Database of Lignin and Cell Wall [151], and nmrdb.org [152]).

9.3. Results and discussion

9.3.1. Comparative assessment of the spectral profiles

Figure 9.1 shows the overlay of ^{1}H–^{13}C HSQC and ^{1}H–^{13}C HMBC NMR spectra of the WSOM and ASOM hydrophobic acids extracted and isolated from the aerosol samples collected in Win. 2010 (Figure 9.1a and Figure 9.1c, respectively) and Sum. B 2010 (Figure

9.1b and Figure 9.1d, respectively) seasons, and the HSQC and HMBC NMR spectra of the aerosol WSOM fraction collected in Sum. A 2010 (Figure 9.1e). Overlaying the complementary heteronuclear 2D NMR spectra enables not only a better discernment of the backbone assignments of the organic structures, but it also provides a depiction of the seasonal variance in molecular diversity for each OA fraction.

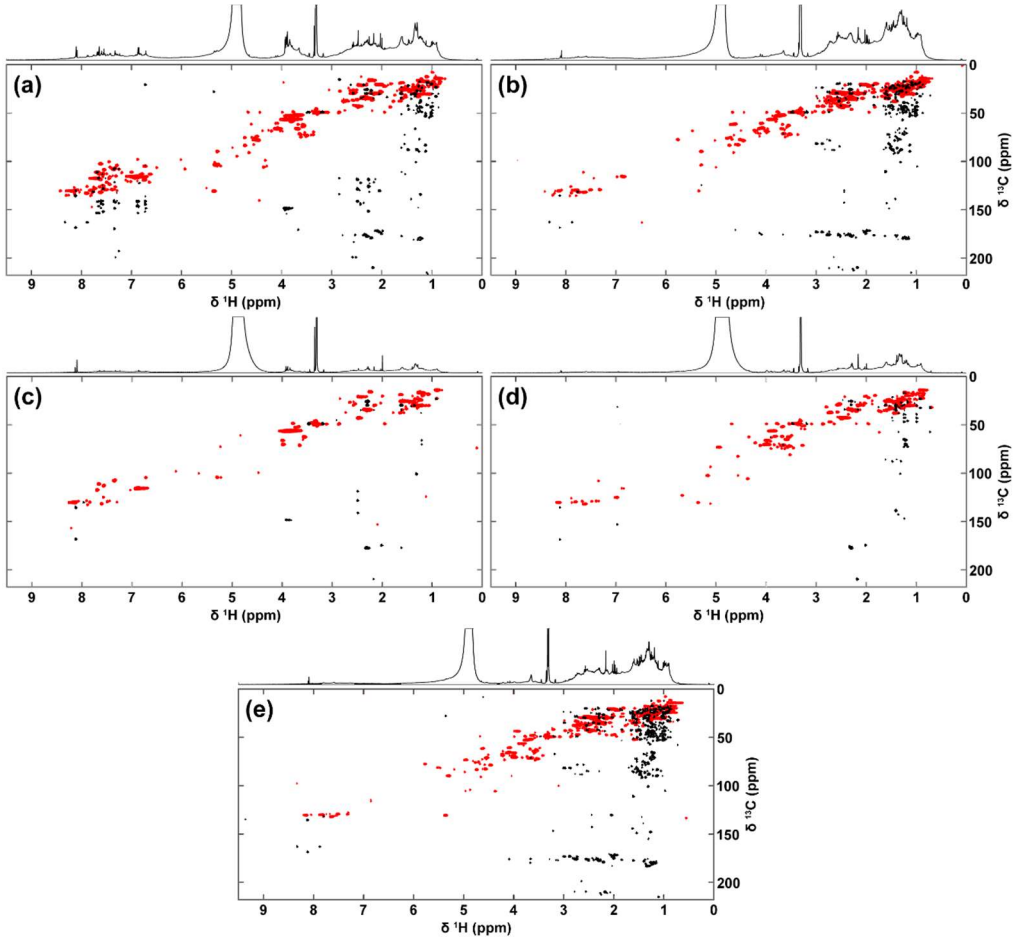

Figure 9.1 ^{1}H–^{13}C HSQC spectrum (●) overlaid onto the ^{1}H–^{13}C HMBC spectrum (●) of WSOM hydrophobic acids from (a) Win. 2010, (b) Sum. B 2010, (e) and Sum. A 2010 seasons, and the ASOM hydrophobic acids from (c) Win. 2010, and (d) Sum. B 2010 samples.

The HSQC NMR spectra of all five OA fractions reveal several important ^{1}H–^{13}C correlations in three major regions of chemical environments, but with very different relative intensities: aliphatic (δ ^{1}H 0.4 – 3.6 ppm / δ ^{13}C 10 – 45 ppm, including also *N*-alkyl groups at δ ^{1}H 2.6 – 3.6 ppm / δ ^{13}C 35 – 42 ppm), *O*-alkyl (δ ^{1}H 3.6 – 6.0 ppm / δ ^{13}C 50 – 107 ppm), and aromatic (δ ^{1}H 6.5 – 8.5 ppm / δ ^{13}C 107 – 160 ppm) regions. Overall, the HSQC (but also the HMBC and COSY (Figure 9.2)) NMR spectra of the WSOM hydrophobic acids are more abundant in cross peaks than those of the ASOM hydrophobic acids. Two possible

explanations for this outcome includes (i) the lower carbon concentration of the ASOM fractions as compared to those of the WSOM fractions (see Table 8.1), and (ii) a lesser atomic mobility due to solubility problems of the ASOM hydrophobic acids in the selected deuterated solvent, with their structural units becoming strongly bound inside the colloidal networks, thereby weakening homonuclear and heteronuclear dipolar interactions. Despite the attenuation of the HSQC signatures for the ASOM hydrophobic acids, the position of the most important cross-peaks agrees with the position of the more intense cross-peaks observed for the WSOM hydrophobic acids. Such similarity does not necessary imply the presence of the same molecules in both OA fractions, but rather suggests a resemblance in terms of their main chemical substructures.

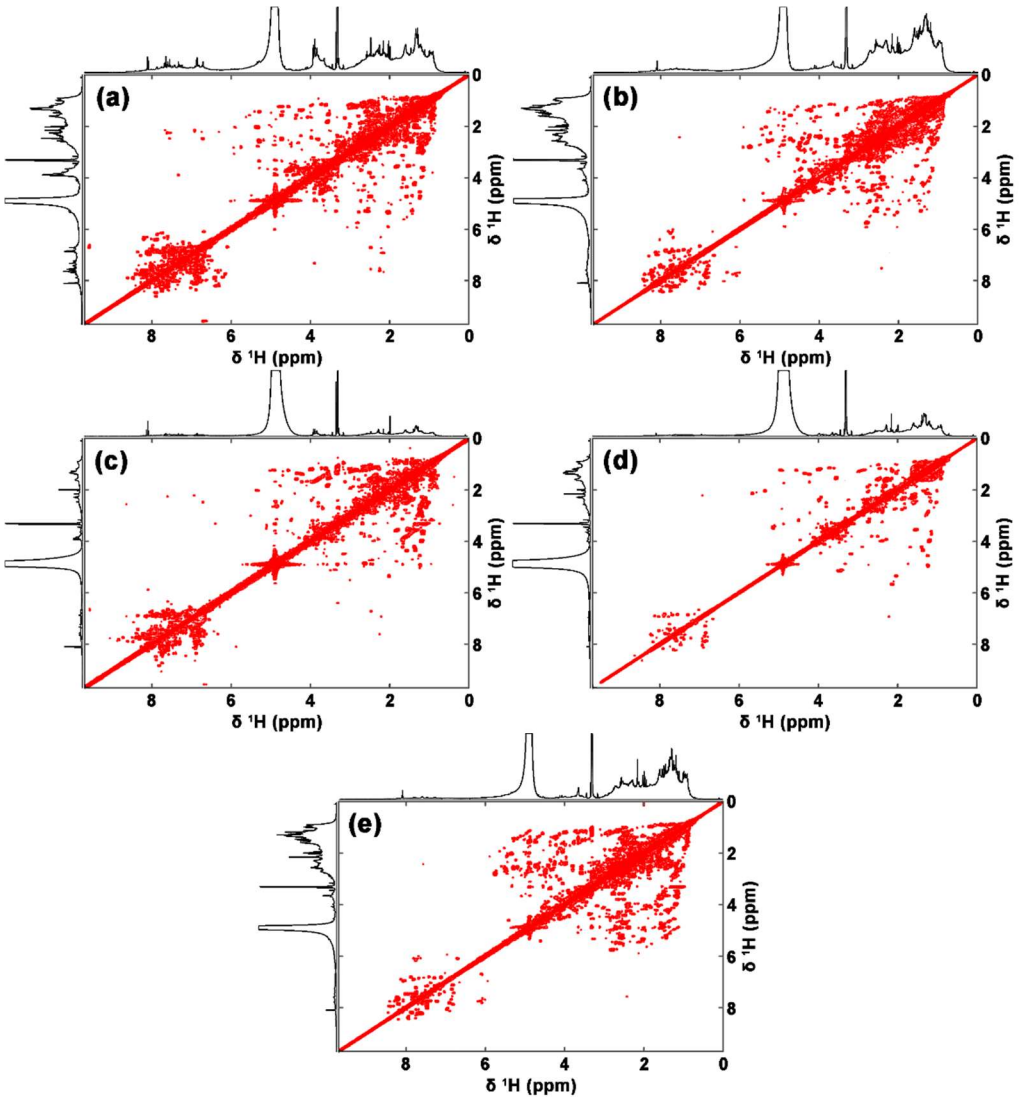

Figure 9.2 ^{1}H–^{1}H COSY NMR spectra of the WSOM hydrophobic acids from (a) Win. 2010, (b) Sum. B 2010, (e) and Sum. A 2010 seasons, and the ASOM hydrophobic acids from (c) Win. 2010, and (d) Sum. B 2010 samples.

Comparing and interpreting additional structural information of the different OA fractions from the 2D NMR data is not straightforward. It becomes, therefore, important to find adequate ways to visualize and compare these datasets by employing a method that should either highlight the systematic pattern between the different OA samples, or the most characteristic differences between the samples. To fulfill this goal, the 2D NMR spectral regional maxima obtained in this study were further identified using the methodology presented in Chapter 5, and published elsewhere [19,20]. This method allows identifying the coordinates of each cross-peak (i.e., ^{1}H and ^{13}C chemical shifts, and signal intensity) in each 2D NMR experiment. The obtained data were then used to reconstruct the 2D NMR spectra (Figure A. 6 in Annexes), and further visualize and distinguish the cross-peaks that are common to all OA fractions from those that are specific of each sample. Figure 9.3a and Figure 9.3b display, respectively, the COSY and the HSQC/HMBC NMR cross-peaks common to all three WSOM hydrophobic acids (i.e., Sum. A 2010, Sum. B 2010, and Win. 2010), whereas Figure 9.3c and Figure 9.3d depict, respectively, the COSY and the HSQC/HMBC NMR cross-peaks common to the two studied ASOM hydrophobic acids (i.e., Sum. B 2010 and Win. 2010). The NMR data regarding the common and specific cross-peaks maxima identified in the 2D NMR spectra of each sample is provided in Annexes (Figure A. 7, Figure A. 8, and Figure A. 9). In seasonal terms, both WSOM and ASOM hydrophobic acids from warm seasons show a prevalence of purely aliphatic (δ ^{1}H 0.8 – 1.8 ppm / δ ^{13}C 10 – 30 ppm) and functionalized aliphatic groups (δ ^{1}H 1.9 – 3.6 ppm / δ ^{13}C 30 – 45 ppm of R^1 –CH groups, where R^1 is an aromatic carbon, NH, C=O or COOH; and δ ^{1}H 3.6 – 6.0 ppm / δ ^{13}C 50-107 ppm of –<u>CH</u>–OH, –O–<u>CH_3</u> , –<u>CH</u>–O, and –O–<u>CH</u>–R^2 groups, where R^2 is an OCH– or OH group) when compared to those collected in winter, which contain more substituted aromatic structures (δ ^{1}H 6.5 – 8.5 ppm / δ ^{13}C 107 – 169 ppm). Compared to the WSOM hydrophobic acids, the ASOM hydrophobic acids appear to have more saturated aliphatic chains and less oxygen-containing functional groups, being therefore less hydrophilic and structurally diverse than its WSOM counterpart.

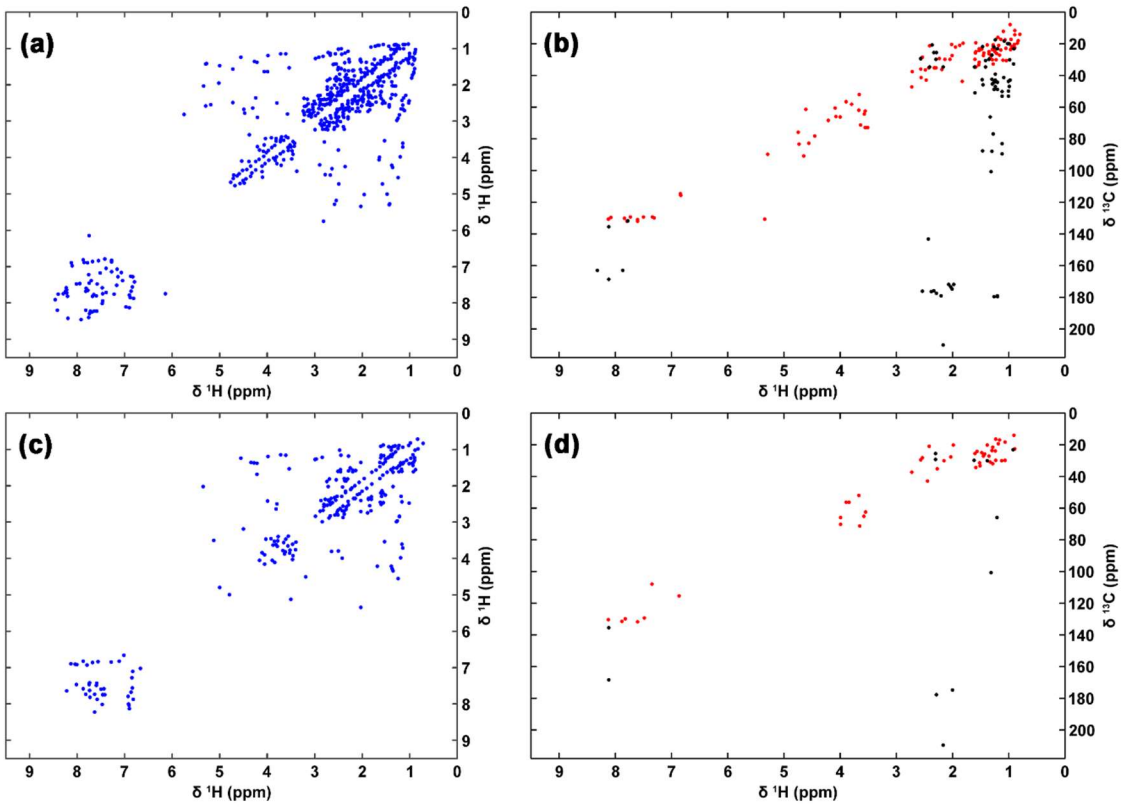

Figure 9.3 (a) ^{1}H–^{1}H COSY and (b) ^{1}H–^{13}C HSQC (●) overlaid onto the ^{1}H–^{13}C HMBC (●) NMR signals maxima common to all three WSOM hydrophobic acids (i.e., Sum. A 2010, Sum. B 2010, and Win. 2010); and (c) ^{1}H–^{1}H COSY and (d) ^{1}H–^{13}C HSQC (●) overlaid onto the ^{1}H–^{13}C HMBC (●) NMR signals maxima common to the two ASOM hydrophobic acids (i.e., Sum. B 2010 and Win. 2010).

The reconstructed 2D NMR spectra in Figure 9.3 have also the unique feature of portraying the annual background of the structural composition of the urban OA, regardless of the seasonal conditions. The WSOM component exhibits a crowded aliphatic region, where the typical aliphatic chemical environment is likely branched with heteroatom-containing functional groups (e.g., OH, NH, N–CO, N–CH_3, COOH, COOR, and COR, where R = H or alkyl group; assignments on the basis of HMBC cross peaks at δ ^{1}H 0.8 – 3.6 ppm / δ ^{13}C 35 – 110 ppm, δ ^{13}C 160 – 200 ppm, and δ ^{13}C 200 – 220 ppm). The superposition of abundant HMBC cross peaks in the δ ^{1}H 0.8 – 1.5 ppm / δ ^{13}C 10 – 35 ppm region also suggests that the aliphatic spin system of the WSOM hydrophobic acids is also likely to be disrupted by the presence of ternary and/or quaternary carbons (i.e., with carbon only environments). In this regard, Figure 9.4 depicts the most important aliphatic substructures – substructures AL-1 to AL-14 – within the urban aerosol WSOM component that are likely to be present throughout the year. The 2D NMR spectral assignments for each

substructure are provided in Table A. 3 in Annexes. It is also noteworthy that substructures AL-1 to AL-7 are also likely to be present in the ASOM component. Apparently, the sources of these branched oxidized polyfunctional aliphatic structures mostly remain identical in the studied urban area on an annual scale. Such type of aliphatic substructures has been recognized as first- and/or second-generation photochemical oxidation products of different gas-phase precursors (e.g., alkanes, isoprene, carbonyl, aliphatic amines, epoxides, and anhydrides) emitted from both anthropogenic (e.g., biomass burning, fossil fuel combustion, and meat cooking) [153–155] and natural sources (e.g., sea-to-air emission of marine organics, and terrestrial vegetation) [156,157]. Additional evidence supporting the predominance of photochemical SOA formation, particularly in summer seasons, is the HSQC cross-peak assigned to aliphatic methyl esters (R_{al}–$COOCH_3$, δ ^{1}H 3.5 – 3.8 ppm / δ ^{13}C 52 – 54 ppm, see Figure A. 10 in Annexes). Their presence in aqueous OA extracts has been considered as an indirect confirmation of sulfate esters present in original SOA [61], which possibly underwent methanolysis prior to NMR measurements during samples isolation/fractionation. Organosulfates are likely to be produced in heterogeneous reactions between partitioned semi-volatile carbonyl compounds and sulfuric acid formed in gas-phase photo-oxidation reactions [61]. Nevertheless, one cannot rule out the contribution of primary sources to some of those structures. Schmitt-Kopplin *et al.* [157] provided evidences of the chemoselective transfer of natural organic molecules, especially of aliphatic compounds (CHO and CHOS molecular series), from the ocean surface water into the atmosphere via bubble bursting processes [157]. Similarly, it has been shown that biomass-burning emissions is a very important primary source for dicarboxylic acids, ketocarboxylic acids, and dicarbonyl compounds at the regional and global scales [155].

Additional chemical structures, whose presence in atmospheric OA seems to be persistent throughout the year, include: (i) amino sugar derivatives (such as structure SAC-1, Figure 9.4, Table A. 3 in Annexes), probably reflecting the contribution of fungal-derived microbial residues in resuspended soil material [158], and (ii) aromatic structures, such as terephthalic acid (structure AR-1, Figure 9.4, Table A. 3 in Annexes), nitrophenyl-derived compounds (structure AR-2, Figure 9.4, Table A. 3 in Annexes), and cinnamic acid and/or cinnamaldehyde (structure AR-3, Figure 9.4, Table A. 3 in Annexes), possibly formed during the oxidation of aromatic hydrocarbons from urban traffic emissions [67,159,160].

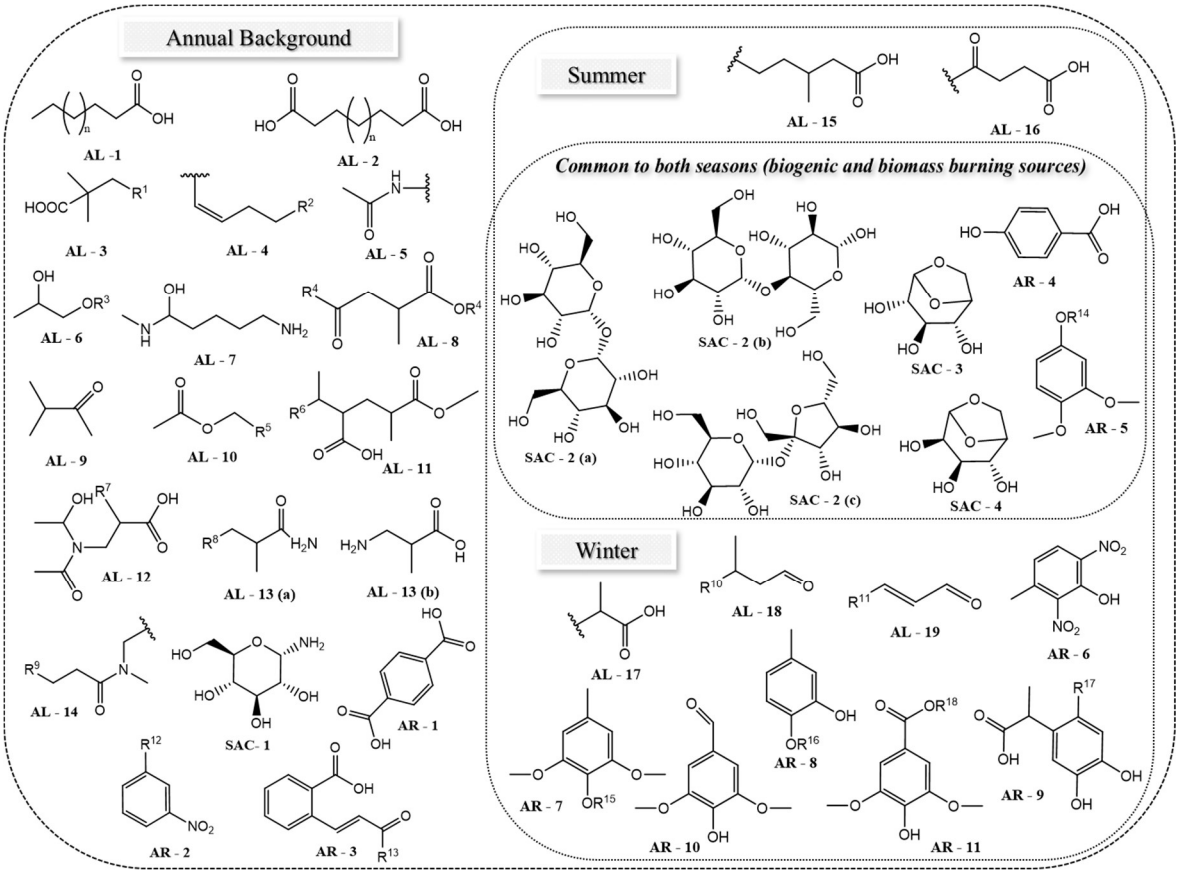

Figure 9.4 Aliphatic, carbohydrate and aromatic substructures identified in the aerosol WSOM and ASOM hydrophobic acids, both on an annual scale ("Annual Background") and specific of each season ("Summer" and "Winter"). See text and Table A. 3 in Annexes, for explanation of labels, and the identity of aliphatic and aromatic substituents (R_1 to R_{18}).

Owing to the diversity of OA sources, the 2D NMR spectra (Figure A. 7, Figure A. 8, and Figure A. 9) also show the existence of substructures that are specific of each season and/or OA fraction. Substructures AL-15 and AL-16 (Figure 9.4 and Table A. 3 in Annexes) were identified in the spectra of WSOM hydrophobic acids collected in summer seasons (Sum. A 2010 and Sum. B 2010). These substructures could conceivably have a secondary origin; e.g., resulting from the ozonolysis of hydrocarbon precursors (namely cycloalkenes) arising from both anthropogenic and biogenic sources [161]. Carbonyl-containing acids (substructure AL-16) have been also used as aromatic SOA anthropogenic tracers likely derived from the processing of fossil fuel or biomass-burning emissions [162]. Branched monocarboxylic acids, such as those represented by substructure AL-17, were also identified as specific to both ASOM hydrophobic acids as well as to WSOM hydrophobic acids collected in winter. These components may be derived from various sources, including fossil fuel combustion, photochemical oxidation of volatile

organic compounds, plant emissions, and bacterial activity [163]. The HMBC/COSY NMR spectra also showed that saturated and unsaturated carbonyl compounds (substructures AL-18 and AL-19, respectively) could be distinguished in both WSOM and ASOM hydrophobic acids collected in winter season. These carbonyl compounds could originate from combustion processes [164], or they could be produced in polluted environments from atmospheric oxidation of hydrocarbons [164,165]. Atmospheric aldehydes could also play an important role in SOA formation, particularly at sufficiently high NO_2 concentrations [165].

As aforementioned, the aerosol WSOM hydrophobic acids collected in winter is rich in aromatic moieties, exhibiting a large proportion of recognizable NMR signatures (Figure 9.1, HSQC: δ 1H = 6.6 – 7.8 ppm / δ ^{13}C = 100 – 125 ppm). The aromatic rings are highly substituted, and the presence of neutral (aliphatic carbon), NO_2, and/or oxygen-containing (namely, OCH_3, OH, COOR, and COR, where R = H or alkyl group) substituents appear to be dominant, as suggested by the HMBC cross-peaks at δ ^{1}H 2.0 – 2.9 ppm / δ ^{13}C 115 – 153 ppm, δ ^{1}H 3.7 – 4.0 ppm / δ ^{13}C 146 – 151 ppm, and δ ^{1}H 7.0 – 7.5 ppm / δ ^{13}C 168 – 200 ppm chemical shift ranges. Structures AR-4 to AR-11 in Figure 9.4 (NMR assignments in Table A. 3 in Annexes) represents some of the key aromatic substructures that are likely to be present in the winter WSOM hydrophobic acids. Based on the 2D NMR assignments, it is clear that these aromatic structures are consistent with residues commonly found in lignin. Their presence in the winter WSOM hydrophobic acids is plausibly explained by the emission of particulates from biomass burning for house heating, and confirms the importance of this source into the chemical composition of OA. The pyrolysis of lignin and wood yield the breakdown products of the biopolymers as phenols, aldehydes, ketones, acids, and alcohols, generally with the same substituent pattern (e.g., OH, OCH_3) on the aromatic rings as the precursor aromatic alcohols from which they were derived [166]. Once in the atmosphere, these structures can also undergo photooxidation, originating highly oxidized SOA species. Iinuma and co-workers [167] provided evidence that *m*-cresol, which is emitted from biomass burning at significant levels, is a precursor of methyl-nitrocatechols (similar to structure AR-6 in Figure 9.4). These SOA compounds originate from the photo-oxidation of *m*-cresol in the presence of NO_x [167].

A closer inspection of the 2D NMR spectra (Figure A. 7, Figure A. 8, and Figure A. 9) also shows that the NMR resonances assigned to substructures AR-4 and AR-5 are also present in both WSOM and ASOM hydrophobic acids collected in summer, during intense forest fires events (i.e., Sum. B 2010). This group of NMR resonances alongside those of structures AR-6 to AR-8 occurred also in the aerosol ASOM hydrophobic acids from Win. 2010 season. Additional NMR resonances attributed to disaccharides (such as trehalose, maltose, and sucrose - structures SAC-2(a) to SAC-2(c), respectively, Figure 9.4, Table A. 3 in Annexes) and anhydrosugars (such as levoglucosan and mannosan - structures SAC-3 and SAC-4, respectively, Figure 9.4, Table A. 3 in Annexes) were also detected in the 2D NMR spectra of the WSOM hydrophobic acids from Sum. B 2010 and Win. 2010 (HSQC cross-peak at δ ^{1}H 5.3 ppm / δ ^{13}C 103 ppm, representative of anomeric C–H pairs from glycosidic linkages between and/or within hexose units). Disaccharides related NMR resonances (i.e., anomeric C–H pairs) are also present, but considerably less intense, in the HSQC spectra of ASOM hydrophobic acids from Sum. B 2010 and Win. 2010 periods, in line with the expectation that these labile constituents are easily soluble in water. Levoglucosan, and to a minor extent mannosan and galactosan, are well-established organic molecular markers of biomass-burning emissions [16,168]. Their contribution to the aerosol WSOM load in both Sum. B 2010 and Win. 2010 periods support the assumption that, biomass burning is an important source of these compounds in the urban OA. Dimeric sugars, such as maltose and sucrose, could conceivably be emitted as well from the combustion of cellulose and hemi-cellulose [169]. Trehalose, on the other hand, is a fungal metabolite and it has been documented as a useful tracer of soil material and associated microbiota [170]. Therefore, the resuspension of soil from agricultural activities in areas nearby the sampling location could be a plausible source of this compound as well.

9.3.2. Semi-quantitative structural model of urban aerosol WSOM

The combined application of 2D NMR techniques enabled detailed structural assignments of the organic components within OA. For the specific case of the aerosol WSOM hydrophobic acids, for which superior ^{1}H–^{13}C and ^{1}H–^{1}H connectivity information have been achieved, a semi-quantitative model of its structural composition can be attempted by computing the numerical integral of the HSQC NMR spectra in four regions of chemical

environments: aliphatic (δ ^{1}H 0.4 – 3.6 ppm / δ ^{13}C 10 – 45 ppm), saccharides-like (δ ^{1}H 3.6 – 6.0 ppm / δ ^{13}C 59.8 – 107 ppm), aromatic (δ ^{1}H 6.5 – 8.5 ppm / δ ^{13}C 107 – 160 ppm), and aromatic –OCH_3 groups (δ ^{1}H 3.6 – 4.5 ppm / δ ^{13}C 54.5 – 59.8 ppm). This model is proposed in Figure 9.5, and it denotes the percentage distribution of the main identified structural fragments within the urban aerosol WSOM hydrophobic acids. It should be emphasized that these structural fragments consist on an average representation of the main organic functionalities identified in each WSOM hydrophobic acids. This model shows the prevalence of heteroatom-rich branched aliphatic (up to 65.4% of total section integrals), with methyl and carbonyl groups (either –COOH or –COR, where R=H or alkyl) as the two main terminating aliphatic units, having both primary (natural and anthropogenic) and secondary origin. The aromatic pool accounts for 13.1 – 23.9% of total section integrals, with biomass-burning emissions having a profound effect in the overall composition of urban aerosol WSOM hydrophobic acids in winter (up to 13% is represented by aromatic –OCH_3). Photooxidation of anthropogenic aromatic hydrocarbons precursors is also an important contributor to WSOM hydrophobic acids throughout the year. Finally, 15.6 – 18.7% of total section integrals are represented by saccharides and anhydrosaccharides, whose composition suggests both biogenic and biomass burning as the main sources of these compounds in urban aerosol WSOM hydrophobic acids.

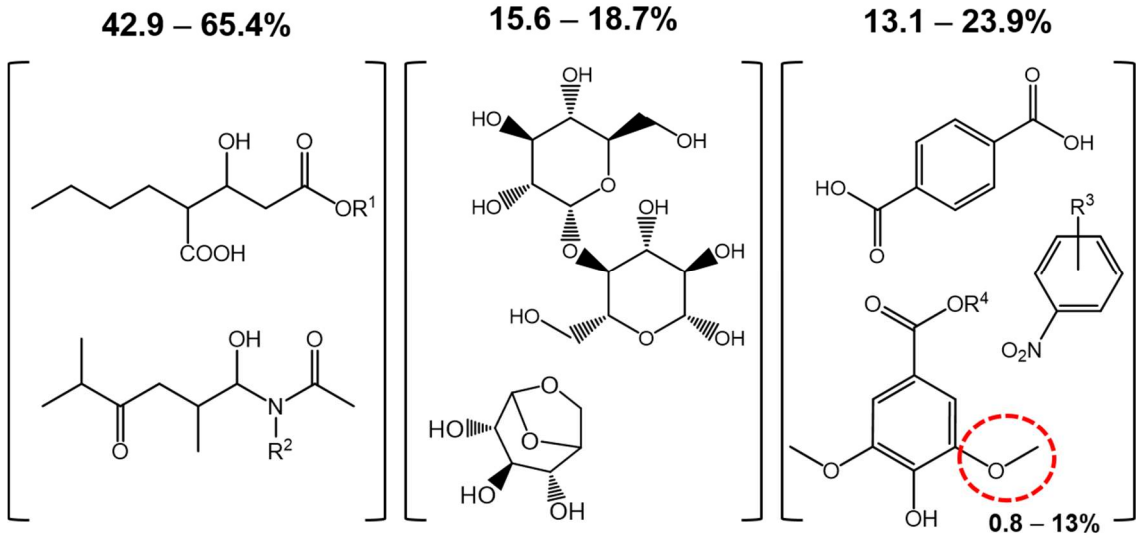

Figure 9.5 Semi-quantitative structural model of WSOM from urban aerosols (R^1 = R^2 = H and/or alkyl group; R^3 = OH and CH_3; R^4 = H and/or CH3). Values near each set of substructures represent the percentage of aliphatic, saccharides-like, aromatic, and aromatic methoxy groups section integrals related to total section integrals as derived from the ^{1}H–^{13}C HSQC NMR spectra of the WSOM samples.

At this point it is not possible to ascertain whether the proposed semi-quantitative structural model of urban WSOM hydrophobic acids can be used for extrapolating the bulk characteristics of the whole OA, even at a wide geographic scale. Future research is needed to refine both the composition and structures of OA in urban, rural, and marine locations, after which a more definite quantification and better constrained model of OA could be possible. Nevertheless, the structural information provided in Figure 9.5 can still be used as a proxy to further distill key features on the atmospheric role of OA.

9.4. Conclusions

A synergistic combination of some 2D NMR techniques was used for decoding the structural features of WSOM and ASOM hydrophobic acids sequentially extracted from fine atmospheric aerosols collected in an urban setting during cold and warm seasons. The 2D NMR spectra showed exceptional resolution and depicted resolved molecular signatures that portrayed the annual background of the structural composition of both WSOM and ASOM hydrophobic acids, as well as deciphering their major sources.

The ASOM hydrophobic acids are less hydrophilic and structurally diverse than their WSOM counterpart. This latter component is mostly composed of heteroatom-rich branched aliphatic, having both primary (natural and anthropogenic) and secondary origin. Lignin, disaccharides, and anhydrosaccharides signatures were also identified in the WSOM hydrophobic acids, reflecting the biomass burning influence, particularly during periods identified as smoke impacted. Contributions of aromatic secondary organics originated from anthropogenic aromatic precursors, as well as primary saccharides and amino sugar derivatives from biogenic emissions were also suggested. The dataset on the H–C molecules backbone was also used to propose a semi-quantitative structural model of urban WSOM, hydrophobic acids which will aid efforts for more realistic studies relating the chemical properties of OA with their atmospheric behavior.

Chapter 10

Knowledge gaps and road map for future research

This final chapter aims to provide an overall reflection and the main conclusions of the work carried out thus far besides discussing how the proposed research project has already contributed to an increase of knowledge in this field as well as to identify knowledge gaps and outline a road map for future research.

In recent years, the study of organic compounds in fine aerosols has become one of the areas of high activity and interest in atmospheric and environmental research. OA, namely the WSOM and the ASOM play an important role in the climate system, atmospheric processes, and public health. However, due to the limited knowledge on the composition, sources, formation mechanisms, and transformation processes of these fractions, their roles are still far from being completely understood. Therefore, in this PhD research project different analytical techniques were used for unravelling the chemical composition of these OA fractions in an attempt to link their structure and functional groups composition to their sources and formation mechanisms.

Although the focus was on urban aerosols, the studies developed under the scope of this PhD research had more emphasis on seasonal variation than in specific features of the same urban aerosols. This fact is easily explained since it has been exploited only a sampling site (i.e., the city of Aveiro), and consequently, the variations observed reflect mainly seasonal sources. In order to assess the specific characteristics of urban sources, it is required to create a larger database with sampling results from different environments (e.g., urban, rural, maritime, and pristine environments) and different seasons, but using the same techniques for sampling, extraction, separation, and targeted and untargeted analysis of aerosols.

Chapter 4, which is based on an extensive forty-three-week urban $PM_{2.5}$ samples dataset, shows that organic matter is the largest portion of the identifiable mass, and a very important fraction of this OC is water-soluble, whose content and structural characteristics are markedly different between colder and warmer seasons. These findings emphasize and enhance the purpose of this dissertation in the study the OA, and especially in its water-soluble fraction. In this fourth chapter it is also pointed out that in addition to the inorganic salts and EC, which also makes up a significant fraction of the total particulate matter mass, there is an important unidentified fraction of the $PM_{2.5}$ mass, usually attributed to water bounded to hygroscopic inorganic and organic material, unidentified species (e.g., water-insoluble crustal materials) or underestimated organic matter content. Future studies should attempt to increase the knowledge on this uncharacterized fraction, as well as, achieve a better understanding of these organic matter-inorganic system in the aerosols, and their importance and role in the atmosphere.

There is no doubt that with the introduction of the first commercial LC×LC systems and the massification of their use with MS/MS detectors, alongside with the explosion in the development of chromatography columns specially designed for each dimension, has made this separation technique a tool of choice for the study of complex matrices. However, its application in environmental samples, particularly in the study of atmospheric aerosols, is still in its infancy and there is a long way to go until they will achieve the full potential of this technique. Chapter 6 presents one of the first applications of this powerful separation technique for unravelling the chemical heterogeneity and mapping the hydrophobicity *vs* M_w distribution of the WSOM hydrophobic acids from urban $PM_{2.5}$ collected over different seasons. Future studies should include the developed technique and optimization of new procedures not only to identify similarities and differences between samples (as described in Chapter 6) but also focus on the target identification of the chemical compounds that contribute for each individual aerosol sample profile. Furthermore, the association of this separation procedure (offline or hyphenated) with high-resolution analytical techniques (e.g., NMR, and HR-MS) will surely be of outstanding added value for unravelling the complexity of the OA. The use of different stationary phases combinations, such as HILIC with RP and ion exchange with RP or HILIC, should also be very valuable since they can provide a larger set of sample fingerprints, and consequently this will allow to extract much more and better discriminated information. Nevertheless, the analysis of a larger number of samples with LC×LC coupled to one or more multidimensional detectors will lead to the need of developing and adapting new and more efficient strategies based on chemometrics for data processing. In Chapter 5 and Chapter 6 a simple method is put forward and employed for obtaining a 3D chemical pattern representation of each sample from the chromatographic and spectral data resulting from the association of multichannel detectors with LC×LC. This method can be quickly and easily applied to a large matrix of data, in order to identify patterns and differences between samples. Nevertheless, by reducing the dimensionality of data there is a loss of quantitative information. The development of methods capable of coping with such large multidimensional data, without losing much of the samples quantitative information will be one of the biggest challenges that have to be met in the near future.

The combination of EEM fluorescence spectroscopy with a PARAFAC-ALS method, as described in Chapter 7, has been proved to be a very useful tool to establish the

link between the WSOM and ASOM fluorescent characteristics with their seasonal variability. WSOM samples collected in the warm seasons have shown differences in the PARAFAC components when compared to WSOM samples collected in the cold seasons, being these changes associated with the decrease of degree of unsaturated π-bond systems in the samples from warmer seasons comparatively to those of the cold seasons. The fluorescent features of urban aerosol ASOM, that account to up 29 and 37% of the particulate OC in cold and warm seasons, respectively, are more constant throughout the year than those of the WSOM, suggesting that ASOM may be enriched in fluorescent compounds with an *in situ* origin. The fluorescence intensity of the PARAFAC components in both fractions appears to be strongly influenced by the season of the year and by the occurrence of biomass burning events. Future work should focus on how to figure out which type of organic fluorophore structure is associated with the components decomposed by the PARAFAC-ALS method. In this sense, the use of chromatographic systems (e.g., HPLC or LC×LC) coupled not only with fluorescence detectors, but also with more discriminating detectors such as MS/MS can be a possible solution. On the other hand, using standards of known organic compounds and the properties of spectral matching of PARAFAC-ALS to identify those organic structures could also be a useful alternative. However, as highlighted by Wunseh *et al.* [171], since many of the organic compounds exhibit highly similar spectral properties, this technique is unlikely to be sufficient to identify individual compounds.

Finally, concerning the use of solution-state ^{1}H NMR spectroscopy and solution-state 2D NMR techniques, namely ^{1}H–^{1}H COSY, ^{1}H–^{13}C HSQC, and ^{1}H–^{13}C HMBC, they have been successfully applied for decoding and characterize the structural and molecular features of WSOM and ASOM hydrophobic acids, as well as, to assess their sources and seasonal variability. The ^{1}H NMR analysis, described in Chapter 8, showed that urban aerosol WSOM and ASOM hydrophobic acids hold similar ^{1}H functional groups but with differences in terms of their relative distribution throughout the sampling campaign I. Moreover, this chapter also highlights that the WSOM and ASOM hydrophobic acids do not fit into any of the pre-established source areas of Decesari *et al.* [37], defined by their source apportionment scheme. As such, it was not possible to associate the WSOM and ASOM hydrophobic acids focused in this study with any specific source (i.e., MOA, SOA, and BBOA) predetermined by the model. Nevertheless, the qualitative and quantitative data derived from the ^{1}H NMR profiles of the samples, suggest the existence of a possible new

area associated with the contribution of urban aerosols. Moreover, it is also suggested that the boundaries of the signature boxes, especially for SOA and biomass burning, might be different at urban locations. In this regard, future work should try to prove and support the existence of this new area in the model, and therefore improve the established ^{1}H NMR source apportionment model to include urban OA. The application of the 2D NMR methods, presented in Chapter 9, allowed to identify the spectral signatures and structural features of the most atmospherically-relevant organic forms present in the WSOM and ASOM hydrophobic acids of the OA, as well as, achieve a comprehensive insight into the C−H backbone of the individual structures in OA. By allowing a unique improvement in the knowledge obtained for these OA samples, the gathered structural information was also crucial for the identification of the sources and some formation mechanisms of OA in the studied urban area, as well as their variability over seasons. The most obvious point for further study is the use of a larger number of samples of more diversified sources and season variability. The potential of these 2D NMR techniques is obvious, even though, in this PhD research project, only 3 WSOM samples and 2 ASOM samples were the subject of the investigation by 2D NMR. Thus, focusing on a larger number of samples will allow to achieve an in-depth knowledge on the composition and atmospheric dynamic of OA. However, as described above for LC×LC technique, one of the biggest challenges for the future, is the development of chemometric methods to deal with the huge amount of data generated. In addition, it is also necessary to develop software capable of combine information withdrawn from the ^{1}H–^{1}H COSY, ^{1}H–^{13}C HSQC, and ^{1}H–^{13}C HMBC spectra, in an automatic or at least semiautomatic way, in order to unambiguously identify the organic structures, present in a given OA sample. In the near future, the research in this scientific field should continue to evolve on the quest for attaining sound conclusions about the structure-origin relationship of both WSOM and ASOM fractions present in urban air particles, and simultaneously build up scientific knowledge in the field of advanced chemical analysis of fine aerosols.

References

[1] H. Horvath, Editorial, J. Environ. Radioact. 51 (2000) 5–25. doi:10.1016/S0265-931X(00)00041-2.

[2] U. Pöschl, Atmospheric aerosols: composition, transformation, climate and health effects., Angew. Chem. Int. Ed. Engl. 44 (2005) 7520–40. doi:10.1002/anie.200501122.

[3] K.A. Prather, C.D. Hatch, V.H. Grassian, Analysis of atmospheric aerosols., Annu. Rev. Anal. Chem. 1 (2008) 485–514. doi:10.1146/annurev.anchem.1.031207.113030.

[4] N.A. Marley, J.S. Gaffney, Introduction to Urban Aerosols and Their Impacts, in: J.S. Gaffney, N.A. Marley (Eds.), Urban Aerosols Their Impacts Lessons Learn. from World Trade Cent. Tragedy, American Chemical Society, Washington, DC, 2005: pp. 2–22. doi:10.1021/bk-2006-0919.ch001.

[5] M. Kanakidou, J.H. Seinfeld, S.N. Pandis, I. Barnes, F.J. Dentener, M.C. Facchini, R. Van Dingenen, B. Ervens, A. Nenes, C.J. Nielsen, E. Swietlicki, J.P. Putaud, Y. Balkanski, S. Fuzzi, J. Horth, G.K. Moortgat, R. Winterhalter, C.E.L. Myhre, K. Tsigaridis, E. Vignati, E.G. Stephanou, J. Wilson, Organic aerosol and global climate modelling: a review, Atmos. Chem. Phys. 5 (2005) 1053–1123. doi:10.5194/acp-5-1053-2005.

[6] J.L. Jimenez, M.R. Canagaratna, N.M. Donahue, A.S.H. Prevot, Q. Zhang, J.H. Kroll, P.F. DeCarlo, J.D. Allan, H. Coe, N.L. Ng, A.C. Aiken, K.S. Docherty, I.M. Ulbrich, A.P. Grieshop, A.L. Robinson, J. Duplissy, J.D. Smith, K.R. Wilson, V.A. Lanz, C. Hueglin, Y.L. Sun, J. Tian, A. Laaksonen, T. Raatikainen, J. Rautiainen, P. Vaattovaara, M. Ehn, M. Kulmala, J.M. Tomlinson, D.R. Collins, M.J. Cubison, J. Dunlea, J.A. Huffman, T.B. Onasch, M.R. Alfarra, P.I. Williams, K. Bower, Y. Kondo, J. Schneider, F. Drewnick, S. Borrmann, S. Weimer, K. Demerjian, D. Salcedo, L. Cottrell, R. Griffin, A. Takami, T. Miyoshi, S. Hatakeyama, A. Shimono, J.Y. Sun, Y.M. Zhang, K. Dzepina, J.R. Kimmel, D. Sueper, J.T. Jayne, S.C. Herndon, A.M. Trimborn, L.R. Williams, E.C. Wood, A.M. Middlebrook, C.E. Kolb, U. Baltensperger, D.R. Worsnop, Evolution of Organic Aerosols in the Atmosphere, Science (80-.). 326 (2009) 1525–1529. doi:10.1126/science.1180353.

[7] H. Yu, Y.J. Kaufman, M. Chin, G. Feingold, L.A. Remer, T.L. Anderson, Y. Balkanski, N. Bellouin, O. Boucher, S. Christopher, P. DeCola, R. Kahn, D. Koch, N. Loeb, M.S. Reddy, M. Schulz, T. Takemura, M. Zhou, A review of measurement-based assessments of the aerosol direct radiative effect and forcing, Atmos. Chem. Phys. 6 (2006) 613–666. doi:10.5194/acp-6-613-2006.

[8] A. Laskin, J. Laskin, S.A. Nizkorodov, Chemistry of Atmospheric Brown Carbon, Chem. Rev. 115 (2015) 4335–4382. doi:10.1021/cr5006167.

[9] C. George, M. Ammann, B. D'Anna, D.J. Donaldson, S.A. Nizkorodov, Heterogeneous Photochemistry in the Atmosphere, Chem. Rev. 115 (2015) 4218–4258. doi:10.1021/cr500648z.

[10] C.I. Davidson, R.F. Phalen, P.A. Solomon, Airborne Particulate Matter and Human Health: A Review, Aerosol Sci. Technol. 39 (2005) 737–749. doi:10.1080/02786820500191348.

[11] A. Mellouki, T.J. Wallington, J. Chen, Atmospheric Chemistry of Oxygenated Volatile Organic Compounds: Impacts on Air Quality and Climate, Chem. Rev. 115 (2015) 3984–4014. doi:10.1021/cr500549n.

[12] B. Nozière, M. Kalberer, M. Claeys, J. Allan, B. D'Anna, S. Decesari, E. Finessi, M. Glasius, I. Grgić, J.F. Hamilton, T. Hoffmann, Y. Iinuma, M. Jaoui, A. Kahnt, C.J. Kampf, I. Kourtchev, W. Maenhaut, N. Marsden, S. Saarikoski, J. Schnelle-Kreis, J.D. Surratt, S. Szidat, R. Szmigielski, A. Wisthaler, The Molecular Identification of Organic Compounds in the Atmosphere: State of the Art and Challenges, Chem. Rev. 115 (2015) 3919–3983. doi:10.1021/cr5003485.

[13] R.M.B.O. Duarte, A.C. Duarte, A critical review of advanced analytical techniques for water-soluble organic matter from atmospheric aerosols, TrAC Trends Anal. Chem. 30 (2011) 1659–1671. doi:10.1016/j.trac.2011.04.020.

[14] M.R. Heal, P. Kumar, R.M. Harrison, Particles, air quality, policy and health., Chem. Soc. Rev. 41 (2012) 6606–30. doi:10.1039/c2cs35076a.

[15] R.M.B.O. Duarte, E.B.H. Santos, C.A. Pio, A.C. Duarte, Comparison of structural features of water-soluble organic matter from atmospheric aerosols with those of aquatic humic substances, Atmos. Environ. 41 (2007) 8100–8113. doi:10.1016/j.atmosenv.2007.06.034.

[16] R.M.B.O. Duarte, A.M.S. Silva, A.C. Duarte, Two-Dimensional NMR Studies of Water-Soluble Organic Matter in Atmospheric Aerosols, Environ. Sci. Technol. 42 (2008) 8224–8230. doi:10.1021/es801298s.

[17] R.M.B.O. Duarte, J.T. V. Matos, A.S. Paula, S.P. Lopes, S. Ribeiro, J.F. Santos, C. Patinha, E.F. da Silva, R. Soares, A.C. Duarte, Tracing of aerosol sources in an urban environment using chemical, Sr isotope, and mineralogical characterization, Environ. Sci. Pollut. Res. (in press) (2016). doi:10.1007/s11356-016-7793-8.

[18] J.T.V. Matos, S.M.S.C. Freire, R.M.B.O. Duarte, A.C. Duarte, Natural organic matter in urban aerosols: Comparison between water and alkaline soluble components using excitation–emission matrix fluorescence spectroscopy and multiway data analysis, Atmos. Environ. 102 (2015) 1–10. doi:10.1016/j.atmosenv.2014.11.042.

[19] J.T. V Matos, R.M.B.O. Duarte, A.C. Duarte, A simple approach to reduce dimensionality from comprehensive two-dimensional liquid chromatography coupled with a multichannel detector., Anal. Chim. Acta. 804 (2013) 296–303. doi:10.1016/j.aca.2013.10.033.

[20] J.T. V. Matos, S.M.S.C. Freire, R.M.B.O. Duarte, A.C. Duarte, Profiling Water-Soluble Organic Matter from Urban Aerosols Using Comprehensive Two-Dimensional Liquid Chromatography, Aerosol Sci. Technol. 49 (2015) 381–389. doi:10.1080/02786826.2015.1036394.

[21] A.S. Paula, J.T.V. Matos, R.M.B.O. Duarte, A.C. Duarte, Two chemically distinct light-absorbing pools of urban organic aerosols: A comprehensive multidimensional analysis of trends, Chemosphere. 145 (2016) 215–223. doi:10.1016/j.chemosphere.2015.11.093.

[22] J.T.V. Matos, R.M.B.O. Duarte, A.C. Duarte, Challenges in the identification and characterization of free amino acids and proteinaceous compounds in atmospheric aerosols: A critical review, TrAC Trends Anal. Chem. 75 (2016) 97–107. doi:10.1016/j.trac.2015.08.004.

[23] S.P. Lopes, J.T.V. Matos, A.M.S. Silva, A.C. Duarte, R.M.B.O. Duarte, 1H NMR studies of water- and alkaline-soluble organic matter from fine urban atmospheric aerosols, Atmos. Environ. 119 (2015) 374–380. doi:10.1016/j.atmosenv.2015.08.072.

[24] J.H. Seinfeld, J.F. Pankow, Organic atmospheric particulate material, Annu. Rev. Phys. Chem. 54 (2003) 121–40. doi:10.1146/annurev.physchem.54.011002.103756.

[25] M.C. Jacobson, H.-C. Hansson, K.J. Noone, R.J. Charlson, Organic atmospheric aerosols: Review and state of the science, Rev. Geophys. 38 (2000) 267–294. doi:10.1029/1998RG000045.

[26] M. Paglione, Advanced spectroscopic techniques and chemometric analysis for atmospheric organic aerosol characterization and source apportionment, University of Bologna, 2013. http://amsdottorato.cib.unibo.it/5218/.

[27] R.M.B.O. Duarte, Balanço mássico e caracterização da matéria orgânica de aerossóis atmosféricos, University of Aveiro, 2006.

[28] M. Lazaridis, Organic Aerosols, in: I. Colbeck (Ed.), Environ. Chem. Aerosols, 1st ed., Blackwell Publishing Ltd., Oxford, UK, 2008: pp. 91–115. doi:10.1002/9781444305388.ch4.

[29] S.S. Park, D. Harrison, J.P. Pancras, J.M. Ondov, Highly time-resolved organic and elemental carbon measurements at the Baltimore Supersite in 2002, J. Geophys. Res. 110 (2005) D07S06. doi:10.1029/2004JD004610.

[30] H.J. Timonen, S.K. Saarikoski, M.A. Aurela, K.M. Saarnio, R.E.J. Hillamo, Water-soluble organic carbon in urban aerosol: concentrations, size distributions and contribution to particulate matter, Boreal Environ. Res. 13 (2008) 335–346.

[31] J. Sun, P. Ariya, Atmospheric organic and bio-aerosols as cloud condensation nuclei (CCN): A review, Atmos. Environ. 40 (2006) 795–820. doi:10.1016/j.atmosenv.2005.05.052.

[32] K.E. Yttri, C.L. Myhre, K. Torseth, The carbonaceous aerosol — A remaining challenge, World Meteorol. Organ. 58 (2009) 54–60.

[33] R.M.B.O. Duarte, A.C. Duarte, Atmospheric Organic Matter, in: eMagRes, John Wiley & Sons, Ltd, Chichester, UK, 2013: pp. 415–426. doi:10.1002/9780470034590.emrstm1331.

[34] P. Saxena, L.M. Hildemann, Water-soluble organics in atmospheric particles: A critical review of the literature and application of thermodynamics to identify candidate compounds, J. Atmos. Chem. 24 (1996) 57–109. doi:10.1007/BF00053823.

[35] G. Kiss, B. Varga, I. Galambos, I. Ganszky, Characterization of water-soluble organic matter isolated from atmospheric fine aerosol, J. Geophys. Res. 107 (2002) 8339. doi:10.1029/2001JD000603.

[36] P. Sannigrahi, A.P. Sullivan, R.J. Weber, E.D. Ingall, Characterization of Water-Soluble Organic Carbon in Urban Atmospheric Aerosols Using Solid-State 13 C NMR Spectroscopy, Environ. Sci. Technol. 40 (2006) 666–672. doi:10.1021/es051150i.

[37] S. Decesari, M. Mircea, F. Cavalli, S. Fuzzi, F. Moretti, E. Tagliavini, M.C. Facchini, Source Attribution of Water-Soluble Organic Aerosol by Nuclear Magnetic Resonance Spectroscopy, Environ. Sci. Technol. 41 (2007) 2479–2484. doi:10.1021/es0617111.

[38] R.M.B.O. Duarte, A.C. Duarte, Unraveling the structural features of organic aerosols by NMR spectroscopy: a review, Magn. Reson. Chem. (2015) doi: 10.1002/mrc.4227. doi:10.1002/mrc.4227.

[39] S. Zappoli, A. Andracchio, S. Fuzzi, M.C. Facchini, A. Gelencsér, G. Kiss, Z. Krivácsy, Á. Molnár, E. Mészáros, H.-C. Hansson, K. Rosman, Y. Zebühr, Inorganic, organic and macromolecular components of fine aerosol in different areas of Europe in relation to their water solubility, Atmos. Environ. 33 (1999) 2733–2743. doi:10.1016/S1352-2310(98)00362-8.

[40] A.P. Sullivan, R.J. Weber, A.L. Clements, J.R. Turner, M.S. Bae, J.J. Schauer, A method for on-line measurement of water-soluble organic carbon in ambient aerosol particles: Results from an urban site, Geophys. Res. Lett. 31 (2004) L13105. doi:10.1029/2004GL019681.

[41] A.S. Willoughby, A.S. Wozniak, P.G. Hatcher, A molecular-level approach for characterizing water-insoluble components of ambient organic aerosol particulates using ultrahigh-resolution mass spectrometry, Atmos. Chem. Phys. 14 (2014) 10299–10314. doi:10.5194/acp-14-10299-2014.

[42] H. Timonen, S. Carbone, M. Aurela, K. Saarnio, S. Saarikoski, N.L. Ng, M.R. Canagaratna, M. Kulmala, V.M. Kerminen, D.R. Worsnop, R. Hillamo, Characteristics, sources and water-solubility of ambient submicron organic aerosol in springtime in Helsinki, Finland, J. Aerosol Sci. 56 (2013) 61–77. doi:10.1016/j.jaerosci.2012.06.005.

[43] K.J. Heaton, R.L. Sleighter, P.G. Hatcher, W.A. Hall IV, M. V. Johnston, Composition Domains in Monoterpene Secondary Organic Aerosol, Environ. Sci. Technol. 43 (2009) 7797–7802. doi:10.1021/es901214p.

[44] A.P. Bateman, S.A. Nizkorodov, J. Laskin, A. Laskin, High-Resolution Electrospray Ionization Mass Spectrometry Analysis of Water-Soluble Organic Aerosols Collected with a Particle into Liquid Sampler †, Anal. Chem. 82 (2010) 8010–8016. doi:10.1021/ac1014386.

[45] T. Feczko, H. Puxbaum, A. Kasper-Giebl, M. Handler, A. Limbeck, A. Gelencsér, C. Pio, S. Preunkert, M. Legrand, Determination of water and alkaline extractable atmospheric humic-like substances with the TU Vienna HULIS analyzer in samples from six background sites in Europe, J. Geophys. Res. 112 (2007) D23S10. doi:10.1029/2006JD008331.

[46] K.A. Pratt, K.A. Prather, Mass spectrometry of atmospheric aerosols — Recent developments and applications. Part I: Off-line mass spectrometry techniques, Mass Spectrom. Rev. 31 (2012) 1–16. doi:10.1002/mas.20322.

[47] K. Hartonen, T. Laitinen, M.-L. Riekkola, Current instrumentation for aerosol mass spectrometry, TrAC Trends Anal. Chem. 30 (2011) 1486–1496. doi:10.1016/j.trac.2011.06.007.

[48] A. Laskin, J. Laskin, S. Nizkorodov, Mass spectrometric approaches for chemical characterisation of atmospheric aerosols: critical review of the most recent advances, Environ. Chem. 9 (2012) 163. doi:10.1071/EN12052.

[49] Q. Zhang, J.L. Jimenez, M.R. Canagaratna, I.M. Ulbrich, N.L. Ng, D.R. Worsnop, Y. Sun, Understanding atmospheric organic aerosols via factor analysis of aerosol mass spectrometry: a review., Anal. Bioanal. Chem. 401 (2011) 3045–67. doi:10.1007/s00216-011-5355-y.

[50] K.A. Pratt, K.A. Prather, Mass spectrometry of atmospheric aerosols — Recent developments and applications. Part II: On-line mass spectrometry techniques, Mass Spectrom. Rev. 31 (2012) 17–48. doi:10.1002/mas.20330.

[51] H. Timonen, M. Aurela, S. Carbone, K. Saarnio, S. Saarikoski, T. Mäkelä, M. Kulmala, V.-M. Kerminen, D.R. Worsnop, R. Hillamo, High time-resolution chemical characterization of the water-soluble fraction of ambient aerosols with PILS-TOC-IC and AMS, Atmos. Meas. Tech. 3 (2010) 1063–1074. doi:10.5194/amt-3-1063-2010.

[52] S. Decesari, M.C. Facchini, E. Matta, F. Lettini, M. Mircea, S. Fuzzi, E. Tagliavini, J.-P. Putaud, Chemical features and seasonal variation of fine aerosol water-soluble organic compounds in the Po Valley, Italy, Atmos. Environ. 35 (2001) 3691–3699. doi:10.1016/S1352-2310(00)00509-4.

[53] B. Graham, O.L. Mayol-Bracero, P. Guyon, G.C. Roberts, S. Decesari, C.M. Facchini, P. Artaxo, W. Maenhaut, P. Köll, M.O. Andreae, Water-soluble organic compounds in biomass burning aerosols over Amazonia 1. Characterization by NMR and GC-MS, J. Geophys. Res. 107 (2002) 8047. doi:10.1029/2001JD000336.

[54] S. Fuzzi, S. Decesari, M.C. Facchini, E. Matta, M. Mircea, E. Tagliavini, A simplified model of the water soluble organic component of atmospheric aerosols, Geophys. Res. Lett. 28 (2001) 4079–4082. doi:10.1029/2001GL013418.

[55] F. Cavalli, M.C. Facchini, S. Decesari, L. Emblico, M. Mircea, N.R. Jensen, S. Fuzzi, Size-segregated aerosol chemical composition at a boreal site in southern Finland, during the QUEST project, Atmos. Chem. Phys. 6 (2006) 993–1002. doi:10.5194/acp-6-993-2006.

[56] M.J. Cleveland, L.D. Ziemba, R.J. Griffin, J.E. Dibb, C.H. Anderson, B. Lefer, B. Rappenglück, Characterization of urban aerosol using aerosol mass spectrometry and proton nuclear magnetic resonance spectroscopy, Atmos. Environ. 54 (2012) 511–518. doi:10.1016/j.atmosenv.2012.02.074.

[57] M. Paglione, S. Saarikoski, S. Carbone, R. Hillamo, M.C. Facchini, E. Finessi, L. Giulianelli, C. Carbone, S. Fuzzi, F. Moretti, E. Tagliavini, E. Swietlicki, K. Eriksson Stenström, A.S.H. Prévôt, P. Massoli, M. Canaragatna, D. Worsnop, S. Decesari, Primary and secondary biomass burning aerosols determined by proton nuclear magnetic resonance (1H-NMR) spectroscopy during the 2008 EUCAARI campaign in the Po Valley (Italy), Atmos. Chem. Phys. 14 (2014) 5089–5110. doi:10.5194/acp-14-5089-2014.

[58] R.M.B.O. Duarte, C.A. Pio, A.C. Duarte, Spectroscopic study of the water-soluble organic matter isolated from atmospheric aerosols collected under different atmospheric conditions, Anal. Chim. Acta. 530 (2005) 7–14. doi:10.1016/j.aca.2004.08.049.

[59] Y. Subbalakshmi, A.F. Patti, G.S.H. Lee, M.A. Hooper, Structural characterisation of macromolecular organic material in air particulate matter using Py-GC-MS and solid state 13C-NMR, J. Environ. Monit. 2 (2000) 561–565. doi:10.1039/b005596o.

[60] R.M.B.O. Duarte, S.M.S.C. Freire, A.C. Duarte, Investigating the water-soluble organic functionality of urban aerosols using two-dimensional correlation of solid-state 13C NMR and FTIR spectral data, Atmos. Environ. 116 (2015) 245–252. doi:10.1016/j.atmosenv.2015.06.043.

[61] P. Schmitt-Kopplin, A. Gelencsér, E. Dabek-Zlotorzynska, G. Kiss, N. Hertkorn, M. Harir, Y. Hong, I. Gebefügi, Analysis of the unresolved organic fraction in atmospheric aerosols with ultrahigh-resolution mass spectrometry and nuclear magnetic resonance spectroscopy: organosulfates as photochemical smog constituents., Anal. Chem. 82 (2010) 8017–26. doi:10.1021/ac101444r.

[62] M.-C.G. Chalbot, G. Gamboa da Costa, I.G. Kavouras, NMR Analysis of the Water-Soluble Fraction of Airborne Pollen Particles, Appl. Magn. Reson. 44 (2013) 1347–1358. doi:10.1007/s00723-013-0492-4.

[63] S. Decesari, E. Finessi, M. Rinaldi, M. Paglione, S. Fuzzi, E.G. Stephanou, T. Tziaras, A. Spyros, D. Ceburnis, C. O'Dowd, M. Dall'Osto, R.M. Harrison, J. Allan, H. Coe, M.C. Facchini, Primary and secondary marine organic aerosols over the North Atlantic Ocean during the MAP experiment, J. Geophys. Res. Atmos. 116 (2011) 1–21. doi:10.1029/2011JD016204.

[64] G.C. Woods, M.J. Simpson, P.J. Koerner, A. Napoli, A.J. Simpson, HILIC-NMR: toward the identification of individual molecular components in dissolved organic matter., Environ. Sci. Technol. 45 (2011) 3880–6. doi:10.1021/es103425s.

[65] A.J. Simpson, L.-H. Tseng, M.J. Simpson, M. Spraul, U. Braumann, W.L. Kingery, B.P. Kelleher, M.H.B. Hayes, The application of LC-NMR and LC-SPE-NMR to compositional studies of natural organic matter., Analyst. 129 (2004) 1216–22. doi:10.1039/b408064e.

[66] R.M.B.O. Duarte, A.C. Barros, A.C. Duarte, Resolving the chemical heterogeneity of natural organic matter: new insights from comprehensive two-dimensional liquid chromatography., J. Chromatogr. A. 1249 (2012) 138–46. doi:10.1016/j.chroma.2012.06.022.

[67] M. Hallquist, J.C. Wenger, U. Baltensperger, Y. Rudich, D. Simpson, M. Claeys, J. Dommen, N.M. Donahue, C. George, A.H. Goldstein, J.F. Hamilton, H. Herrmann, T. Hoffmann, Y. Iinuma, M. Jang, M.E. Jenkin, J.L. Jimenez, A. Kiendler-Scharr, W. Maenhaut, G. McFiggans, T.F. Mentel, A. Monod, A.S.H. Prévôt, J.H. Seinfeld, J.D. Surratt, R. Szmigielski, J. Wildt, The formation, properties and impact of secondary organic aerosol: current and emerging issues, Atmos. Chem. Phys. 9 (2009) 5155–5236. doi:10.5194/acp-9-5155-2009.

[68] W. Welthagen, J. Schnelle-Kreis, R. Zimmermann, Search criteria and rules for comprehensive two-dimensional gas chromatography–time-of-flight mass spectrometry analysis of airborne particulate matter, J. Chromatogr. A. 1019 (2003) 233–249. doi:10.1016/j.chroma.2003.08.053.

[69] J. Hamilton, P. Webb, A. Lewis, J. Hopkins, S. Smith, P. Davy, Partially oxidised organic components in urban aerosol using GCXGC-TOF/MS, Atmos. Chem. Phys. Discuss. 4 (2004) 1393–1423. doi:10.5194/acpd-4-1393-2004.

[70] M. Kallio, M. Jussila, T. Rissanen, P. Anttila, K. Hartonen, A. Reissell, R. Vreuls, M. Adahchour, T. Hyötyläinen, Comprehensive two-dimensional gas chromatography coupled to time-of-flight mass spectrometry in the identification of organic compounds in atmospheric aerosols from coniferous forest., J. Chromatogr. A. 1125 (2006) 234–43. doi:10.1016/j.chroma.2006.05.050.

[71] J. Pól, B. Hohnová, M. Jussila, T. Hyötyläinen, Comprehensive two-dimensional liquid chromatography-time-of-flight mass spectrometry in the analysis of acidic compounds in atmospheric aerosols., J. Chromatogr. A. 1130 (2006) 64–71. doi:10.1016/j.chroma.2006.04.050.

[72] J.-K. Kim, S.N. Jackson, K.K. Murray, Matrix-assisted laser desorption/ionization mass spectrometry of collected bioaerosol particles., Rapid Commun. Mass Spectrom. 19 (2005) 1725–9. doi:10.1002/rcm.1982.

[73] Y. Wei, T. Cao, J.E. Thompson, The chemical evolution & physical properties of organic aerosol: A molecular structure based approach, Atmos. Environ. 62 (2012) 199–207. doi:10.1016/j.atmosenv.2012.08.029.

[74] M. Alier, B.L. van Drooge, M. Dall'Osto, X. Querol, J.O. Grimalt, R. Tauler, Source apportionment of submicron organic aerosol at an urban background and a road site in Barcelona (Spain) during SAPUSS, Atmos. Chem. Phys. 13 (2013) 10353–10371. doi:10.5194/acp-13-10353-2013.

[75] M.K. Shrivastava, R. Subramanian, W.F. Rogge, A.L. Robinson, Sources of organic aerosol: Positive matrix factorization of molecular marker data and comparison of results from different source apportionment models, Atmos. Environ. 41 (2007) 9353–9369. doi:10.1016/j.atmosenv.2007.09.016.

[76] S.M.C. Freire, Characterization of water-soluble organic matter from urban aerosols, University of Aveiro, 2014.

[77] A.F. Stein, R.R. Draxler, G.D. Rolph, B.J.B. Stunder, M.D. Cohen, F. Ngan, NOAA's HYSPLIT Atmospheric Transport and Dispersion Modeling System, Bull. Am. Meteorol. Soc. 96 (2015) 2059–2077. doi:10.1175/BAMS-D-14-00110.1.

[78] G.D. Rolph, Real-time Environmental Applications and Display sYstem (READY), NOAA Air Resour. Lab. Silver Spring, MD. (2016).

[79] M.E. Birch, R.A. Cary, Elemental carbon-based method for occupational monitoring of particulate diesel exhaust: methodology and exposure issues., Analyst. 121 (1996) 1183–90. http://www.ncbi.nlm.nih.gov/pubmed/8831275.

[80] U. Lohmann, J. Feichter, Global indirect aerosol effects: a review, Atmos. Chem. Phys. 5 (2005) 715–737. doi:10.5194/acp-5-715-2005.

[81] N. Mahowald, D.S. Ward, S. Kloster, M.G. Flanner, C.L. Heald, N.G. Heavens, P.G. Hess, J.-F. Lamarque, P.Y. Chuang, Aerosol Impacts on Climate and Biogeochemistry, Annu. Rev. Environ. Resour. 36 (2011) 45–74. doi:10.1146/annurev-environ-042009-094507.

[82] B.B.B. Booth, N.J. Dunstone, P.R. Halloran, T. Andrews, N. Bellouin, Aerosols implicated as a prime driver of twentieth-century North Atlantic climate variability, Nature. 484 (2012) 228–232. doi:10.1038/nature10946.

[83] E. Dinar, I. Taraniuk, E.R. Graber, S. Katsman, T. Moise, T. Anttila, T.F. Mentel, Y. Rudich, and Physics Cloud Condensation Nuclei properties of model and atmospheric, Atmos. Chem. Phys. Discuss. 6 (2006) 2465–2482. doi:10.5194/acp-6-2465-2006.

[84] W. Li, J. Chi, Z. Shi, X. Wang, B. Chen, Y. Wang, T. Li, J. Chen, D. Zhang, Z. Wang, C. Shi, L. Liu, W. Wang, Composition and hygroscopicity of aerosol particles at Mt. Lu in South China: Implications for acid precipitation, Atmos. Environ. 94 (2014) 626–636. doi:10.1016/j.atmosenv.2014.06.003.

[85] J.P. Reid, R.M. Sayer, Heterogeneous atmospheric aerosol chemistry: laboratory studies of chemistry on water droplets, Chem. Soc. Rev. 32 (2003) 70–79. doi:10.1039/b204463n.

[86] F.R. Cassee, M.-E. Héroux, M.E. Gerlofs-Nijland, F.J. Kelly, Particulate matter beyond mass: recent health evidence on the role of fractions, chemical constituents and sources of emission, Inhal. Toxicol. 25 (2013) 802–812. doi:10.3109/08958378.2013.850127.

[87] M.S. Callén, A. Iturmendi, J.M. López, Source apportionment of atmospheric PM2.5-bound polycyclic aromatic hydrocarbons by a PMF receptor model. Assessment of potential risk for human health, Environ. Pollut. 195 (2014) 167–177. doi:10.1016/j.envpol.2014.08.025.

[88] A. Saffari, N. Daher, M.M. Shafer, J.J. Schauer, C. Sioutas, Global Perspective on the Oxidative Potential of Airborne Particulate Matter: A Synthesis of Research Findings, Environ. Sci. Technol. 48 (2014) 7576–7583. doi:10.1021/es500937x.

[89] R.W. Atkinson, I.C. Mills, H.A. Walton, H.R. Anderson, Fine particle components and health—a systematic review and meta-analysis of epidemiological time series studies of daily mortality and hospital admissions, J. Expo. Sci. Environ. Epidemiol. 25 (2015) 208–214. doi:10.1038/jes.2014.63.

[90] J.-P. Putaud, F. Raes, R. Van Dingenen, E. Brüggemann, M.-C. Facchini, S. Decesari, S. Fuzzi, R. Gehrig, C. Hüglin, P. Laj, G. Lorbeer, W. Maenhaut, N. Mihalopoulos, K. Müller, X. Querol, S. Rodriguez, J. Schneider, G. Spindler, H. ten Brink, K. Tørseth, A. Wiedensohler, A European aerosol phenomenology - 2: chemical characteristics of particulate matter at kerbside, urban, rural and background sites in Europe, Atmos. Environ. 38 (2004) 2579–2595. doi:10.1016/j.atmosenv.2004.01.041.

[91] X. Querol, A. Alastuey, C.R. Ruiz, B. Artiñano, H.C. Hansson, R.M. Harrison, E. Buringh, H.M. ten Brink, M. Lutz, P. Bruckmann, P. Straehl, J. Schneider, Speciation and origin of PM10 and PM2.5 in selected European cities, Atmos. Environ. 38 (2004) 6547–6555. doi:10.1016/j.atmosenv.2004.08.037.

[92] R. Ocskay, I. Salma, W. Wang, W. Maenhaut, Characterization and diurnal variation of size-resolved inorganic water-soluble ions at a rural background site, J. Environ. Monit. 8 (2006) 300. doi:10.1039/b513915e.

[93] C.A. Pio, M. Legrand, T. Oliveira, J. Afonso, C. Santos, A. Caseiro, P. Fialho, F. Barata, H. Puxbaum, A. Sanchez-Ochoa, A. Kasper-Giebl, A. Gelencsér, S. Preunkert, M. Schock, Climatology of aerosol composition (organic versus inorganic) at nonurban sites on a west-east transect across Europe, J. Geophys. Res. 112 (2007) D23S02. doi:10.1029/2006JD008038.

[94] L. Tositti, E. Brattich, M. Masiol, D. Baldacci, D. Ceccato, S. Parmeggiani, M. Stracquadanio, S. Zappoli, Source apportionment of particulate matter in a large city of southeastern Po Valley (Bologna, Italy), Environ. Sci. Pollut. Res. 21 (2014) 872–890. doi:10.1007/s11356-013-1911-7.

[95] J.-P. Putaud, R. Van Dingenen, A. Alastuey, H. Bauer, W. Birmili, J. Cyrys, H. Flentje, S. Fuzzi, R. Gehrig, H.C. Hansson, R.M. Harrison, H. Herrmann, R. Hitzenberger, C. Hüglin, A.M. Jones, A. Kasper-Giebl, G. Kiss, A. Kousa, T.A.J. Kuhlbusch, G. Löschau, W. Maenhaut, A. Molnar, T. Moreno,

J. Pekkanen, C. Perrino, M. Pitz, H. Puxbaum, X. Querol, S. Rodriguez, I. Salma, J. Schwarz, J. Smolik, J. Schneider, G. Spindler, H. ten Brink, J. Tursic, M. Viana, A. Wiedensohler, F. Raes, A European aerosol phenomenology – 3: Physical and chemical characteristics of particulate matter from 60 rural, urban, and kerbside sites across Europe, Atmos. Environ. 44 (2010) 1308–1320. doi:10.1016/j.atmosenv.2009.12.011.

[96] L. Solorzano, Determination of ammonia in natural waters by the phenolhypochlorite method, Limnol. Oceanogr. 14 (1969) 799–801. doi:10.4319/lo.1969.14.5.0799.

[97] K.M. Shakya, P.F. Place, R.J. Griffin, R.W. Talbot, Carbonaceous content and water-soluble organic functionality of atmospheric aerosols at a semi-rural New England location, J. Geophys. Res. Atmos. 117 (2012) n/a-n/a. doi:10.1029/2011JD016113.

[98] R.J. Park, D.J. Jacob, M. Chin, R. V. Martin, Sources of carbonaceous aerosols over the United States and implications for natural visibility, J. Geophys. Res. 108 (2003) 4355, doi: 10.1029/2002JD003190. doi:10.1029/2002JD003190.

[99] A.S. Wozniak, J.E. Bauer, R.M. Dickhut, Characteristics of water-soluble organic carbon associated with aerosol particles in the eastern United States, Atmos. Environ. 46 (2012) 181–188. doi:10.1016/j.atmosenv.2011.10.001.

[100] E. Mantas, E. Remoundaki, I. Halari, P. Kassomenos, C. Theodosi, A. Hatzikioseyian, N. Mihalopoulos, Mass closure and source apportionment of PM2.5 by Positive Matrix Factorization analysis in urban Mediterranean environment, Atmos. Environ. 94 (2014) 154–163. doi:10.1016/j.atmosenv.2014.05.002.

[101] M. Yang, B.J. Huebert, B.W. Blomquist, S.G. Howell, L.M. Shank, C.S. McNaughton, A.D. Clarke, L.N. Hawkins, L.M. Russell, D.S. Covert, D.J. Coffman, T.S. Bates, P.K. Quinn, N. Zagorac, A.R. Bandy, S.P. de Szoeke, P.D. Zuidema, S.C. Tucker, W.A. Brewer, K.B. Benedict, J.L. Collett, Atmospheric sulfur cycling in the southeastern Pacific – longitudinal distribution, vertical profile, and diel variability observed during VOCALS-REx, Atmos. Chem. Phys. 11 (2011) 5079–5097. doi:10.5194/acp-11-5079-2011.

[102] E. Terzi, G. Argyropoulos, A. Bougatioti, N. Mihalopoulos, K. Nikolaou, C. Samara, Chemical composition and mass closure of ambient PM10 at urban sites, Atmos. Environ. 44 (2010) 2231–2239. doi:10.1016/j.atmosenv.2010.02.019.

[103] S. Reis, R.W. Pinder, M. Zhang, G. Lijie, M.A. Sutton, Reactive nitrogen in atmospheric emission inventories, Atmos. Chem. Phys. 9 (2009) 7657–7677. doi:10.5194/acp-9-7657-2009.

[104] S.N. Behera, M. Sharma, V.P. Aneja, R. Balasubramanian, Ammonia in the atmosphere: a review on emission sources, atmospheric chemistry and deposition on terrestrial bodies, Environ. Sci. Pollut. Res. 20 (2013) 8092–8131. doi:10.1007/s11356-013-2051-9.

[105] A.M. Jones, R.M. Harrison, Interpretation of particulate elemental and organic carbon concentrations at rural, urban and kerbside sites, Atmos. Environ. 39 (2005) 7114–7126. doi:10.1016/j.atmosenv.2005.08.017.

[106] C. Pio, M. Cerqueira, R.M. Harrison, T. Nunes, F. Mirante, C. Alves, C. Oliveira, A. Sanchez de la Campa, B. Artíñano, M. Matos, OC/EC ratio observations in Europe: Re-thinking the approach for apportionment between primary and secondary organic carbon, Atmos. Environ. 45 (2011) 6121–6132. doi:10.1016/j.atmosenv.2011.08.045.

[107] A. Gelencsér, B. May, D. Simpson, A. Sánchez-Ochoa, A. Kasper-Giebl, H. Puxbaum, A. Caseiro, C. Pio, M. Legrand, Source apportionment of PM2.5 organic aerosol over Europe: Primary/secondary, natural/anthropogenic, and fossil/biogenic origin, J. Geophys. Res. 112 (2007) D23S04. doi:10.1029/2006JD008094.

[108] D.R. Stoll, J.D. Cohen, P.W. Carr, Fast, comprehensive online two-dimensional high performance liquid chromatography through the use of high temperature ultra-fast gradient elution reversed-phase liquid chromatography., J. Chromatogr. A. 1122 (2006) 123–37. doi:10.1016/j.chroma.2006.04.058.

[109] G. Guiochon, N. Marchetti, K. Mriziq, R.A. Shalliker, Implementations of two-dimensional liquid chromatography., J. Chromatogr. A. 1189 (2008) 109–68. doi:10.1016/j.chroma.2008.01.086.

[110] J.T.V. Matos, R.M.B.O. Duarte, A.C. Duarte, Trends in data processing of comprehensive two-dimensional chromatography: State of the art, J. Chromatogr. B. 910 (2012) 31–45. doi:10.1016/j.jchromb.2012.06.039.

[111] S.E.G. Porter, D.R. Stoll, S.C. Rutan, P.W. Carr, J.D. Cohen, Analysis of four-way two-dimensional liquid chromatography-diode array data: application to metabolomics., Anal. Chem. 78 (2006) 5559–69. doi:10.1021/ac0606195.

[112] H.P. Bailey, S.C. Rutan, Chemometric resolution and quantification of four-way data arising from comprehensive 2D-LC-DAD analysis of human urine, Chemom. Intell. Lab. Syst. 106 (2011) 131–141. doi:10.1016/j.chemolab.2010.07.008.

[113] S.E. Reichenbach, X. Tian, C. Cordero, Q. Tao, Features for non-targeted cross-sample analysis with comprehensive two-dimensional chromatography., J. Chromatogr. A. 1226 (2012) 140–8. doi:10.1016/j.chroma.2011.07.046.

[114] M.R. Filgueira, C.B. Castells, P.W. Carr, A simple, robust orthogonal background correction method for two-dimensional liquid chromatography., Anal. Chem. 84 (2012) 6747–52. doi:10.1021/ac301248h.

[115] R.M.B.O. Duarte, J.T. V Matos, A.C. Duarte, A new chromatographic response function for assessing the separation quality in comprehensive two-dimensional liquid chromatography., J. Chromatogr. A. 1225 (2012) 121–31. doi:10.1016/j.chroma.2011.12.082.

[116] IUPAC, Compendium of Chemical Terminology, 2nd ed., Blackwell Scientific Publication, Oxford, 1997. doi:10.1351/goldbook.L03540.

[117] J.T.V. Matos, R.M.B.O. Duarte, A.C. Duarte, Chromatographic response functions in 1D and 2D chromatography as tools for assessing chemical complexity, TrAC Trends Anal. Chem. 45 (2013) 14–23. doi:10.1016/j.trac.2012.12.013.

[118] S. Fuzzi, M.O. Andreae, B.J. Huebert, M. Kulmala, T.C. Bond, M. Boy, S.J. Doherty, A. Guenther, M. Kanakidou, K. Kawamura, V.-M. Kerminen, U. Lohmann, L.M. Russell, U. Pöschl, Critical assessment of the current state of scientific knowledge, terminology, and research needs concerning the role of organic aerosols in the atmosphere, climate, and global change, Atmos. Chem. Phys. Discuss. 5 (2005) 11729–11780. doi:10.5194/acpd-5-11729-2005.

[119] E.R. Graber, Y. Rudich, Atmospheric HULIS: How humic-like are they? A comprehensive and critical review, Atmos. Chem. Phys. 6 (2006) 729–753. doi:10.5194/acp-6-729-2006.

[120] Y. Chin, G. Aiken, E. O'Loughlin, Molecular weight, polydispersity, and spectroscopic properties of aquatic humic substances, Environ. Sci. Technol. 28 (1994) 1853–1858. doi:10.1021/es00060a015.

[121] C. Pelekani, G. Newcombe, V.L. Snoeyink, C. Hepplewhite, S. Assemi, R. Beckett, Characterization of natural organic matter using high performance size exclusion chromatography, Environ. Sci. Technol. 33 (1999) 2807–2813. doi:10.1021/es9901314.

[122] A. Gelencsér, A. Hoffer, Z. Krivácsy, G. Kiss, A. Molnár, E. Mészáros, On the possible origin of humic matter in fine continental aerosol, J. Geophys. Res. 107 (2002) 4137. doi:10.1029/2001JD001299.

[123] R.M.B.O. Duarte, A.C. Duarte, Optimizing size-exclusion chromatographic conditions using a composite objective function and chemometric tools: application to natural organic matter profiling., Anal. Chim. Acta. 688 (2011) 90–8. doi:10.1016/j.aca.2010.12.031.

[124] Á. Andrade-Eiroa, M. Canle, V. Cerdá, Environmental Applications of Excitation-Emission Spectrofluorimetry: An In-Depth Review II, Appl. Spectrosc. Rev. 48 (2013) 77–141. doi:10.1080/05704928.2012.692105.

[125] R.M.B.O. Duarte, C.A. Pio, A.C. Duarte, Synchronous Scan and Excitation-Emission Matrix Fluorescence Spectroscopy of Water-Soluble Organic Compounds in Atmospheric Aerosols, J. Atmos. Chem. 48 (2004) 157–171. doi:10.1023/B:JOCH.0000036845.82039.8c.

[126] N. Mladenov, L. Alados-Arboledas, F.J. Olmo, H. Lyamani, A. Delgado, A. Molina, I. Reche, Applications of optical spectroscopy and stable isotope analyses to organic aerosol source discrimination in an urban area, Atmos. Environ. 45 (2011) 1960–1969. doi:10.1016/j.atmosenv.2011.01.029.

[127] K.R. Murphy, C.A. Stedmon, D. Graeber, R. Bro, Fluorescence spectroscopy and multi-way techniques. PARAFAC, Anal. Methods. 5 (2013) 6557. doi:10.1039/c3ay41160e.

[128] K.R. Murphy, K.D. Butler, R.G.M. Spencer, C.A. Stedmon, J.R. Boehme, G.R. Aiken, Measurement of dissolved organic matter fluorescence in aquatic environments: an interlaboratory comparison., Environ. Sci. Technol. 44 (2010) 9405–12. doi:10.1021/es102362t.

[129] C.A. Andersson, R. Bro, The N-way Toolbox for MATLAB, Chemom. Intell. Lab. Syst. 52 (2000) 1–4. doi:10.1016/S0169-7439(00)00071-X.

[130] R. Bro, H.A.L. Kiers, A new efficient method for determining the number of components in PARAFAC models, J. Chemom. 17 (2003) 274–286. doi:10.1002/cem.801.

[131] Á. Andrade-Eiroa, M. Canle, V. Cerdá, Environmental Applications of Excitation-Emission Spectrofluorimetry: An In-Depth Review I, Appl. Spectrosc. Rev. 48 (2013) 1–49. doi:10.1080/05704928.2012.692104.

[132] U. Lorenzo-seva, J.M.F. Berge, Tucker's Congruence Coefficient as a Meaningful Index of Factor Similarity, Methodol. Eur. J. Res. Methods Behav. Soc. Sci. 2 (2006) 57–64. doi:10.1027/1614-1881.2.2.57.

[133] I. Salma, R. Ocskay, X. Chi, W. Maenhaut, Sampling artefacts, concentration and chemical composition of fine water-soluble organic carbon and humic-like substances in a continental urban atmospheric environment, Atmos. Environ. 41 (2007) 4106–4118. doi:10.1016/j.atmosenv.2007.01.027.

[134] K. Hautala, J. Peuravuori, K. Pihlaja, Measurement of aquatic humus content by spectroscopic analyses, Water Res. 34 (2000) 246–258. doi:10.1016/S0043-1354(99)00137-2.

[135] N. Havers, P. Burba, J. Lambert, D. Klockow, Spectroscopic characterization of humic-like substances in airborne particulate matter, J. Atmos. Chem. 29 (1998) 45–54. doi:10.1023/A:1005875225800.

[136] P. Kowalczuk, M.J. Durako, H. Young, A.E. Kahn, W.J. Cooper, M. Gonsior, Characterization of dissolved organic matter fluorescence in the South Atlantic Bight with use of PARAFAC model: Interannual variability, Mar. Chem. 113 (2009) 182–196. doi:10.1016/j.marchem.2009.01.015.

[137] C.A. Stedmon, S. Markager, Resolving the variability of dissolved organic matter fluorescence in a temperate estuary and its catchment using PARAFAC analysis, Limnol. Oceanogr. 50 (2005) 686–697. doi:10.4319/lo.2005.50.2.0686.

[138] S.A. Baghoth, S.K. Sharma, G.L. Amy, Tracking natural organic matter (NOM) in a drinking water treatment plant using fluorescence excitation-emission matrices and PARAFAC., Water Res. 45 (2011) 797–809. doi:10.1016/j.watres.2010.09.005.

[139] S. Singh, E.J. D'Sa, E.M. Swenson, Chromophoric dissolved organic matter (CDOM) variability in Barataria Basin using excitation-emission matrix (EEM) fluorescence and parallel factor analysis (PARAFAC)., Sci. Total Environ. 408 (2010) 3211–22. doi:10.1016/j.scitotenv.2010.03.044.

[140] C. Stedmon, S. Markager, R. Bro, Tracing dissolved organic matter in aquatic environments using a new approach to fluorescence spectroscopy, Mar. Chem. 82 (2003) 239–254. doi:10.1016/S0304-4203(03)00072-0.

[141] G.-H. Yu, Y.-H. Luo, M.-J. Wu, Z. Tang, D.-Y. Liu, X.-M. Yang, Q.-R. Shen, PARAFAC modeling of fluorescence excitation-emission spectra for rapid assessment of compost maturity., Bioresour. Technol. 101 (2010) 8244–51. doi:10.1016/j.biortech.2010.06.007.

[142] M.S. Callén, M.T. de la Cruz, J.M. López, R. Murillo, M. V Navarro, A.M. Mastral, Some inferences on the mechanism of atmospheric gas/particle partitioning of polycyclic aromatic hydrocarbons (PAH) at Zaragoza (Spain)., Chemosphere. 73 (2008) 1357–65. doi:10.1016/j.chemosphere.2008.06.063.

[143] S. Decesari, M.C. Facchini, S. Fuzzi, E. Tagliavini, Characterization of water-soluble organic compounds in atmospheric aerosol: A new approach, J. Geophys. Res. Atmos. 105 (2000) 1481–1489. doi:10.1029/1999JD900950.

[144] E. Tagliavini, F. Moretti, S. Decesari, M.C. Facchini, S. Fuzzi, W. Maenhaut, Functional group analysis by H NMR/chemical derivatization for the characterization of organic aerosol from the

SMOCC field campaign, Atmos. Chem. Phys. 6 (2006) 1003–1019. doi:10.5194/acp-6-1003-2006.

[145] P.M. Fine, G.R. Cass, B.R.T. Simoneit, Chemical Characterization of Fine Particle Emissions from Fireplace Combustion of Woods Grown in the Northeastern United States, Environ. Sci. Technol. 35 (2001) 2665–2675. doi:10.1021/es001466k.

[146] R.M.B.O. Duarte, C.L. Mieiro, A. Penetra, C.A. Pio, A.C. Duarte, Carbonaceous materials in size-segregated atmospheric aerosols from urban and coastal-rural areas at the Western European Coast, Atmos. Res. 90 (2008) 253–263. doi:10.1016/j.atmosres.2008.03.003.

[147] F. Moretti, E. Tagliavini, S. Decesari, M.C. Facchini, M. Rinaldi, S. Fuzzi, NMR Determination of Total Carbonyls and Carboxyls: A Tool for Tracing the Evolution of Atmospheric Oxidized Organic Aerosols, Environ. Sci. Technol. 42 (2008) 4844–4849. doi:10.1021/es703166v.

[148] A.J. Simpson, J. Burdon, C.L. Graham, M.H.B. Hayes, N. Spencer, W.L. Kingery, Interpretation of heteronuclear and multidimensional NMR spectroscopy of humic substances, Eur. J. Soil Sci. 52 (2001) 495–509. doi:10.1046/j.1365-2389.2001.00402.x.

[149] N. Hertkorn, A. Kettrup, Molecular Level Structural Analysis of Natural Organic Matter and of Humic Substances by Multinuclear and Higher Dimensional NMR Spectroscopy, in: I. V. Perminova, K. Hatfield, N. Hertkorn (Eds.), Use Humic Subst. to Remediat. Polluted Environ. From Theory to Pract., Springer, 2005: pp. 391–435. doi:10.1007/1-4020-3252-8_21.

[150] National Institute of Advanced Industrial Science and Technology, SDBSWeb:, (2015). http://sdbs.db.aist.go.jp (accessed October 1, 2015).

[151] S.A. Ralph, John Ralph, L.L. Landucci, NMR Database of Lignin and Cell Wall Model Compounds, (2009). http://www.glbrc.org/databases_and_software/nmrdatabase/ (accessed June 20, 2002).

[152] D. Banfi, L. Patiny, www.nmrdb.org: Resurrecting and Processing NMR Spectra On-line, Chim. Int. J. Chem. 62 (2008) 280–281. doi:10.2533/chimia.2008.280.

[153] I. Barnes, G. Solignac, A. Mellouki, K.H. Becker, Aspects of the atmospheric chemistry of amides, ChemPhysChem. 11 (2010) 3844–3857. doi:10.1002/cphc.201000374.

[154] S. Liu, D.A. Day, J.E. Shields, L.M. Russell, Ozone-driven daytime formation of secondary organic aerosol containing carboxylic acid groups and alkane groups, Atmos. Chem. Phys. 11 (2011) 8321–8341. doi:10.5194/acp-11-8321-2011.

[155] S. Kundu, K. Kawamura, T.W. Andreae, A. Hoffer, M.O. Andreae, Molecular distributions of dicarboxylic acids, ketocarboxylic acids and α-dicarbonyls in biomass burning aerosols: implications for photochemical production and degradation in smoke layers, Atmos. Chem. Phys. 10 (2010) 2209–2225. doi:10.5194/acp-10-2209-2010.

[156] L.M. Russell, R. Bahadur, P.J. Ziemann, Identifying organic aerosol sources by comparing functional group composition in chamber and atmospheric particles., Proc. Natl. Acad. Sci. U. S. A. 108 (2011) 3516–3521. doi:10.1073/pnas.1006461108.

[157] P. Schmitt-Kopplin, G. Liger-Belair, B.P. Koch, R. Flerus, G. Kattner, M. Harir, B. Kanawati, M. Lucio, D. Tziotis, N. Hertkorn, I. Gebef??gi, Dissolved organic matter in sea spray: A transfer study from marine surface water to aerosols, Biogeosciences. 9 (2012) 1571–1582. doi:10.5194/bg-9-1571-2012.

[158] R.G. Joergensen, F. Wichern, Quantitative assessment of the fungal contribution to microbial tissue in soil, Soil Biol. Biochem. 40 (2008) 2977–2991. doi:10.1016/j.soilbio.2008.08.017.

[159] M.C.G. Chalbot, J. Brown, P. Chitranshi, G. Gamboa Da Costa, E.D. Pollock, I.G. Kavouras, Functional characterization of the water-soluble organic carbon of size-fractionated aerosol in the southern Mississippi Valley, Atmos. Chem. Phys. 14 (2014) 6075–6088. doi:10.5194/acp-14-6075-2014.

[160] H.J. Lee, P.K. Aiona, A. Laskin, J. Laskin, S.A. Nizkorodov, Effect of solar radiation on the optical properties and molecular composition of laboratory proxies of atmospheric brown carbon, Environ. Sci. Technol. 48 (2014) 10217–10226. doi:10.1021/es502515r.

[161] S. Gao, M. Keywood, N.L. Ng, J. Surratt, V. Varutbangkul, R. Bahreini, R.C. Flagan, J.H. Seinfeld, Low-Molecular-Weight and Oligomeric Components in Secondary Organic Aerosol from the Ozonolysis of Cycloalkenes and α-Pinene, J. Phys. Chem. A. 108 (2004) 10147–10164. doi:10.1021/jp047466e.

[162] R.Q. Shen, X. Ding, Q.F. He, Z.Y. Cong, Q.Q. Yu, X.M. Wang, Seasonal variation of secondary organic aerosol tracers in Central Tibetan Plateau, Atmos. Chem. Phys. 15 (2015) 8781–8793. doi:10.5194/acp-15-8781-2015.

[163] K. Kawamura, K. Matsumoto, E. Tachibana, K. Aoki, Low molecular weight (C1–C10) monocarboxylic acids, dissolved organic carbon and major inorganic ions in alpine snow pit sequence from a high mountain site, central Japan, Atmos. Environ. 62 (2012) 272–280. doi:10.1016/j.atmosenv.2012.08.018.

[164] D. Grosjean, Atmospheric Chemistry of Toxic Contaminants. 3. Unsaturated Aliphatics: Acrolein, Acrylonitrile, Maleic Anhydride, J. Air Waste Manage. Assoc. 40 (1990) 1664–1669. doi:10.1080/10473289.1990.10466814.

[165] A.W.H. Chan, M.N. Chan, J.D. Surratt, P.S. Chhabra, C.L. Loza, J.D. Crounse, L.D. Yee, R.C. Flagan, P.O. Wennberg, J.H. Seinfeld, Role of aldehyde chemistry and NOx concentrations in secondary organic aerosol formation, Atmos. Chem. Phys. 10 (2010) 7169–7188. doi:10.5194/acp-10-7169-2010.

[166] B.R.T. Simoneit, W.F. Rogge, M.A. Mazurek, L.J. Standley, L.M. Hildemann, G.R. Cass, Lignin pyrolysis products, lignans, and resin acids as specific tracers of plant classes in emissions from biomass combustion, Environ. Sci. Technol. 27 (1993) 2533–2541. doi:10.1021/es00048a034.

[167] Y. Iinuma, O. Böge, H. Herrmann, Methyl-nitrocatechols: Atmospheric tracer compounds for biomass burning secondary organic aerosols, Environ. Sci. Technol. 44 (2010) 8453–8459. doi:10.1021/es102938a.

[168] B.R.T. Simoneit, J.J. Schauer, C.G. Nolte, D.R. Oros, V.O. Elias, M.P. Fraser, W.F. Rogge, G.R. Cass, Levoglucosan, a tracer for cellulose in biomass burning and atmospheric particles, Atmos. Environ. 33 (1999) 173–182. doi:10.1016/S1352-2310(98)00145-9.

[169] C.G. Nolte, J.J. Schauer, G.R. Cass, B.R.T. Simoneit, Highly polar organic compounds present in wood smoke and in the ambient atmosphere, Environ. Sci. Technol. 35 (2001) 1912–1919. doi:10.1021/es001420r.

[170] B.R.T. Simoneit, V.O. Elias, M. Kobayashi, K. Kawamura, A.I. Rushdi, P.M. Medeiros, W.F. Rogge, B.M. Didyk, Sugars - Dominant water-soluble organic compounds in soils and characterization as tracers in atmospheric participate matter, Environ. Sci. Technol. 38 (2004) 5939–5949. doi:10.1021/es0403099.

[171] U.J. Wünsch, K.R. Murphy, C.A. Stedmon, Fluorescence Quantum Yields of Natural Organic Matter and Organic Compounds : Implications for the Fluorescence-based Interpretation of Organic Matter Composition, Front. Mar. Sci. 2 (2015) 1–15. doi:10.3389/fmars.2015.00098.

Annexes

Table A. 1 Sampling dates for each collected sample and for each sample campaign (*I, II, III*).

Sampling campaign I		
	Sampling Period	
s01	23/11/2009	30/11/2009
s02	30/11/2009	07/12/2009
s03	07/12/2009	14/12/2009
s04	14/12/2009	21/12/2009
s05	08/03/2010	15/03/2010
s06	30/03/2010	06/04/2010
s07	06/04/2010	13/04/2010
s08	20/04/2010	27/04/2010
s09	27/04/2010	04/05/2010
s10	04/05/2010	11/05/2010
s11	11/05/2010	18/05/2010
s12	18/05/2010	25/05/2010
s13	01/06/2010	08/06/2010
s14	15/06/2010	22/06/2010
s15	22/06/2010	29/06/2010
s16	05/07/2010	12/07/2010
s17	12/07/2010	19/07/2010
s18	19/07/2010	26/07/2010
s19	26/07/2010	02/08/2010
s20	02/08/2010	09/08/2010
s21	09/08/2010	16/08/2010
s22	20/09/2010	27/09/2010
s23	27/09/2010	04/10/2010
s24	04/10/2010	11/10/2010
s25	02/11/2010	09/11/2010
s26	09/11/2010	16/11/2010
s27	16/11/2010	23/11/2010
s28	23/11/2010	30/11/2010
s29	30/11/2010	07/12/2010
s30	27/12/2010	03/01/2011
s31	11/01/2011	18/01/2011
s32	18/01/2011	25/01/2011
s33	25/01/2011	01/02/2011
s34	01/03/2011	08/03/2011
s35	08/03/2011	15/03/2011
s36	15/03/2011	22/03/2011
s37	22/03/2011	29/03/2011

Sampling campaign II		
	Sampling Period	
s01	30/01/2013	06/02/2013
s02	06/02/2013	13/02/2013
s03	13/02/2013	20/02/2013
s04	20/02/2013	27/02/2013
s05	05/04/2013	12/04/2013
s06	12/04/2013	19/04/2013
s07	19/04/2013	26/04/2013
s08	26/04/2013	03/05/2013
s09	01/07/2013	08/07/2013
s10	08/07/2013	15/07/2013
s11	19/07/2013	26/07/2013
s12	26/07/2013	02/08/2013
s13	02/09/2013	09/09/2013
s14	09/09/2013	16/09/2013
s15	16/09/2013	23/09/2013
s16	30/09/2013	07/10/2013
s17	07/10/2013	14/10/2013
s18	14/10/2013	21/10/2013
s19	21/10/2013	28/10/2013
s20	11/11/2013	18/11/2013
s21	18/11/2013	25/11/2013
s22	25/11/2013	02/12/2013
s23	02/12/2013	09/12/2013

Sampling campaign III		
	Sampling Period	
s01	08/01/2014	15/01/2014
s02	15/01/2014	22/01/2014
s03	22/01/2014	29/01/2014
s04	29/01/2014	05/02/2014
s05	19/02/2014	26/02/2014
s06	26/02/2014	05/03/2014
s07	05/03/2014	12/03/2014
s08	12/03/2014	19/03/2014
s09	03/04/2014	10/04/2014
s10	10/04/2014	17/04/2014
s11	17/04/2014	24/04/2014
s12	24/04/2014	01/05/2014
s13	19/05/2014	26/05/2014
s14	26/05/2014	02/06/2014
s15	02/06/2014	09/06/2014
s16	09/06/2014	16/06/2014
s17	30/06/2014	07/07/2014
s18	07/07/2014	14/07/2014
s19	14/07/2014	21/07/2014
s20	21/07/2014	28/07/2014

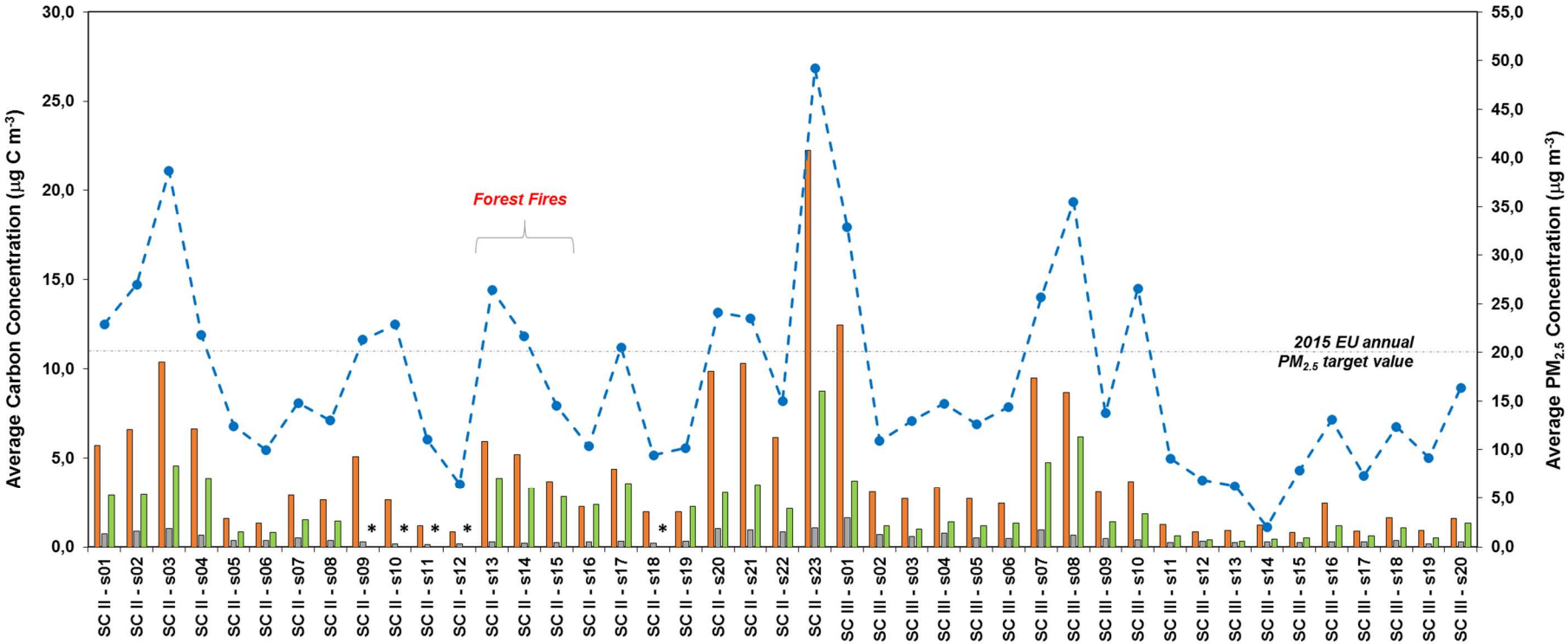

Figure A. 1 Atmospheric concentrations of ■ OC (µg C m^{-3}), ■ EC (µg C m^{-3}), ■ WSOC (µg C m^{-3}), and -●- urban $PM_{2.5}$ (µg m^{-3}) for each collected sample of the Sampling campaign II (SC II) and Sampling campaign III (SC III). (*) denotes data unavailable for the content of WSOC fraction in $PM_{2.5}$ samples. The $PM_{2.5}$ limit of 20 µg m^{-3} fixed by 2008/50/EC for the year 2015 is represented by a dashed dot grey line. The samples collected under forest fire events are also highlighted.

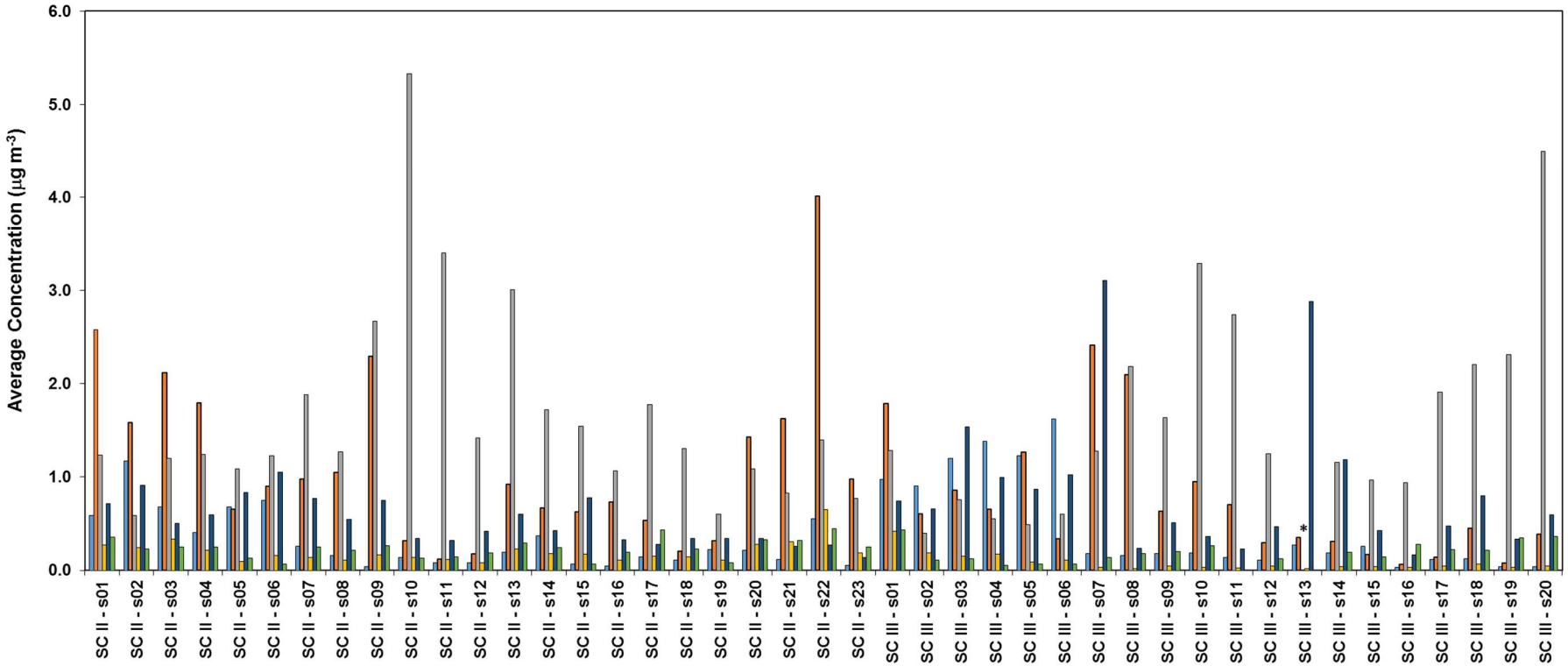

Figure A. 2 Atmospheric concentrations (µg m^{-3}) of water-soluble ions Cl^-, NO_3^-, SO_4^{2-}, K^+, Na^+, and NH^{4+} in urban $PM_{2.5}$ for each collected sample of the Sampling campaign II (SC II) and Sampling campaign III (SC III). (*) denotes data unavailable for the content of SO_4^{2-} ion in $PM_{2.5}$ samples.

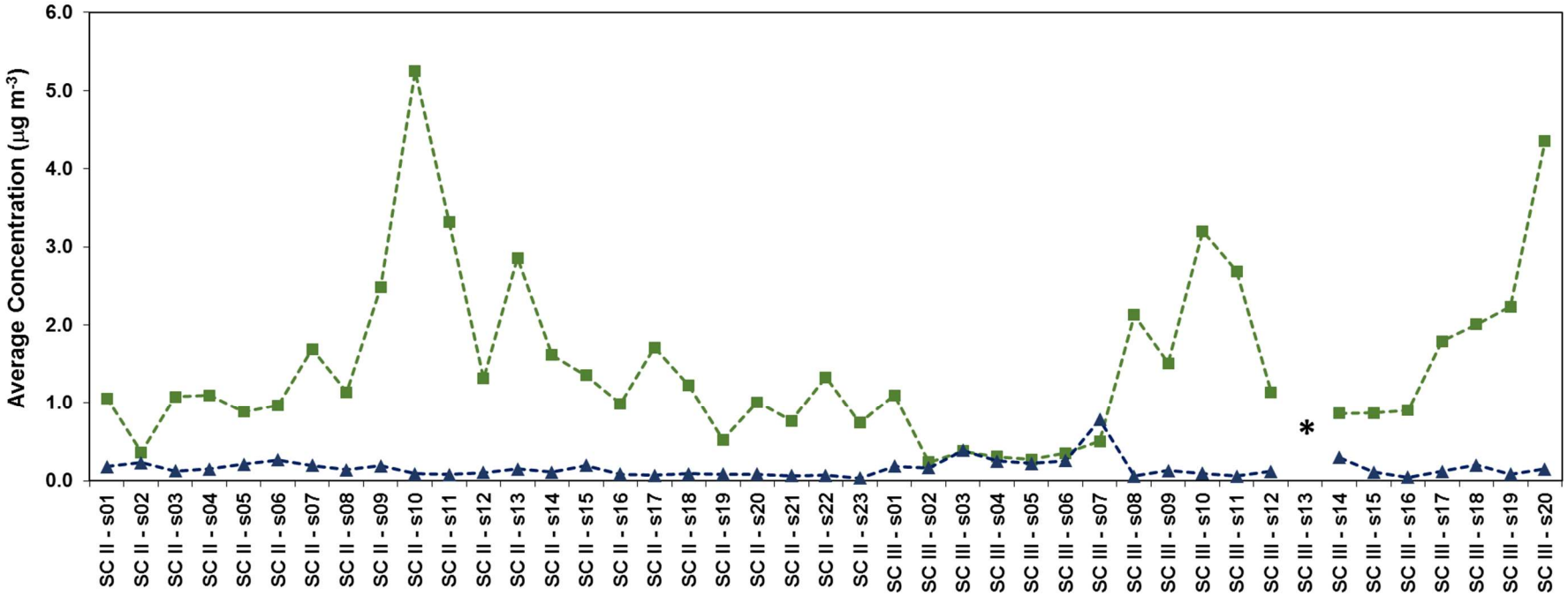

Figure A. 3 Atmospheric concentrations (μg m^{-3}) of -■- non-sea-salt SO_4^{2-} and -▲- sea-salt SO_4^{2-} in urban $PM_{2.5}$ for each collected sample of the Sampling campaign II (SC II) and Sampling campaign III (SC III). (*) denotes data unavailable for the content of of non-sea-salt and sea-salt SO_4^{2-} in $PM_{2.5}$ samples.

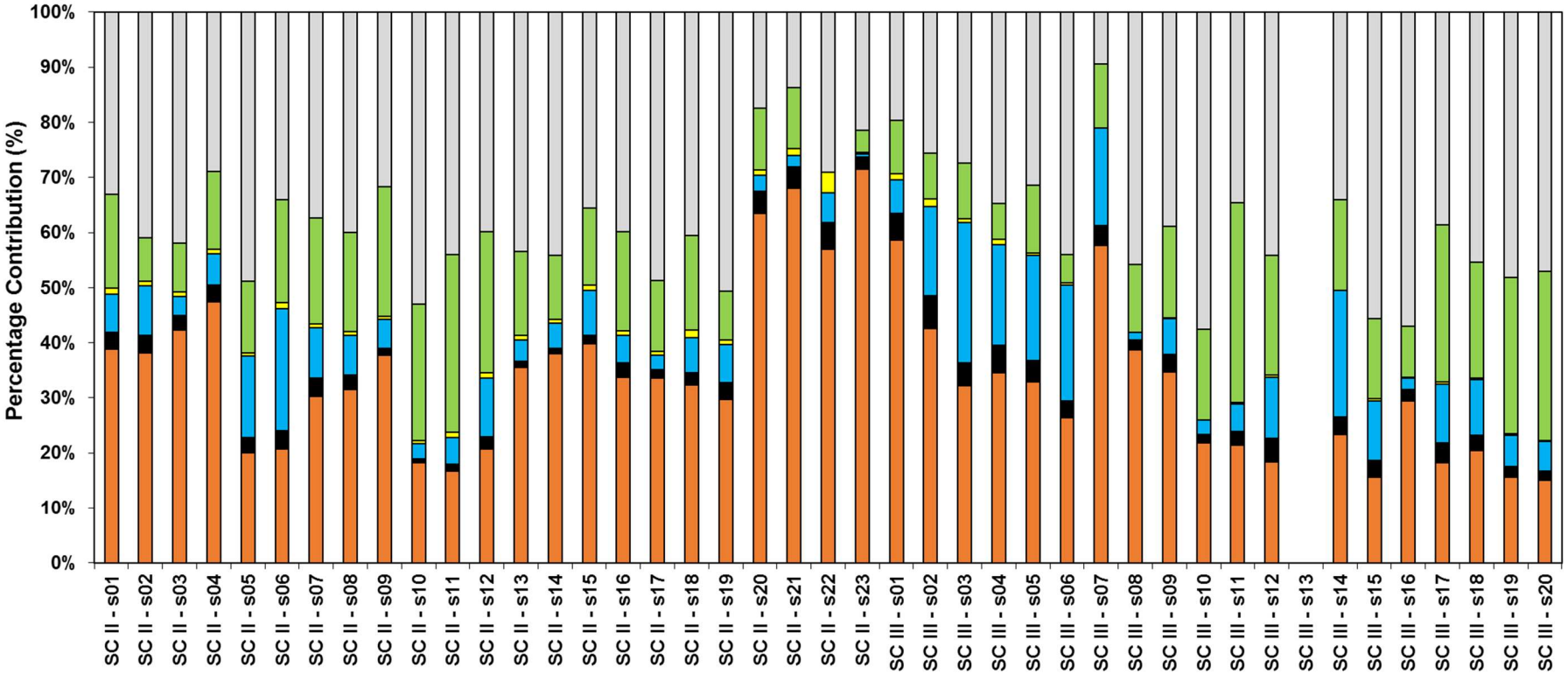

Figure A. 4 Percentage contribution of organic matter, EC, sea salt, non-sea-salt K+, and SIA to the urban $PM_{2.5}$ mass for each collected sample of the Sampling campaign II (SC II) and Sampling campaign III (SC III). "Unknown" represents the difference between total mass, measured by gravimetry, and total analysed mass. (*) denotes data unavailable for the $PM_{2.5}$ samples.

Table A. 2 Pearson Correlation between the average atmospheric concentrations of $PM_{2.5}$, OC, EC, WSOC, water-soluble Cl^-, NO_3^-, SO_4^{2-}, K^+, Na^+, and NH_4^+ ions, sea-salt, SIA, and median air temperature.

	$PM_{2.5}$ (µg m^{-3})	**OC (µg C m^{-3})**	**EC (µg C m^{-3})**	**WSOC (µg C m^{-3})**	**Cl^- (µg m^{-3})**	**NO_3^- (µg m^{-3})**	**SO_4^{2-} (µg m^{-3})**	**K^+ (µg m^{-3})**	**Na^+ (µg m^{-3})**	**NH_4^+ (µg m^{-3})**	**Sea Salt (µg m^{-3})**	**SIA (µg m^{-3})**	**T_{median} ºC**
$PM_{2.5}$ (µg m^{-3})	1 (n=43)												
OC (µg C m^{-3})	0.896** (p=0.000; n=43)	1 (n=43)											
EC (µg C m^{-3})	0.385* (p =0.011; n=43)	0.513** (p=0.000; n=43)	1 (n=43)										
WSOC (µg C m^{-3})	0.924** (p=0.000; n=39)	0.917** (p=0.000; n=39)	0.305 (p=0.059; n=39)	1 (n=43)									
Cl^- (µg m^{-3})	0.055 (p=0.724; n=43)	0.033 (p=0.833; n=43)	0.282 (p=0.067; n=43)	-0.128 (p=0.436; n=39)	1 (n=43)								
NO_3^- (µg m^{-3})	0.521** (p=0.000; n=43)	0.537** (p=0.000; n=43)	0.385* (p=0.011; n=43)	0.508** (p=0.001; n=39)	0.184 (p=0.238; n=43)	1 (n=43)							
SO_4^{2-} (µg m^{-3})	0.100 (p=0.522; n=43)	-0.167 (p=0.284; n=43)	-0.432** (p=0.004; n=43)	0.016 (p=0.922; n=39)	-0.454** (p=0.002; n=43)	-0.111 (p=0.480; n=43)	1 (n=43)						
K^+ (µg m^{-3})	0.172 (p=0.270; n=43)	0.282 (p=0.067; n=43)	0.780** (p=0.000; n=43)	0.130 (p=0.429; n=39)	0.199 (p=0.200; n=43)	0.431** (p=0.004; n=43)	-0.282 (p=0.066; n=43)	1 (n=43)					
Na^+ (µg m^{-3})	-0.001 (p=0.993; n=43)	0.033 (p=0.836; n=43)	0.037 (p=0.813; n=43)	0.014 (p=0.932; n=39)	0.348* (p=0.022; n=43)	0.229 (p=0.140; n=43)	-0.161 (p=0.303; n=43)	-0.210 (p=0.176; n=43)	1 (n=43)				
NH_4^+ (µg m^{-3})	0.351* (p=0.024; n=41)	0.358* (p=0.022; n=41)	0.316* (p=0.044; n=41)	0.264 (p=0.114; n=37)	-0.304 (p=0.053; n=41)	0.402** (p=0.009; n=41)	0.228 (p=0.151; n=41)	0.486** (p=0.001; n=41)	-0.332* (p=0.034; n=41)	1 (n=41)			
Sea Salt (µg m^{-3})	-0.022 (p=0.891; n=43)	0.007 (p=0.967; n=43)	0.321* (p=0.036; n=43)	-0.093 (p=0.572; n=39)	0.699** (p=0.000; n=43)	0.220 (p=0.157; n=43)	-0.377* (p=0.013; n=43)	0.094 (p=0.547; n=43)	0.870** (p=0.000; n=43)	-0.387* (p=0.012; n=41)	1 (n=43)		
SIA (µg m^{-3})	0.415** (p=0.006; n=42)	0.210 (p=0.182; n=42)	0.089 (p=0.576; n=42)	0.344* (p=0.035; n=38)	-0.320* (p=0.039; n=42)	0.540** (p=0.000; n=42)	0.745** (p=0.000; n=42)	0.329* (p=0.033; n=42)	-0.148 (p=0.350; n=42)	0.550** (p=0.000; n=41)	-0.254 (p=0.104; n=42)	1 (n=42)	
T_{median} ºC	-0.463** (p=0.003; n=40)	-0.617** (p=0.000; n=40)	-0.630** (p=0.000; n=40)	-0.429** (p=0.009; n=36)	-0.534** (p=0.000; n=40)	-0.563** (p=0.000; n=40)	0.544** (p=0.000; n=40)	-0.441** (p=0.004; n=40)	-0.094 (p=0.564; n=40)	-0.128 (p=0.445; n=38)	-0.318* (p=0.046; n=40)	0.053 (p=0.750; n=39)	1 (n=40)

** Correlation is significant at the 0.01 level (2-tailed);

* Correlation is significant at the 0.05 level (2-tailed).

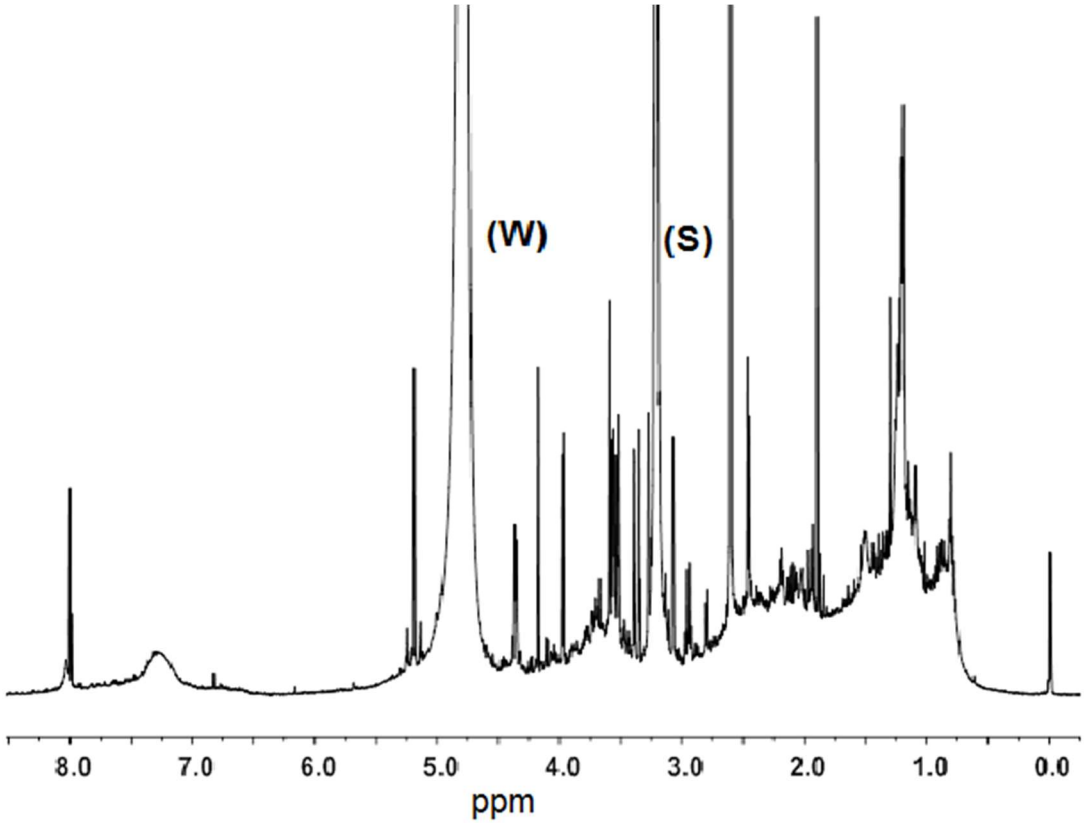

Figure A. 5 500 MHz solution-state ^{1}H NMR spectra of WSOM extract from a seven-day $PM_{2.5}$ sample collected in the early autumn of 2014 (October). Resonance signals: Water (W), and Solvent (S) – MeOH–*d4*.

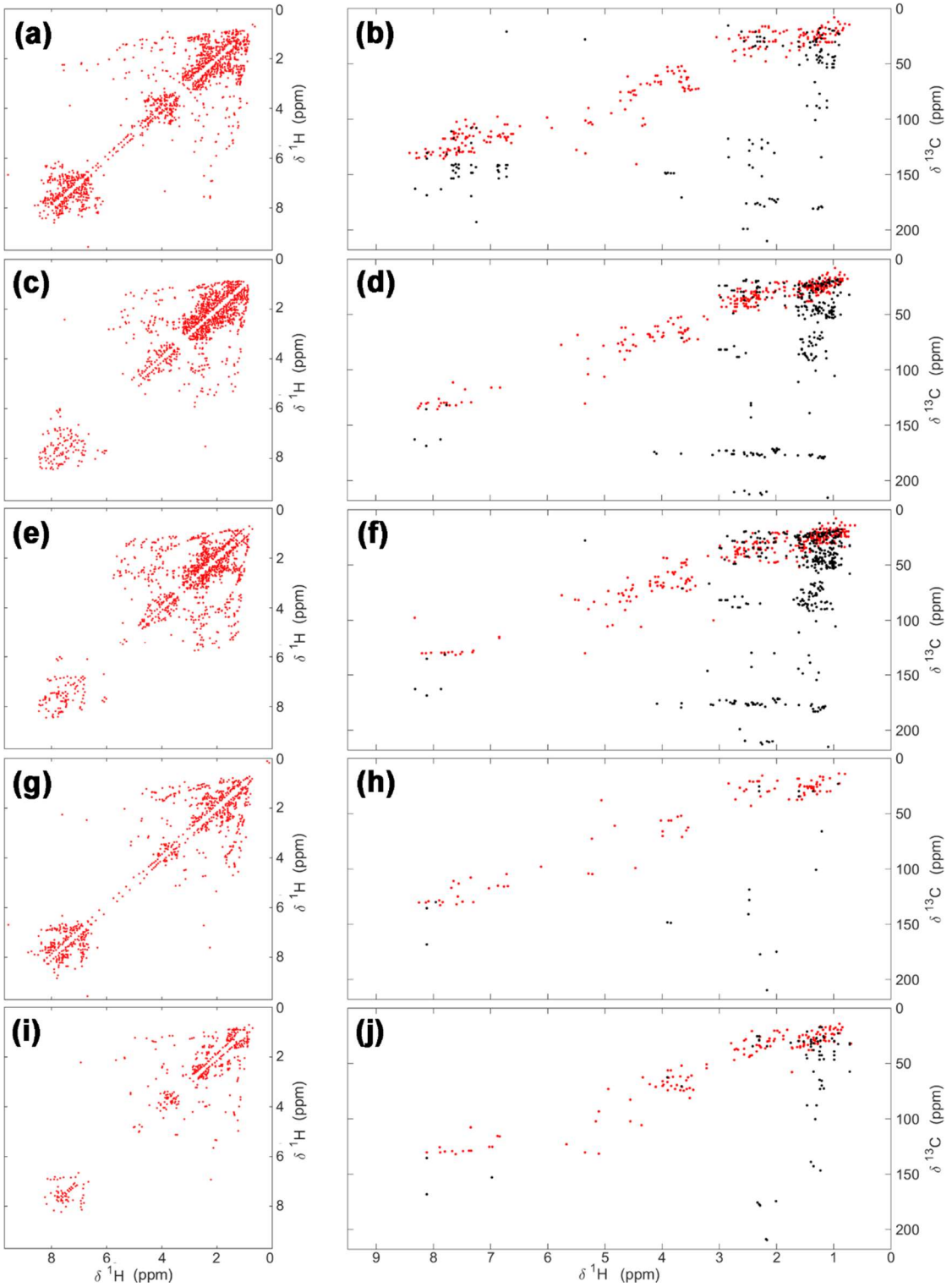

Figure A. 6 ^{1}H–^{1}H COSY NMR signals maxima of the (a) WSOM Win. 2010, (c) WSOM Sum. B 2010, (e) WSOM Sum. A 2010, (g) ASOM Win. 2010, and (i) ASOM Sum. B 2010 hydrophobic fraction samples; and ^{1}H–^{13}C HSQC NMR signals maxima (●) overlaid onto the ^{1}H–^{13}C HMBC signals maxima (●) of the (b) WSOM Win. 2010, (d) WSOM Sum. B 2010, (f) WSOM Sum. A 2010, (h) ASOM Win. 2010, and (j) ASOM Sum. B 2010 hydrophobic fraction samples.

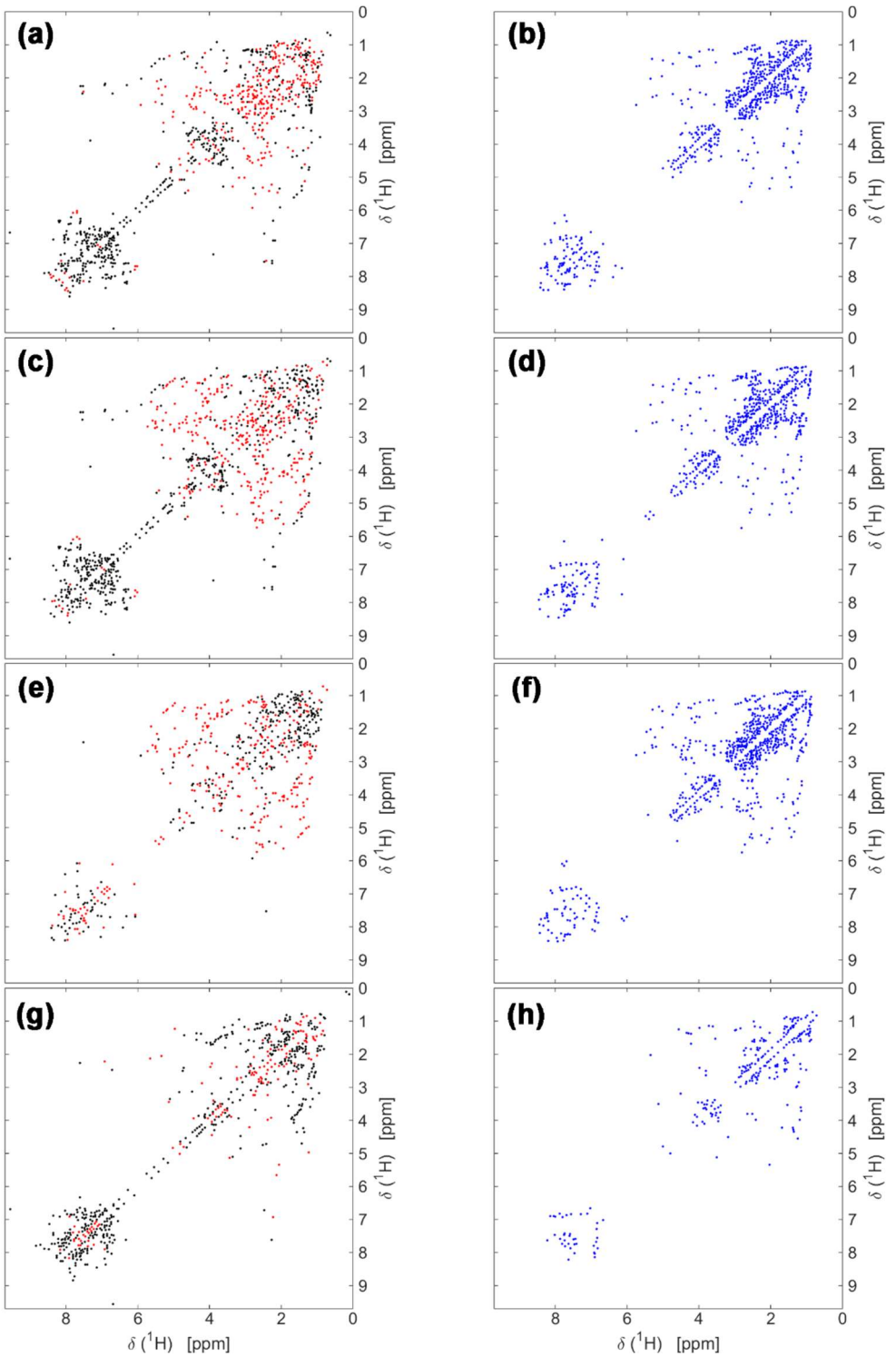

Figure A. 7 ^{1}H–^{1}H COSY NMR signals maxima: (a) non-common between WSOM Win. 2010 (●) and Sum. B 2010 (●) samples; (b) common to both WSOM Win. 2010 and Sum. B 2010 samples; (c) non-common between WSOM Win. 2010 (●) and Sum. A 2010 (●) samples; (d) common to both WSOM Win. 2010 and Sum. A 2010 samples; (e) non-common between WSOM Sum. B 2010 (●) and Sum. A 2010 (●) samples; (f) common to both WSOM Sum. B 2010 and Sum. A 2010 samples; (g) non-common between ASOM Win. 2010 (●) and Sum. B 2010 (●) samples; and (h) common to both ASOM Win. 2010 and Sum. B 2010 samples.

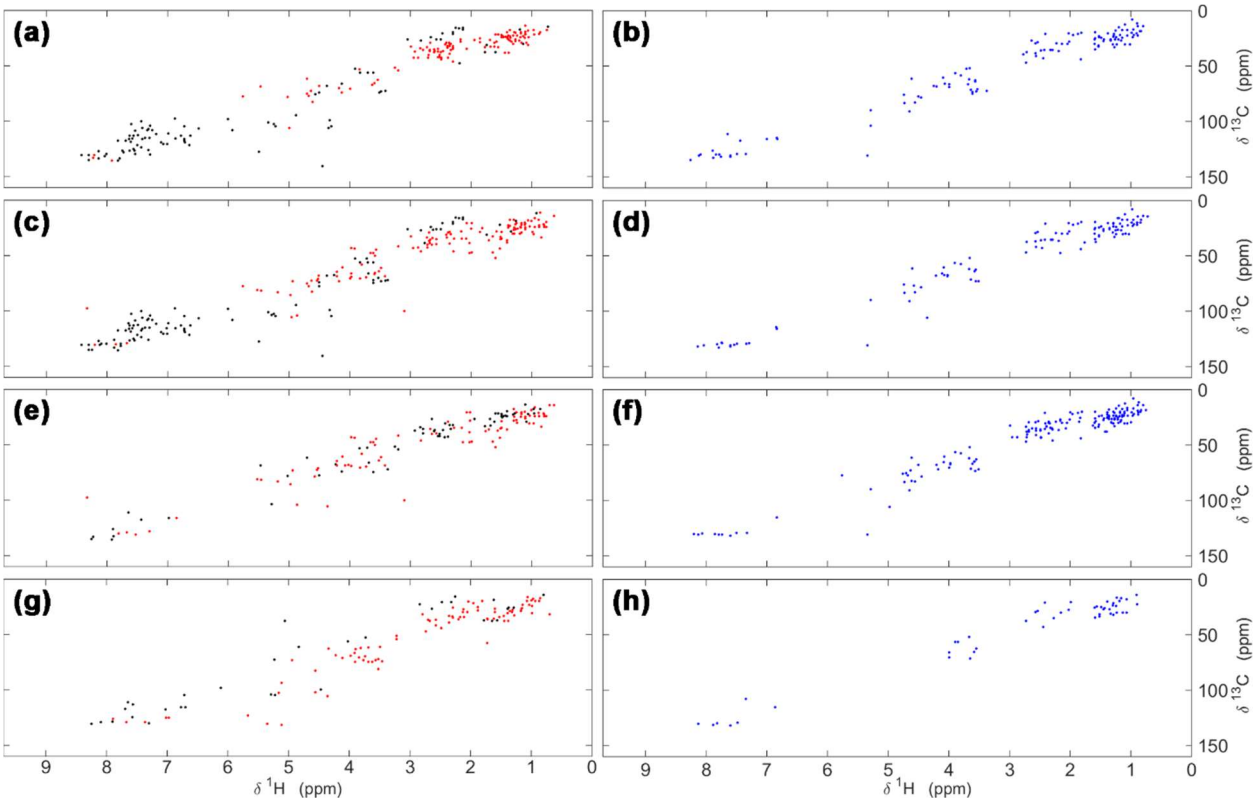

Figure A. 8 $^{1}H–^{13}C$ HSQC NMR signals maxima: (a) non-common between WSOM Win. 2010 (●) and Sum. B 2010 (●) samples; (b) common to both WSOM Win. 2010 and Sum. B 2010 samples; (c) non-common between WSOM Win. 2010 (●) and Sum. A 2010 (●) samples; (d) common to both WSOM Win. 2010 and Sum. A 2010 samples; (e) non-common between WSOM Sum. B 2010 (●) and Sum. A 2010 (●) samples; (f) common to both WSOM Sum. B 2010 and Sum. A 2010 samples; (g) non-common between ASOM Win. 2010 (●) and Sum. B 2010 (●) samples; and (H) common to both ASOM Win. 2010 and Sum. B 2010 samples.

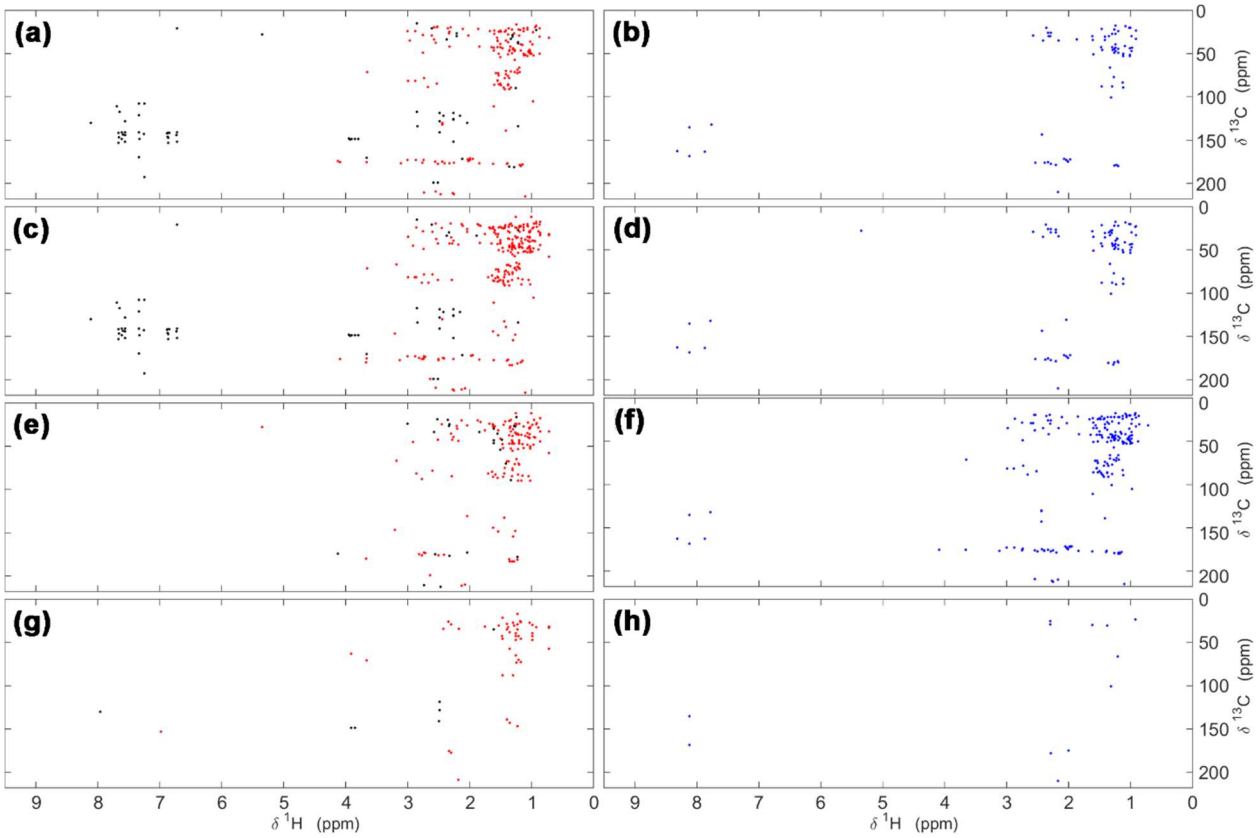

Figure A. 9 $^{1}H–^{13}C$ HMBC NMR signals maxima: (a) non-common between WSOM Win. 2010 (●) and Sum. B 2010 (●) samples; (b) common to both WSOM Win. 2010 and Sum. B 2010 samples; (c) non-common between WSOM Win. 2010 (●) and Sum. A 2010 (●) samples; (d) common to both WSOM Win. 2010 and Sum. A 2010 samples; (e) non-common between WSOM Sum. B 2010 (●) and Sum. A 2010 (●) samples; (f) common to both WSOM Sum. B 2010 and Sum. A 2010 samples; (g) non-common between ASOM Win. 2010 (●) and Sum. B 2010 (●) samples; and (H) common to both ASOM Win. 2010 and Sum. B 2010 samples.

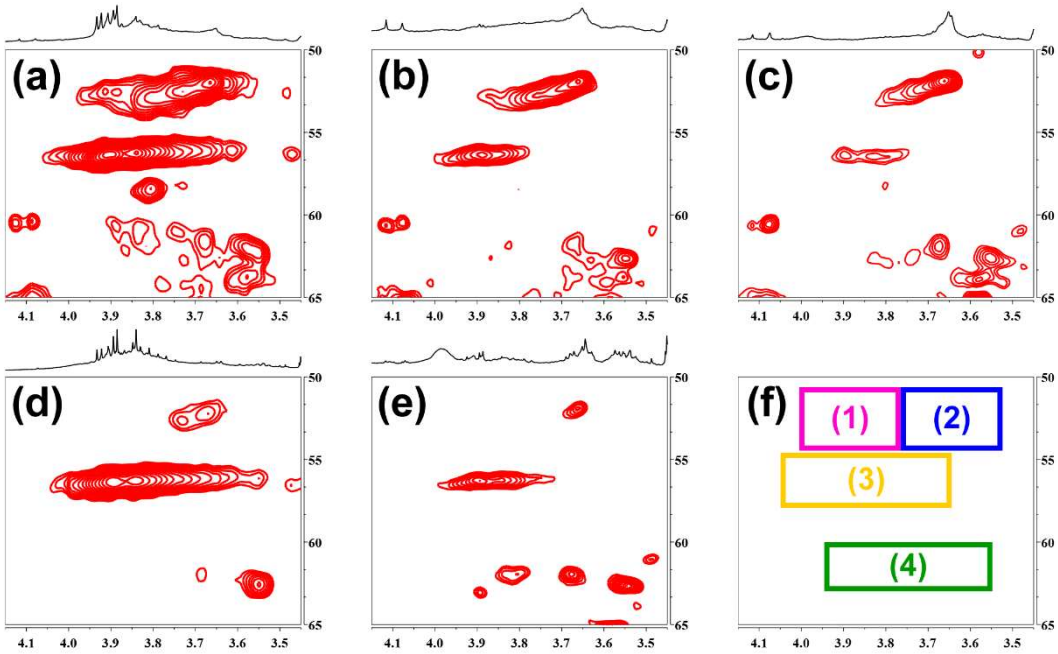

Figure A. 10 Expanded heteroatom-alkane substituted region of the $^{1}H–^{13}C$ HSQC 2D NMR spectra of the WSOM hydrophobic fraction extracted from the aerosol samples collected in Win. 2010 (a), Sum. B 2010 (b), and Sum. A 2010 (c), and of the ASOM hydrophobic fraction sequentially extracted from Win. 2010 (d) and Sum. B 2010 (e) samples. The regions defined in (f) are: (1) aromatic methyl esters ($R_{ar}–COO\mathbf{CH_3}$), (2) aliphatic methyl esters ($R_{al}–COO\mathbf{CH_3}$), (3) aromatic methyl ethers ($R_{ar}–O\mathbf{CH_3}$), and (4) oxymethylene ($\mathbf{CH_2}–O–$), likely from carbohydrates.

Table A. 3 2D NMR spectral assignments of the substructures identified in WSOM and ASOM fraction.

Substructure		Sample	Spectral assignments
Aliphatics			
AL - 1	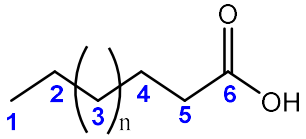	WSOM Win. 2010 WSOM Sum. A 2010 WSOM Sum. B 2010 ASOM Win. 2010 ASOM Sum. B 2010	**COSY:** δH**1** 0.9 / δH**2** 1.3 ppm; δH**3** 1.3 / δH**4** 1.5 ppm; δH**4** 1.5 / δH**5** 2.3 ppm **HSQC:** δH**1** 0.9 / δC**1** 14 ppm; δH**2** 1.3 / δC**2** 23.4 – 26.0 ppm; δH**3** 1.3 / δC**3** 30.0 – 32.6 ppm; δH**4** 1.5 / δC**4** 25.5-26.0 ppm; δH**5** 2.3 / δC**5** 35.0 ppm **HMBC:** δH**1** 0.9/ δC**2** 23.4, δC**3** 32.6 ppm; δH**4** 1.5/ δC**5** 35.0, δC**6** 177.0 ppm; δH**5** 2.3/ δC**4** 25.5, δC**6** 177.0 ppm
AL - 2	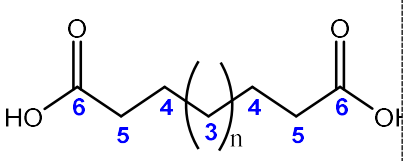		
AL - 3	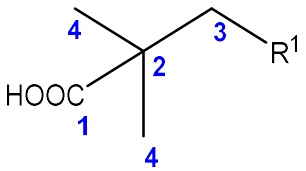 R^1 = Alkyl group (with a withdrawing unit)	WSOM Win. 2010 WSOM Sum. A 2010 WSOM Sum. B 2010 ASOM Win. 2010 ASOM Sum. B 2010	**HSQC:** δH**4** 1.24 / δC**4** 24.0 ppm **HMBC:** δH**4** 1.24 / δC**3** 39.2, δC**2** 43.1, δC**1** 181.5 ppm
AL - 4	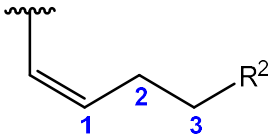 R^2 = Alkyl group bearing a methyl ester group in its spin system (δ_C 173.3 ppm; δ_H 3.5 – 3.8 / δ_C 52 – 54 ppm)	WSOM Win. 2010 WSOM Sum. A 2010 WSOM Sum. B 2010 ASOM Win. 2010 ASOM Sum. B 2010	**COSY:** δH**2** 2.03 / δH**1** 5.36 ppm **HSQC:** δH**2** 2.04 / δC**2** 27.9 ppm; δH**3** 1.33 / δC**3** 29.9 ppm; δH**1** 5.36 / δC**1** 130.6 ppm **HMBC:** δH**2** 2.04 / δC**3** 30.6, δC**1** 130.6, δC 173.3 ppm; δH**1** 5.36 / δC**2** 27.9 ppm
AL - 5	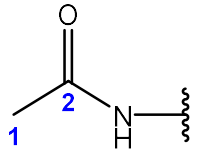	WSOM Win. 2010 WSOM Sum. A 2010 WSOM Sum. B 2010 ASOM Win. 2010 ASOM Sum. B 2010	**HSQC:** δH**1** 2.03–2.07 / δC**1** 20.2–20.5 ppm **HMBC:** δH**1** 2.03–2.07 / δC**2** 173.3 ppm

AL - 6	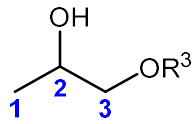 R^3 = H or alkyl group	WSOM Win. 2010 WSOM Sum. A 2010 WSOM Sum. B 2010 ASOM Win. 2010 ASOM Sum. B 2010	**HSQC:** δH**1** 1.18 / δC**1** 19.5 ppm; δH**2** 3.99 / δC**2** 66.2 ppm; δH**3** 3.99 / δC**3** 70.4 ppm **HMBC:** δH**1** 1.18 / δC**2** 66.1, δC**3** 70.3 ppm
AL - 7	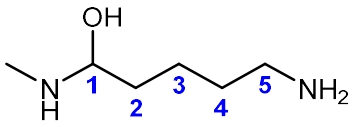	WSOM Win. 2010 WSOM Sum. A 2010 WSOM Sum. B 2010 ASOM Sum. B 2010	**HSQC:** δH**3** 1.29 / δC**3** 21.9 ppm; δH**4** 1.46 / δC**4** 27.3 ppm; δH**5** 2.46 / δC**5** 42.9 ppm; δH**1** 4.66 / δC**1** 90.8 ppm **HMBC:** δH**3** 1.30 / δC**4** 27.3, δC**5** 42.5, δC**1** 87.8 ppm; δH**4** = 1.48 / δC**5** 42.5, δC**1** 87.8 ppm
AL - 8	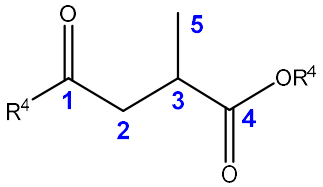 R^4 = H or CH_3	WSOM Win. 2010 WSOM Sum. A 2010 WSOM Sum. B 2010	**HSQC:** δH**5** 1.00 / δC**5** 20.2 ppm; δH**3** 2.57 / δC**3** 29.6 ppm **HMBC:** δH**5** 1.0 / δC**3** 30.0, δC**2** 50.0 ppm; δH**3** 2.57 / δC**5** 20.2, δC**4** 176.0, δC**1** 209.0 ppm
AL - 9	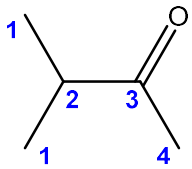	WSOM Win. 2010 WSOM Sum. A 2010 WSOM Sum. B 2010	**COSY:** δH**1** 0.96 / δH**2** = 2.5 ppm **HSQC:** δH**1** 0.96 / δC**1** 17.6 ppm; δH**4** 2.03 / δC**4** 27.9 ppm; δH**2** 2.47 / δC**2** 42.7 ppm **HMBC:** δH**1** 1.0 / δC**2** 42.7, δC**3** 215.0 ppm
AL - 10	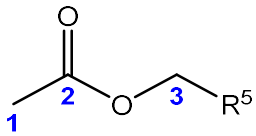 R^5 = Alkyl group	WSOM Win. 2010 WSOM Sum. A 2010 WSOM Sum. B 2010	**HSQC:** δH**1** 1.96 / δC**1** 21.9 ppm; δH**3** 4.08 – 4.12 / δC**3** 60.0 – 60.6 ppm **HMBC:** δH**1** 1.96 / δC**2** 172.3 ppm; δH**3** 4.08 – 4.12 / δC**2** 174.5 – 175.8 ppm

AL - 11	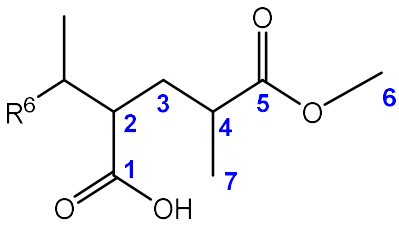 R^6 = H or alkyl group	WSOM Win. 2010 WSOM Sum. A 2010 WSOM Sum. B 2010	**HSQC:** δH**7** 0.97 / δC**7** 17.5 ppm; δH**3** 1.21 / δC**3** 30.1 ppm; δH**4** 2.36 – 2.58 / δC**4** 39.2 ppm; δH**6** 3.5 – 3.8 / δC**6** 52.0 – 54.0 ppm **HMBC:** δH**7** 0.97 / δC**3** 30.1, δC**4** 39.2, δC**2** 46.8 ppm; δH**3** 1.21 / δC**4** 17.5, δC**4** 39.2, δC**2** 47.0, δC**1** 181.4 ppm; δH**4** 2.36 – 2.58 / δC**5** 176.6 ppm
AL - 12	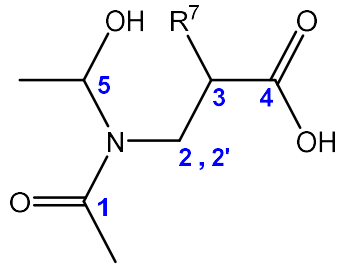 R^7 = H or alkyl group	WSOM Win. 2010 WSOM Sum. A 2010 WSOM Sum. B 2010	**COSY:** δH**3** 2.28 / δH**2** 2.88 ppm **HSQC:** δH**3** 2.28 / δC**3** 34.6 ppm; δH**2** 2.88 / δC**2** 42.7 ppm; δH**2'** 2.97 / δC**2'** 42.9 ppm **HMBC:** δH**3** 2.28 / δC**2** 42.5, δC**4** 177.0 ppm; δH**2** 2.88 / δC**5** 81.8, δC**1** 173.0 ppm; δH**2'** 2.97 / δC**5** 81.8, δC**1** 173.0 ppm
AL - 13	**(a)** 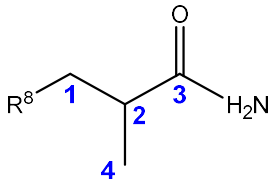 R^8 = Withdrawing group (e.g.,COOH) **(b)** 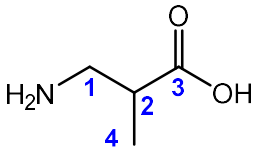	WSOM Win. 2010 WSOM Sum. A 2010 WSOM Sum. B 2010	**HSQC:** δH**4** 1.18 / δC**4** 22.1 ppm; **HMBC:** δH**4** 1.18 / δC**1** 44.3, δC**2** 49.0, δC**3** 179.8 ppm

AL - 14	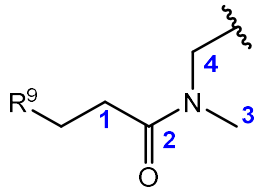 R^9 = Withdrawing group (e.g.,COOH)	WSOM Win. 2010 WSOM Sum. A 2010 WSOM Sum. B 2010	**HSQC:** δH**1** 2.53 / δC**1** 28.2 ppm; δH**3** 2.73 / δC**3** 37.6 ppm; δH**4** 3.77 / δC**4** 48.78 ppm **HMBC:** δH**1** 2.53 / δC**3** 37.6, δC**2** 176.2 ppm; δH**3** 2.73 / δC**1** 28.2, δC**4** 48.78, δC**2** 176.2 ppm
AL - 15	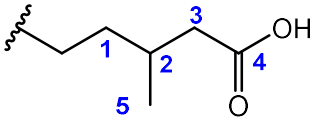	WSOM Sum. A 2010 WSOM Sum. B 2010	**COSY:** δH**5** 0.96 / δH**2** 1.82 ppm; δH**2** 1.82 / δH**1** 2.35 ppm **HSQC:** δH**5** 0.96 / δC**5** 24.2 ppm; δH**2** 1.82 / δC**2** 25.3 ppm; δH**1** 2.35 / δC**1** 39.3 ppm; δH**3** 2.72 / δC**3** 46.9 ppm **HMBC:** δH**5** 0.96 / δC**2** 25.4, δC**1** 39.3, δC**3** 46.9 ppm; δH**2** 1.82 / δC**4** 176.7 ppm; δH**3** 2.72 / δC**4** 176.0 ppm
AL - 16	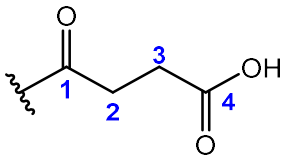	WSOM Sum. A 2010 WSOM Sum. B 2010	**HSQC:** δH**3** 2.53/ δC**3** 28.4 ppm; δH**2** 2.71 / δC**2** 37.6 ppm **HMBC:** δH**3** 2.53 / δC**2** 37.6, δC**4** 176.2, δC**1** 209.6 ppm; δH**2** 2.71 / δC**3** 28.4, δC**4** 176.2 ppm
AL - 17	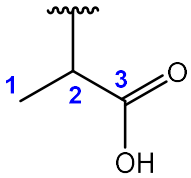	WSOM Win. 2010 ASOM Win. 2010 ASOM Sum. B 2010	**COSY:** δH**1** 1.2 / δH**2** 2.7 ppm **HSQC:** δH**1** 1.2 / δC**1** 16.4 – 16.8 ppm; δH**2** 2.7 / δC**2** 36.7 – 37.3 ppm **HMBC:** δH**1** 1.2 / δC**2** 36.7, δC**3** 179.8 ppm

AL - 18	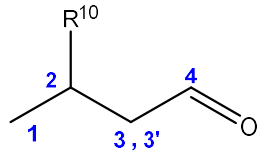 R^{10} = OH or alkyl group	WSOM Win. 2010	**HMBC:** δH**3** 2.52 / δC**4** 199.4 ppm; δH**3'** 2.59 / δC**1** 20.6, δC**4** 199.2 ppm
AL - 19	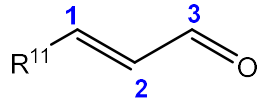 R^{11} = alkyl unit	WSOM Win. 2010 ASOM Win. 2010	**COSY:** δH**1** 6.69 / δH**3** 9.57 ppm
Saccharides			
SAC - 1	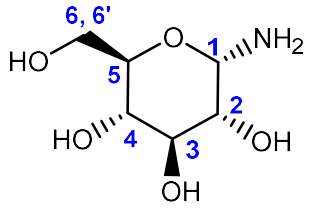	WSOM Win. 2010 WSOM Sum. A 2010 WSOM Sum. B 2010 ASOM Sum. B 2010	**HSQC:** δH**6** 3.57 / δC**6** 62.0 ppm; δH**6'** 3.67 / δC**6'** 61.6 ppm; δH**1** 5.29 / δC**1** 89.6 ppm; δH**2**,**3**,**4** 3.6 – 3.4 / δC**2**,**3**,**4** 69.5 – 74.7 ppm
SAC - 2	**(a)** 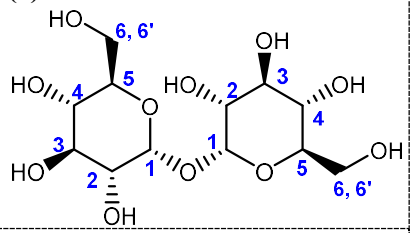 **(b)** 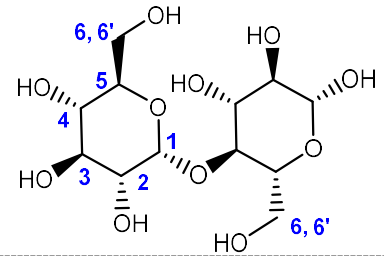 **(c)** 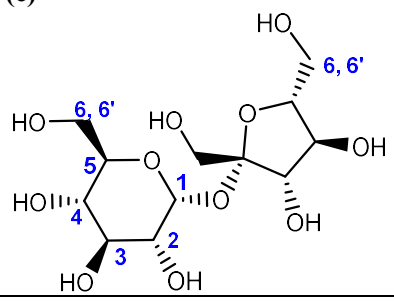	WSOM Win. 2010 WSOM Sum. B 2010 ASOM Win. 2010 ASOM Sum. B 2010	**HSQC:** δH**6** 3.57 / δC**6** 62.0 ppm; δH**6'** 3.67 / δC**6'** 61.6 ppm; δH**1** 5.30 / δC**1** 103.4 ppm; δH**2**,**3**,**4** 3.4 – 3.6 / δC**2**,**3**,**4** 69.5 – 74.7 ppm

SAC - 3	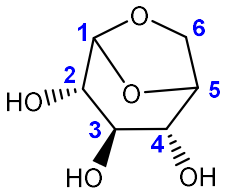	WSOM Win. 2010 WSOM Sum. B 2010	**HSQC:** δH**6** 3.6 – 3.7 / δC**6** 66.2 ppm; δH**6** 4.0 – 4.1 / δC**6** 66.2 ppm; δH**1** 5.30 / δC**1** 103.4 ppm; δH**2**,**3**,**4** 3.4 – 3.6 / δC**2**,**2**,**4** 69.5 – 74.7 ppm
SAC - 4	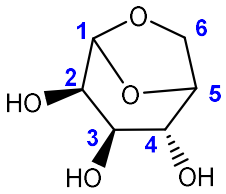	WSOM Win. 2010 WSOM Sum. B 2010	
Aromatics			
AR - 1	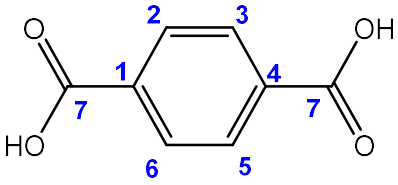	WSOM Win. 2010 WSOM Sum. A 2010 WSOM Sum. B 2010 ASOM Win. 2010 ASOM Sum. B 2010	**HSQC:** δH**2**,**3**,**5**,**6** 8.12 / δC**2**,**3**,**5**,**6** 130.5 ppm **HMBC:** δH**2**,**3**,**5**,**6** 8.12 / δC**1**,**4** 135.5, δC**7** 168.5 ppm
AR - 2	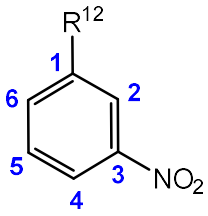 R^{12} = Oxygenated alkyl group	WSOM Win. 2010 WSOM Sum. A 2010 WSOM Sum. B 2010 ASOM Win. 2010 ASOM Sum. B 2010	**COSY:** δH**5** 7.60 / δH**6** 7.77 ppm **HSQC:** δH**5** 7.60 / δC**5** 131.8 ppm; δH**6** 7.77 / δC**6** 129.7 ppm; **HMBC:** δH**5** 7.60 / δC**1** 143.6, δC**3** 148.4 ppm; δH**6** 7.77 / δC**5** 131.8 ppm
AR - 3	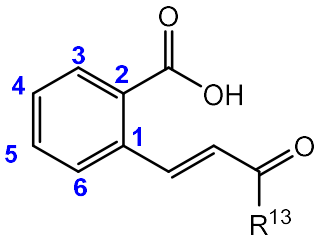 R^{13} = H, OH	WSOM Win. 2010 WSOM Sum. A 2010 WSOM Sum. B 2010 ASOM Win. 2010 ASOM Sum. B 2010	**COSY:** δH**4** 7.51 / δH**3** 8.02 ppm **HSQC:** δH**4** 7.51 / δC**4** 129.2ppm; δH**3** 8.02 / δC**3** 131.8 ppm;

AR - 4	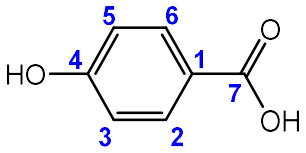	WSOM Win. 2010 WSOM Sum. B 2010 ASOM Win. 2010 ASOM Sum. B 2010	**COSY:** δH**3,5** 6.82 (d, *J* = 9.1 Hz) / δH**2,6** 7.88 ppm (d, *J* = 9.1 Hz) **HSQC:** δH**3,5** 6.82 / δC**3,5** 115.8 ppm; δH**2,6** 7.89 / δC**2,6** 132.6 ppm; **HMBC:** δH**3,5** 6.82 / δC**1** 122.3 ppm; δH**2,6** 7.89 / δC**4** 163.2 ppm
AR - 5	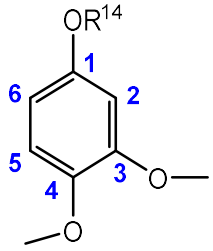 R^{14} = Alkyl group	WSOM Win. 2010 WSOM Sum. B 2010 ASOM Win. 2010 ASOM Sum. B 2010	**COSY:** δH**5** 6.86 (d, *J* = 8.8 Hz) / δH**6** 7.68 ppm (dd, *J* = 8.8, 2.7 Hz) **HSQC:** δH**5** 6.86 / δC**5** 115.3 ppm; δH**2** 7.64 (d, *J* = 2.7 Hz) / δC**2** 111.2 ppm; δH**6** 7.68 / δC**6** 117.5 ppm; **HMBC:** δH**5** 6.86 / δC**4** 141.5, δC**3** 146.3, δC**1** 153.6 ppm; δH**2** 7.64 / δC**6** 117.5, δC**4** 141.5, δC**3** 146.3, δC**1** 153.6 ppm; δH**6** 7.68 / δC**2** 111.2, δC**1** 153.6 ppm
AR - 6	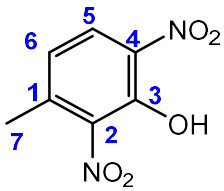	WSOM Win. 2010 ASOM Win. 2010	**COSY:** δH**7** 2.25 / δH**6** 7.60 ppm (WSOM); δH**7** 2.26 / δH**6** 7.61 ppm (ASOM) **HSQC:** δH**7** 2.25 / δC**7** 15.8 ppm; δH**6** 7.62 / δC**6** 118.6 ppm (WSOM); δH**7** 2.25 / δC**7** 15.7 ppm; δH**6** 7.62 / δC**6** 118.8 ppm (ASOM) **HMBC:** δH**7** 2.25 / δC**6** 118.6, δC**5** 125.7, δC**3** 151.7 ppm; (WSOM); δH**6** 7.56 / δC**5** 128.4, δC**1** 144.3, δC**3** 152.0 ppm; (WSOM); δH**7** 2.25 / δC**6** 118.4, δC**5** 125.5, δC**3** 151.6 ppm (ASOM)

AR - 7	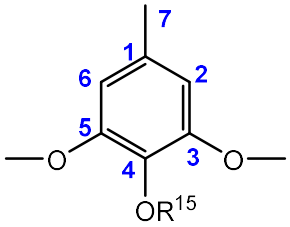 R^{15} = H, CH_3	WSOM Win. 2010 ASOM Win. 2010	**HSQC:** δH**7** 2.47 / δC**7** 20.6 ppm; δH**2,6** 6.72 / δC**2,6** 104.8 ppm **HMBC:** δH**7** 2.47 / δC**1** 141.2 ppm; δH**2,6** 6.71 / δC**7** 20.6, δC**2,6** 104.3, δC**4** 136.4, δC**3,5** 152.0 ppm
AR - 8	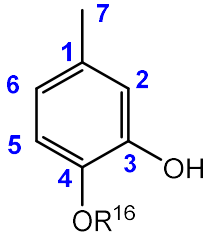 R^{16} = H, CH_3	WSOM Win. 2010 ASOM Win. 2010	**HSQC:** δH**7** 2.47 / δC**7** 20.6 ppm; δH**2** 6.72 / δC**2** 118.9 ppm **HMBC:** δH**7** 2.47 / δC**2** 118.8, δC**1** 128.5 ppm; δH**2** 6.72 / δC**7** 20.6, δC**3** 144.4, δC**4** 148.5 ppm
AR - 9	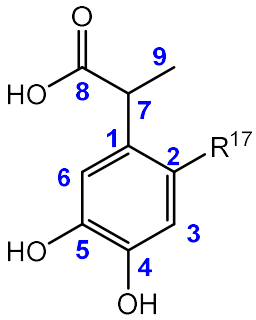 R^{17} = NH_2, NO_2	WSOM Win. 2010	**COSY:** δH**9** 1.21 / δH**7** 2.83 ppm **HSQC:** δH**9** 1.21 / δC**9** 15.2 ppm; δH**7** 2.83 / δC**7** 42.9 ppm; δH**6** 6.73 / δC**6** 117.5 ppm **HMBC:** δH**9** 1.21/ δC**7** 42.9, δC**1** 134.2, δC**8** 179.0 ppm; δH**7** 2.83/ δC**9** 15.2, δC**6** 117.4, δC**1** 134.2, δC**2** 141.0 ppm
AR - 10	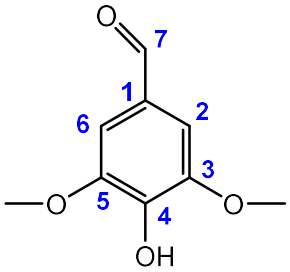	WSOM Win. 2010	**HSQC:** δH**2,6** 7.24 / δC**2,6** 107.8 ppm **HMBC:** δH**2,6** 7.24 / δC**2,6** 107.8, δC**4** 143.3, δC**7** 192.7 ppm

AR - 11	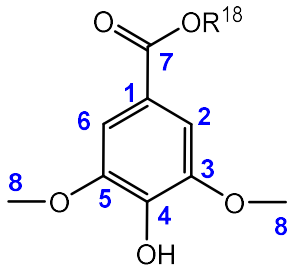 R^{18} = H, CH_3	WSOM Win. 2010	**HSQC:** δH**2,6** 7.35 / δC**2,6** 108.0 ppm; δH**8** 3.91 / δC**8** 56.4 ppm **HMBC:** δH**8** 3.91 / δC**3,5** 148.5 ppm; δH**2,6** 7.35 / δC**2,6** 108.0, δC**1** 121.5, δC**4** 141.3, δC**3,5** 148.5, δC**7** 169.7 ppm